STRUCTURE PROPERTY RELATIONSHIPS FOR DIRHODIUM ANTITUMOR ACTIVE COMPOUNDS: REACTIONS WITH BIOMOLECULES AND *IN CELLULO* STUDIES

A Dissertation

by

JESSICA DAFHNE AGUIRRE FLORES

Submitted to the Office of Graduate Studies of
Texas A&M University
in partial fulfillment of the requirements for the degree of

DOCTOR OF PHILOSOPHY

December 2009

Major Subject: Chemistry

STRUCTURE PROPERTY RELATIONSHIPS FOR DIRHODIUM ANTITUMOR ACTIVE COMPOUNDS: REACTIONS WITH BIOMOLECULES AND *IN CELLULO* STUDIES

A Dissertation

by

JESSICA DAFHNE AGUIRRE FLORES

Submitted to the Office of Graduate Studies of
Texas A&M University
in partial fulfillment of the requirements for the degree of

DOCTOR OF PHILOSOPHY

Approved by:

Chair of Committee,	Kim R. Dunbar
Committee Members,	Françoise Gabbaï
	Jean-Philippe Pellois
	Wenshe Liu
Head of Department,	David H. Russell

December 2009

Major Subject: Chemistry

ABSTRACT

Structure Property Relationships for Dirhodium Antitumor Active Compounds: Reactions with Biomolecules and *In Cellulo* Studies.

(December 2009)

Jessica Dafhne Aguirre Flores, B.S., Pontificia Universidad Católica del Perú

Chair of Advisory Committee: Dr. Kim R. Dunbar

The molecular characteristics that affect the activity of various dirhodium complexes are reported. The importance of the axial position in the action of dirhodium compounds was studied. Three dirhodium complexes with increasing number of accessible axial coordination sites were synthesized and characterized. In *cis*-$[Rh_2(\mu\text{-}OAc)_2(np)_2]^{2+}$ (np = 1,8-naphthyridine) both axial sites are available for coordination, whereas for *cis*-$[Rh_2(\mu\text{-}OAc)_2(np)(pynp)]^{+2}$ (pynp = 2-(2-pyridyl)1,8-naphthyridine) and *cis*-$[Rh_2(\mu\text{-}OAc)_2(pynp)_2]^{+2}$ the pyridyl arm on the ligand pynp blocks one and two axial sites, respectively. The availability of the axial positions affects the *in vitro* and *in cellulo* activity of these complexes demonstrating that open axial coordination sites are necessary for biological activity.

The inhibitory activity of derivatives of dirhodium-dppz complexes (dppz = dipyrido[3,2-a:2′,3′-c]phenazine) has also been investigated. The dppz derivatives included compounds with electron-withdrawing (Cl, CN, and NO_2) as well as electro-donating (MeO and Me) substituents. These compounds inhibit transcription of T7-RNA polymerase by reducing accessible cysteine residues. The activity correlates with the electron-

withdrawing character of the substituent on the dppz ligand. Density functional theory (DFT) calculations reveal that the lowest unoccupied molecular orbitals (LUMOs) in the series are ligand-based π* orbitals localized on the phenazine ring. These complexes represent the first family of dirhodium complexes whose inhibitory ability can be tuned by controlling their redox properties.

The effect of the presence of diimine ligands in the dirhodium core in both *in vitro* and *in cellulo* activity is discussed. The presence of one diimine ligand allows for dual binding, intercalation and covalent, as observed by melting temperature and relative viscosity measurements, as well as electrophoretic mobility shift assay (EMSA). The mono-substituted dirhodium complexes are effective against HeLa and COLO-316 cell lines, with $[Rh_2(\mu\text{-}O_2CCH_3)_2(\eta^1\text{-}O_2CCH_3)(dppz)]^+$ being the most effective compound of the series. Results of the comet assay indicate that all of the mono-substituted complexes studied damage nuclear DNA, although in different degrees. The cytotoxic effect of these complexes is not affected by the presence of glutathione. The addition of the second diimine ligand hinders the ability of the complexes to damage DNA. The bis-substituted complexes are also slightly less cytotoxic than their mono-substituted congeners. Thus, the number of equatorial positions occupied by diimine ligands play a critical role in the mechanism of cytotoxicity of dirhodium(II,II) complexes.

Finally, the results also demonstrate that improving the internalization of the dirhodium complexes can be achieved by co-incubation with cell penetrating peptides. This work provides a foundation for the preparation of new and more effective dirhodium complexes.

Para mis adorados padres Francisco y Aurora.

ACKNOWLEDGEMENTS

I would like to extend my heartfelt thanks to my academic advisor, Dr. Kim Dunbar, my mentor and friend. Working on this project was the most rewarding and motivating academic challenge that I have ever faced. I would like to thank her for being supportive, enthusiastic, and optimistic. I am especially grateful to her for giving me the freedom to shape this project and especially for trusting my instincts. I would also like to thank Dr. Claudia Turro, our collaborator from The Ohio State University, who was there to give me her support and always encourage me to continue and never give up. I am especially grateful to Dr. Jean-Phillipe Pellois for helping me every time, for his optimism, for making me laugh, but especially for lending me his laboratory facilities, without which I would have never been able to obtain such beautiful results. My thanks also go to my committee members, Dr. Wenshen Liu and Dr. François Gabbaï.

Thanks also to my colleagues and friends Carolina Avendaño, Mathew Hilfiger, Ferdi Karadaş and Alfredo Angeles for their friendship, for all the good times we spent together, and for simply being there during the hard times. Thanks to all the current and past members of the Dunbar group Sarah Lane, Ian Giles, Kristen Funk, Edward Funk, Nazario Lopez, Zhongyue Zhang, Dr. Hanhua Zhao, Dr. Xinyi Wang, Heather Southerland, Dr. Akira Ota, Dr. Andrey Prosvirin, Codi Sanders, Dr. Abdellatif Chouai and Prof. Mikhail Shatruk for an enjoyable atmosphere and their unconditional help.

My gratitude goes to the members of the Pellois group, especially Ja-yung Lee, Dr. Didvia Mani Srinivasan and Alfredo Erazo for accepting me as part of their lab, for always trying to assist me, for never complaining about

the long hours I took to finish my experiments, and cheering me up every time I got a result, bad or good. I would also like to thank Dr. Lisa Pérez for her time and help with the DFT calculations.

I would like to thank my parents, Francisco and Aurora, for their support and unconditional love. Without them this effort would have been worth nothing. To the rest of my family, although not being here with me, they gave me the strength to continue by giving me all their love. Finally, my thanks go to my husband Alfredo for his love, patience, help and support.

LIST OF ABBREVIATIONS

ssDNA	Single Strand DNA
dsDNA	Double Strand DNA
DFT	Density Functional Theory
TDDFT	Time Dependent Density Functional Theory
ct-DNA	Calf Thymus DNA
ddH_2O	Double Distilled Water
dH_2O	Distilled Water
IC_{50}	Concentration for 50% Inhibition
LC_{50}	Lethal Concentration
MTT	3-(4,5-dimethylthiazol-2-yl)-2,5-diphenyltetrazolium
SDS	Sodium Dodecyl Sulphate
Å	Anstrongs
MLCT	Metal to Ligand Charge Transfer
Tm	Melting Temperature
Kb	Binding Constant
HOMO	Highest Occupied Molecular Orbital
LUMO	Lowest Unoccupied Molecular Orbital
ε	Epsilon
PBS	Phosphate Buffer Saline

ax	Axial
eq	Equatorial
EtBr	Ethidium Bromide
Log P	Partition Coefficient
R	Arginine
K	Lysine

TABLE OF CONTENTS

CHAPTER Page

LIST OF FIGURES

FIGURE Page

FIGURE Page

FIGURE Page

FIGURE Page

FIGURE Page

FIGURE Page

FIGURE Page

LIST OF TABLES

TABLE Page

CHAPTER I

INTRODUCTION

Medicinal Inorganic Chemistry

A New Field or an Old Concept?

The field of modern *medicinal inorganic chemistry* was officially launched at the end of the 1970's with the introduction of cisplatin for the treatment of various forms of reproductive cancers, most notably that of testicular tumors.[1] Medicinal inorganic chemistry, however, has been around for a long time.[2, 3] In fact there is documented evidence that inorganic compounds have been used for medicinal purposes for over 5000 years. In Egypt, for example, copper was used to sterilize water, and zinc compounds were used to heal wounds.[2] Meanwhile, gold was very popular in Arabia and China for a variety of medical applications.[4] During the Renaissance period, Europeans used mercury in the form of mercurous chloride as a diuretic and recognized the nutritional value of iron.[2, 4-6]

During the early 1900's, the development of biologically active inorganic compounds began to be explored in a rational manner. Notable among these efforts is the use of $K[Au(CN)_2]$ for tuberculosis and various gold salts as antibacterial agents,[4, 6] as well as the implementation of antimony-based compounds to treat leishmaniasis,[4, 7, 8] a parasitic disease spread by the bite of the sandfly.[9, 10] Paul Ehrlich, known as the father of chemotherapy, was the first scientist to establish structure-activity relationship (SAR) studies, a method that is widely used in modern pharmacology.[7, 11] Early on, Ehrlich realized that certain dyes were able to

---

This dissertation follows the style and format of the *Journal of the American Chemical Society*.

stain specific microbes. He then proposed that they could be chemically modified to be pharmacologically active for killing harmful microbes without endangering the host. He discovered that trypan red had activity against sleeping sickness caused by the protozoa *trypanosome brucei gambiense* in chickens (Figure I-1). Ehrlich hypothesized that the azo group (-N=N-) was key to the activity of the dye and he decided to study other compounds containing this moiety. The position of arsenic in the periodic table, just under nitrogen, was the main reason that Ehrlich began studying arsenic derivatives. Several hundreds of arsenic based compounds were synthesized and their biological activity and cytotoxicity were tested. Atoxyl, arsacetin and arsenophenylglycine (Figure I-2), all arsenic compounds, were the first hugely successful compounds used to treat sleeping sickness protozoa. These compounds were also found to be active against *Spirochaeta pallidum*, the organism that causes syphilis. In particular, Ehrlich observed that the compound arsephanamine was able to cure the blood infection spirillosis and relapsing fever in chickens as well as to heal rabbits infected with syphilis. The compound was given the name Salvarsan, which derives from the Latin word *salvus*, meaning alive and well.[7, 9, 11-14]

Despite the long history of salvarsan, its structure has been a source of much controversy. Ehrlich believed that the molecule was a dimer joined by a double As=As bond.[5] In the early 1980's, the structure was proposed to be a linear polymer.[5] Finally, in 2005, there was sufficient evidence to conclude that there is no simple structure to describe Salvarsan. In reality, the active compound is a mixture of cyclic structures, predominantly three and five membered rings, with significant presence of four, six or even larger As rings (Figure I-3).[15]

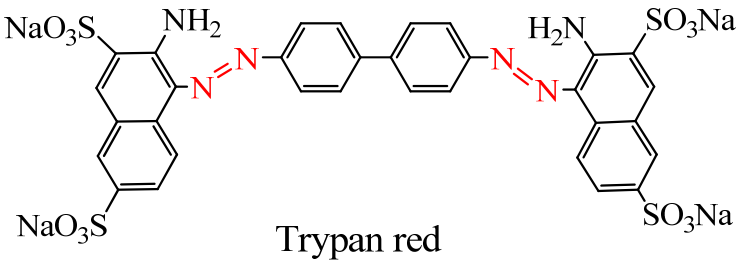

Trypan red

Figure I-1. Schematic representation of the structure of trypan red.

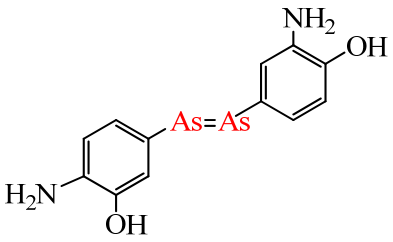

Ehrlich's Salvarsan

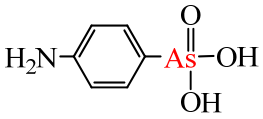

Atoxyl

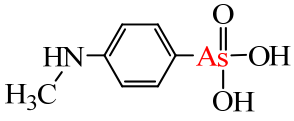

Arsacetin

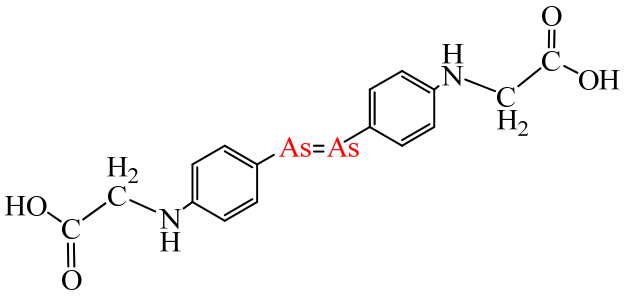

Arsenophenylglycine

Figure I-2. Schematic representations of arsenic base drugs used to treat sleeping sickness.

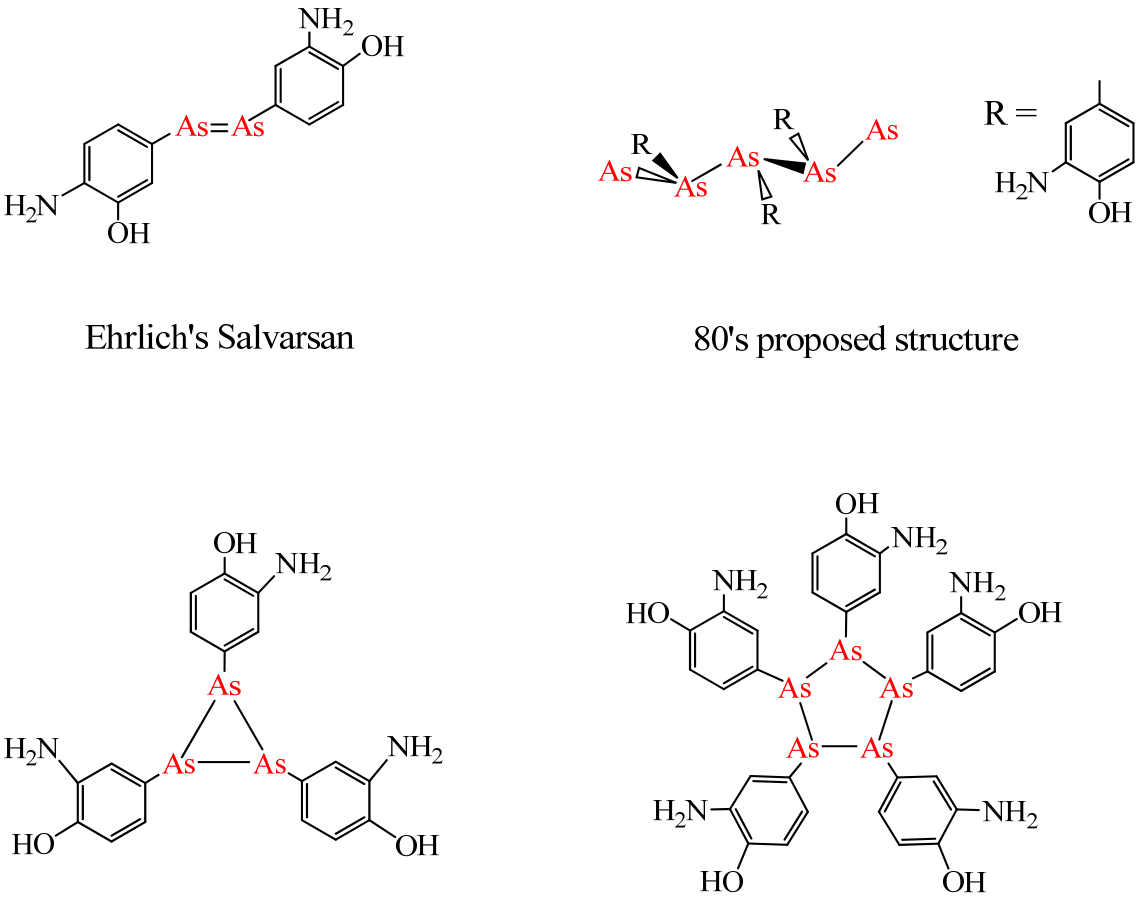

Figure I-3. Schematic representations of Salvarsan's proposed structures.

As the understanding of inorganic compounds in biological environments is expanding, the clinical use of inorganic compounds with medicinal applications is also being introduced, although very slowly, by pharmaceutical companies. Still, sometimes the fact that an inorganic compound is used as a main ingredient or active ingredient is concealed. The reluctance of using inorganic based drugs is mainly due to the lack of information about the fate and behavior of inorganic compounds *in vivo*.[2, 3] There is a general belief that all inorganic compounds are highly toxic.[2] The dictionary defines toxicity as containing or being a poisonous material especially when capable of causing death or serious debilitation.[16] In a scientific context, however, toxicity is a relative term. Any compound, regardless of its origin, organic or inorganic, synthetic or natural, has an inherent toxicity that depends on its concentration.[2, 17] The physiological effect of a compound varies non-monotonically with its concentration, as first noted and formalized by the French nutritionist Gabriel Bertrand in 1912.[18] A general Bertrand diagram is shown in Figure I-4, where the parameters of the function are specific to particular compounds or elements.[17]

One of the advantages of inorganic compounds is that their optimum physiological response profile can be varied depending on the type of metal ion, oxidation state and the ligands surrounding the metal ion or ions. Ligand modification plays an important role since they can help in the refinement of the biological properties of the metal complex, its delivery and absorption. Currently there are numerous inorganic compounds that are used as medicinal agents for the management and diagnosis of numerous diseases and dysfunctions,[2, 3, 19-21] and as main ingredients in every day cosmetics and toiletries.[2, 5] Excellent examples of the former type are lithium carbonate for the treatment of depression;[22-24] and barium sulfate ($BaSO_4$) as a radiocontrast agent for gastrointestinal X-ray imaging.[3, 25] In the field of

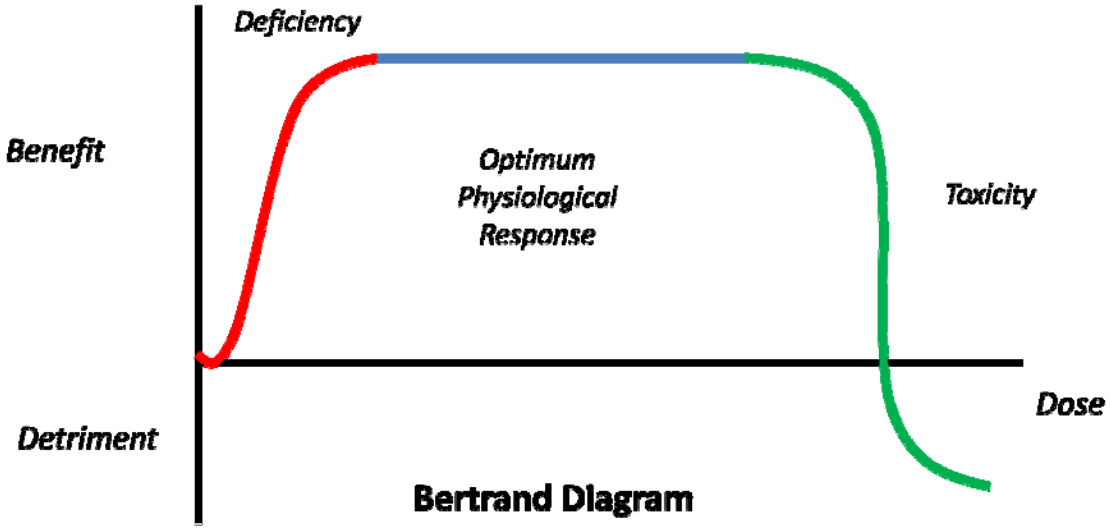

Figure I-4. Bertrand diagram illustrating the relationship between benefit and detriment from an element and its concentration.[2]

radiopharmaceutical diagnostics, *α*-emitting radiopharmaceuticals based on ^{99m}Tc are widely employed.[5, 26] Additionally, drugs containing gold, such as K[Au(CN)$_2$], are used to treat tuberculosis.[27] There are also many diseases in which the only line of defense is an inorganic-based drug, such as in the case of various tropical maladies that are only treated with arsenic and tin complexes.[8, 28] In this vein, arsenic trioxide (Trisenox®) was recently approved by the FDA as the only treatment for acute promyelocytic leukemia (APL).[14, 28, 29]

Finally, compounds of aluminum and bismuth are also employed in antacids, whereas fluorine, zinc, strontium and tin are typical ingredients in toothpaste.[3] A great variety of antiperspirants contain aluminum and zirconium as ingredients in their formulations.[5] Magnesium, selenium and zinc are also common ingredients in antiseborrheic products.[5] Zinc is also employ in healing ointments (Zincofax®), and tin is used in formulations for the treatment of boils and acne (Stanoxyl®).[3, 5, 19]

Cisplatin

A Serendipitous Beginning

Cis-diamminodichloro platinum (II), cisplatin, the most successful inorganic drug in history, was first synthesized and characterized by Peyrone in 1845. Later on, in 1983, Alfred Werner deduced its structure and separated it from its *trans* isomer. During the mid-1960s, the biological activity of cisplatin was accidentally discovered by Bernard Rosenberg and Loretta van Camp.[30] Initially, Rosenberg wanted to study how cell mitosis was affected by electromagnetic radiation of a resonant frequency. In order to test their initial set up, *Escherichia coli* bacterial cells were used instead of mammalian cells, which are more difficult to handle. The experimental design included a pair of platinum electrodes; which were chosen due to the fact that platinum is normally a chemically "inert" metal, and in this way Rosenberg wished to avoid any side chemical reaction on the electrodes. The results revealed that the bacterial cells formed rod-like filaments (Figure I-5), a characteristic of bacteria that are not able to divide (DNA inhibition but not protein synthesis). Numerous control experiments supported the conclusion that the source of the halted cell division of the bacteria was caused by $Pt(NH_4)_2Cl_2$, a compound generated by an electrochemical reaction between the cell culture media and the platinum electrode.[30]

After the identity of the active compound was determined, several other platinum derivatives were tested along with other transition metal compounds including platinum group metals and non-platinum group metals such as cobalt (Co), iridium (Ir), nickel (Ni), osmium (Os), palladium (Pd), rhodium (Rh), and ruthenium (Ru). The complexes tested were divided in three groups, depending on their effects on bacterial growth (Table I-1). The first group included compounds that were able to cause elongation of the

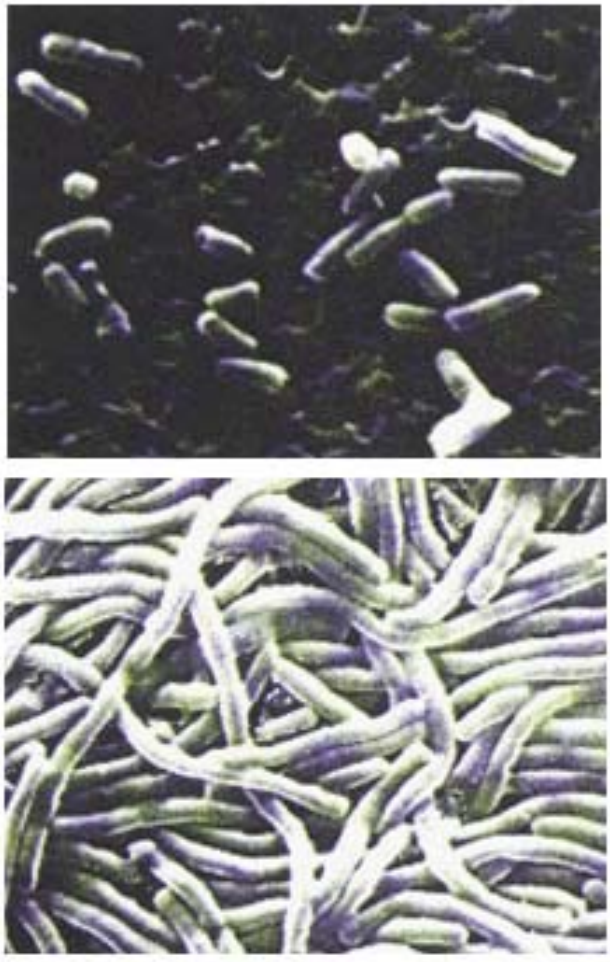

Figure I-5. Scanning electron photography of *E. coli.* Top picture: normal *E. coli* (Gram-negative rods). Bottom picture: *E. coli* grown in a medium containing a low concentration of *cisplatin.*[30]

bacterial cells. The second, compounds with no effect and the final class were toxic to the cells. Interestingly, these studies revealed that rhodium compounds were nearly as effective as the platinum compounds being analyzed.[1]

Table I-1. Effects of transition metal compounds on bacterial growth.

Caused elongation	Caused no change	Caused bacterial death
$K_2[PtCl_6]$	$[Co(NH_3)_6]Cl_2$	$CoCl_2$
$(NH_4)_2[PtCl_6]$	$K_2Ir(NO_2)_6$	$(NH_4)_2IrCl_6$
$H_2[PtCl_6]$	$[Ni(NH_3)_6]Cl_2$	$NiCl_2$
$(NH_4)_2PtBr_6$	*Cis*-$[Rh(en)_2Cl_2]NO_3$	$(NH_4)_2OsCl_6$
$(NH_4)_2PtI_6$	*Trans*-$[Rh(en)_2Cl_2]NO_3$	$(NH_4)_2PdCl_4$
$[Pt(en)_3]Cl_4$		$[Rh(NH_3)_5Cl]Cl_2$
$RhCl_3$		$PdCl_2$
$(NH_4)_3RhCl_6$		
$[Ru(NH_3)_4ClOH]Cl$		

After these unprecedented results, the *in vitro* activity against two murine cancer lines, namely Sarcoma 180 and Leukemia L1210, of four platinum complexes, *cis*-$Pt^{IV}(NH_3)_2Cl_4$, *cis*-$Pt^{II}(NH_3)_2Cl_2$, $Pt^{II}(NH_2CH_2CH_2NH_2)Cl_2$, and $Pt^{IV}(NH_2CH_2CH_2NH_2)Cl_4$, was investigated in mice. The c*is*-$Pt^{II}(NH_3)_2Cl_2$ complex proved to be the most successful at reducing the size of the tumor and curing the mouse completely.[1] These results prompted clinical studies that wound up with FDA (Food and Drug Administration) approval of the first platinum anti-tumor agent, cisplatin (Platinol®, Bristol-Myers Squibb) in 1979. Since that time, cisplatin has been shown to have a 90% success rate to treat testicular cancer and it is used in

the treatment of ovarian, cervical, bladder, head and neck, esophageal and small cell lung cancer.[19, 31, 32]

Despite the success of cisplatin in the treatment of cancer, its use is still problematic due to its toxicity and side effects such as nephrotoxicity, ototoxicity, neurotoxicity and emesis (vomiting).[31-33] Another problem associated with the use of cisplatin is that certain tumors that are initially sensitive to the treatment become resistant.[32, 33] Carboplatin,[34] Oxaliplatin[35, 36] and Nedaplatin[37-39] belong to the second generation of cisplatin derivatives that are currently in use (Table I-2, Figure I-6).[21, 32, 34-40] Carboplatin (Paraplatin®, Bristol-Myers Squibb) was approved in 1989 by the FDA,[21, 34, 40] while Oxaliplatin (Eloxatin®, Sanofi-Synthelabo) was first approved by the European Agency for the evaluation of Medicinal Products (EMEA) in 1986; however, it was not until 2002 that the FDA granted its approval in the United States.[21, 35, 36, 40] Nedaplatin (Aqupla®, Shionogi & Co) is another derivative that has been used in Japan since 1995 to treat ovarian and cervical cancer, but it is still undergoing clinical trials in the United States.[21, 37-40] Other derivatives in clinical trials are Lobaplatin and Heptaplatin (Figure I-6), both of which are commercially available in China and South Korea respectively. Both compounds are more soluble than cisplatin and have shown better activity against human lung, gastric, testicular, and ovarian cancer xenografts.[40]

Table I-2. Spectrum of activity and side effects of commercially available platinum-based drugs.

Compound	Spectrum of Activity	Side Effects
Cisplatin	lung, ovarian, and germ cell tumors	Damage to the nerves and to the kidneys
Carboplatin	ovarian and lung cancers	Cumulative dose-related toxicity resulting in slow bone marrow recovery
Oxaliplatin	colorectal cancer	Peripheral nerve damage

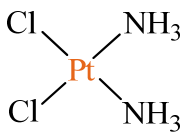

Cisplatin

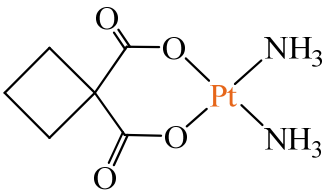

Carboplatin

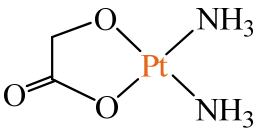

Nedaplatin

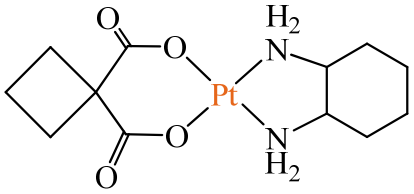

Oxaliplatin

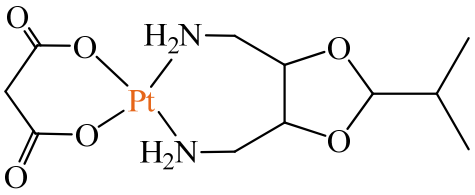

Heptaplatin

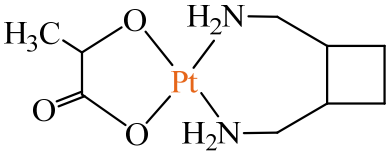

Lobaplatin

Figure I-6. Schematic representation of platinum based drugs commercially available.

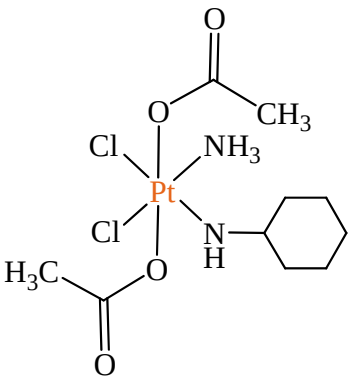

Satraplatin
JM216

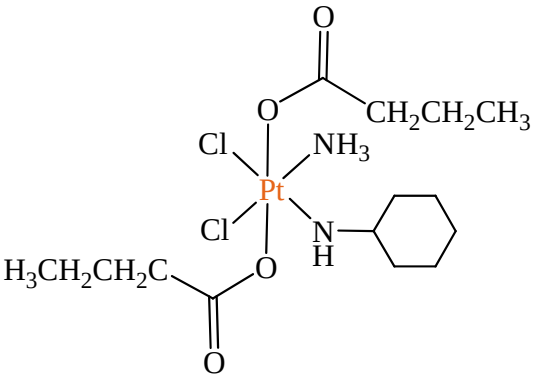

JM221

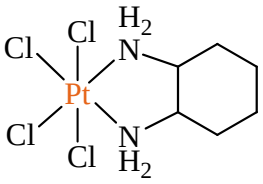

Tetraplatin
Ormaplatin

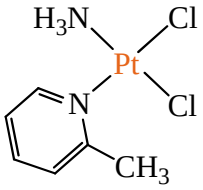

Picoplatin
JM473

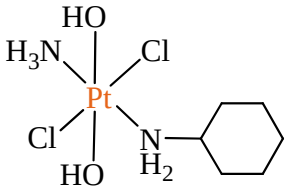

JM335

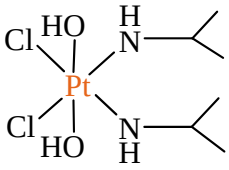

Iproplatin

Figure I-7. Schematic representation of platinum compounds currently undergoing clinical trials.

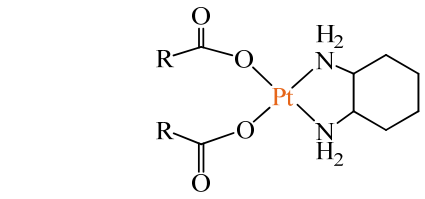

Miriplatin R = $C_{13}H_{27}$
Aroplatin R = C_9H_{19}

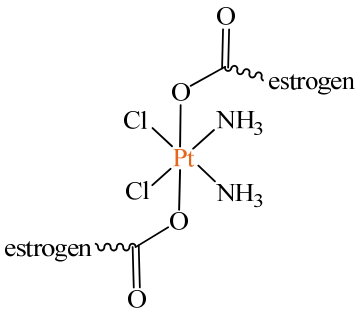

Pt (IV)-estrogen carboxylate

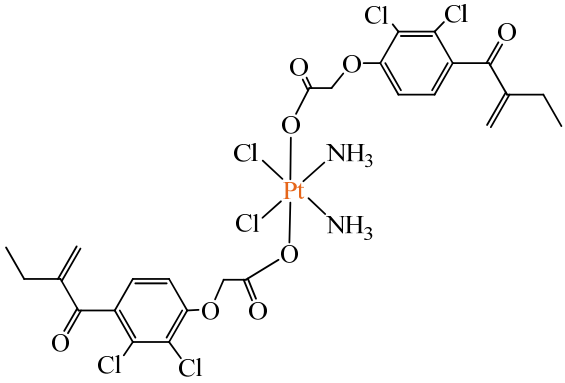

Ethacraplatin

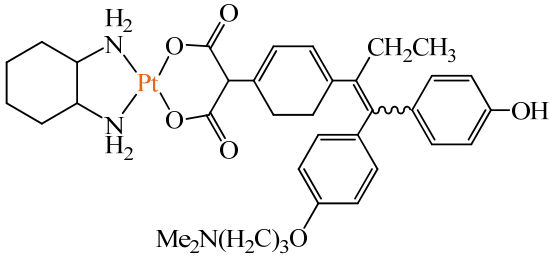

Pt (II) tamoxifen

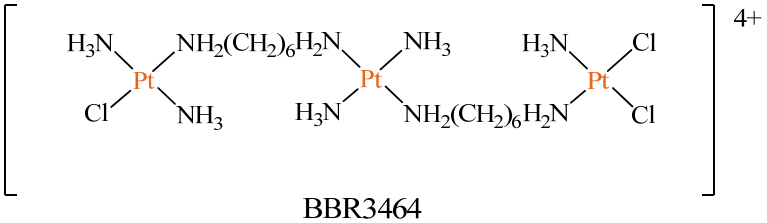

BBR3464

Figure I-8. Platinum compounds that differ from the classical cisplatin model.

After many years of research, it is evident that, in order to overcome the side effects and to circumvent the intrinsic and acquired resistance associated with the use of these platinum-based drugs, new compounds, that are structurally different (non-classical platinum derivatives) from the lead compound cisplatin, should be studied. Several platinum derivatives both mononuclear and polynuclear, compounds with oxidation states of IV and even with *trans*- geometries have been investigated and found to be active; several of these compounds are undergoing clinical trials at the present time (Figures I-7 and I-8).[21, 33, 40-42] These compounds have been shown to hold certain advantages over the classical platinum derivatives currently used, such as increased activity (Picoplatin-JM473), improved water solubility (Iroplatin, Satraplatin-JM216), and activity against cisplatin-resistant tumors (Ormaplatin, *trans*-platinum derivatives) (Figure I-7).[21, 40]

Compounds from the main group metals such as gallium,[43-47] germanium,[46, 48] tin[49, 50] and bismuth[46, 51] are also being investigated. Vanadium, titanium, niobium, molybdenum, rhenium, ruthenium, rhodium, iridium, copper and gold are among the transition metals whose complexes have been studied and found to be active (Figure I-9).[3, 6, 20, 40, 41, 46, 52-58] The most exciting results are observed with ruthenium derivatives such as NAMI-A (imidazolium [*trans*-tetrachloro(dimethylsulfoxide)-imidazoleruthenate(III)]) and KP1019 (indazolium [*trans*tetrachlorobis) 1H-indazole)ruthenate(III)] that are currently undergoing clinical trials.[59] Despite their structural similarities (Figure I-9) and the fact that both can target DNA, these two compounds seem to have a different biological activity. NAMI-A has a low impact on primary tumors, but it inhibits their growth and reduces their ability to metastasize.[6, 21, 58, 60, 61] The compound KP1019, with a lower cytotoxicity than cisplatin, is active against primary tumors, especially colorectal cancer.[21, 40, 41]

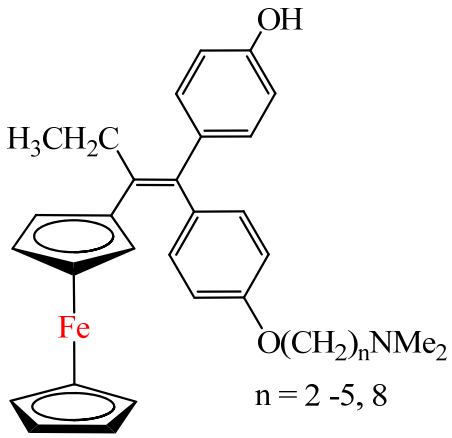

Ferrocifenes

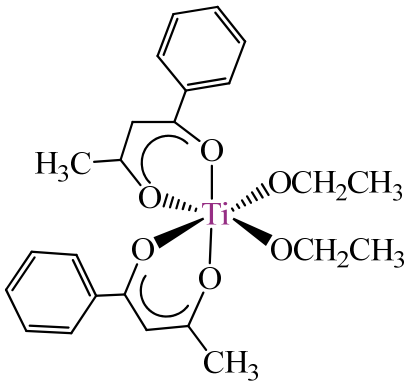

Budotitanium

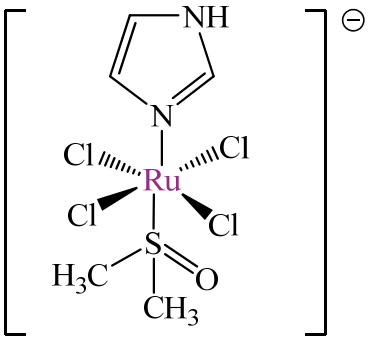

NAMI-A

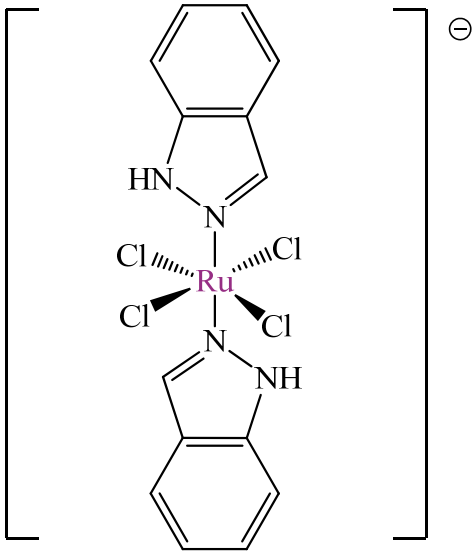

KP1019

Figure I-9. Schematic representation of inorganic complexes that exhibit anticancer activity.

Mechanism of Action of Cisplatin

What Is Known to Date

Almost 40 years have passed since the introduction of cisplatin to the chemotherapeutic drug market. Despite its great success in the treatment of a variety of cancers that include testicular, ovarian, bladder, cervical, head and neck, oesophageal and small cell lung cancer, the mechanism of action is still under investigation.[31-33, 42] Studies have showed that, depending on the type of cancer cells and maturity of the tumor, cisplatin can cause necrosis or apoptosis.[62] Of general consensus is the fact that cisplatin and other platinum based drugs form cross-links with DNA, and in this way interfere with the mechanisms of DNA replication and transcription, which in turn, leads to cell death.[31, 33, 41]

The detailed nature of the mechanism is not completely known in part due to the lack of methodologies and also because the biochemical behavior of inorganic compounds is extremely complicated. The active form of the compound may differ greatly from the original compound. The rich chemistry of the cellular media can change the oxidation state and ligand substitutions can occur. In addition, many cancer cells can become resistant to the drug.[42]

Upon administration of an intravenous saline solution, cisplatin is initially distributed to all tissues and accumulates especially in the kidneys, liver, muscle and skin. Approximately 90 % of the total cisplatin is deactivated in the blood stream due to reactions with the sulfur rich plasma proteins.[31, 63, 64] Cisplatin is able to transverse the cell membrane, either as a neutral specie or as a cation, through multiple pathways including passive diffusion[42] and active transporters such as copper homeostasis proteins (CTR1)[65, 66] and organic cation transporters (OCT) (Figure I-10).[33, 42, 63-66] During passive diffusion some cisplatin is deactivated due to coordination

with constituents of the lipid bilayer, in particular with nitrogen, sulfur and phosphorous atoms present in glycoproteins, phospholipids and phosphatidylserine, decreasing its uptake and causing changes in the membrane protein that eventually lead to cell damage and increased side effects.[33, 63]

Once inside the cell, the lower concentration of chloride ions in the cytosol promotes hydrolysis of cisplatin (activated cisplatin) allowing the formation of highly reactive aquo species. Activated cisplatin can effectively react with nuclear DNA, but it can also react with important cellular components such as peptides, proteins, cytoskeletal microfilaments and RNA. Reactions with proteins occur through the nitrogen atoms of histidine residues and sulfur atoms of cysteine and methionine residues. RNA coordinates to cisplatin mainly through its phosphorous atoms. Two important components of the cellular milieu that bind preferentially to cisplatin are metallothionein (MT) and glutathione (GSH). These molecules are responsible for the efflux of cisplatin, and are found in increased levels in several cancer cell lines resistant to cisplatin.[33, 63] It is important to note that the binding of cisplatin to the sulfur atoms of MT and GSH is under kinetic and not under a thermodynamic control. Because of this, the migration of platinum from sulfur donor ligands to DNA bases is possible, the result of which is that MT and GSH act as platinum reservoirs.[33]

After reaching the nucleus, cisplatin binds to DNA and forms several types of adducts. The main products are 1,2-GpG intrastrand (~65%), 1,2-ApG intrastrand (~25%), and 1,3-GpXpG (~5%). There is also a small, but important, percentage of monofunctional adducts and ternary complexes between DNA, platinum and protein that have been indicated to cause damage to the cell (Figure I-11).[33, 63, 64]

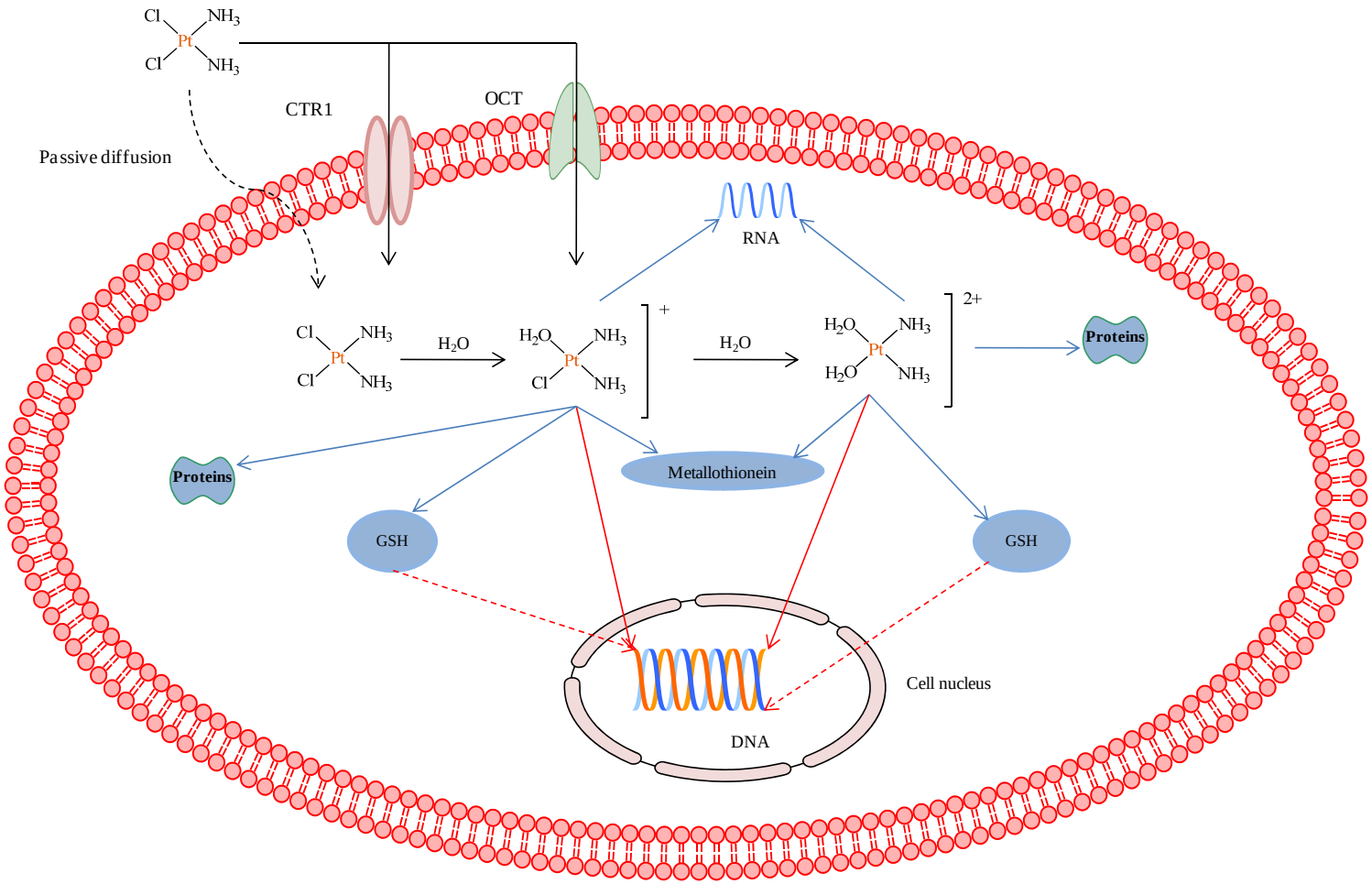

Figure I-10. Scheme that depicts the proposed mechanism of cisplatin action.

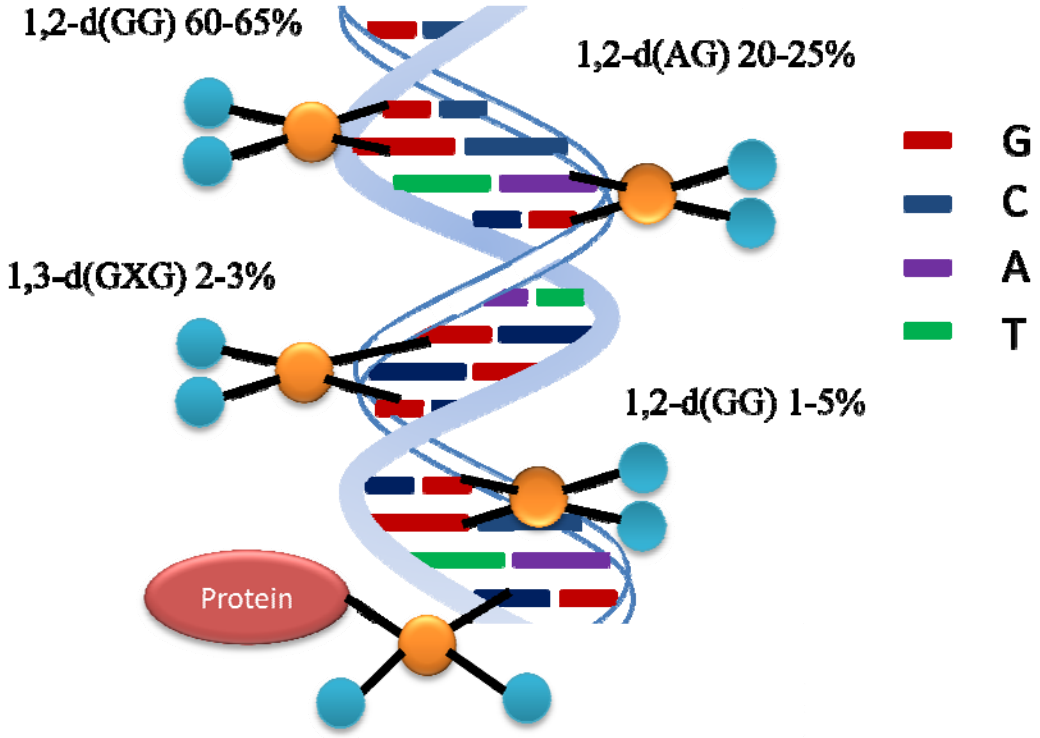

Figure I-11. Adducts formed after binding of cisplatin to DNA.

Medicinal Applications of Dirhodium Compounds

Dirhodium tetraacetate was first synthesized in 1963, but it was not until 1970 that the structure was definitively characterized by X-ray crystallography.[67] The complex $Rh_2(\mu\text{-}O_2CCH_3)_4$ and its derivatives exhibit a paddlewheel structure in which four bridging ligands span the equatorial positions of the two rhodium atoms and the axial positions are often occupy by solvent molecules (Figure I-12).[67, 68] A distinctive characteristic of these compounds is the sensitivity of their electronic spectral properties in the visible region (*i.e.*, colors) due to the nucleophilic nature of the axial ligand. This sensitivity is due to the influence on the energy of the LUMO (σ^*) orbital. Oxygen donors produce blue or green adducts, nitrogen donors generate red or violet, whereas sulfur and phosphorous donors deliver burgundy and orange adducts, respectively. The length of the Rh – Rh single bond, 2.35 – 2.45 Å, is not particularly sensitive to the nature of the σ-donor axial ligands.[67]

Despite the fact that these compounds, with their lantern-type structures and high molecular weights, defy the most traditional considerations of medicinal chemistry, they have shown that they not only exhibit activity against various cancer lines, but in many cases they have proven to be less toxic than cisplatin.

The first dirhodium complexes to be studied are the carboxylate derivatives of general formula $Rh_2(\mu\text{-}O_2CR)_4$ (R= CH_3, C_2H_5, C_3H_7).[69, 70] These dirhodium carboxylate compounds showed activity against Ehrlich ascites tumor,[69, 71, 72] Leukemia L1210,[73] and sarcoma 180 cell lines.[69, 71] It was observed that the activity in the series increases as the hydrophobicity of the R group increases. The results also showed that further lengthening of the carboxylate group beyond the pentanoate group was detrimental to the

efficacy of the complexes, a finding that highlights the importance of the delicate balance between hydrophobicity and activity.[72]

Further studies revealed that the substitution of the acetate bridging groups with ligands possessing more electron withdrawing groups renders compounds with better activity. The trifluoroacetate derivative increases the survival rate of mice bearing Ehrlich ascites tumor[74] while the trifluoroacetamide derivative not only increases the survival rate of the mice population on 90 % but also has LD_{50} values of the same order as that of cisplatin *in vitro*.[75, 76] Conversely, substitution of the four carboxylate ligands with the formamidinate ligands DTolF (DTolF= $(p\text{-}CH_3C_6H_4N)_2CH^-$) did not result in any biological activity. It is worth mentioning, that later studies on the heteroleptic compound $Rh_2(\mu\text{-}O_2CCF_3)_2(DTolF)_2$ showed that this compound has an antitumor activity comparable to that of cispaltin against Yoshida ascites and T8 sarcomas with considerably reduced toxicity.[77]

During the early 1980's, the cationic $Rh_2(\mu\text{-}O_2CCH_3)_2(diimine)_2$ complexes, (where diimine = 2,2′-bipyridine (bpy) and 1,10-phenantroline (phen)) were developed and quickly tested for anticancer activity.[78] These molecules were shown to be more effective than the neutral parent compound, being active against human oral carcinoma KB cell lines.[79] Additionally, these compounds were also observed to have antibacterial activity.[78-80]

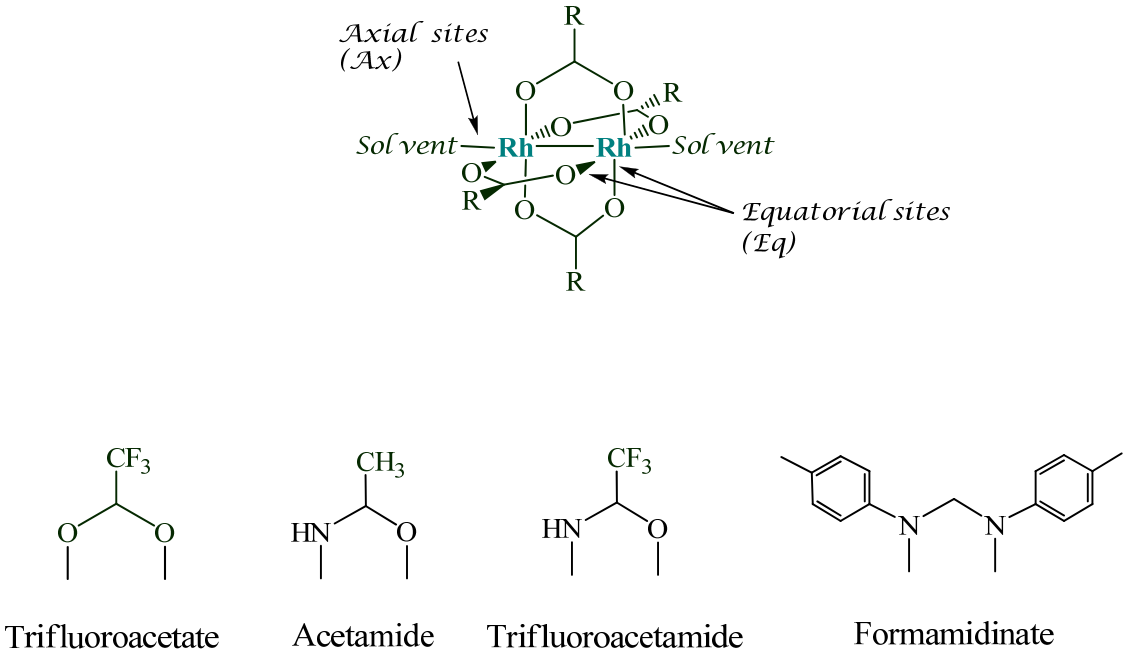

Figure I-12. Schematic representation of dirhodium tetracarboxylate (Top). Bridging ligands of compounds studied as anticancer agents (Bottom).

Interaction of Dirhodium Complexes and Nucleobases, Dinucleosides and Dinucleotides

Model systems of nucleic acid binding to metal complexes have proven to be invaluable tools as they provide excellent illustrations of the diverse nucleobase chemistry of these compounds. In the case of dirhodium compounds, adenine and guanine binding has been found to occur either through the axial position or in a bridging fashion through the equatorial sites.[69, 71, 81-86]

$Rh_2(\mu\text{-}O_2CCH_3)_4$ binds to 1-methyladenosine, a model of adenosine, through the axial position.[83] This is possible due to the existence of hydrogen-bonding interactions between the exocyclic amine group and an oxygen atom from the carboxylato bridge as observed in a crystallographic study of the bis(1-methyladenosine) adduct of $Rh_2(\mu\text{-}O_2CCH_3)_4$ (Figure I-13).[83, 84] In the case of guanosine/guanine, the use of model compounds failed to produce axial adducts with $Rh_2(\mu\text{-}O_2CCH_3)_4$. It was hypothesized that this was a result of repulsive interactions between the O6 of the purine and the carboxylate oxygen atoms.[84, 87] On the other hand, when $Rh_2(\mu\text{-}HNOCCF_3)_2(\mu\text{-}O_2CCH_3)_2$ was reacted with 9-ethylguanine, Aoki was able to observe an axial adduct (Figure I-14). This was possible since in this case, the guanine O6 can form a hydrogen bond with the trifluoroacetamido bridge.[88]

Reactions of $Rh_2(\mu\text{-}O_2CCH_3)_4$ with 9-ethylguanine produce a dimetal complex with the two rhodium atoms bridged via N7/O6 of the nucleobase derivative (Figure I-15).[87] A similar product has been observed when $Rh_2(\mu\text{-}O_2CCF_3)_4$ reacts with two equivalents of 9-ethylguanine.[87]

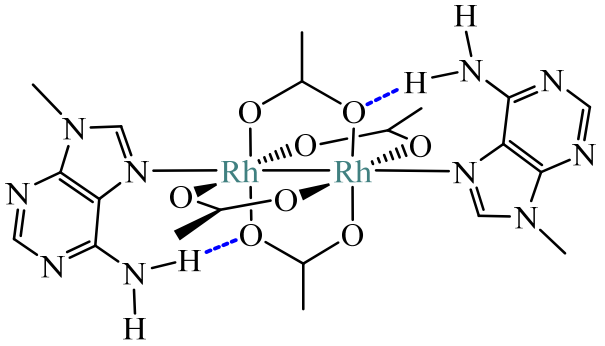

Figure I-13. Schematic representation of the adduct formed between $Rh_2(\mu\text{-}O_2CCH_3)_4$ and 1-methyladenosine.

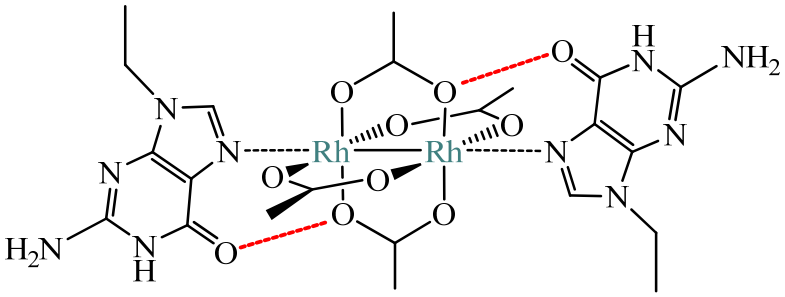

Figure I-14. Schematic representation of the repulsive interaction (shown in red) between $Rh_2(\mu\text{-}O_2CCH_3)_4$ and the O6 of 9-ethylguanine.

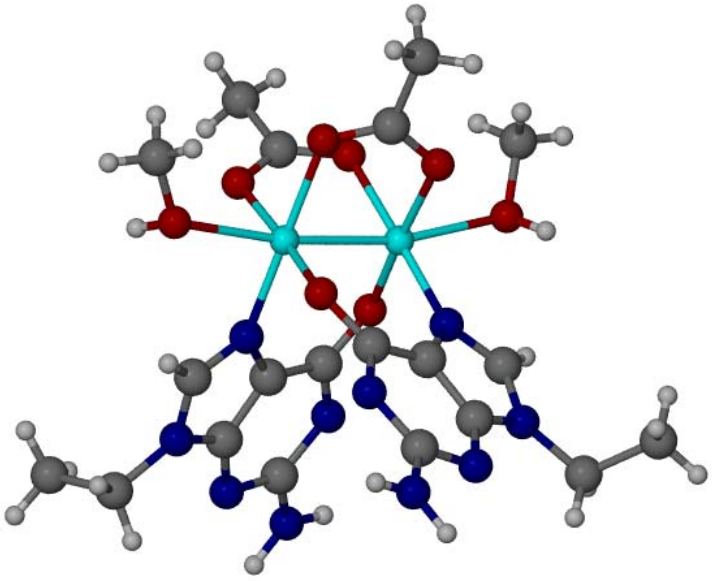

(a)

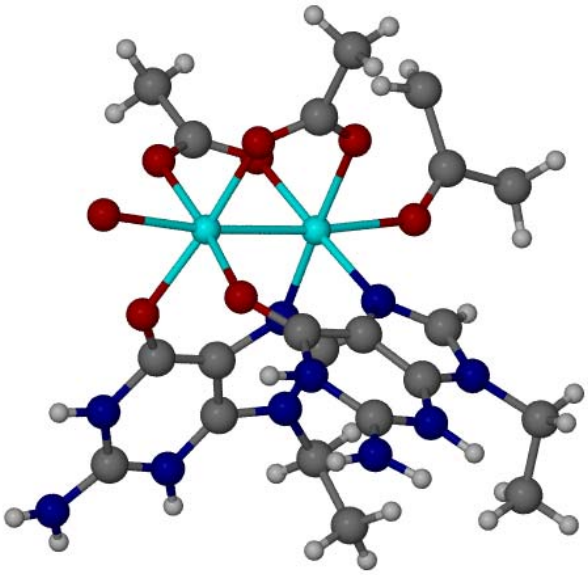

(b)

Figure I-15. Molecular structure of (a) H-T *cis*-[$Rh_2(\mu\text{-}O_2CCH_3)_2(9\text{-EtGua})_2(CH_3OH)_2$] and (b) H-H *cis*-[$Rh_2(\mu\text{-}O_2CCH_3)_2(9\text{-EtGua})_2((CH_3)_2CO)(H_2O)]^{2+}$.

Adenine can also bind equatorially to the dirhodium unit. Reactions of $[Rh_2(DTolF)_2(CH_3CN)_6](BF_4)_2$ with two equivalents of 9-EtAdeH afford *cis*-$[Rh_2(DTolF)_2(9\text{-}EtAdeH)_2(CH_3CN)](BF_4)_2$ with the 9-EtAdeH molecules bridging at *eq* sites via N7/N6 (Figure I-16).[89, 90] ^{1}H-NMR studies indicate that in *cis*-$[Rh_2(DTolF)_2(9\text{-}EtAdeH)_2(CH_3CN)](BF_4)_2$, 9-EtAdeH is stabilized in its less common imino form.[89] If this adduct is also form *in vivo*, it will alter the hydrogen bonding scheme of the nucleobase resulting in its mispairing and the appearance of cell mutations that could be deleterious to cells (Figure I-17).[91]

The reactions of $Rh_2(\mu\text{-}O_2CCH_3)_4$ and $[Rh_2(DTolF)_2(CH_3CN)_6](BF_4)_2$ with the dinucleotides d(GpG) and d(pGpG) have been studied in the Dunbar group and they have revealed that the bridging binding mode of guanine is also possible when the two guanine bases are joined by a phosphodiester bond.[92-94] These adducts are very similar to those formed by cisplatin. Even more important is the fact that the aforementioned results provide evidence that these adducts might also exist *in vivo*.[92, 93]

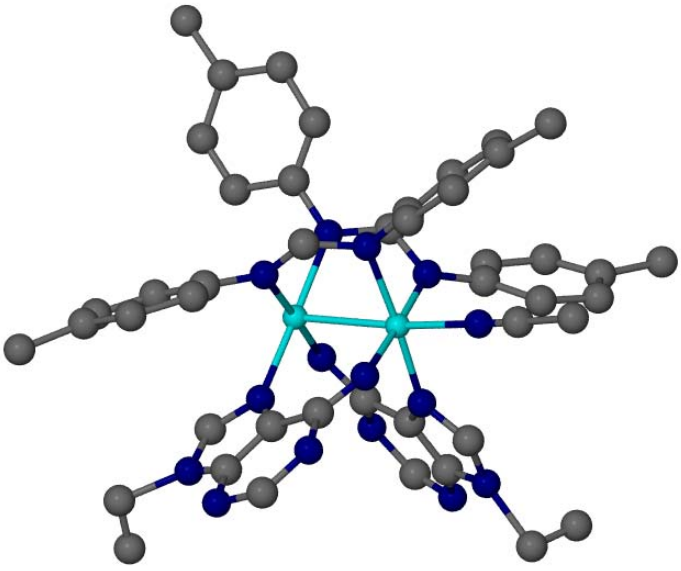

Figure I-16. Molecular structure of H-T *cis*-$[Rh_2(DTolF)_2(9\text{-}EtAdeH)_2(CH_3CN)]^{2+}$.

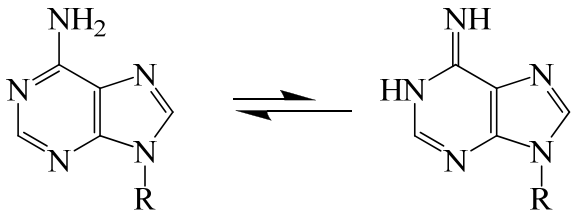

Amino form Imino form

Figure I-17. Amino and imino structures in adenine.

Dirhodium Complexes and Their Interactions with Double-stranded DNA

Reactions of $Rh_2(\mu\text{-}O_2CCH_3)_4$, $[Rh_2(\mu\text{-}O_2CCH_3)_2(CH_3CN)_6]^{2+}$, and $Rh_2(\mu\text{-}O_2CCF_3)_4$ with single-stranded oligonucleotide tetramers, octamers, and dodecamers have also been studied.[95] Due to the complexity of these reactions, matrix-assisted laser desorption ionization (MALDI) and nanoelectrospray ionization (nanoESI) coupled to time-of-flight mass spectrometry (TOF MS) were used to elucidate the products formed. The sequences were designed to contain AA, GG, GA, and AG dipurine sites to gain information on the site preference of these dirhodium complexes. The study established that both GG, as well as AA sites are the targeted residues in these oligomers. It also revealed that the the dirhodium bis-acetate oligonucleotide adducts are the main products of the reactions.[95] From these studies, a relative order of reactivity of the dirhodium complexes studied as well as cisplatin and *cis*-$[Pt(NH_3)_2(OH_2)_2]^{2+}$ (activated cisplatin) was established: *cis*-$[Pt(NH_3)_2(OH_2)_2]^{2+}$ ~ $Rh_2(\mu\text{-}O_2CCF_3)_4$ > *cis*-$[Pt(NH_3)_2Cl_2]$ (cisplatin) >> $[Rh_2(\mu\text{-}O_2CCH_3)_2(CH_3CN)_6]^{2+}$ > $Rh_2(\mu\text{-}O_2CCH_3)_4$.[96] This order of reactivity correlates with the known relative lability of the leaving group(s) for each complex.

Collaborative work in the Dunbar and Dunham laboratories has established that dirhodium tetraacetate, and its derivatives are capable of forming DNA interstrand crosslinks (Figure I-18). The study investigated the interactions of dsDNA with the dirhodium carboxylate compounds $Rh_2(\mu\text{-}O_2CCH_3)_4$**,** $Rh_2(\mu\text{-}O_2CCF_3)_4$, and $[Rh_2(\mu\text{-}O_2CCH_3)_2(CH_3CN)_6]^{2+}$ (Figure I-18). Besides the DNA interstrand crosslinks, other adducts were also observed Monofunctional and intrastrand adducts are also formed during the reaction.[97]

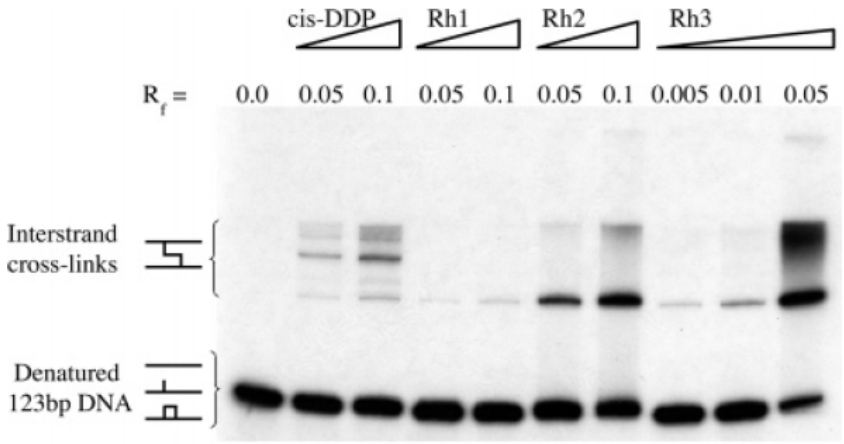

Figure I-18. Denaturating PAGE (5%) of reactions between cisplatin (cis-DDP), $Rh_2(\mu\text{-}O_2CCH_3)_4$ (Rh1), $[Rh_2(\mu\text{-}O_2CCH_3)_2(CH_3CN)_6]^{2+}$ (Rh2), and $Rh_2(\mu\text{-}O_2CCF_3)_4$ (Rh3) (taken from ref. 97).

Inhibition of Transcription by Dirhodium Complexes

Recently, it has been reported that several dirhodium compounds inhibit transcription, a process by which cells produce RNA from a DNA template by action of RNA polymerase.[98, 99] A collaborative effort between the Turro and Dunbar groups found that two dirhodium complexes, $Rh_2(\mu\text{-}O_2CCH_3)_4$ and *cis*-$[Rh_2(\mu\text{-}O_2CCH_3)_2(phen)_2]^{2+}$ (phen = 1,10-phenanthroline), were able to inhibit transcription *in vitro* (Figure I-19).[98] Interestingly, it was also observed that, unlike cisplatin, the mechanism of the inhibition of transcription by $Rh_2(\mu\text{-}O_2CCH_3)_4$ and *cis*-$[Rh_2(\mu\text{-}O_2CCH_3)_2(phen)_2]^{2+}$ involves the binding of the complexes to the enzyme T7-RNA polymerase (T7-RNAP).[98] Additional studies have shown that the mechanism of inhibition depends on the coordination sphere of the dirhodium core. For example, $Rh_2(\mu\text{-}O_2CCF_3)_4$, $Rh_2(\mu\text{-}HNOCCF_3)_4$, and *cis*-$[Rh_2(\mu\text{-}O_2CCH_3)_2(CH_3CN)_6]^{2+}$ inhibit T7-RNAP in a manner similar to $Rh_2(\mu\text{-}O_2CCH_3)_4$ and *cis*-$[Rh_2(\mu\text{-}O_2CCH_3)_2(phen)_2]^{2+}$, whereas $Rh_2(\mu\text{-}HNOCCH_3)_4$ does not bind T7-RNAP.[99]

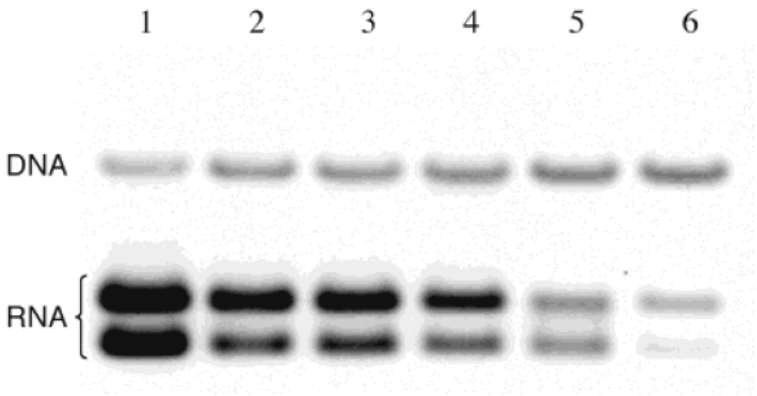

Figure I.19. Agarose gel of transcribed RNA in the presence of *cis*-[$Rh_2(\mu$-$O_2CCH_3)_2(phen)_2]^{2+}$at various complex/[template DNA base] ratios, *R*. Lanes 1-6, *R* = 0.0000, 0.0005, 0.0010, 0.0015, 0.0020, 0.0025 (taken from ref. 98).

Photodynamic Therapy

The observation of a transient species formed upon excitation of $Rh_2(\mu\text{-}O_2CCH_3)_4(L)_2$ (L = CH_3OH, tetrahydrofuran, PPh_3, pyridine) with a short laser pulse have resulted on a new research avenue for dirhodium complexes.[100] Turro et al. have investigated the photochemistry of dirhodium tetracetate and found that the transient species are long-lived. Although no emission from the transient complexes is observed, energy transfer from the excited state to the $^3\pi\text{–}\pi^*$ excited state of perylene is possible.[100] Further studies indicated that excitation of $Rh_2(\mu\text{-}O_2CCH_3)_4(H_2O)_2$ with visible light in the presence of an electron-acceptor produces the one-electron-oxidized complex, $[Rh_2(\mu\text{-}O_2CCH_3)_4(H_2O)_2]^+$, which efficiently cleaves dsDNA.[101]

Later generations have incorporated the electron acceptor in the first coordination sphere of the complex.[102-104] The Turro and Dunbar groups have reported that $[Rh_2(\mu\text{-}O_2CCH_3)_2(dppz)_2]^{2+}$ and $[Rh_2(\mu\text{-}O_2CCH_3)_3(dppz)(CH_3OH)]^+$, where dppz = dipyrido[3,2,2',3'-phenazine (dppz), have the ability to direct DNA photocleavage upon irradiation with visible light in the absence of a electron acceptor molecule.[102, 103] Furthermore, these compounds photocleave DNA non-stoichiometrically in the presence and absence of molecular oxygen. These results hint at the possibility of their use as agents for photodynamic therapy (PDT), in particular for the treatment of hypoxic cells. Hypoxic cells are difficult to treat by PDT due to the fact that most compounds investigated need the presence of O_2.[104]

Despite the short time since the discovery of the photocleavage properties of dirhodium complexes, great advances have been made towards the search of a compound with good PDT properties. For example, a requirement for compounds to be an adequate PDT agent is to have cytotoxicity to photocytotoxicity ratio large enough so the compound does not damage any tissues before activation. In this sense, ratios of about 1:5 are

considered good.[103, 104] Three compounds, $[Rh_2(\mu\text{-}O_2CCH_3)_2(dppz)_2]^{2+}$, $[Rh_2(\mu\text{-}O_2CCH_3)_3(dppz)(CH_3OH)]^{+}$ and $[Rh_2(\mu\text{-}O_2CCH_3)_2(dppz)(bpy)]^{2+}$, have cytotoxicity to photocytotoxicity ratios in that range and are attractive lead compounds for the development of a clinically attractive PDT agent (Table I-3).[102-104]

Table I-3. Comparison of cytotoxicity / photocytotoxicity ratios for leading rhodium compounds and hematoporphyrin.

Compound	LC_{50} μM	LC^*_{50} μM	Ratio LC_{50} / LC^*_{50}
Hematoporphyrin	21 ± 1	3.8 ± 0.2	5.6
$[Rh_2(\mu\text{-}O_2CCH_3)_2](dppz)_2]^{2+}$	135 ± 7.2	39 ± 1.3	3.5
$[Rh_2(\mu\text{-}O_2CCH_3)_2](bpy)(dppz)]^{2+}$	208 ± 10	44 ± 2	4.7
$[Rh_2(\mu\text{-}O_2CCF_3)_2](dppz)_2]^{2+}$	58 ± 2.9	27 ± 1.4	2.1

It is obvious from the research conducted to date, that dirhodium (II,II) complexes are a diverse and promising class of cytotoxic compounds. Since cellular organization is very complex, the number of biomolecules, other than DNA, that can act as possible targets is large. Among other biomolecules of high importance RNA, proteins and enzymes directly related to the cellular cycle, can be considered possible targets. In order to obtain compounds with improved activity, less toxic towards healthy cells and with enhanced cell penetrating ability, the interactions with DNA and other biomolecules need to be better understood.

My research along these years has focused on the study of several families of dirhodium compounds both in cell free medium and *in cellulo*. From the introductory remarks, it is clear that the interaction of dirhodium complexes with biologically relevant molecules, as well as *in cellulo* activity cannot be generalized since it greatly depends on the coordination sphere of the dirhodium core. Therefore, I have divided the dirhodium compounds in closely related families and studied their *in vitro* properties and *in cellulo* behavior. In chapter II, I have focused on the importance of the axial position by studying three dirhodium complexes that differ in their availability of the axial site. Chapter III uncovers a novel enzyme inhibition strategy through tuning of the electronic properties of the metal complex. In chapters IV and V, the influence of diimine ligands on the activity of dirhodium complexes is revealed. The results show that this influence covers target interaction as well as cellular localization of the compounds. Finally, in chapter VI, attempts to improve the internalization of dirhodium complexes are described.

CHAPTER II

ROLE OF THE AXIAL COORDINATION ON THE BIOLOGICAL ACTIVITY OF DIRHODIUM (II,II) COMPLEXES*

Introduction

Although the antitumor effect of dirhodium carboxylate and derivatives has been known since the early 1970's,[67, 68, 71, 105-107] the mechanism by which they exert their activity remains unknown.[105, 106] Metal-metal bonded dirhodium (II,II) complexes possess ten possible coordination sites, with eight of them being equatorial and two which are axial.[67] The large number of bonding sites leads to diverse chemistry that can be tuned by donor atoms in the two different types of positions, but they also result in complications for those who strive to unravel the chemistry behind the biological properties of these compounds. Until now, all of the structure activity relationship (SAR) studies have focused on the exchange of the equatorial ligands, with less interest in the role of the axial positions which are considered too weak to have an effect on the activity of dirhodium complexes. SAR studies have been performed with different carboxylate ligands such as propionate, butyrate, benzoate,[72] trichloroacetate,[108] trifluoroacetate,[74, 108] as well as many other diverse ligands such as formamidinates,[109] acetamidinates,[75, 76] cyclophosphamides[110] and chelating nitrogen ligands[78] (Figure II-1).

---

*Reprinted in part from "Effect of Axial Coordination on the Electronic Structure and Biological Activity of Dirhodium (II,II) Complexes" J. Dafhne Aguirre, Daniel A. Lutterman, Alfredo M. Angeles-Boza, Kim R. Dunbar, and Claudia Turro. *Inorg. Chem*. **2007**, *46* (18), 7494 – 7502. Copyright 2007, with permission from the American Chemical Society.

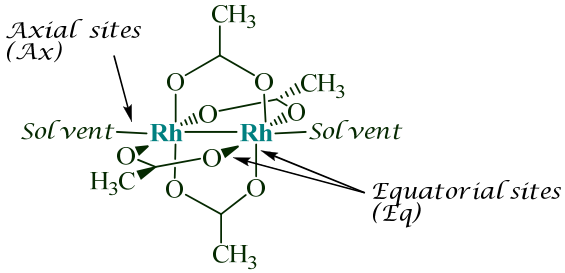

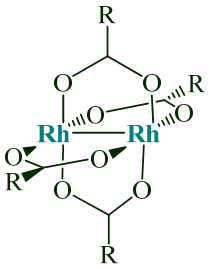

Carboxylates
R = Me, Et, Pr

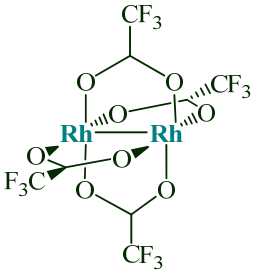

Trifluroacetates

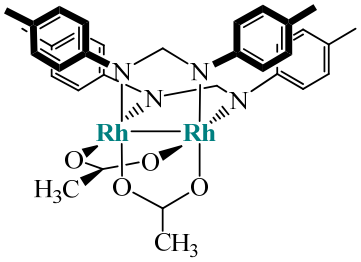

Formamidinates

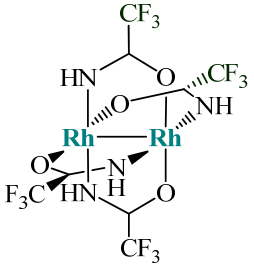

Acetamidates

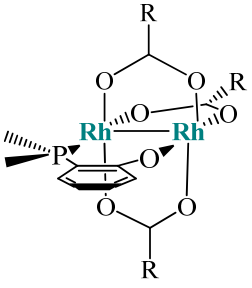

Carboxylates with phosphine ligands
R = Me, Et, Pr

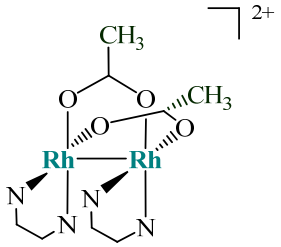

Carboxylates with chelating nitrogen ligands

Figure II-1. Dirhodium compounds that have been studied for their antitumor activity.

In terms of the axial position and what is known about its importance vis-à-vis anticancer properties, it was reported long ago that $Rh_2(\mu\text{-}O_2CCH_3)_4$ used in conjunction with arabinosylcytosine, a DNA polymerase inhibitor, was active against L1210 tumors.[111, 112] The proposed mechanism suggested that $Rh_2(\mu\text{-}O_2CCH_3)_4$ was able to inhibit the deammination of arabinosylcytosine by cytidine deaminase in cells, thereby increasing the efficacy of arabinosylcytosine.[112] The synergistic effect was achieved because of the ability of $Rh_2(\mu\text{-}O_2CCH_3)_4$ to bind near the active site of the cytidine deaminase through its axial positions.[111, 112]

Later studies revealed that dirhodium complexes bind to nucleobases,[83, 87, 89, 90, 113-115] dinucleotides,[92] and DNA dodecamer single strands,[95] through both axial and equatorial ligand substitution reactions. It is believed, however, that reactions of complexes for which equatorial substitution takes place proceed via an initial axial interaction which is followed by a rearrangement of the new axial ligand to an equatorial position (Figure II-2).[116-118] Given this situation, one might expect that the presence of strong, non-labile donor ligands in the axial position of a dirhodium(II,II) complex would lower the observed bioactivity through decreased interactions or binding of the compounds to biomolecules.

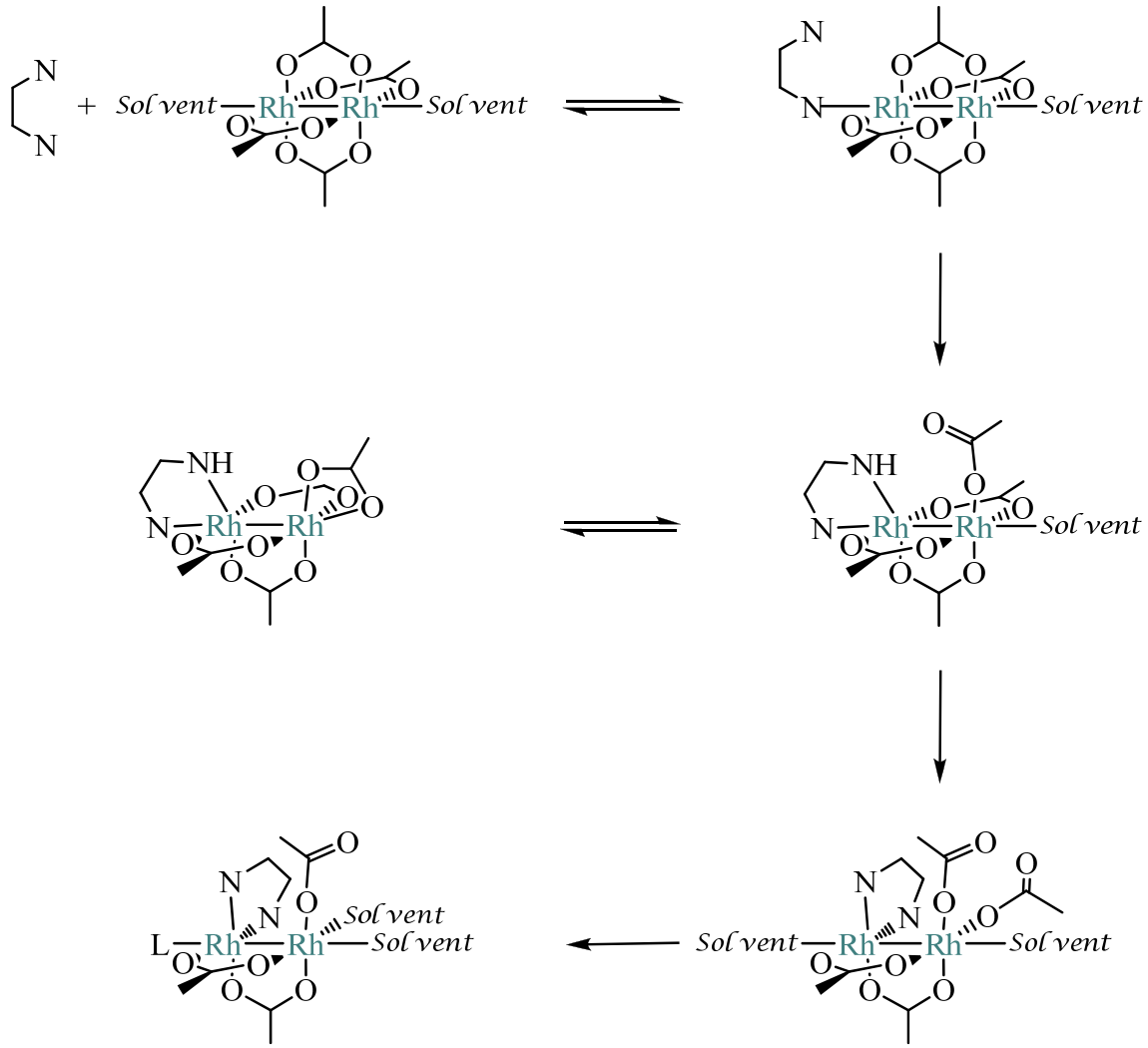

Figure II-2. Proposed mechanism for the reaction of dirhodium tetraacetate with adjacent nucleobases (modified from ref. 117).

In the present chapter complexes that possess one or two accessible axial coordination sites are compared to a compound in which the axial positions are blocked. In the case of cis-$[Rh_2(OAc)_2(np)_2]^{2+}$ (**1**; np = 1,8-naphthyridine) both axial sites are available for coordination, whereas for *cis*-$[Rh_2(OAc)_2(np)(pynp)]^{+2}$ (**2**; pynp = 2-(2-pyridyl)1,8-naphthyridine) and *cis*-$[Rh_2(OAc)_2(pynp)_2]^{+2}$ (**3**) the bridging pynp ligand blocks one and two of the axial coordination sites in the complexes, respectively. The structures of **1**–**3** are shown in Figure II-3.

A variety of properties of these compounds were studied including their electrochemical properties, their interactions with biological relevant molecules in cell free medium, in assays such as transcription inhibition, binding constant, melting temperature and photocleavage. Data gathered against a panel of two different cancer cell lines revealed that these compounds do not exhibit cytotoxicity at values of up to 400 μM. The ability of the complexes to inhibit transcription *in vitro* shows a profound effect on the availability of an axial coordination site, indicating the need of metal binding for biological activity in these complexes.

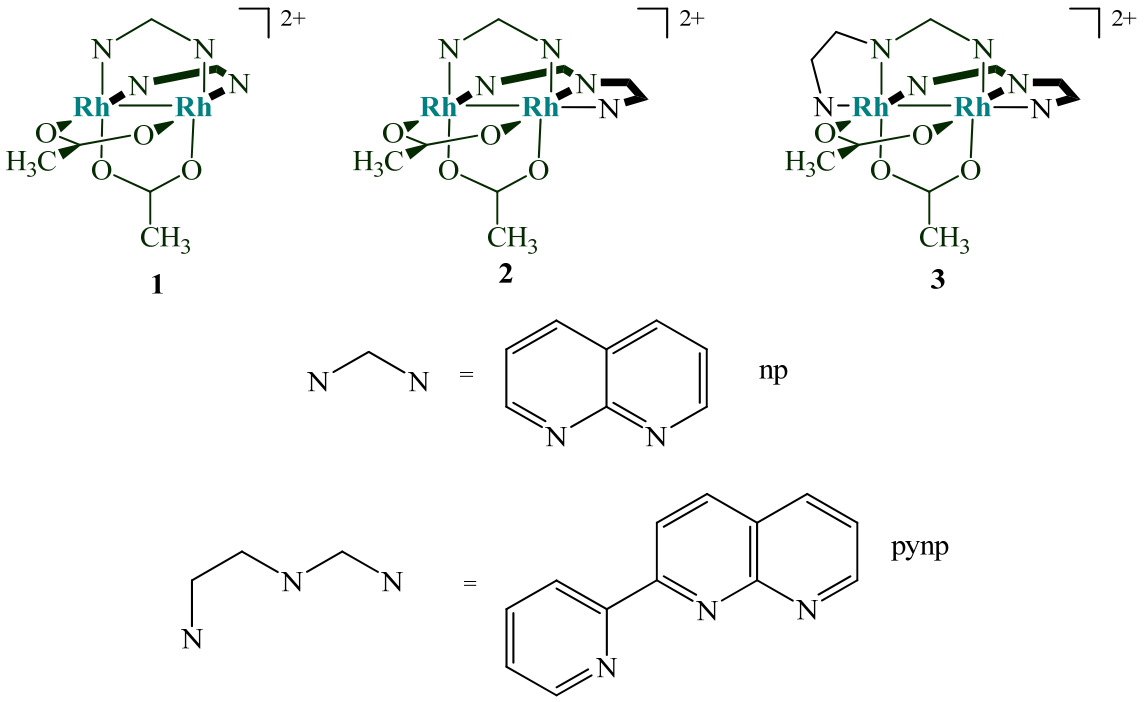

Figure II-3. Schematic representations of the molecular structures of **1** – **3** and the np and pynp ligands.

Experimental Section

Materials

Biotech grade acetonitrile was purchased from Sigma-Aldrich. The tetra-*n*-butylammonium hexafluorophosphate ($TBAPF_6$) salt was purchased from Fluka. Agarose, ethidium bromide, EDTA, Tris/HCl, $MgCl_2$, and RNA loading solution were purchased from Sigma and used as received. The pGEM linear DNA control template (3,995 bp) was purchased from Promega, and the T7-RNA polymerase (50 units/μL) and 5x RNA transcription buffer were purchased from Life-Technologies (Rockville, MD). The starting material $RhCl_3 \cdot xH_2O$ was purchased from Pressure Chemicals and $Rh_2(\mu\text{–}O_2CCH_3)_4$ and *cis*-$[Rh_2(\mu\text{–}O_2CCH_3)_2(CH_3CN)_6](BF_4)_2$ were prepared following literature procedures.[119] The bridging ligand np was purchased from TCI and the pynp ligand was prepared according to literature procedures.[120] The compounds *cis*-$[Rh_2(\mu\text{-}O_2CCH_3)_2(pynp)_2]^{2+}$ and *cis*-$[Rh_2(\mu\text{-}O_2CCH_3)_2(np)_2]^{2+}$ were synthesized from *cis*-$[Rh_2(\mu\text{-}O_2CCH_3)_2(CH_3CN)_6]^{2+}$ using a modified literature procedure as described in detail below.[120]

Synthesis of *cis*-$[Rh_2(\mu\text{-}O_2CCH_3)_2(np)_2](BF_4)_2$ (1)

The tetrafluoroborate salt of *cis*-$[Rh_2(\mu\text{-}O_2CCH_3)_2(CH_3CN)_6]^{2+}$ (0.1 g, 0.13 mmol) was dissolved in acetonitrile (20 mL) to afford a purple solution, and two equivalents of the naphthyridine ligand (0.034 g, 0.26 mmol) were added. The mixture was refluxed and stirred overnight, the solution was evaporated, and a dark red powder was obtained by filtration. The product was then dissolved in a minimum amount of acetonitrile, and toluene was added to precipitate the orange product, which was then collected and dried

(0.074 g, 74%). ^{1}H NMR in CH_3CN-d_6, δ / ppm : 9.05 (q, 4H), 8.37 (d, 4H), 7.61 (m, 4H), 2.40 (s, 6H).

Synthesis of *cis*-[Rh_2(μ-O_2CCH_3)$_2$(pynp)$_2$](BF_4)$_2$ (2)

A procedure similar to that for the preparation of *cis*-[Rh_2(μ-O_2CCH_3)$_2$(np)$_2$]$^{2+}$ was used, with the addition of 2 equivalents (0.056 g, 0.27 mmol) of pynp ligand to *cis*-[Rh_2(μ-O_2CCH_3)$_2$(CH_3CN)$_6$]$^{2+}$ (0.1 g, 0.13 mmol) in acetonitrile (20 mL), to obtain a dark red solid (0.084 g, 84%). ^{1}H NMR in CH_3CN-d_6, δ / ppm (splitting): 9.70 (d, 2H), 8.87 (m, 4H), 8.70(d, 2H) 8.67(m, 4H), 8.50 (dd, 2H), 8.37 (td, 2H), 7.48 (q, 2H), 2.25 (s, 6H).

Synthesis of *cis*-[Rh_2(μ-O_2CCH_3)$_2$(np)(pynp)](BF_4)$_2$ (3)

A solution of Rh_2(μ-O_2CCH_3)$_4$ (0.2 g, 0.39 mmol) was stirred overnight in acetone (20 mL) in the presence of one equivalent of pynp (0.08 g, 0.39 mmol). The product precipitated from the reaction mixture and was collected by filtration. The solid was suspended in methanol (40 mL) and stirred at r.t. until it went into solution. To this solution was added 4 equivalents of $NaBF_4$ (0.16 g, 1.44 mmol), and one equivalent of np (0.05g, 0.38mmol). The mixture was stirred overnight, the volume of the solution was decreased to ~ 6 mL, and the solution was filtered through a fine frit. The red/orange solution was treated with toluene to afford a red/orange powder (0.06 g, 30%). ^{1}H NMR in CH_3CN-d_6, δ / ppm (splitting): 10.04 (d, 1H), 9.81 (d, 1H), 9.71 (d, 1H), 9.02 (d, 1H), 8.87 (m, 2H), 8.71 (d, 1H), 8.64 (m, 2H), 8.52 (m, 2H), 8.33 (dd, 1H), 8.15 (dd, 1H), 7.87 (dd, 1H), 7.56 (dd, 1H), 2.21 (s, 6H), 1.82 (s, 6H). MS m/z = 330.5 ([Rh_2(μ-O_2CCH_3)$_2$(pynp)(np)]$^{2+}$). Anal. Calcd for $Rh_2C_{25}H_{21}N_5O_4B_2F_8$: C, 35.97; H, 2.54; N, 8.39. Found: C, 35.93; H, 2.39; N, 8.41.

Instrumentation

X-ray diffraction data were collected on a Bruker SMART 1000 CCD diffractometer with graphite monochromated Mo-K_α radiation (λ = 0.71073 Å). The frames were integrated with the Bruker SAINT software[121] and a semi-empirical absorption correction using multiple-measured reflections was applied using SADABS.[122] The structures were solved and refined using X-SEED, a graphical interface to SHELX97.[123]

Cyclic voltammetric measurements were performed on a H-CH Electrochemical Analyzer model 620A. Absorption measurements were performed on a Shimadzu UV 1601PC spectrophotometer or a HP diode array spectrometer (HP 8453) with HP8453 Win System software or a Perkin-Elmer Lambda 900 spectrometer. The ethidium bromide stained agarose gels (1%) were imaged on an AlphaImager 2000 transilluminator (Alpha Innotech Corporation).

Methods

X-Ray Structural Study of *cis*-[$Rh_2(\mu$-$O_2CCH_3)_2(np)_2](BF_4)_2$ (1)

For the X-ray crystallographic analysis, a red prismatic crystal of **1** of dimensions: 0.20 x 0.16 x 0.10 mm^3 was selected. The crystal was coated with Paratone oil, transferred to a nylon loop, and placed in a cold N_2 stream at 110(2) K. An indexing of the preliminary diffraction patterns indicated that the crystal was monoclinic. A total of 24,689 reflections was collected in the range $2.36 \leq \theta \leq 26.37^o$. The data collection covered approximately a hemisphere of reciprocal space, by a combination of three or four sets of exposures; each set had a different ϕ angle for the crystal and each exposure covered 0.3° in Ω. Crystal decay, which was monitored by analyzing duplicate

reflections, was found to be less than 1%, therefore, no decay correction was applied. During the final cycles of refinement, all atoms, with the exception of hydrogen, were refined anisotropically. All hydrogen atoms were placed at calculated positions. The structure was solved and refined in the space group $P2_1/n$.

Computational Studies

The molecular and electronic structure calculations were performed with density functional theory (DFT) using the Gaussian03 (G03) program package.[124] The B3LYP[125-127] functional along with the 6–31G* basis set was used for H, C, N, and O,[128] along with the Stuttgart/Dresden (SDD) energy-consistent pseudopotentials for Rh.[129] Formate ligands were used instead of acetate ligands in the computationally modeled complexes. This procedure has been found to be acceptable in other reported computational studies.[130] All geometries were fully optimized under the conditions of the respective programs. Orbital analysis was completed with Molekel 4.3.[131] Vertical electronic transitions were calculated using TDDFT methods implemented within G03. All calculations shown in this chapter were performed at The Ohio State University by Dr. Daniel Lutterman.

Electrochemical Characterization

Electrochemical studies were performed in CH_3CN with 0.1 M $TBAPF_6$ as the supporting electrolyte, a BAS Pt disk as the working electrode, a Ag/AgCl reference electrode, and a Pt wire as the auxiliary electrode. Ferrocene was used as an internal reference and under the same experimental conditions the ferrocene/ferrocenium couple was observed at

$E_{1/2}$ = +0.52 V versus Ag/AgCl electrode.[132] The reduction and oxidation potentials were converted to SCE by subtraction of 0.45 V.[133]

Melting Point Experiments

The melting temperature experiments were carried out by monitoring the absorption change at 260 nm while varying the temperature from 25 °C to 95 °C at a rate of 0.5 °C/min of a mixture containing 20 μM complex and 100 μM ct-DNA in 1 mM phosphate buffer, 2 mM NaCl, pH 7.2. The value of T_m was determined as the temperature corresponding to a maximum on the first-derivative profile of the melting curves.[103, 134]

DNA Binding Constant Determination

The binding constant, K_b, was determined by optically titrating 5 μM metal complexes in a 5 mM Tris/HCl, pH 7.2 buffer at room temperature with ct-DNA up to a final concentration of 200 μM. The dilution of the compound concentration at the end of each titration was negligible. The K_b values were calculated from fits of the absorption changes as a function of DNA to eq 1,[103]

$$\frac{\varepsilon_a - \varepsilon_f}{\varepsilon_b - \varepsilon_f} = \frac{b - (b^2 - 2K_b{}^2 C_t [DNA]_t / s)^{1/2}}{2K_b C_t} \quad (1)$$

where $b = 1 + K_b C_t + K_b [DNA]_t / 2s$, C_t and $[DNA]_t$ represent the total complex and DNA concentrations, respectively, *s* is the base pair binding site size, and ε_a, ε_f, and ε_b represent the apparent, free complex, and bound complex molar extinction coefficients, respectively. The value of ε_b was determined from the plateau of the DNA titration where addition of DNA did not result in further changes to the absorption spectrum.

Relative Changes in Viscosity Studies

The relative changes in viscosity were measured on a Cannon-Manning semi-micro viscometer. The viscometer was immersed in a constant temperature water bath (25 °C) controlled by a Neslab (model RTE-100) circulator. Data are presented as:

$$(\frac{\eta}{\eta_\circ})^{1/3} \text{ vs } \frac{[M]}{[DNA]}$$

$$\eta = t_1 - t_2$$

$$\eta_0 = t_n - t_0$$

where η is viscosity of DNA in the presence of the complex and η_0 is viscosity of DNA in the absence of complex.[134]

Transcription Inhibition Studies

The transcription assay has been previously reported.[135-137] In the *in vitro* transcription experiment, the pGEM linear DNA template (120 μM bases) was used with T7-RNAP, resulting in two transcripts of length 1,065 and 2,346 bases; each trial was conducted three times. The transcription reaction was conducted for 45 min at 37 ºC (40 mM Tris/HCl, pH = 8.0) in nuclease-free water in the presence of 1.25 units of T7-RNAP, 25 mM NaCl, and 1.0 mM of each ATP, CTP, GTP and UTP. The inhibition of RNA production by the dirhodium complexes was detected *in vitro* by the measurement of the RNA generated upon addition of increasing amounts of metal complex to the assay. The concentration of each complex at which 50% of the RNA is transcribed, IC_{50}, was calculated by interpolation of the integrated areas of the imaged RNA signal of each lane of the gel conducted with various concentrations of a given complex. Modifications of these methods were used in the various control assays, including those designed to

determine the role of binding of the complexes to T7-RNAP. All stock solutions of the metal complexes were prepared in pure H_2O.

DNA Photocleavage Experiments

The DNA photocleavage experiments were carried out using 20 μL of total sample volume in 0.5 mL transparent eppendorf tubes containing 100 μM pUC18 plasmid, 25 μM of metal complex and 2 mM of 3-cyano-1-methylpyridinium tetrafluoroborate (3-CN-1-Me-py^+). Irradiation of the solutions was performed under a positive pressure of nitrogen or in the presence of oxygen. Following irradiation, 5 μl of the DNA gel loading buffer was added to each 20 μL of sample. The electrophoresis was carried out using 1% agarose gel stained with 0.5 mg/L ethidium bromide in 1X TAE buffer (40 mM tris-acetate, 1 mM EDTA, pH ~ 8.2).

***In Vitro* Cytotoxicity**

The viability of COLO-316 and HeLa cells in the presence of the compounds under investigation was tested using the 3-(4,5-dimethylthiazol-2-yl)-2,5-diphenyltetrazolium bromide (MTT) assay (Invitrogen). Subconfluent (50-80% confluent) monolayers of cells at a concentration of 5000-10000 cells/μL were used. Cells were plated in 96-well sterile plates at a density of 20-30 cells/μL (volume of 100 μL per well) and were pre-incubated for 48 h. After the cells reached 100% confluency, the medium was replaced by 100 μL of L-15 medium containing different complex concentrations. The plates were incubated for either 24 or 48 hours. A 10 μL aliquot of fresh MTT solution was added, followed by incubation for 3 hours. A 100 μL volume of fresh SDS solution in 0.01 M HCl was then added and, after 16 hours of incubation, the absorbance at 570 nm was measured using a Bio-Rad plate reader.

Results and Discussion

Synthesis and Structural Characterization

The homoleptic complexes were prepared by substitution of the four equatorial CH_3CN ligands of *cis*-$[Rh_2(\mu\text{-}O_2CCH_3)_2(CH_3CN)_6]^{2+}$ with the polydentate ligands, np (1,8-naphthyridine) and pynp (2-(2-pyridyl)1,8-naphthyridine), to generate *cis*-$[Rh_2(\mu\text{-}O_2CCH_3)_2(np)_2]^{2+}$ (**1**) and *cis*-$[Rh_2(\mu\text{-}O_2CCH_3)_2(pynp)_2]^{2+}$ (**3**), respectively. The synthesis of the new heteroleptic complex *cis*-$[Rh_2(\mu\text{-}O_2CCH_3)_2(np)(pynp)]^{2+}$ (**2**) was carried out by stepwise addition of pynp followed by np to an acetone solution of $Rh_2(\mu\text{-}O_2CCH_3)_4$ at room temperature (Figure II-4).

The crystal structure of the tetrafluoroborate salt of **1**, which has not been previously reported, is shown in Figure II-5a. Selected refinement parameters are provided in Table II-1. The asymmetric unit contains the cationic *cis*-$[Rh_2(\mu\text{-}O_2CCH_3)_2(np)_2]^{2+}$ molecule with two chloride ions coordinated to the axial positions, and two methanol solvent molecules of crystallization. The final refinement cycle was based on 5,224 unique reflections (4,302 with $F_\sigma^2 > 2\sigma(F_\sigma^2)$), 327 parameters, and no restraints ($R1$ = 0.0508, $wR2$ = 0.1193). The maximum and minimum peaks in the final difference Fourier map corresponded to 3.27 and –0.89 e/Å^3, respectively, with a goodness-of-fit value of 1.158.

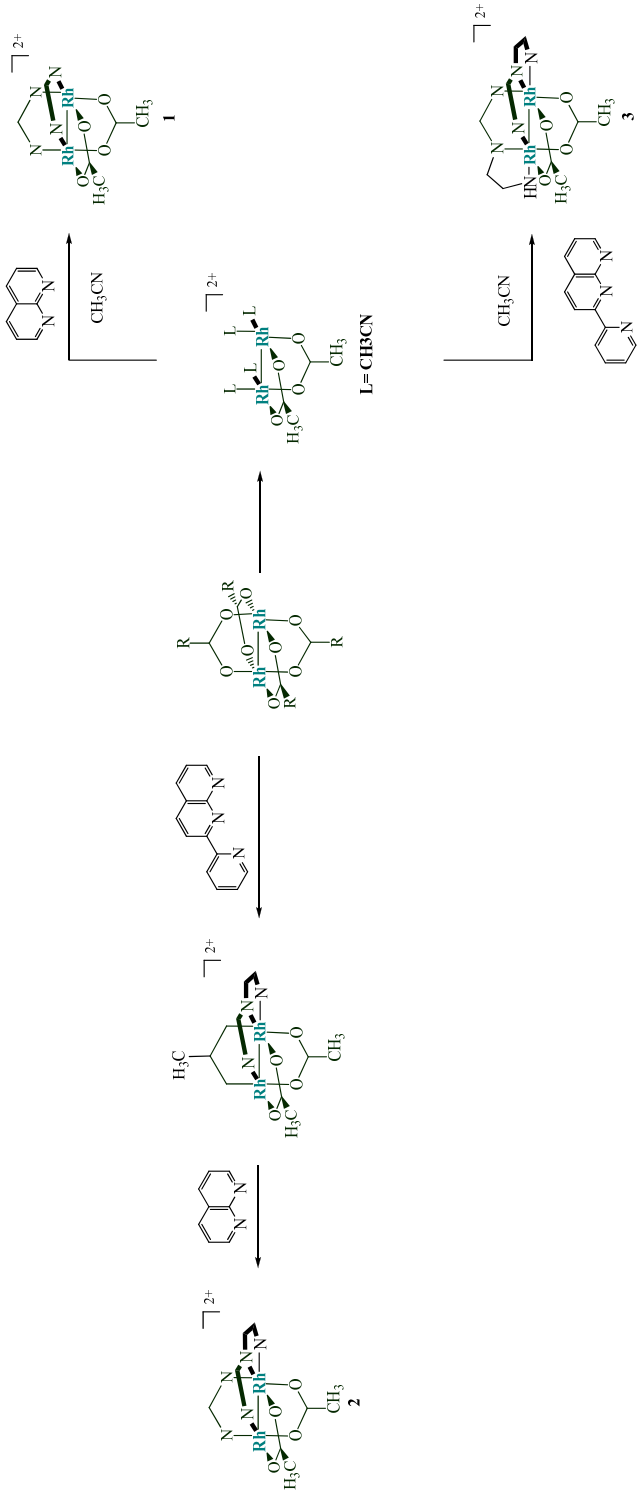

Figure II-4. Schematic representation of the syntheses of compounds **1** – **3**.

Table II-1. Crystal data and structure refinement for compound **1**.

Empirical formula	$C_{46}\,H_{41}\,B\,F_4\,N_8\,O_8\,Rh_2$	
Formula weight	719.19	
Crystal system	Monoclinic	
Space group	$P2_1$	
Unit cell dimensions	a = 8.812 (1) Å	α= 90°
	b = 17.293(2) Å	β= 104.574(2)°
	c = 17.336(2) Å	γ = 90°
Volume	2556.8(5) $Å^3$	
Z	4	
Density (calculated)	1.868 Mg/m^3	
Absorption coefficient	1.545 mm^{-1}	
Crystal size	0.20 x 0.16 x 0.10 mm^3	
Reflections collected	24689	
Independent reflections	5224 [R_{int} = 0.0395]	
Goodness-of-fit on F^2	1.158	
Final R indices [I>2sigma(I)][a]	$R1$ = 0.0508, $wR2$ = 0.1193	
R indices (all data)[a]	$R1$ = 0.0604, $wR2$ = 0.1266	

[a] $R_1 = \Sigma||F_o| - |F_c||/\Sigma|F_o|$; $wR_2 = [\Sigma[w(F_0^2-F_c^2)^2]/\Sigma[w(F_0^2)^2]]^{1/2}$

(a)

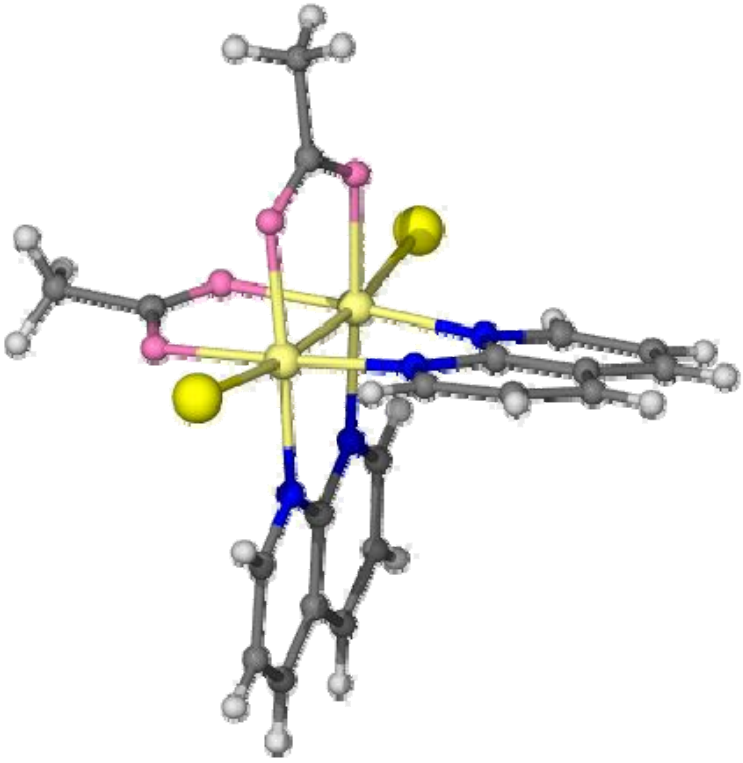

(b)

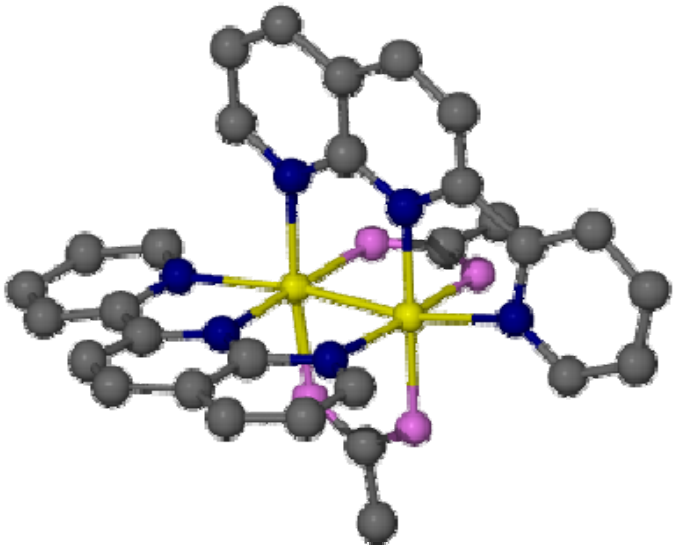

Figure II-5. X-ray structure of (a) compound 1 and (b) compound 3 (taken from ref. 120).

The molecular structure of **1**, determined by X-ray crystallographic methods, consists of a dinuclear Rh_2(II,II) core with a pair of bridging naphthyridine ligands coordinated to each Rh atom and two bridging acetate groups occupying the remaining equatorial sites. Two chloride ions complete a distorted octahedral coordination sphere around each Rh atom. The structure of **1** is shown in Figure II-5a and is similar to those reported for related dirhodium complexes (Figure. II-5b).[120, 138, 139] Selection of bond distances and angles are provided in Table II-2 and Table II-3 respectively. The Rh-Rh distance in **1**, 2.4251(5) Å, is in the expected range for a Rh-Rh single bond. The distance is longer than that reported for *cis*-$[Rh_2(\mu\text{-}O_2CCH_3)_2(pynp)_2]^{2+}$ (pynp = 2-(2-pyridyl)-1,8-naphtyridine), 2.206(9) Å, and shorter than those reported $Rh_2(\mu\text{-}O_2CCH_3)_2(phen)_2Cl_2$ (phen = 1,10-phenanthroline), and $[Rh_2(np)_4(O_2CCH_3)_2]^{2+}$, 2.6011(11) and 2.448(1) Å, respectively. The average Rh-N bond length in **1**, 2.027(4) Å, is similar to that of $[Rh_2(\mu\text{-}O_2CCH_3)_2(pynp)_2]^{2+}$, 2.018(4) Å, and longer than the reported $Rh\text{-}N_{av}$ distance of 2.010(5) Å in $Rh_2(\mu\text{-}O_2CCH_3)_2$ $(phen)_2Cl_2$ and somewhat shorter than that found for $[Rh_2(np)_4(O_2CCH_3)_2]^{2+}$, 2.054(3). The average Rh-axial chloride distance is 2.563(1) Å in **1** as compared to the reported Rh-Cl distance for $Rh_2(\mu\text{-}O_2CCH_3)_2(phen)_2Cl_2$ which is 2.532(2) Å. This increase of 0.03 Å, as compared to the bis-phenanthroline analogue, is attributed to the presence of the hydrogen atoms on the np ligands pointing towards the chloride ions.

Table II-2. Selected bond distances (Å) for compound **1**.

	Bond Distances
Rh(1)-Rh(2)	2.4251(5)
Rh(1)-N(1)	2.025(4)
Rh(1)-N(3)	2.028(4)
Rh(2)-N(4)	2.022(4)
Rh(2)-N(2)	2.031(4)
Rh(1)-O(3)	2.043(3)
Rh(1)-O(1)	2.046(3)
Rh(2)-O(4)	2.058(3)
Rh(2)-O(2)	2.063(3)

Table II-3. Selected bond angles (°) for compound **1**.

	Bond Angles
Rh(1)-Cl(1)	2.582(1)
Rh(2)-Cl(2)	2.544(1)
Rh(2)-Rh(1)-Cl(1)	173.46(3)
Rh(1)-Rh(2)-Cl(2)	171.92(3)
N(1)-Rh(1)-N(3)	92.2 (2)
O(3)-Rh(1)-O(1)	87.5(1)
N(4)-Rh(2)-N(2)	88.9(2)
O(4)-Rh(2)-O(2)	89.0(1)

Electronic Absorption Spectroscopy and Electrochemistry

The absorption maxima and molar extinction coefficients of complexes **1** – **3** are listed in Table II-4. Given that the free np ligand exhibits π–π* transitions at 258, 300, and 309 nm in CH_3OH/H_2O (50:50 v:v), it is likely that the peaks observed in **1** at 268 and 307 nm are centered on the np ligand. Similarly, the free pynp ligand exhibits absorption maxima at 271, 322, and 333(sh) nm (CH_3OH/H_2O 50:50 v:v), which leads to the assignment of the peaks at 316 and 329 nm in **3** as ligand-centered. In the mixed-ligand complex **2**, the peaks observed at 266 and 320 nm are likely due to a superposition of π–π* transitions of the np and pynp ligands. Additional absorption peaks in the UV and near-UV region are observed with maxima at 315 nm (ε = 5,830 $M^{-1}cm^{-1}$) in **1** and at 356 nm in **2** (ε = 5,410 $M^{-1}cm^{-1}$) and **3** (ε = 12,790 $M^{-1}cm^{-1}$), which are attributed to MLCT transitions. The latter is likely to be due to $Rh_2 \rightarrow$ pynp, which is expected to occur at a lower energy than the corresponding MLCT transition involving the np ligand in **1**. Complexes **1** – **3** also exhibit an absorption peak in the 393 to 465 nm region with intensities that range from 3,380 to 4,880 $M^{-1}cm^{-1}$. In the related complex $Rh_2(\mu\text{-}O_2CCH_3)_4$, the transitions observed in water in the visible region are weak (441 nm, ε = 106 $M^{-1}cm^{-1}$ and 585 nm, ε = 241 $M^{-1}cm^{-1}$); these absorptions were previously assigned to $Rh–O(\sigma) \rightarrow Rh_2(\sigma^*)$ and $Rh_2(\pi^*) \rightarrow Rh_2(\sigma^*)$ transitions respectively.[120, 140] Owing to the intensity of the transitions observed in **1** – **3** in the visible region, the transitions can be assigned as arising from MLCT from Rh_2 to the np and/or pynp ligand, depending on the complex. The positions and intensities of these transitions are comparable to those observed for *cis*-$[Rh_2(\mu\text{-}O_2CCH_3)_2(bpy)_2]^{2+}$ (bpy = 2,2′-

bipyridine, λ_{abs} = 408 nm, ε = 2,920 $M^{-1}cm^{-1}$ in CH_3CN) and *cis*-[$Rh_2(\mu$-$O_2CCH_3)_2(phen)_2]^{2+}$ (phen = 1,10-phenanthroline, λ_{abs} = 408 nm, ε = 3,050 $M^{-1}cm^{-1}$ in CH_3CN), which also possess aromatic ligands coordinated to the dirhodium core and have been previously assigned as MLCT transitions from the Rh_2 to the bpy and phen ligand, respectively.[141]

Additional evidence for the assignment of the lowest energy transition in complexes **1** – **3** as MLCT can be found by examining the spectra of **1** with axially coordinated pyridine (py). The presence of strong σ-donor axial ligands has been shown to have a profound effect on the electronic structure of dirhodium complexes. For example, in $Rh_2(\mu$-$O_2CCH_3)_4$, addition of ligands that bind to the axial positions result in a blue-shift of the lowest energy, $Rh_2(\pi^*) \rightarrow Rh_2(\sigma^*)$ metal-centered (MC) transition.[142-145] This shift is due to interaction of the antisymmetric linear combination of the filled orbitals on the axial ligands with the $Rh_2(\sigma^*)$ molecular orbital, which raises the energy of the latter.[130, 140, 146, 147] Addition of excess py (547 μM) to **1** (22 μM) in H_2O does not result in spectral shifts in the UV/visible regions. This result is consistent with the assignment of these low energy transitions as $Rh_2 \rightarrow$ np MLCT, which are not expected to be affected greatly by the presence of axial ligands.

The reduction and oxidation potentials of **1** – **3** are listed in Table II-4. The first reduction is dependent on the identity of the aromatic ligand. Complexes **2** and **3**, with one and two coordinated pynp ligands, respectively, exhibit $E_{1/2}$ ~ –0.64 V vs SCE. In contrast, complex **1** is more difficult to reduce by ~0.17 V, with the first reduction being observed at –0.82 V vs SCE. Free pynp ligand is easier to reduce than np, with $E_{1/2}$ values of –1.68 and –

1.88 vs SCE (CH_3CN, 0.1 M Bu_4NPF_6), respectively. The difference in the reduction potentials of the free ligands, 0.20 V, is comparable to that between **1** and complexes **2** and **3**. The values of the first reduction waves of complexes **1** – **3** are similar to those reported for other dirhodium complexes possessing aromatic ligands, such as *cis*-$[Rh_2(\mu\text{-}O_2CCH_3)_2(bpy)_2]^{2+}$ ($E_{1/2}$ = –0.93 vs SCE in CH_3CN) and *cis*-$[Rh_2(\mu\text{-}O_2CCH_3)_2(phen)_2]^{2+}$ ($E_{1/2}$ = –0.87 vs SCE in CH_3CN). The oxidation potentials of **1** – **3** range from +1.30 to +1.50 vs SCE and are quasi-reversible or irreversible. These values are similar to those previously reported for the metal-centered oxidation of related dirhodium complexes, such as $Rh_2(\mu\text{-}O_2CCH_3)_4$, with $E_{1/2}$ = +1.17 V vs SCE in CH_3CN.[148] These results support the conclusion that the oxidations for **1** – **3** are centered on the dirhodium core.

Electronic Structure Calculations

Electronic structure calculations were conducted in order to aid in the assignments of the absorption spectra and electrochemistry of complexes **1** – **3**, and comparisons can be made regarding the structural and electronic changes that take place upon axial coordination of solvent and as the bridging ligands are varied. As shown in Figure II-6, the electronic structures of the model complexes cis-$[Rh_2(\mu\text{-}O_2CH)_2(np)_2]^{2+}$ (**1a**) and cis-$[Rh_2(\mu\text{-}O_2CH)_2(pynp)(np)]^{2+}$ (**2a**) are sensitive to the nature of the coordinating solvent in the axial position, as previously reported for other dirhodium complexes.[130]

Table II-4. Electronic absorption and electrochemical properties of **1** – **3**.

Complex	λ_{abs} / nm (ε / $M^{-1}cm^{-1}$) [a]			$E_{1/2}$ / V [b]
1	268 (16,260),	307 (5,980),	315 (5,830),	–0.82
2	266 (21,320),	320 (19,490),	356 (5,410),	–0.63, –1.35
3	316 (31,390),	329 (31,400),	356 (12,790),	–0.64, –1.03

[a]In CH_3OH/H_2O (50:50 v/v). [b]In acetonitrile with 0.1 M Bu_4NPF_6; vs SCE.

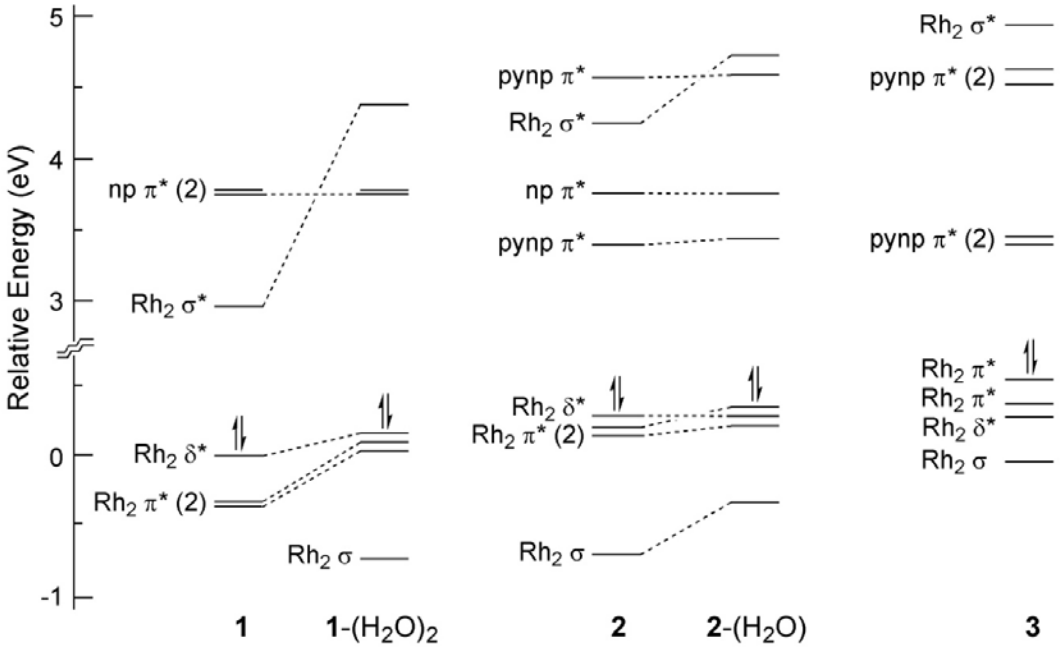

Figure II-6. MO diagrams of (a) **1a** and **1a**–$(H_2O)_2$, (b) **2a** and **2a**–(H_2O), and (c) **3a**. For reference, the $Rh_2(\delta^*)$ MO in 1a was set to 0 eV.

In aqueous solution, water molecules coordinate to the open axial sites of **1a** and **2a**, generating **1a**–$(H_2O)_2$ and **2a**-H_2O, respectively (Figure II-6).

Interaction of the symmetric and antisymmetric linear combinations of the axial water molecules with metal-centered MOs in **1a** result in the destabilization the $Rh_2(\sigma)$and $Rh_2(\sigma^*)$ orbitals in **1a**–$(H_2O)_2$ (Figure II-6a). As shown in Figure II-6a, these axial interactions change the identity of the LUMO from $Rh_2(\sigma^*)$ in **1a** to np(π^*) in **1a**–$(H_2O)_2$. The electronic structure calculations with NCH axial ligands as models for acetonitrile molecules also result in np(π^*) LUMO in **1a**–$(NCH)_2$. These results are in agreement with the observation of ligand-centered reduction of **1** in CH_3CN. DFT calculations on **2a**, **2a**–(H_2O), and cis-$[Rh_2(\mu\text{-}O_2CH)_2(pynp)_2]^{2+}$ (**3a**) also result in ligand-centered LUMO, in agreement with the electrochemical reduction discussed above (Figure II-6). It should be noted that the calculations also predict that the reduction potentials of **2** and **3** should be similar in a coordinating solvent, whereas **1** should be more difficult to reduce (Figure II-6). Selected molecular orbitals of **1a**–$(H_2O)_2$, **2a**–(H_2O), and **3a** are shown in Figure II-7.

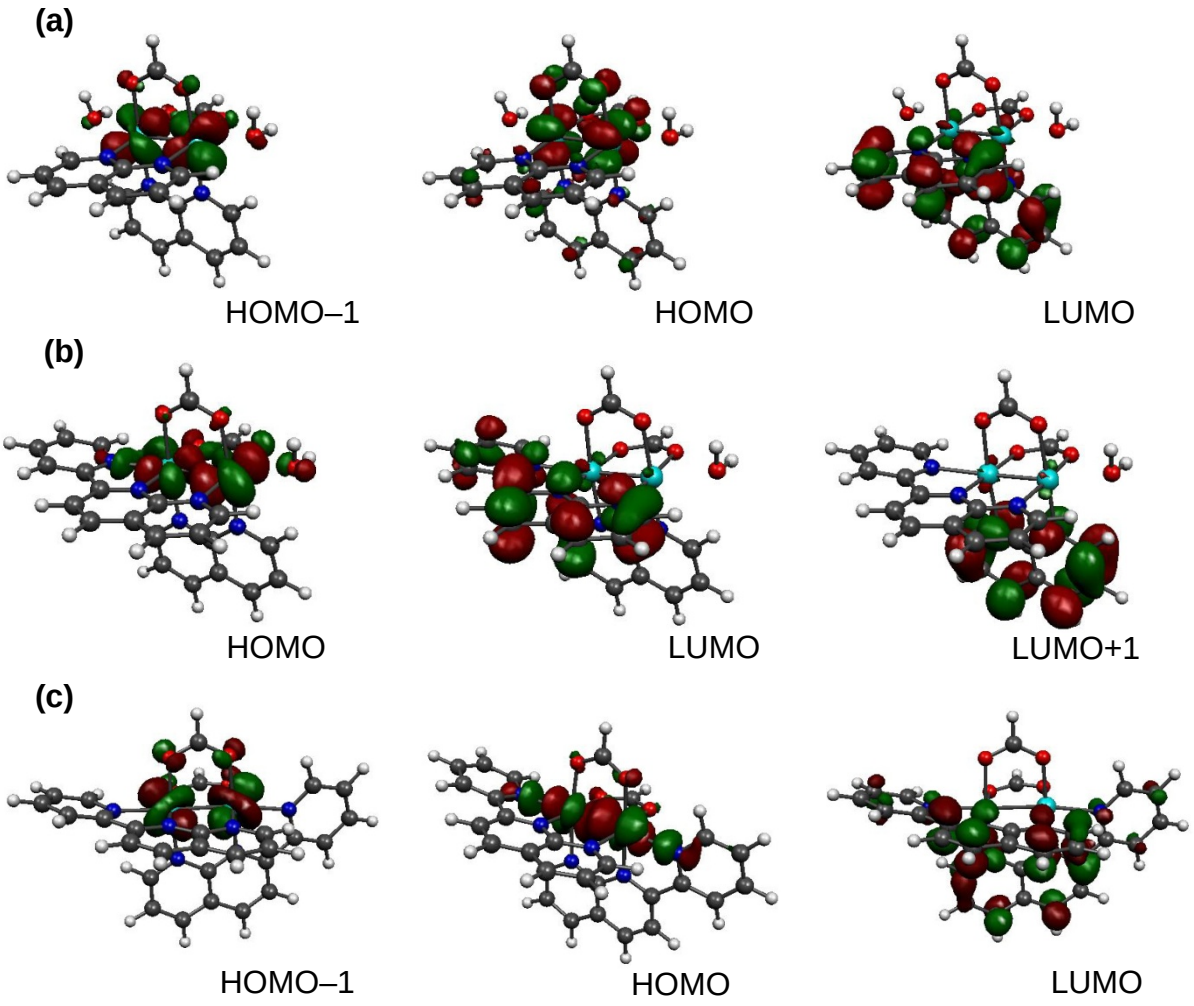

Figure II-7. Selected molecular orbital representations of (a) **1a**–$(H_2O)_2$, (b) **2a**–(H_2O), and (c) **3a** drawn with isovalues = 0.4.

The changes to the orbital energies of **1a**–$(H_2O)_2$ upon the substitution of one and two np ligand(s) for pynp to generate **2a**–H_2O and **3a**, respectively, are also shown in Figure II-6. In order to make a semi-quantitative comparison among the complexes, the energy of the Rh_2 (δ^*) MO of **1a** was set to 0.0 eV. In addition, the lowest energy np(π^*) orbitals of **1a**, **1a**–$(H_2O)_2$, **2a**, and **2a**–(H_2O) were matched in energy in Figure II-6, since this orbital is not expected to be affected by axial substitution. Similarly, the lowest energy pynp(π^*) in **2a**–(H_2O) and **3a** were set to the same energy. As expected, substitution of H_2O molecules in the axial position for the stronger pyridine portion of the pynp ligand results in an increase in the energy of both the $Rh_2(\sigma)$ and $Rh_2(\delta^*)$ MOs (Figure II-6).

Time-dependent DFT (TDDFT) calculations can be used to predict observed transition energies and can be used to elucidate their parentage. As discussed above, the peaks observed in UV region can be ascribed to π–π^* transitions centered on the aromatic ligands, while the two lowest energy transitions were assigned as $Rh_2 \rightarrow$np/pynp MLCT. In general, the MCLT peaks red-shift across the series **1** – **3** (Table II-4). TDDFT calculations on **1a**–$(H_2O)_2$ predict a strong np-centered transition at 259 nm and four weaker ones in the 261– 275 nm range. Two low energy vertical $Rh_2(\pi^*) \rightarrow$np(π^*) MLCT transitions are calculated at 402 nm and 410 nm. The latter exhibits the highest oscillator strength (Table II-5) and may be correlated to the peak observed at 393 nm in the complex (Table II-4). In **3a**, MLCT transitions from $Rh_2(\delta^*)$ and $Rh_2(\sigma^*)$ to pynp(π^*) are calculated at 466 nm and 489 nm, respectively (Table II-5), which is correlated with the absorption peak with maximum at 465 nm in **3**. Additional MLCT

transitions of **3a** are predicted at 315 nm, 320 nm, and 331 nm, however, a very strong pynp-centered transition of significantly greater intensity is calculated at 326 nm (Table II-5). The latter is associated with the observed peak at 356 nm in **3**. A transition at 340 nm calculated to exhibit both MLCT and LC character in **3a** may also contribute to the peak observed at 356 nm in **3**. Owing to the presence of both np and pynp ligands in the heteroleptic complex, there is a greater number of calculated transitions for **2a**–(H_2O) in the same energy range. Two low-lying MLCT transitions of similar intensity from $Rh_2(\pi*)$ to pynp($\pi*$) and np($\pi*$) are calculated at 471 nm and 423 nm, respectively. These occur at significantly lower energies than the MLCT peak observed for **2** with a maximum at 398 nm (Table II-4). A fairly strong pynp π–$\pi*$ transition is calculated at 342 nm for **2a**–(H_2O) with several additional peaks with MLCT character between 318 nm and 335 nm. Owing to the number of calculated peaks, a correlation with the experiment in solution in this complex is not possible, but it is noted that the calculated transitions lie in the region where peaks are observed. As previously assigned, the calculations show that the lowest energy transition in each of these complexes is MLCT in character.

As discussed above, the metal-centered $Rh_2(\pi*)\rightarrow Rh_2(\sigma*)$ transition of the parent complex $Rh_2(\mu\text{-}O_2CCH_3)_4$ is known to shift to higher energy as a function of the axial ligands.[149, 150] Although this weak transition is not observed experimentally in complexes **2** and **3** because of the overlapping high intensity MLCT peaks, its position can be calculated. As expected, the calculated energy of $Rh_2(\pi*)\rightarrow Rh_2(\sigma*)$ transition shifts as the number of pynp ligands with strong axial coordination is increased in the series **1a**–

$(H_2O)_2$, **2a**–(H_2O), and **3a**, with predicted maxima at 521 nm (f = 0.0011), 474 nm (f = 0.0022), and 455 nm (f = 0.0008), respectively. The calculated maximum of the metal-centered transition for **1a**–$(H_2O)_2$ agrees well with the observed shoulder for **1** in water at ~519 nm.

Table II-5. Calculated vertical singlet excitations, oscillator strength (f), and assignments for **1a**-$(H_2O)_2$, **2a**-(H_2O), and **3a**.*a*

1a-$(H_2O)_2$		**2a**-(H_2O)		**3a**	
λ_{abs} / nm (f)	Assignment [b]	λ_{abs} / nm (f)	Assignment [b]	λ_{abs} / nm (f)	Assignment [b]
259 (0.1108)	ππ*	318 (0.1495)	MLCT	306 (0.0117)	MLCT
259 (0.0148)	MLCT	322 (0.0345)	MLCT	315 (0.0688)	MLCT
261 (0.0175)	ππ*	327 (0.0111)	MLCT	320 (0.0490)	MLCT
262 (0.0143)	ππ*	335 (0.0107)	MLCT	326 (0.2520)	MLCT / ππ*
273 (0.0362)	ππ*	342 (0.0586)	pynp ππ*	331 (0.0110)	MLCT
275 (0.0545)	ππ*	417 (0.0181)	MLCT	340 (0.0217)	MLCT / ππ*
402 (0.0431)	MLCT	423 (0.0374)	MLCT	466 (0.0182)	MLCT
410 (0.0855)	MLCT	471 (0.0521)	MLCT	489 (0.0871)	MLCT

[a]Only transitions with $f \geq 0.01$ are listed. [b]Assignments were made from the character of the orbitals with greatest contribution to each transition.

DNA Binding

The binding constants of **1** – **3** to DNA, K_b, determined from fits of the changes in the absorption of each complex as a function of nucleic acid concentration (Figures II-8 – II-10) are listed in Table II-6. The values of K_b vary with the availability of the axial position. For complex **1**, with both axial positions available for coordination with Lewis bases, $K_b = 5.6\times10^5$ M^{-1} (s = 1.1) was measured, while $K_b = 3.4\times10^5$ M^{-1} (s = 0.9) was calculated for **2**. The value of K_b measured for **3**, 5.9×10^3 M^{-1} (s = 1.2), which has the two axial positions blocked by the pynp ligand, is approximately two orders of magnitude smaller than the DNA binding constants of **1** and **2**. The magnitude of K_b obtained for **3** is consistent with electrostatic interactions with DNA; similar values have been reported in the literature for $[Ru(tpy)(bpy)OH]^+$ ($K_b = 1.3\times10^4$ M^{-1}), $[Ru(tpy)(bpy)(OH_2)]^{2+}$ (tpy = [2,2´; 6',2´´]-terpyridine, $K_b = 6.6\times10^2$ M^{-1}), and $[Ru(bpy)_3]^{2+}$ ($K_b = 6.8\times10^2$ M^{-1}), respectively, which bind DNA through electrostatic interactions.[151, 152] For comparison, the DNA binding constant for the partial intercalator $[Ru(phen)_3]^{2+}$ was reported[151] to be 4.8×10^3 M^{-1}, while a K_b value of 1.7×10^5 M^{-1} has been reported for the intercalator ethidium bromide.[153, 154] Since complexes **1** – **3** have the same overall charge, the differences in measured K_b values are not due to electrostatic interactions. Previous reports have shown that dirhodium compounds can interact with DNA forming a variety of interstrand crosslink adducts.[97] Therefore, it is possible that there is a covalent interaction between the open axial position of the compound and the DNA, such that the decrease in the value of the binding constant from **1** to **2** is related to the difference in the number of open axial positions.

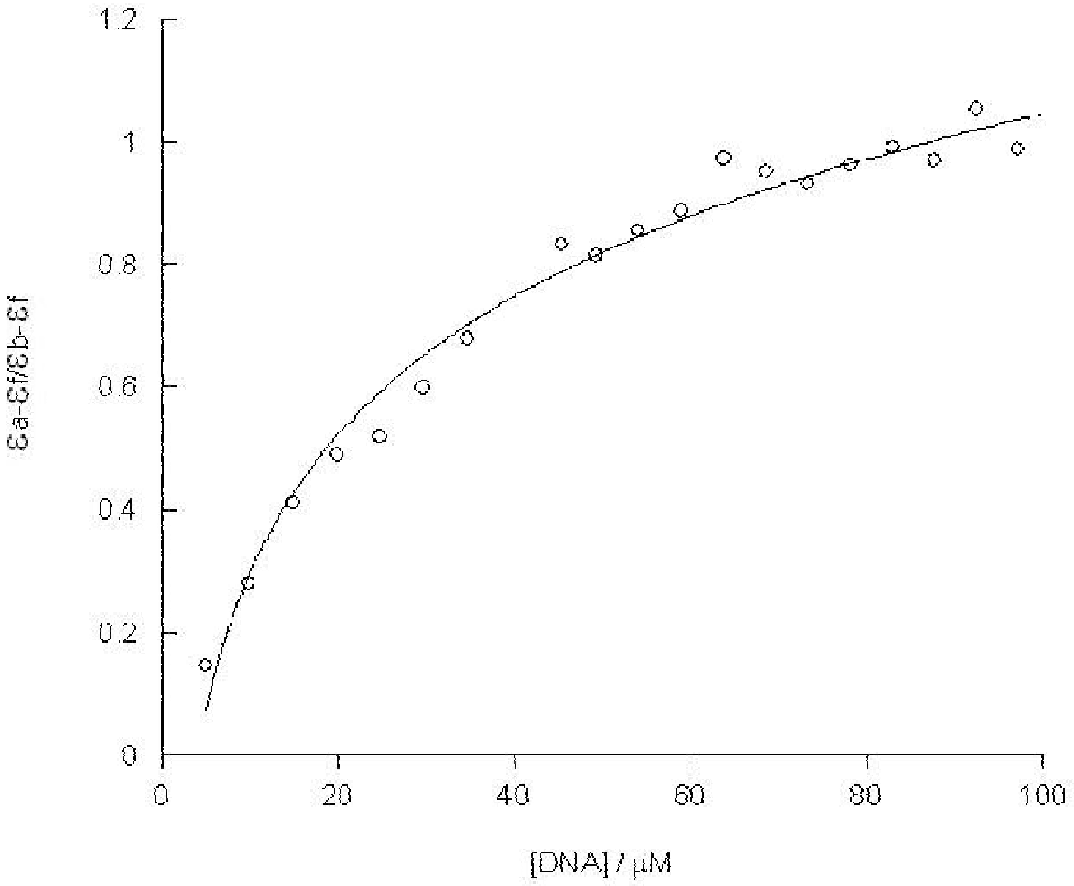

Figure II-8. Changes to the absorption of 5 μM **1** monitored at 390 nm upon addition of DNA in 5 mM Tris, pH = 7.5, 50 mM NaCl.

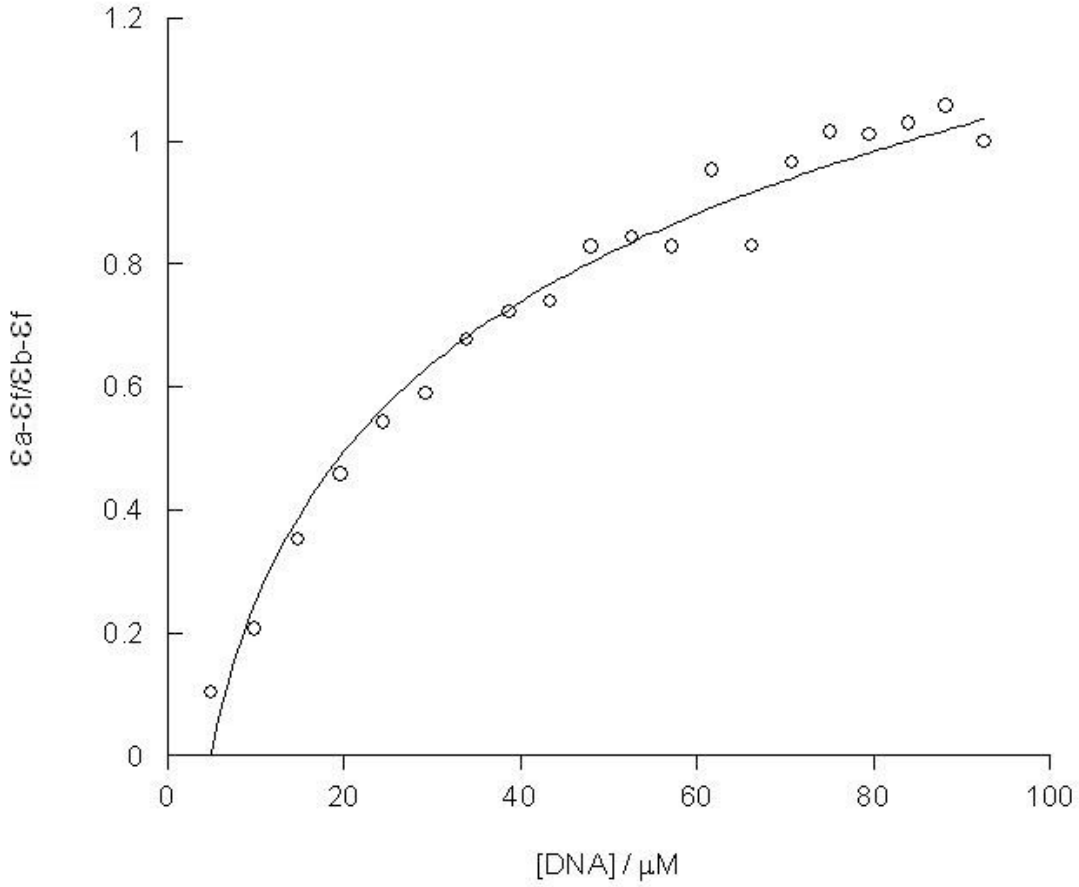

Figure II-9. Changes to the absorption of 5 μM **2** monitored at 390 nm upon addition of DNA in 5 mM Tris, pH = 7.5, 50 mM NaCl.

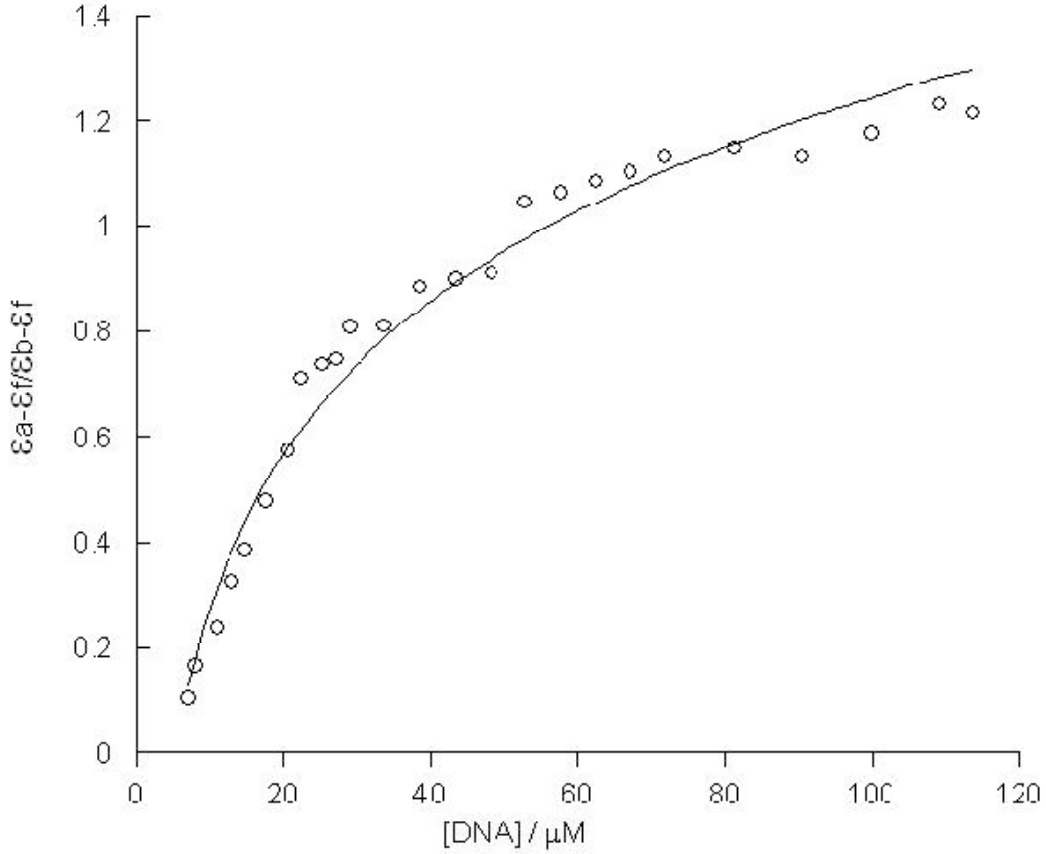

Figure II-10. Changes to the absorption of 5 μM **3** monitored at 390 nm upon addition of DNA in 5 mM Tris, pH = 7.5, 50 mM NaCl.

Table II-6. DNA binding constants, ΔT_m values, and IC_{50} of **1** – **3**.

Complex	K_b / M^{-1}	ΔT_m / °C [a]	IC_{50} / μM[b]
1	5.9×10^3	10.3	3.4
2	3.4×10^5	7.0	54
3	5.6×10^5	4.2	>600

[a]T_m = 61(1) °C was measured for DNA alone. [b]The value measured for cisplatin under the same experimental conditions is 4.1 μM.

The shift in the melting temperature of 100 μM DNA, ΔT_m, in the presence of each complex (20 μM) was measured relative to that of DNA alone, for which T_m = 61(1) °C (1 mM phosphate buffer, 2 mM NaCl, pH 7.2). The largest shift, ΔT_m = +10(2) °C, was observed for compound **1**, followed by **2** with ΔT_m = +7(2) °C. Only a modest shift in the DNA melting temperature was measured for **3**, ΔT_m = +4(2) °C (Figure II-12). Intercalating complexes possessing a phi (phi = 9,10-phenanthrenequinone diimine) ligand in their coordination sphere, such as $[Rh(phen)_2phi]^{3+}$ and $[Ru(phen)_2phi]^{2+}$, have been shown to raise the melting temperature of the duplex by 7 °C and 11 °C, respectively.[136] Similar stabilization of the DNA double helix has been reported for other intercalators, such as $[Ru(bpy)_2(DAP)]^{2+}$ (DAP = 1,12-diazaperylene) and ethidium bromide.[134] Therefore, it is possible that the shift in T_m observed for **1** is due to DNA intercalation by the complex. Intercalation of molecules between DNA bases is known to increase the viscosity of the solution due to unwinding and elongation of the double helix.[155] Experiments using 1 mM herring sperm DNA in the presence of up to 300 μM of **1** did not result in an increase of the relative viscosity of the solution (Figure II-11). Since relative viscosity measurements are the most reliable means to determine intercalation,[155] these results indicate that the

greater DNA binding constant and ΔT_m value measured for **1** is not due to intercalation.

A possible explanation for these observations is the presence of one and two axial sites available for coordination in **1** and **2**, respectively, while the two rhodium centers in **3** are coordinatively saturated, since the pynp ligands blocks both axial sites in the complex. It is well known that cations, such as Na^+ and Mg^{2+}, stabilize the duplex DNA structure by charge screening through interaction with the anionic phosphate groups in the phosphodiester backbone. It has been previously shown that divalent alkaline earth ions are able to stabilize the duplex structure to a significantly greater extent than monovalent cations.[156-158] For example, the melting temperature of a duplex composed of the sequence d(GCCAGTTAA) and its complementary strand was reported to increase from 32.0 ^oC in the presence of 100 mM NaCl (10 mM Na_2HPO_4, 1 mM Na_2EDTA, pH = 7.0) to 39.0 °C in 100 mM $MgCl_2$ (10 mM sodium cacodylate, pH = 7.0). A similar shift in T_m was measured for the same duplex in the presence of 10 mM $MgCl_2$ (T_m = 36.0 °C), and in mixtures of 100 mM NaCl with 10 mM $MgCl_2$ (T_m = 35.1 °C) and with 100 mM $MgCl_2$ (T_m = 38.5 °C).[159] These results show the greater activity of divalent ions in duplex stablization as compared to monovalent cations. In contrast to the increase in the DNA melting temperature typically observed for divalent alkaline earth ions, transition metal cations, such as Co^{2+}, Ni^{2+}, and Cd^{2+} result in destabilization of the duplex.[160] It is believed that cations which are capable of interacting with the phosphate backbone stabilize the duplex DNA structure, while those that coordinate to the nucleobases exert a destabilizing effect.[160]

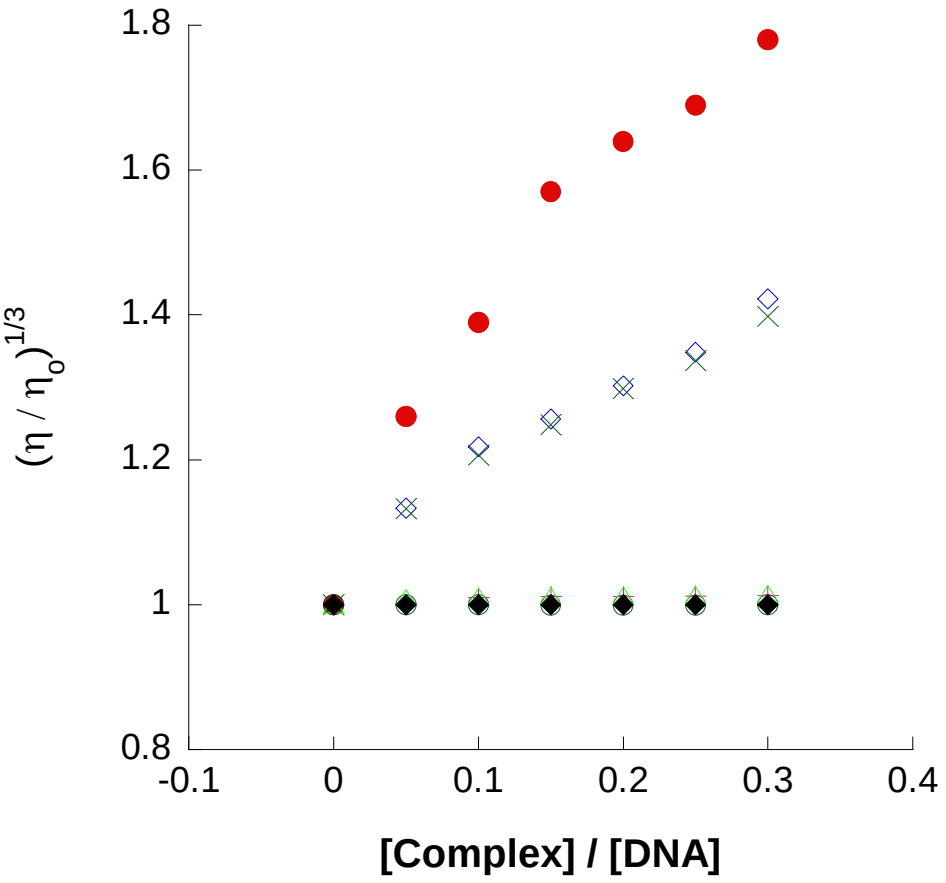

Figure II-11. Relative viscosity measurements of 1 mM sonicated herring sperm DNA (50 mM NaCl, 5 mM tris, pH = 7.5) upon addition of increasing concentrations of ethidium bromide (●), Hoecht 33258 (○), **1** (◊), **2** (×), **3** (+), **4** (Δ) and **5** (♦).

Similarly, non-intercalating mononuclear cationic transition metal complexes that interact with the phosphodiester backbone of duplex DNA exhibit positive ΔT_m values consistent with electrostatic screening of the negative phosphate charges charges.[161, 162] Modest increases in DNA melting temperature, +5 °C, were previously reported for $[Ru(phen)_3]^{2+}$ and $Rh(phen)_3]^{3+}$.[136] Monofunctional cationic complexes, such as $[Pt(NH_3)_3Cl]^+$ and $[Pt(dien)Cl]^+$ (dien = diethylenetriamine) that interact through coordination to the N7 position of guanine typically shift the T_m values to lower temperatures.[163-165] In these systems, however, the destabilization results from conformational changes that take place upon guanine coordination competes with electrostatic screening, thus making shifts in T_m highly dependent on nucleic acid sequence and salt concentration.[164, 165]

Complexes **1** and **2** may be able to efficiently screen the charge on the DNA backbone through axial interactions with the oxygen atoms of the phosphodiester backbone of the duplex, thus resulting in ΔT_m values of +10(2) °C and + 7(2) °C, respectively. The blue-shift in the $Rh_2(\pi^*) \rightarrow Rh_2(\sigma^*)$ transition observed in the absorption spectrum of $Rh_2(\mu\text{-}O_2CCH_3)_4$ upon addition of DNA is indicative of axial coordination,[166] however, due to its neutral charge, no shift in the DNA melting temperature was observed. The lower shift in T_m of **3**, +4 °C, may be due to the inability of the complex to interact effectively with the DNA backbone, thus reducing charge screening.

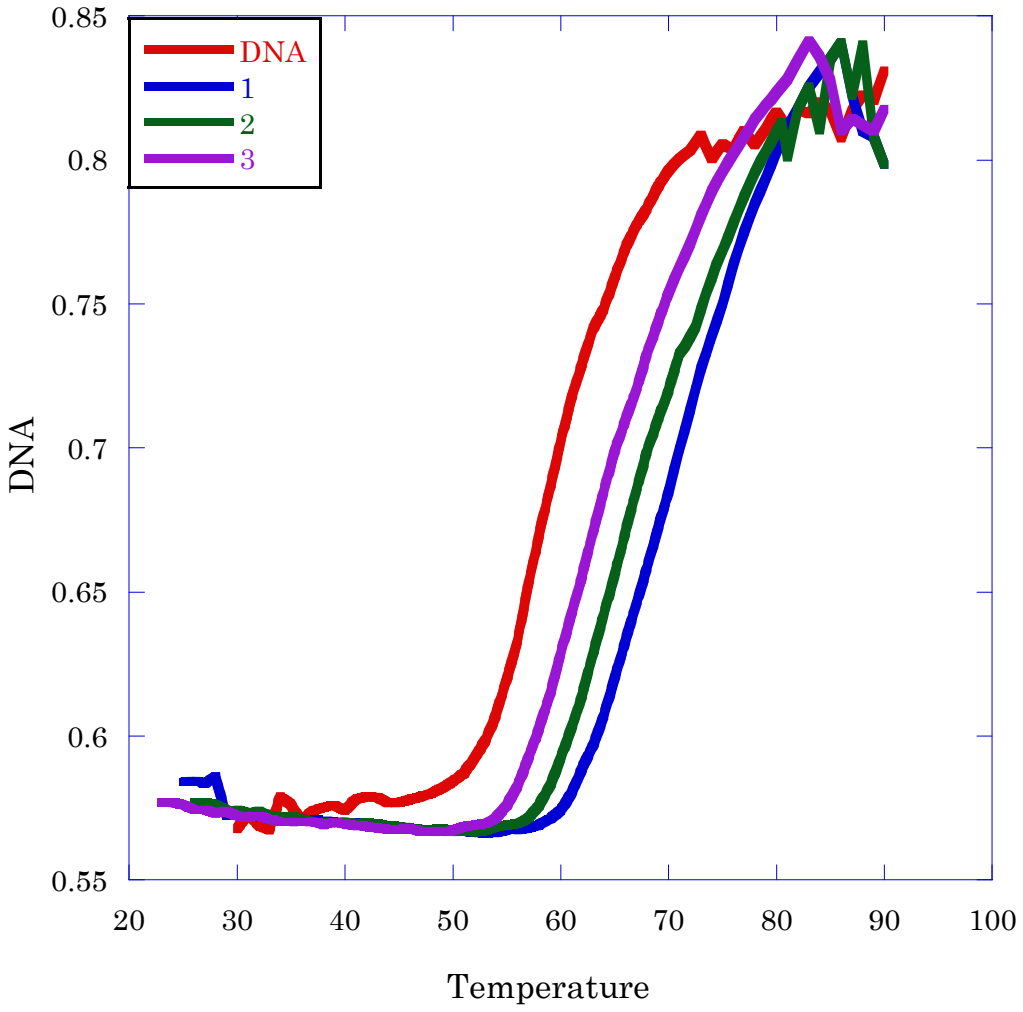

Figure II-12. Melting temperature profile of 100 μM calf-thymus DNA (1mM phosphate, 2mM NaCl, pH = 7.2) alone (▬), and with 20 μM **1** (▬), **2** (▬) and **3** (▬).

Transcription Inhibition

The inhibition of transcription by each metal complex was determined by recording the imaged RNA produced during the transcription reaction as a function of complex concentration, while keeping the concentrations of all other components constant. For complex **1** (Figure II-13), the RNA produced decreases relative to the control lane (no metal complex, Lane 1) as the complex concentration is increased from 1.5 to 7.5 μM (Lanes 2 – 5). In contrast, no decrease in the RNA transcribed is observed upon addition of up to 300 μM of **3** (Figure II-14). The concentration of each complex required to inhibit 50% of the transcription, IC_{50}, was determined from interpolation of plots of percent inhibition as a function of increasing complex concentration. The value of IC_{50} for **1** and **2** are 3.4 μM and 54 μM, respectively, while that of **3** could not be measured but is greater than 300 μM (Table II-6).

A strong correlation between the DNA melting temperature of mononuclear Ru(II) and Rh(III) complexes with transcription inhibition has been previously reported.[136] It is believed that the stabilization of the DNA duplex structure suppresses bubble formation, thus reducing the amount of transcribed RNA. In the present work, this trend is also observed, with an increase in transcription inhibition with greater duplex stabilization.

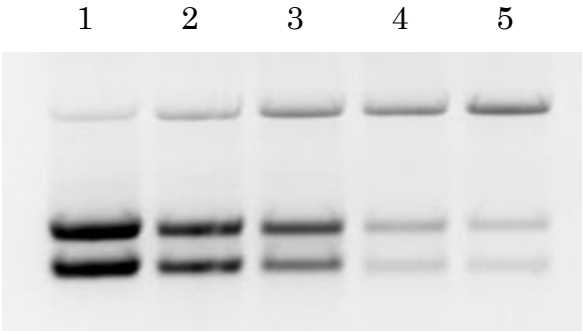

Figure II-13. Ethidium bromide stained agarose gel showing RNA produced in the transcription reaction in the absence (lane 1) and in the presence of 2 μM (lane 2), 4 μM (lane 3), 6 μM (lane 4), and 10 μM (lane 5) complex **1**.

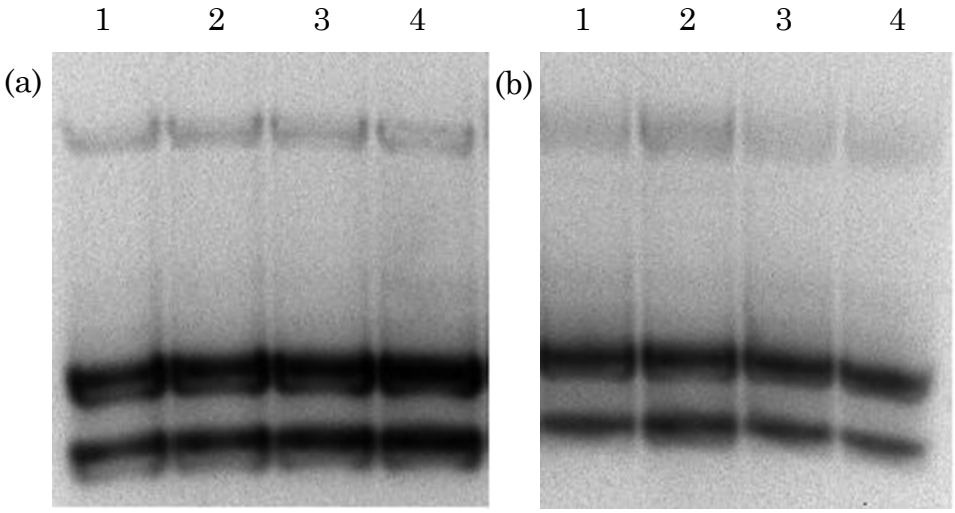

Figure II-14. Ethidium bromide stained agarose gels showing RNA produced in the transcription in the presence of complex **3**: (a) lane 1, 0 μM; lane 2, 10 μM, lane 3, 20 μM; lane 4, 30 μM; (b) lane 1, 0 μM; lane 2, 50 μM; lane 3, 100 μM; lane 4 300 μM.

DNA Photocleavage Experiments

As the data in Figure II-15 attest, compound 1 photocleaves plasmid DNA upon absorption of photons in the visible region ($\lambda_{irr} \geq 395$ nm, 15 min) and in the presence of an electron acceptor (3-CN-1-Me-py$^+$). The control line in Figure II-15 (Line 1), which contains 100 μM pUC18 plasmid alone in the dark, shows the position of the undamaged supercoiled pUC18 plasmid (Form I) with a small amount of nicked, circular DNA (Form II). It is evident from Lanes 2 and 5 that exposure of 100 μM pUC18 plasmid to 25 μM **1** and **3** in the dark, respectively, and in presence of an electron acceptor, does not result in DNA cleavage. Irradiation of 100 μM pUC18 in the presence of 25 μM **1** ($\lambda_{irr} \geq 395$ nm, 15 min) results in the formation of nicked DNA (Form II) as shown in Lanes 3 and 4, either in presence or absence of oxygen, respectively. Compound **3**, with no open axial positions, does not show DNA cleavage in presence or absence of oxygen, as observed from the results in Lanes 6 and 7.

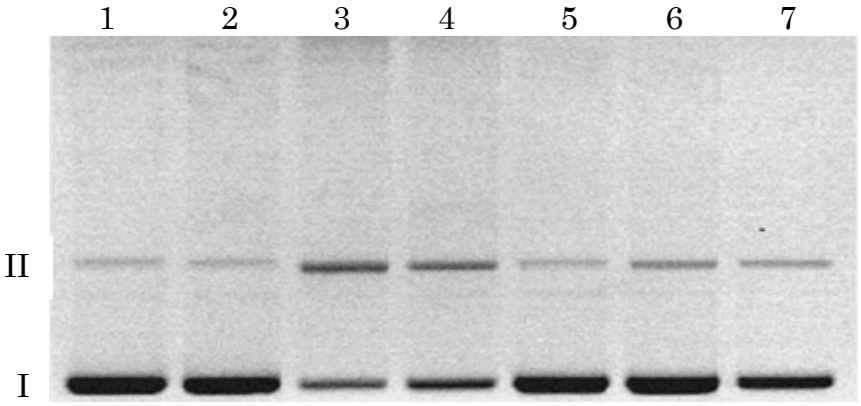

Figure II-15. Ethidium bromide agarose gel (1%) of 100 μM pUC18 plasmid in the presence of 25 μM metal complex in 5 mM Tris, 50 mM NaCl (pH = 7.5) and 2 mM of 3-CN-1-Me-py$^+$, irradiated with $\lambda_{irr} \geq 395$ nm. Lane 1: plasmid only, dark; Lane 2: plasmid + **1**, dark; Lane 3: plasmid + **1**, irr. 15 min in the presence of oxygen; Lane 4: plasmid + **1**, irr. 15 min in the absence of oxygen; Lane 5: plasmid + **3**, dark; Lane 6: plasmid + **3**, irr. 15 min in the presence of oxygen; Lane 7: plasmid + **3**, irr. 15 min in the absence of oxygen.

In Vitro *Cytotoxicity*

The compounds in this study were tested using the MTT cell proliferation assay on two human cell lines, *viz*., HeLa and COLO-316. Cells were incubated with different concentrations of compounds for 24 h and 48 h, determination of a LC_{50} value was not possible due to the low cytotoxicity of these compounds. As shown in Table II-7, none of the compounds are able to kill more than 15% of either cancer cell lines at concentrations as high as 400 μM even at 48 h incubation. It also seems that COLO-316 cells are more sensitive than HeLa cells to this series of compounds (Table II-7).

Table II-7. Percentage of death cells after incubation with compounds **1** – **3** compared with a control of 100 % live cells.

Complex	HeLa		COLO-316	
	24 h	**48 h**	**24 h**	**48 h**
1	10.0 %	13.2 %	11.7 %	14.3 %
2	9.6 %	12.4 %	9.8 %	10.3 %
3	9.6 %	12.3 %	9.1 %	9.9 %

Conclusions

The properties of dirhodium(II,II) complexes that possess one or two accessible axial coordination sites, *cis*-$[Rh_2(\mu\text{-}O_2CCH_3)_2(np)_2]^{2+}$ (**1**) and *cis*-$[Rh_2(\mu\text{-}O_2CCH_3)_2(np)(pynp)]^{2+}$ (**2**), respectively, were compared to a compound in which the axial sites positions are blocked, namely *cis*-$[Rh_2(\mu\text{-}O_2CCH_3)_2(pynp)_2]^{2+}$ (**3**). In the latter compound, the bridging pynp ligand blocks both the axial coordination sites. The electronic and electrochemical properties of the complexes were investigated, and TDDFT calculations were used to aid in the assignments. The ability of the complexes to stabilize duplex DNA and to inhibit transcription *in vitro* show a profound effect on the availability of an axial coordination site on reactivity toward biomolecules.

The importance of the availability of a free axial coordination posititon is also evident from the photocleavage studies. DNA photocleavage activity is only observed with compound **1** in the presence of an electron acceptor, whereas compound **3** does not nick the plasmid DNA. *In cellulo* studies were not conclusive due to the lack of an LC_{50} value. Compounds with LC50 values higher than 500 μM are not very appealing to the medicinal chemistry arena, since they are considered to be no-toxic towards cancer cells. From the MTT assay it could be inferred that compound **1**, with both axial positions free, has the most potential to become cytotoxic. The combine results agree with the fact that an accessible axial position is required for the complex to interact with DNA and/or accomplish biological functions.

CHAPTER III
ROLE OF THE DISTAL SUBSTITUENT ON THE BIOLOGICAL ACTIVITY OF DIRHODIUM (II,II) COMPLEXES*

Introduction

Anti-cancer agents such as actinomycin D,[167-170] anthracyclines,[171-173] daunorubicin,[174-176] and cisplatin,[42, 177] among others[178-189] have been shown to inhibit transcription. In general, the mechanism of transcription inhibition by these drugs takes place via their modification of, interaction with, or damage of template DNA.[42, 167-177] In other cases, the mechanism involves the binding of the drug to the active site of RNA polymerase, blocking of the DNA/RNA channel,[190, 191] or by targeting transcription factors.[192] In recent years, studies have shown that several dirhodium compounds are capable of inhibiting the synthesis of RNA *in vitro* when linear DNA template and T7-RNA polymerase (T7-RNAP) are used.[98, 99]

Studies aimed at unearthing the mechanism of transcription inhibition by dirhodium complexes revealed that this mechanism is dependent on the coordination environment of the dirhodium core, and that it involves the binding of the compound to either the DNA template or the polymerase.[98, 99] Specifically, the complexes $Rh_2(\mu\text{-}O_2CCF_3)_4$, $Rh_2(\mu\text{-}HNCOCF_3)_4$ and $[Rh_2(\mu\text{-}O_2CCH_3)_2(CH_3CN)_6]^{2+}$ appear to inhibit transcription via binding to the enzyme T7-RNAP, whereas $Rh_2(\mu\text{-}HNCOCH_3)_4$ does not proceed in a similar fashion.[99] Table III-1 lists a compilation of the known targets for various transcription inhibitors including dirhodium complexes.

---

*Reprinted in part from "Redox-regulated Inhibition of T7 RNA Polymerase via Establishment of Disulfide Linkages by Substituted DPPZ Dirhodium (II,II) Complexes" J. Dafhne Aguirre, Helen T. Chifotides, Alfredo M. Angeles-Boza, Abdellatif Chouai, Claudia Turro, and Kim R. Dunbar. *Inorg. Chem*. **2009**, *48* (10), 4435 – 4444. Copyright 2009, with permission from the American Chemical Society.

Table III-1. Transcription Inhibition of Various Compounds and their Binding Mechanism.

Compound	Binding
Actinomycin D	DNA Template[181, 193]
Anthracycline	DNA Template[181]
Daunorubicin	DNA Template[181]
Cisplatin	DNA Template[42]
$Rh_2(\mu\text{-}O_2CCF_3)_4$	T7-RNAP[99]
$Rh_2(\mu\text{-}HNCOCF_3)_4$	T7-RNAP[99]
$[Rh_2(\mu\text{-}O_2CCH_3)_2(CH_3CN)_6]^{2+}$	T7-RNAP[99]
$Rh_2(\mu\text{-}O_2CCH_3)_4$	T7-RNAP[98, 99]
cis-$[Rh_2(O_2CCH_3)_2(phen)_2]^{2+}$	T7-RNAP[98]
Rifampicim[a]	DNA/RNA channel[190]
Captan[b]	DNA/RNA channel[191]
Flavopiridol[c]	Transcription factors[169, 185, 192]

[a]Rifampicim is an antituberculosis agent, [b]Captan is a fungicide, [c]Flavopiridol is anticancer and anti HIV agent.

This chapter presents the results of a study aimed at probing the effect of a series of cationic dirhodium complexes on the transcription process. The *cis*-$[Rh_2(\mu\text{-}O_2CCH_3)_2(R_1R_2dppz)_2]^{2+}$ (R_1R_2dppz = substituted dppz; Figure III-1) compounds used in this study are equipped with dppz ligands that have either electron donating or withdrawing substituents on the ring (Figure III-2). A combination of DFT calculations, EPR spectroscopy and electrochemistry were used to probe the electronic/redox effect of the electron withdrawing or donating substituent ligand on the transcription inhibition experiment.

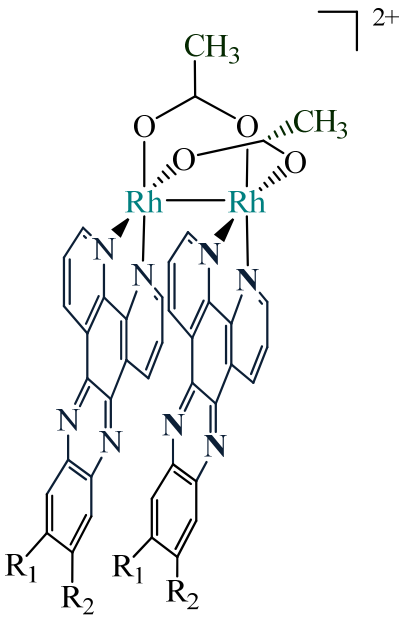

$R_1 = R_2 = H$, **1**
$R_1 = R_2 = OCH_3$, **2**
$R_1 = R_2 = CH_3$, **3**
$R_1 = R_2 = Cl$, **4**
$R_1 = H$, $R_2 = CN$, **5**
$R_1 = R_2 = NO_2$, **6**

Figure III-1. Dirhodium complexes *cis*-$[Rh_2(O_2CCH_3)_2(R_1R_2dppz)_2]^{2+}$.

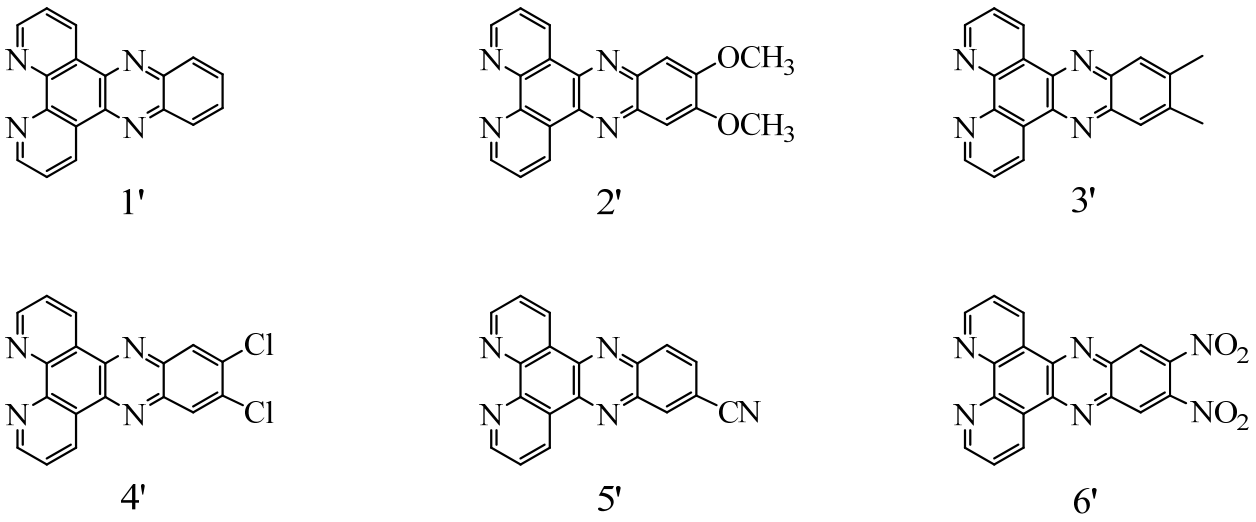

Figure III-2. Structure of ligands described in this chapter.

Experimental Section

Materials

Agarose, ethidium bromide, EDTA, Tris/HCl and RNA loading solution were purchased from Sigma and used as received. The pGEM linear DNA control template (3995 bp) was purchased from Promega; the T7-RNAP (50 units/μL) and 5X RNA transcription buffer were purchased from Invitrogen. The protein marker Precision 'Plus Protein Dual Color Standards' was purchased from Bio-Rad.

The reagents 1,10-phenanthroline, 1,2-phenylenediamine, nitric acid, sulfuric acid and potassium bromide were purchased from Acros. Anhydrous (99.9%) DMF (N,N-dimethylformamide) was purchased from Aldrich. The reagents 4,5-dimethoxy-1,2-phenylenediamine dihydrochloride and 4,5-dichloro-1,2-phenylenediamine were obtained from Alfa-Aesar. The reagents 4,5-dimethyl-1,2-phenylenediamine and 4-cyano-*o*-phenylenediamine were purchased from TCI and Sigma-Aldrich, respectively. The complex $RhCl_3{\cdot}H_2O$ was purchased from Pressure Chemicals. The ligands phendione, dipyrido[3,2-α:2′,3′-*c*]phenazine (dppz),[194] 7,8-dimethyldipyrido[3,2-α:2′,3′-*c*]phenazine (Me_2dppz),[195] 7,8-dinitrodipyrido[3,2-α:2′,3′-*c*]phenazine ($(NO_2)_2$dppz),[196] and 7,8-dichlorodipyrido[3,2-α:2′,3′-*c*]phenazine (Cl_2dppz)[197] were prepared according to published literature procedures. The compounds $Rh_2(\mu\text{-}O_2CCH_3)_4(CH_3OH)_2$[198] and *cis*-$[Rh_2(\mu\text{-}O_2CCH_3)_2(dppz)_2](O_2CCH_3)_2$[103] (**1**) were prepared according to published procedures.[194-197]

Synthesis of *cis*-{$Rh_2(O_2CCH_3)_2[(OMe)_2dppz]_2$}$(O_2CCH_3)_2$ (2)

A solution of $Rh_2(O_2CCH_3)_4$ (161 mg, 0.36 mmol) in acetonitrile (12 mL) was treated with solid $(OMe)_2$dppz (250 mg, 0.73 mmol) and the suspension was refluxed for 24 h under nitrogen. After this time period, the resulting brown solid was collected by filtration in air, washed with acetonitrile and dried under *vacuo* (81% yield). ESI-MS for $\{Rh_2(O_2CCH_3)_2[(OMe)_2dppz]_2\}^{2+}$ *m/z*: 504.1. ^{1}H NMR (CD_3OD), δ (ppm): 1.70 (s, 6H, CH_3CO_2), 2.60 (s, 6H, CH_3CO_2), 4.0 (s, 12H, OMe), 7.10 (s, 4H, dppz), 7.71 (m, 4H, dppz), 8.58 (m, 4H, dppz), 8.98 (m, 4H, dppz). Elemental, Calculated for $Rh_2C_{48}H_{40}N_8O_{12}\cdot 8H_2O$: C 45.36, N 8.82, H 4.44. Found: C 45.00, N 8.91, H 4.25.

Synthesis of *cis*-{$Rh_2(O_2CCH_3)_2(Me_2dppz)_2$}$(O_2CCH_3)_2$ (3)

A solution of $Rh_2(O_2CCH_3)_4(CH_3OH)_2$ (163 mg, 0.32 mmol) in acetonitrile (12 mL) was treated with solid Me_2dppz (200 mg, 0.65 mmol) and the suspension was refluxed for 24 h under nitrogen. The resulting brown-red solid was collected by suction filtration in air, washed with acetonitrile and dried *in vacuo* (84% yield). ESI-MS for $[Rh_2(O_2CCH_3)_2(Me_2dppz)_2]^{2+}$ *m/z*: 472.0 ^{1}H NMR (CD_3OD), δ (ppm): 1.75 (s, 6H, CH_3CO_2), 2.58 (s, 12H, Me), 2.60 (s, 6H, CH_3CO_2), 7.50 (s, 4H, dppz), 7.71 (m, 4H, dppz), 8.60 (m, 4H, dppz), 8.93 (m, 4H, dppz). Elemental, Calculated for $Rh_2C_{48}H_{40}N_8O_8\cdot 10H_2O$: C 41.39, N 8.04, H 3.62. Found: C 41.99, N 8.01, H 3.75.

Synthesis of *cis*-{$Rh_2(O_2CCH_3)_2(Cl_2dppz)_2$}$(O_2CCH_3)_2$ (4)

A solution of $Rh_2(O_2CCH_3)_4(CH_3OH)_2$ (72 mg, 0.14 mmol) in acetonitrile (12 mL) was treated with solid Cl_2dppz (100 mg, 0.28 mmol) and the suspension was refluxed for 24 h under nitrogen. The dark brown product

was collected by suction filtration, washed with acetonitrile and dried in *vacuo* (96% yield). ESI-MS for $[Rh_2(O_2CCH_3)_2(Cl_2dppz)_2]^{2+}$ *m/z*: 512.9 Elemental, Calculated for $Rh_2C_{44}H_{28}N_8O_8Cl_4.7H_2O$: C 38.03, N 8.05, H 2.76. Found: C 38.42, N 8.16, H 2.56.

Synthesis of *cis*-{$Rh_2(O_2CCH_3)_2(CNdppz)_2$}$(O_2CCH_3)_2$ (5)

A solution of $Rh_2(O_2CCH_3)_4$ (100 mg, 0.23 mmol) in acetonitrile (12 mL) was treated with solid CNdppz (139 mg, 0.45 mmol) and the suspension was refluxed for 24 h under nitrogen. The brown solid was collected by suction filtration, washed with acetonitrile and dried *in vacuo* (86% yield). ESI-MS for $[Rh_2(O_2CCH_3)_2(CNdppz)_2]^{2+}$ *m/z*: 469.0. ^{1}H NMR (CD_3OD), δ (ppm): 1.62 (s, 6H, CH_3CO_2), 2.60 (s, 6H, CH_3CO_2), 7.78, 7.95, 8.18, 8.30, 8.72, 8.98, 9.08, 9.18 (dppz). Elemental, Calculated for $Rh_2C_{46}H_{30}N_{10}O_8.3H_2O.CH_3CN$: C 48.17, N 12.87, H 3.03. Found: C 47.95, N 12.30, H 3.11.

Synthesis of *cis*-{$Rh_2(O_2CCH_3)_2[(NO_2)_2dppz]_2$}$(O_2CCH_3)_2$ (6)

A solution of $Rh_2(O_2CCH_3)_4(CH_3OH)_2$ (68 mg, 0.13 mmol) in acetonitrile (12 mL) was treated with solid $(NO_2)_2$dppz (100 mg, 0.27 mmol) and the suspension was refluxed for 24 h under nitrogen. The resulting dark brown/black suspension was cooled to room temperature and filtered. The resulting product was washed with acetonitrile and dried to afford a dark brown solid (91% yield). Elemental, Calculated for $Rh_2C_{44}H_{28}N_{12}O_{16}.4H_2O.CH_3CN$: C 40.63, N 13.39, H 2.59. Found: C 40.91, N 13.77, H 2.68.

Instrumentation

The ^{1}H NMR spectra were recorded on Varian 300 MHz spectrometers and referenced to the residual proton impurities in the relevant deuterated

solvents. The UV absorption measurements were performed with a Shimadzu UV 1601PC spectrophotometer. X-band EPR spectra were recorded on a Bruker EMX spectrometer using a Hewlett-Packard 5352B microwave frequency counter, the ER4102 ST cavity and the Oxford Instruments ESR 900 Cryostat. The ethidium bromide stained agarose gels (1 %) were imaged on an AlphaImager 2000 transilluminator (Alpha Innotech Corporation).

Methods

Cyclic Voltammetric Measurements

Electrochemical measurements were carried out by using an H-CH Electrochemical Analyzer model 620A. The cyclic voltammetric experiments were performed in 99.9% dry dimethylformamide (DMF), with 0.2 M tetra-*n*-butyl ammonium hexafluorophosphate ($TBAPF_6$) as the supporting electrolyte. The working electrode was a BAS Pt disk electrode, the reference electrode was Ag/AgCl (in a saturated NaCl solution) and the auxiliary electrode was a Pt wire.

Density Functional Theory (DFT) Calculations

DFT calculations were performed on the dirhodium complexes **1**-**6** with the hybrid Becke-3 parameter exchange functional and the Lee-Yang-Parr non-local correlation functional (B3LYP) implemented in the Gaussian 98 program suite.[124, 126, 127] Geometry optimizations were carried out using the SDD basis set-relativistic effective core potential (RECP), which combines the Huzinaga–Dunning double-ζ basis set on the main group elements with the Stuttgart–Dresden basis set-RECP combination for the rhodium atoms, while for all other atoms, the 6-311G(d) basis set was

employed.[129] Formate ligands were used instead of acetates in the computationally modeled complexes to simplify the calculations. The molecules were embedded in a dielectric medium as an approximation to include solvent polarization effects. The inclusion of the dielectric medium was considered using the Tomasi's Polarized Continuum Model (PCM) reaction field model for the optimization of the molecular geometry.[199, 200] All calculations were performed on an Altix 3700 128-processor SGI computer or a p575 640-processor IBM computer located at the Laboratory for Molecular Simulations at Texas A&M University.

Transcription Inhibition Experiments

In vitro transcription experiments were conducted by triplicate using T7-RNAP (2.3 units). The DNA template was the pGEM linear plasmid (120 μM bases) which results in two transcripts of length 1065 and 2346 bases. The transcription reaction was performed for 45 min at 37 ºC using transcription buffer (40 mM Tris/HCl pH = 8.0, 8 mM $MgCl_2$, 25 mM NaCl), 1.0 mM of each ATP, CTP, GTP and UTP. The inhibition of mRNA production by the dirhodium compounds was detected *in vitro* by the measurement of the RNA generated upon addition of increasing amounts of metal complex to the assay. The concentration of each complex at which 50% of the RNA is transcribed, IC_{50}, was calculated by interpolation of the integrated areas of the imaged RNA signal of each lane of the gel conducted with various concentrations of a given complex. All stock solutions of the metal complexes were prepared in 1% DMSO in double-distilled H_2O (ddH_2O). For the experiments, the metal stock solutions were diluted 100 fold with ddH_2O making them 0.01% in DMSO. Control experiments indicate

that the amount of DMSO introduced into each transcription assay does not interfere with the process. All water used during the assay and for dilution of the compounds was nuclease free grade. The concentration of T7-RNAP purchased from Invitrogen was determined by measuring the absorbance at 280 nm with an extinction coefficient ε_{280} = 1.4 x 10^5 M^{-1} cm^{-1};[201, 202] the T7-RNAP concentration in each well for the transcription assays was approximately 10 μM.

Electrophoretic Mobility Shift Assay

Aliquots of 1.5 μL of T7-RNAP were incubated with the dirhodium complexes at a concentration equal to their IC_{50} value calculated from the transcription inhibition assay (for each complex), 3.5 μL transcription buffer and water to a total volume of 15 μL. After incubation for 1 hour at 37 °C, the samples were mixed with 5X loading buffer and loaded on a non-denaturing 10% polyacrylamide gel. Electrophoresis was run at 120 V for a period of 5 hours. The gel was stained with Brilliant Blue solution and subsequently imaged.

Results and Discussion

Synthesis and Characterization

The dirhodium complexes **1-6** were prepared by refluxing $Rh_2(\mu\text{-}O_2CCH_3)_4(CH_3OH)_2$ with the appropriate dppz ligand (Figure III-3); the reactions involve substitution of two acetate groups on the dirhodium core by the unsubstituted/substituted dppz ligands (Figure III-2).

Complexes **1-6** were characterized by MS, ^{1}H NMR and UV spectroscopies. The UV/Vis data for the ligands from the present or previous spectroscopic studies are listed in Table III-2. The absorption bands of the ligands and the complexes in the 360-370 nm region are assigned to dppz π-π* ligand centered (LC) transitions. Stronger LC transitions are observed at energies higher than 300 nm. Apart from the LC transitions, the complexes exhibit several broad and intense bands that may are assigned as MLCT bands.

Electrochemistry

Electrochemical data for the dppz ligands are summarized in Table III-3. As expected, substitution of positions 7,8 of dppz with electron withdrawing groups (Cl, CN and NO_2) results in less negative reduction potentials as compared to unsubstituted dppz, whereas electron donating groups (OMe, Me) in the same positions have the opposite effect.[203, 204] For the investigated region in DMF (1.3 – -2.0 V), the ligands CNdppz and $(NO_2)_2$dppz, exhibit two reversible reduction processes (Table III-3). All of the other ligands, namely Cl_2dppz, dppz, $(OMe)_2$dppz and $(Me)_2$dppz exhibit a single reversible one-electron reduction process.

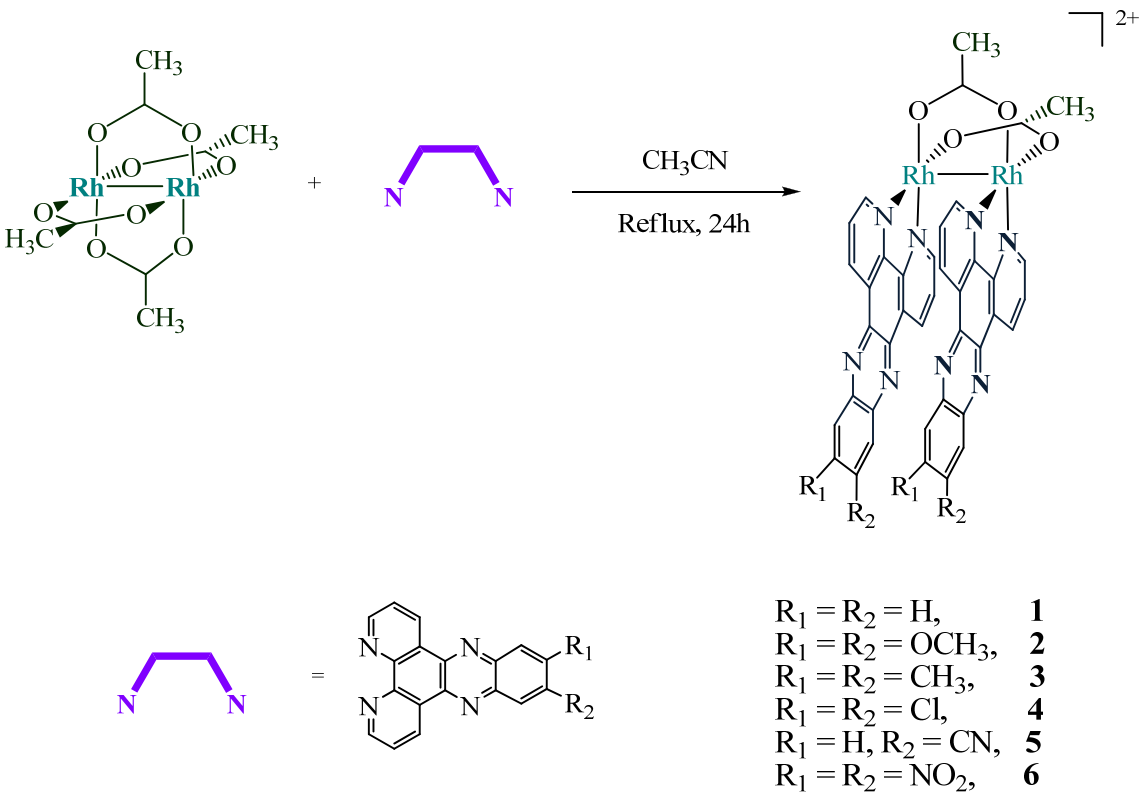

Figure III-3. Schematic representation of the syntheses of compounds **1** – **6**.

Table III-2. Electronic absorption data for Dppz ligands and dirhodium complexes

Compound	λ_{max}/nm ($\varepsilon/10^4 M^{-1}$ cm^{-1})	Solvent	Ref.
$(OMe)_2$dppz	280 (3.62), 379 (1.22), 400 (2.23)	CH_2Cl_2	Pres. work
2	213 (7.96), 295 (9.0), 396 (3.75)	MeOH	Pres. work
Me_2dppz	274 (6.11), 347 (0.75), 355 (0.95), 366 (1.39), 374 (1.22), 386 (1.82)	CH_2Cl_2	197,203
3	210 (63.2), 285 (10.68), 380 (18.7)	MeOH	Pres. work
dppz	269 (5.12), 343 (0.91), 351 (1.01), 360 (1.23), 368 (1.11), 379 (1.29)	CH_2Cl_2	203
1	203 (6.94), 276 (8.64), 363 (1.52), 434 (0.55)	H_2O	103
Cl_2dppz	272 (5.39), 370 (1.54), 391 (2.13)	CH_2Cl_2	197
4	218 (3.5), 279 (6.85), 371 (1.56), 391 (1.55)		Pres. work
CNdppz	271 (5.86), 295 (3.79), 305 (2.7), 367 (1.7), 387 (1.8)	CH_2Cl_2	Pres. work
5	211 (9.81), 271 (16.87), 347 (2.89)	MeOH	Pres. work
$(NO_2)_2$dppz	228 (5.45), 233 (5.25), 249 (4.40), 293 (2.01), 304 (1.67), 389 (0.61)	CH_2Cl_2	196
6	284 (9.77), 387 (2.18)	MeOH	Pres. work

The ligand-based reduction potentials of complexes **1**-**6** are expected to follow the same trend as the corresponding ligands. It is well established that, for complexes with ligand-based reductions, binding of the metal centers shifts the reductions to more positive potentials[197, 203, 205] thus giving rise to the corresponding order **2** < **3** < **1** < **4** < **5** < **6** for the ease of reduction for the series of dirhodium compounds under investigation.

Table III-3. Electrochemical reduction potentials (vs. Ag/AgCl) in dry DMF for substituted Dppz ligands.

L	E_{red} (V)[a]
$(OMe)_2$dppz	–1.25
Me_2dppz	–1.14
dppz	–1.06
Cl_2dppz	–0.83
CNdppz	–0.74, –1.50
$(NO_2)_2$dppz	+0.10, –0.27

[a]The reduction potentials were measured in dry DMF with a Ag/AgCl reference electrode. All reduction processes were reversible.

Transcription Inhibition

The effect of the distal substituent on the efficiency of each dirhodium complex to inhibit transcription was studied using a T7-RNA polymerase transcription system. Due to the fact that the compounds are not very soluble in water, a study about the effect of the solvent on the transcription reaction was performed (Figure III-4). Solvents in which usually dirhodium compounds are the most soluble were chosen to perform this assay. Different percentages of acetonitrile, DMSO and methanol were used. A concentration of up to 3.5% DMSO used for the transcription reaction does not cause a significant reduction in the transcription efficiency (Figure III-4).

The inhibition of transcription was determined by recording the imaged RNA produced during the transcription reaction as a function of complex concentration, while keeping the concentrations of all other components constant. Figure III-5 shows a typical imaged gel obtained for *cis*-$\{Rh_2(O_2CCH_3)_2(Cl_2dppz)_2\}(O_2CCH_3)_2$ (**4**); the produced RNA decreases relative to the control lane (no metal complex, lane 1) as the complex concentration increases (lanes 2 – 5). The IC_{50} values, the concentration of each complex required to inhibit 50% of the transcription in vitro, are listed in Table III-4. For the sake of comparison, the transcription inhibition assay was conducted in the presence of increasing amounts of cisplatin and dirhodium tetraacetate. The measured IC_{50} values for cisplatin and dirhodium tetraacetate are 10.9 and 13.6 μM, respectively under the same experimental conditions as for compounds **1**-**6**.

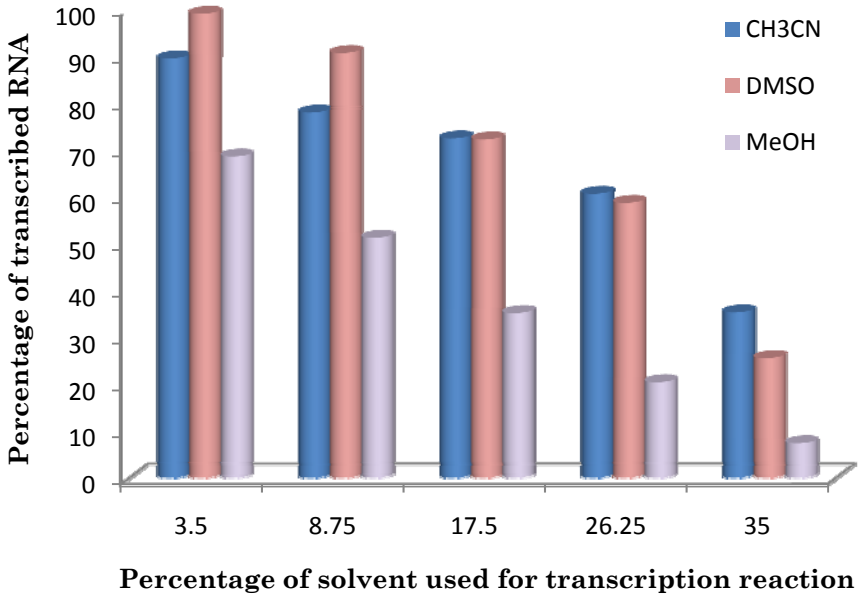

Figure III-4. Solvent effect on the transcription reaction.

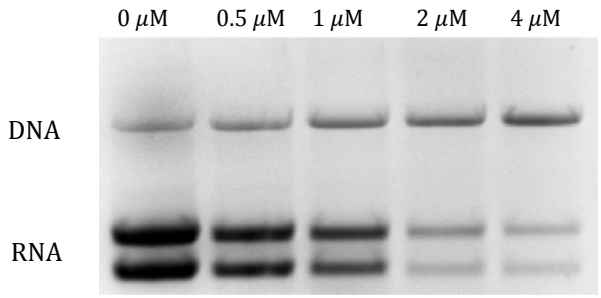

Figure III-5. Ethidium bromide stained agarose gel (1%) of transcribed RNA produced from the transcription reaction in the absence (lane 1; control) and in the presence of increasing concentrations of compound **4** in μM.

Table III-4. *IC50* values for compounds **1**-**6**.

Complex	L	*IC50* (μM)[a]
2	$(OMe)_2$dppz	1.1
3	Me_2dppz	1.5
1	dppz	2.0
4	Cl_2dppz	2.4
5	CNdppz	2.5[b]
6	$(NO_2)_2$dppz	3.2

[a]The complex solutions were prepared in 1% DMSO/99% H_2O; The *IC50* values recorded for cisplatin and dirhodium tetraacetate under the same experimental conditions are 10.9 and 13.6 μM, respectively. [b]If the complex is dissolved in 1% MeOH/99% H_2O, the *IC50* value is the same.

An assessment of the *IC50* values for the complexes studied in this chapter (Table III-4) reveals that a higher concentration of dirhodium complex is required to inhibit the transcription reaction as the substituents on the dppz ligand become more electron-withdrawing. A mechanism of transcription inhibition that involves binding of complexes **1**-**6** to the DNA was ruled out for several reasons. Previous studies in our laboratories with the unsubstituted bis dppz complex *cis*-$[Rh_2(\mu\text{-}O_2CCH_3)_2(dppz)_2]^{2+}$ showed that it does not intercalate between the DNA bases.[103] Additionally, binding of **1**-**6** to the NTP's can be ruled out as a mechanism of transcription inhibition because each NTP is present in large excess (1 mM) relative to the concentration of the metal complexes (< 5 μM) in the transcription assays. The aforementioned observations for **1**-**6** along with the good electron-accepting properties of dppz,[203, 206, 207] led us to consider an alternative

mechanism of transcription inhibition involving redox reactions with the cysteine residues of T7-RNA.

Interaction of Dirhodium Complexes with Sulfhydryl Groups

The T7-RNA polymerase, a relative easy and fairly well studied system,[208-214] has 12 cysteine residues in the free sulfhydryl forms.[202, 215] Studies have shown that substitution of seven of these residues with serine residues can be accomplished without considerable reduction of the activity, while substitution of the remaining five resulted in complete loss of activity.[216] Moreover, reactions of the enzyme with sulfhydryl binding compounds such as iodoacetamide[217, 218] or p-hydroxymercuribenzoate[219] resulted in complete inactivation of the T7-RNAP enzyme as well. Given this information, the interaction of the complexes with cysteine was studied by assessing their effect on the cysteine residues of T7-RNAP by PAGE mobility shift assay. These studies were complemented with an analysis of the product of reduction of the compounds after interaction with cysteine by ESI-MS spectrometry.

Formation of disulfide bonds in T7-RNAP after incubation with the dirhodium complexes at a concentration equal to their IC_{50} at 37 ºC for 1h, was evaluated by polyacrylamide gel electrophoresis under non-reducing conditions. Migration on the PAGE gel is sensitive to modifications in the conformation of the protein. Formation of intraprotein disulfide bonds between proximal cysteine thiol groups[220, 221] and other oxidized related species such as sulfenic (S-OH)/sulfinic (SO_2H) acids and disulfide S-oxide,[220, 221]leads to species that migrate slightly slower on the gel than the reduced enzyme.[222] Formation of high molecular weight species such as trimers is

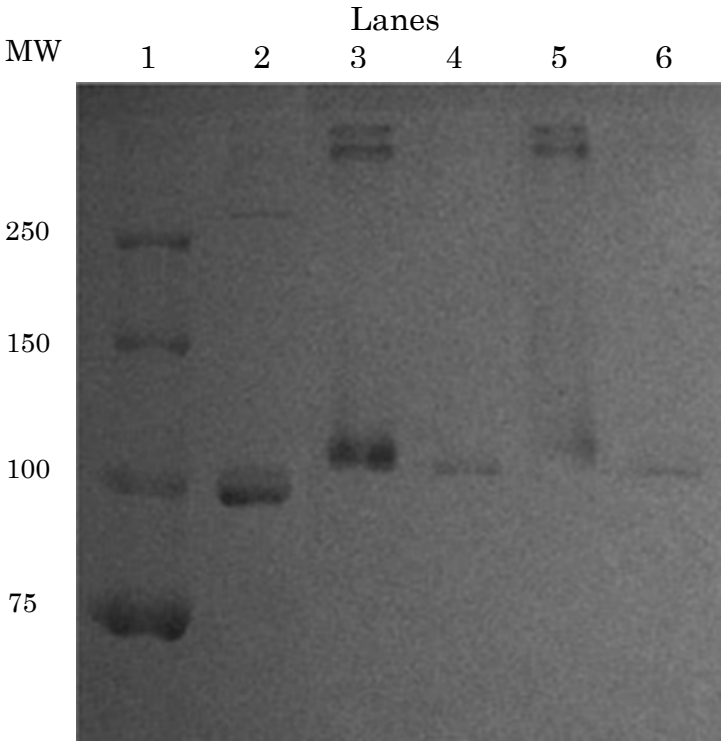

Figure III-6. PAGE non-denaturing gel; Protein marker (lane 1; labeled on the side in kDa); T7 RNPA incubated at 37 ºC (lane 2); T7 RNPA incubated at 37 ºC in the presence of **1** (lane 3); T7 RNPA incubated at 37 ºC in the presence of **1** followed by addition of DTT (dithiothreitol) (lane 4); T7 RNPA incubated at 37 ºC in the presence of **2** (lane 5); T7 RNPA incubated at 37 ºC in the presence of **2** followed by addition of DTT (lane 6).

also possible due to the formation of interprotein disulfide bonds between the cysteine thiol groups on the surface of T7-RNAP.[220] For the dirhodium species under investigation, the formation of all of the aforementioned high molecular species is feasible to conclude from the data in Figure III-6.

Figure III-6 shows a native PAGE gel of the reaction product after incubation of T7-RNAP with compounds **1** and **2**. In lanes 3 and 5, the product of reaction of the compound and the enzyme migrates slightly slower as compared to the native enzyme in lane 2. Additionally, at the top of these lanes, two new bands appear at higher molecular weights (> 250 kDa) than T7-RNAP. Upon addition of the reducing agent dithiothreitol (DTT) to the incubated reaction solutions of the dirhodium compounds (lanes 4 and 6), the intermolecular disulfide cross-links responsible for the high molecular weight bands of the T7-RNAP disappear, thus indicating that the interprotein disulfide bonds are completely cleaved by reduction. The oxidation products in the bands close to the 100 kDa marker are only partially reversed. Similar results for the PAGE gels were recorded for complexes **3**-**6**. These findings indicate that the oxidation products formed between T7-RNAP and complexes **1**-**6** are partially or completely reversible.

The oxidizing capability of complexes **1**-**6** was also monitored by mass spectrometry. Accordingly, each complex was reacted with cysteine in a 1:1 ratio and the resulting paramagnetic reduction products were immediately subjected to mass spectrometry analysis. Addition of cysteine to the red-brown dirhodium solutions leads to the instantaneous appearance of an intensely colored blue/violet solution with an intense absorption band at ~ 800 nm. An analogous intense blue color was previously reported for the

reduced dirhodium species $[Rh_2(O_2CCH_3)_2(bpy)_2(MeCN)_2]^+$.[141] The ESI-MS spectra for these reactions contains a peak corresponding to the $[Rh_2(\mu\text{-}O_2CCH_3)_2(R_1R_2dppz)_2(Cyst) + 1]^+$ species (Figure III-7). The appearance of this peak suggest that the dirhodium product is axially coordinated to the cysteine thiol, which leads to an electron transfer to the dirhodium species to form the radical species $[Rh_2(O_2CCH_3)_2(Me_2dppz)_2]^{\bullet+}$. Subsequently the thiyl radical ($RS^{\bullet}$) is released and couples with another thiyl radical to form the cysteine disulfide product (RS-RS).[221, 223] As has been suggested in other cases, thiol oxidation can also take place in two steps through oxidation to the sulfenic acid (S-OH) or the disulfide S-oxide.[220, 221, 223]

Density Functional Theory (DFT) Calculations

Electronic structure calculations were conducted on the cations $[Rh_2(O_2CCH_3)_2(R_1R_2dppz)_2]^{2+}$ (R_1 and R_2 defined in Figure III-1) to assess the effect of the R_1R_2 groups of the dppz ligands on the molecular orbitals of **1**-**6**. As indicated from the results in Table III-5 and visualized from the orbitals depicted in Figure III-8, in general, all of the complexes possess LUMO orbitals that are primarily of ligand (dppz) character (> 95%), with **1**-**3** having a slightly higher metal contribution as compared to **4**-**6** which possess electron-donating substitutents on the dppz ligand (Table III-5). In particular, it is obvious that the LUMO orbitals of the complexes are phenazine-centered[203, 206, 207] with the percent phenazine contribution increasing as the electron-donating character of the dppz-substituents increases (Table III-6).

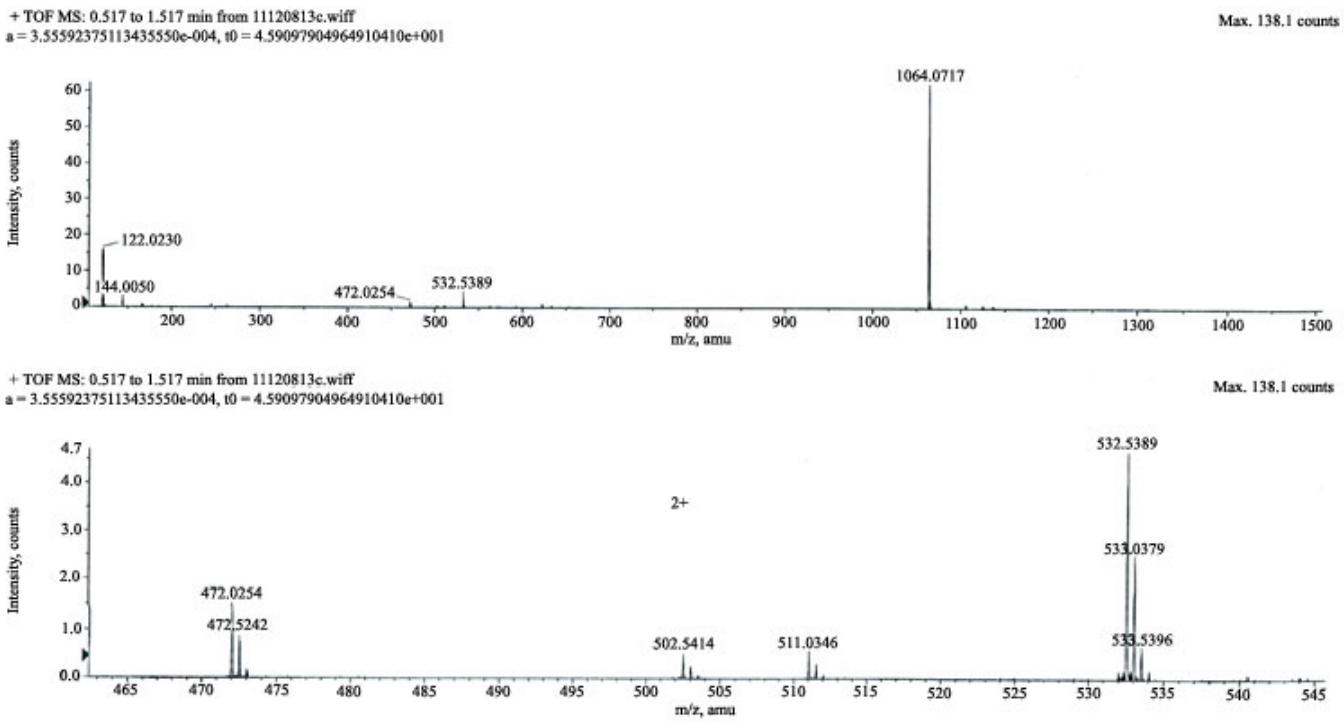

Figure III-7. ESI-MS spectrum for the reaction of $[Rh_2(O_2CCH_3)_2(Me_2dppz)_2]^{2+}$ with cysteine [peak at *m/z* 1064 corresponding to $[Rh_2(O_2CCH_3)_2(Me_2dppz)_2(Cyst) + 1]^+$.]

Compound	HOMO	LUMO
2	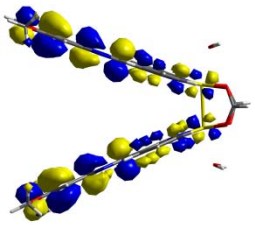	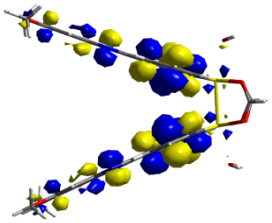
3	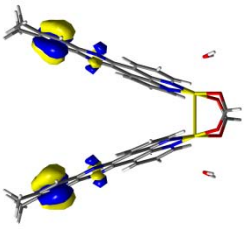	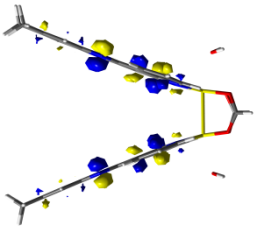
1	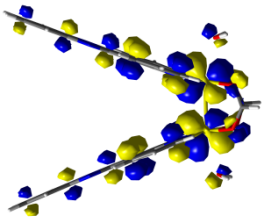	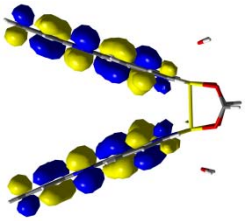
4	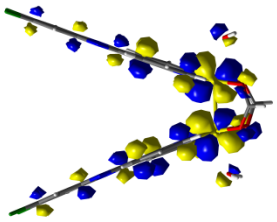	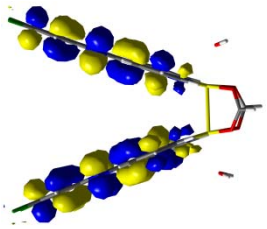
5	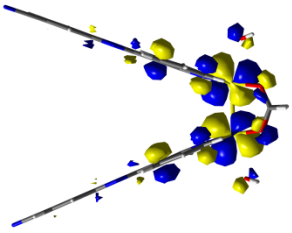	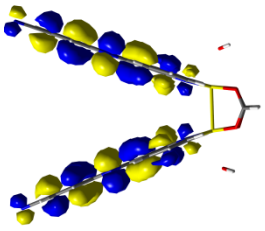
6	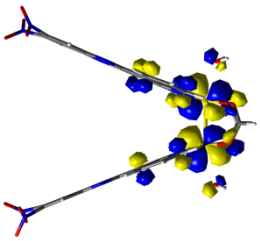	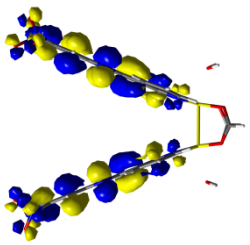

Figure III-8. HOMO and LUMO Orbitals for Compounds **1**-**6**.

Table III-5. Metal orbital contribution to the HOMO's and LUMO's of **1**-**6**.

Complex	L	HOMO (%)	LUMO (%)
2	$(OMe)_2$dppz	6.7	4.3
3	Me_2dppz	0.4	1.7
1	dppz	74.8	1.2
4	Cl_2dppz	73.8	0.6
5	CNdppz	79.7[a], 79.8[b]	0.6,[a] 0.6[b]
6	$(NO_2)_2$dppz	82.4	0.4

[a]Calculated for the *anti* isomer. [b]Calculated for the *syn* isomer.

Table III-6. Phenazine orbital contribution to the LUMO's of complexes **1**-**6**.

Complex	L	phenazine (%)
2	$(OMe)_2$dppz	51.3
3	Me_2dppz	75.9
1	dppz	80.7
4	Cl_2dppz	87.2
5	CNdppz	87.8,[a] 69.5[b]
6	$(NO_2)_2$dppz	90.8

[a]Calculated for the *anti* isomer. [b]Calculated for the *syn* isomer.

Conclusions

In the present study, the combined application of electrochemical, spectroscopic, computational and biochemical methods has established that the dirhodium complexes *cis*-$[Rh_2(O_2CCH_3)_2(R_1R_2dppz)_2]^{2+}$ (R_1R_2dppz = substituted dppz, Figure III-1) comprise a sensitive redox-regulated series of T7-RNAP inhibitors. The behavior can be readily tuned by changing the electron–withdrawing or –donating ability of the dppz substituents which affects the ease of the complex reduction and ultimately their reactivity with the T7-RNAP accessible thiol groups. The process of transcription is inhibited *in vitro* by small amounts of **1**-**6** via formation of intra- and inter-protein disulfide bonds that affect the critical sulfhydryl cysteine groups of the T7-RNAP. The dominant phenazine character of the LUMO orbitals for the complexes **1**-**6** was corroborated by electronic structure calculations which demonstrated that the unpaired electron is completely delocalized in the phenazine orbitals in the case of **4**-**6** which possess electron withdrawing substituents on the dppz ligands. The high sensitivity of these dirhodium complexes and the potential to tune their redox activity towards T7-RNAP by modifying the dppz substituents render them promising candidates for the control and/or inhibition of other important biochemical processes.

CHAPTER IV
MONOSUBSTITUTED DIRHODIUM (II,II) COMPLEXES : TARGETING NUCLEAR DNA*

Introduction

Dirhodium carboxylate complexes are among the most promising non-platinum compounds known to date, but the mechanism of their antitumor activity has not been elucidated.[69, 71, 106, 112, 224, 225] The first study aimed at revealing the cellular target(s) of these complexes focused on the binding affinity of $Rh_2(\mu\text{-}O_2CCH_3)_4$ towards biological relevant molecules such as DNA, ribonuclease, and albumin among others.[69, 71] The experiment revealed the affinity of $Rh_2(\mu\text{-}O_2CCH_3)_4$ as follows: poly-C < native DNA ≤ poly-G < albumin < denature DNA < ribonuclease A << poly-A.[69] Because of this result, native DNA was dismissed as a possible target in a cellular environment for all dirhodium complexes,[225-227] not taking into account the differences in reactivity among the distinct dirhodium compounds.

In 2005, a study aimed at investigating the interactions of ds-DNA and dirhodium carboxylate compounds revealed that $Rh_2(\mu\text{-}O_2CCH_3)_4$, $Rh_2(\mu\text{-}O_2CCF_3)_4$, and $[Rh_2(\mu\text{-}O_2CCH_3)_2(CH_3CN)_6]^{2+}$ are capable of forming DNA interstrand crosslinks.[97] It was also observed that other adducts, namely monofunctional and intrastrand adducts, are formed during the reaction

---

*Reprinted in part from "Live Cell Cytotoxicity Studies: Documentation of the Interactions of Antitumor Active Dirhodium Compounds with Nuclear DNA" J. Dafhne Aguirre, Alfredo M. Angeles-Boza, Abdellatif Chouai, Jean-Philippe Pellois, Claudia Turro, and Kim R. Dunbar. *J. Am. Chem. Soc.* **2009**, *131* (32), 11353 – 11360. Copyright 2009, with permission from the American Chemical Society.

between these complexes and DNA. The adducts formed between DNA and the dirhodium core most likely involve the full variety of coordination modes observed in model complexes, including *axial*/*axial* (*ax*/*ax*), *axial*/*equatorial* (*ax*/*eq*), and *equatorial*/*equatorial* (*eq*/*eq*).[96, 97] All these experiments, however, were performed in cell free media using a 123 bp DNA sequence, and the issue that they could reach nuclear DNA was still under debate.

It is possible to increase the affinity of a dirhodium complex for DNA by attaching a small organic molecule that will impart the compound with properties that differ from the parent $Rh_2(\mu\text{-}O_2CCH_3)_4$. The ligand dppz has been shown to be an effective ligand for binding to DNA, by interacting through intercalation,[102, 228, 229] which is a mode of binding characteristic of a large number of drugs that target DNA. The intercalating driving force added to the charge of the dirhodium compounds and their ability to form covalent interactions with DNA,[230] render it possible to design compounds with different biological properties and improved cytotoxicity.

The research described in this chapter involves the reactivity of a series of complexes $[Rh_2(\mu\text{-}O_2CCH_3)_2(\eta^1\text{-}O_2CCH_3)(L)]^+$, where L= bpy (2,2'-bipyridine) (**1**), phen (1,10-phenanthroline) (**2**), dpq (dipyrido[3,2-f:2',3'-h]quinoxaline) (**3**), dppz (dipyrido[3,2-a:2',3'-c]phenazine) (**4**), dppn (benzo[i]dipyrido[3,2-a:2',3'-c]phenazine) (**5**) and dap (4,7-dihydrodibenzo[de,gh][1,10]phenanthroline) (**6**) (Figure IV-1) with DNA in cell free medium as *in cellulo*. The effect of the diimine ligand on the biological properties of the compounds, the impact of the hydrophobicity as well as the effect of glutathione on the *in cellulo* activity of these complexes were also explored.

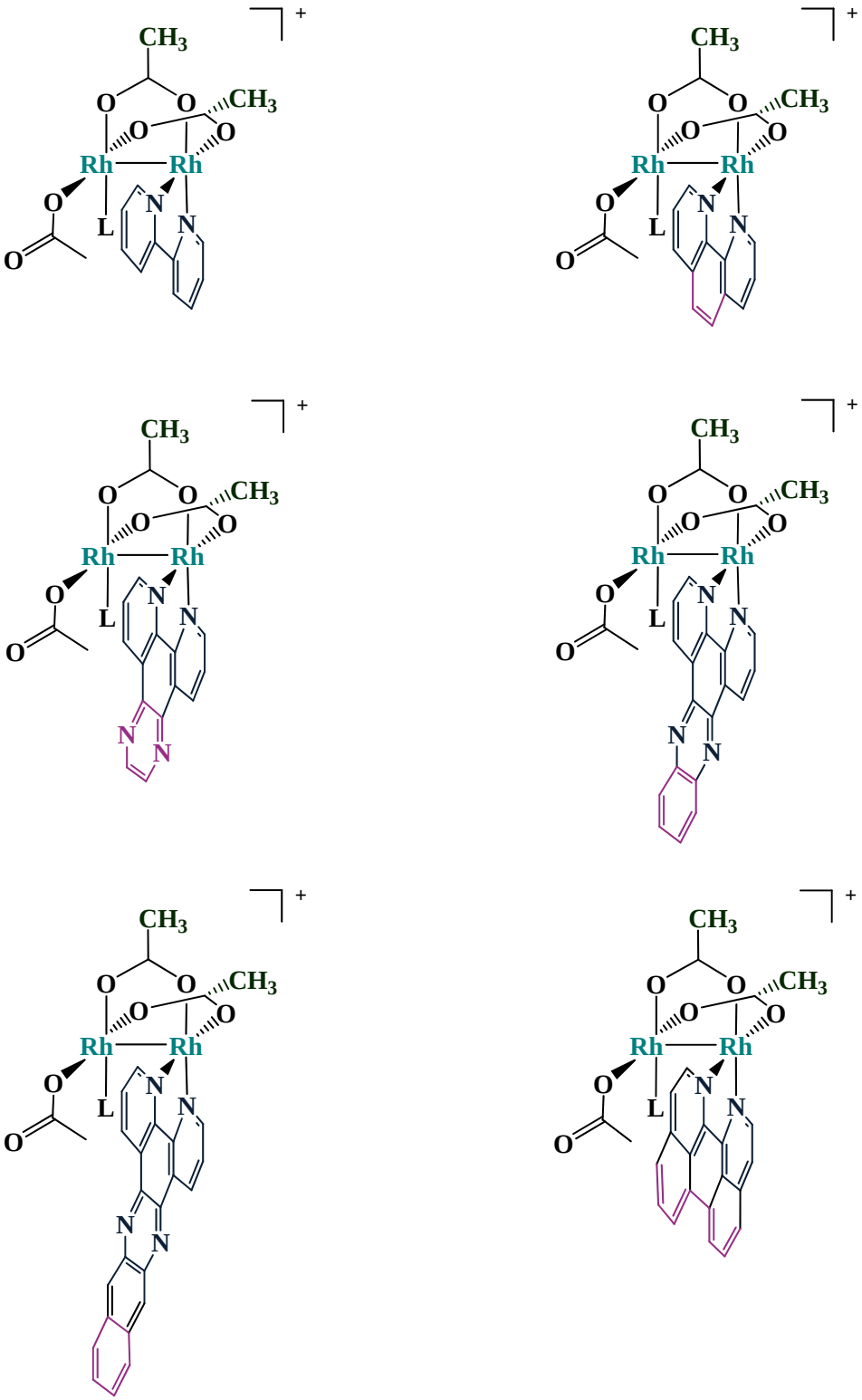

Figure IV-1. Structures of Compounds **1**-**6** (L = CH_3OH).

Experimental Section

Materials

The reagents 2,2′-bipyridine (bpy), 1,10-phenanthroline (phen), diaminoethylene and 2,3-diaminonaphthalene were purchased from Acros. Calf thymus DNA, ethidium bromide, Hoechst 33258, n-octanol, 1,10-phenantroline-5,6-dione, L-buthionine-sulfoximine (BSO) and *N*-acetyl-L-cysteine (NAC) were purchased from Sigma-Aldrich and used as received. The circular plasmid pUC18 was purchased from Fermentas. The DNA oligonucleotide (5'-ATCACCTAAAATGGCG-3') and its complementary strand were purchased from The Midland Certified Reagent Company (Midland, TX) as pure materials. The starting material $RhCl_3.H_2O$ was purchased from Pressure Chemicals and was used as received.

The ligands pyrazino[2,3-f][1,10]phenanthroline (dpq),[231] dipyrido[3,2-*a*:2′,3′-*c*]phenazine (dppz),[232] benzodipyrido[3,2-*a*:2′,3′-*c*]phenazine (dppn),[233] and 4,7-dihydrodibenzo [de,gh][1,10]phenanthroline (dap)[234] were synthesized according to reported procedures.[231-234] The complexes $Rh_2(\mu\text{-}O_2CCH_3)_4$,[198] cis-$[Rh_2(\mu\text{-}O_2CCH_3)_2(\eta^1\text{-}O_2CCH_3)(bpy)(CH_3OH)](O_2CCH_3)$ (**1**),[117] cis-$[Rh_2(\mu\text{-}O_2CCH_3)_2(\eta^1\text{-}O_2CCH_3)(phen)(CH_3OH)](O_2CCH_3)$ (**2**),[117] cis-$[Rh_2(\mu\text{-}O_2CCH_3)_2(\eta^1\text{-}O_2CCH_3)(dppz)(CH_3OH)](O_2CCH_3)$ (**4**),[102, 104] cis-$[Rh_2(\mu\text{-}O_2CCH_3)_2(\eta^1\text{-}O_2CCH_3)(dppn)(CH_3OH)](O_2CCH_3)$ (**5**)[235] and cis-$[Rh_2(\mu\text{-}O_2CCH_3)_2(\eta^1\text{-}O_2CCH_3)(dap)(CH_3OH)](O_2CCH_3)$ (**6**)[230] were all prepared according to previously described procedures.

Synthesis of *cis*-[$Rh_2(\mu\text{-}O_2CCH_3)_2(\eta^1\text{-}O_2CCH_3)(dpq)(CH_3OH)][O_2CCH_3]$ (3)

A suspension of dpq (200 mg, 0.86 mmol) and $Rh_2(\mu\text{-}O_2CCH_3)_4(CH_3OH)_2$ (381 mg, 0.86 mmol) in acetone (30 mL) was stirred at room temperature under N_2 for 48 h. The resulting green precipitate was collected by filtration in air and washed with acetone (3 × 5 mL). The solid was suspended in CH_3OH (50 mL) and stirred at room temperature for 24 h. The resulting green solution was filtered and concentrated under reduced pressure to 2 mL, and the product was precipitated by addition of Et_2O. The green solid was collected by filtration, washed with Et_2O, and dried *in vacuum* (260 mg, 47%). ESI-MS: *m*/*z* 646.93 ($[Rh_2(\mu\text{-}O_2CCH_3)_2(\eta^1\text{-}O_2CCH_3)(dpq)(CH_3OH)]^+$) 614.85 ($[Rh_2(\mu\text{-}O_2CCH_3)_2(\eta^1\text{-}O_2CCH_3)(dpq)]^+$). ^1H NMR (CD_3OD) δ (ppm): 1.07 (s, 3H, CH_3CO_2), 1.88 (s, 3H, CH_3CO_2), 2.34 (s, 3H, CH_3CO_2), 2.40 (s, 3H, CH_3CO_2), 3.31 (s, 3H, CH_3OH), 8.14 (m, 2H, dpq), 8.86 (dd, 2H, dpq), 9.22 (s, 2H, dpq), 9.643 (m, 2H, dpq). Anal. Calc.: C, 38.95; H, 3.27; N, 8.66. Found: C, 39.27; H, 4.09; N, 8.41.

Instrumentation

The ^1H NMR spectra of the new complexes were recorded on a Varian spectrometer at 300 MHz and referenced to the residual proton impurities in the deuterated solvents. Mass spectra were acquired on a PE SCIEX QSTAR Pulsar electrospray ionization mass spectrometer at Texas A & M University. Elemental analyses were performed by Atlantic Microlab Inc., P.O. Box 2288, Norcross, GA 30091. The UV-visible measurements were performed on a UV-1601PC Shimadzu spectrophotometer or on a Cary 100 Bio Thermal UV/vis Spectrometer equipped with a Cary temperature

controller for thermal denaturation studies. The ethidium bromide stained agarose gels were imaged on an Alpha Imager 2000 transilluminator (Alpha Innotech Corporation). Confocal microscopy was performed using an Olympus IX81 Confocal microscope.

Methods

DNA Binding Constant Determination

Binding titration experiments were performed by titrating a fixed concentration of calf thymus DNA (120 μM) and increasing the concentration of metal complex (0 to 100 μM) in 5 mM Tris/HCl buffer, pH 7.5, 20 mM NaCl. The dilution of metal complex concentration at the end of each titration was negligible. The DNA binding constant, K_b, was determined from fits of the change in the absorption of each complex as a function of the DNA concentration using eq 1,[103]

$$\frac{\varepsilon_a - \varepsilon_f}{\varepsilon_b - \varepsilon_f} = \frac{b - (b^2 - 2K_b{}^2 C_t [DNA]_t / s)^{1/2}}{2K_b C_t} \quad (1)$$

where $b = 1 + K_b C_t + K_b [DNA]_t / 2s$, C_t and $[DNA]_t$ represent the total complex and DNA concentrations, respectively, s is the base pair binding site size, and ε_a, ε_f, and ε_b represent the apparent, free complex, and bound complex molar extinction coefficients, respectively. The value of ε_b was determined from the plateau of the DNA titration at which point addition of DNA did not result in further changes to the absorption spectrum.

Relative Changes in Viscosity Studies

The relative change in viscosity was measured using an Ubbelodhe viscometer maintained at constant temperature (27 °C) in a thermostatic bath. Sonicated herring sperm DNA (200 μM), 5mM Tris/HCl, 20 mM NaCl,

pH 7.5, and increasing concentrations of complexes were used.[134] Data are presented as:

$$(\frac{\eta}{\eta_\circ})^{1/3} \text{ vs } \frac{[M]}{[DNA]}$$

$$\eta = t_1 - t_2$$

$$\eta_0 = t_n - t_0$$

where η is viscosity of DNA in the presence of the complex and η_0 is viscosity of DNA in the absence of complex.

Melting Temperature Experiments

Melting temperature experiments were recorded by measuring the absorbance at 260 nm. The experiment was performed using 20 μM complex and a 100 μM solution of DNA (5'-ATCACCTAAAATGGCG-3') in 1 mM phosphate buffer, 2 mM NaCl at a pH of 7.2. The value of T_m was determined as the temperature corresponding to a maximum on the first-derivative profile of the melting curves.[103, 134]

Electrophoretic Mobility Shift Assay

Aliquots of 50 μM native pUC18 were incubated in the dark with different compound concentrations (5, 10 and 25 μM) at room temperature using a 10 mM phosphate buffer. After incubation for 24 h, electrophoresis was carried out using 1% agarose gel, 1X TAE buffer (40 mM tris-acetate, 1 mM EDTA, pH ~ 8.2). The applied voltage was 40 V and the gels were run for a period of 16 h. After electrophoresis, the gels were stained with 0.5 mg/L ethidium bromide and imaged under UV light.[236-239]

Partition Coefficient Determination

The lipophilicity of the complexes was determined by the "shake flask" method using a pH 7.4 phosphate buffer (0.129 M NaCl) and *n*-octanol as solvents.[240] Each compound was dissolved in the phase in which it is most soluble, resulting in typical concentrations of 50 to 350 μM. Duplicate determinations using three different solvent ratios were performed for each complex. Following mixing and phase separation according to literature methods,[240] each phase was analyzed for solute content and the concentration was determined using spectrophotometric methods. All the *n*-octanol/water partition coefficients were determined by UV/vis spectroscopy. Octanol and buffer solutions were pre-saturated with each other prior to use. Fifty rotations were performed by hand followed by one hour of settling time. Equilibration and absorption measurements were made at 20 °C.[235]

Cell Culture

The HeLa cell line was obtained from the American Type Culture Collection, cell line CCL-2. COLO-316 cell line was kindly provided by Robert Burghardt (Texas A&M, Department of Veterinary Anatomy and Public Health). Both cells lines were cultured in Dulbecco's modified Eagle medium, containing 10% fetal bovine serum (Invitrogen), 50 μg/mL gentamicin, 4.5 mg/mL glucose, and 4 mM L-glutamine (Invitrogen). Cell cultures were incubated in a humidified atmosphere containing 5% CO_2 at 37 °C.

***In Vitro* Cytotoxicity**

The viability of COLO-316 and HeLa cells in the presence of the compounds under investigation was tested using the 3-(4,5-dimethylthiazol-2-yl)-2,5-diphenyltetrazolium bromide (MTT) assay[241] (Invitrogen).

Subconfluent (50-80% confluent) monolayers of cells at a concentration of 5000-10000 cells/μL were used. Cells were plated in 96-well sterile plates, at a density of 20-30 cells/ μL (volume of 100 μL per well) and were pre-incubated for 48 h. After the cells reached 100% confluency, the medium was replaced by 100 μL of L-15 medium containing different complex concentrations. The plates were incubated for 24 hours. 10 μL of fresh MTT solution was added, followed by incubation for 4 hours. A 100 μL aliquot of fresh SDS solution in 0.01 M HCl was added, and after 16 hours of incubation absorbance at 570 nm was measured using a Bio-Rad plate reader.

Alkaline Comet Assay

Single cell gel electrophoresis was performed using a commercially available kit (R&D Systems). HeLa cells were incubated with metal complexes at a concentration that allows for 75% viability. After 4 h, cells were harvested and embedded in 0.75% low-melting point agarose at a volume of 1:10 on microscope slides. Cells were lysed in the dark for a minimum of 1 h at 4 °C. Cells were incubated in an alkaline solution containing NaOH (0.3 M), for a period of 1 h. Electrophoresis was performed for 30 min, at 28 V, in TBE buffer (pH=13). After electrophoresis, the cells were stained with SYBR® green dye and imaged using an inverted microscope. A total of 100 cells were scored per sample, using the CometScore® software.[242]

Glutathione Modulation

COLO-316 cells were plated in 96-well sterile plates, at a density of 20-30 cell/μL (volume of 100 μL per well) and were pre-incubated for 48 h. After the cells reached 100% confluency, the medium was replaced by 100 μL of

fresh medium containing either 500 μM of L-buthionine-sulfoximine (BSO) or 5 mM of *N*-acetyl-L-cysteine (NAC). Incubation with NAC was performed for a period of 2 h whereas BSO-containing plates were incubated overnight. After the respective incubation period, cells were washed twice with sterile PBS and L-15 medium containing a concentration of the dirhodium complex corresponding to its LC_{50} was added and cells incubated overnight. To assess cell viability, an MTT assay was performed as described above.

SYTOX® Blue Assay

HeLa cells, at a concentration of 5000-10000 cell/µL, were harvested, 75 μL of cells were seeded in an 8-well sterile plate, and 125 μL of fresh medium was added to give a total volume of 250 μL. Cells were pre-incubated at 37 °C. After 24 h, cells were washed with sterile PBS and the medium was replaced by 250 μL of L-15 medium containing the different complexes at their LC_{50} concentration. Plates were incubated for 4 h after which time they were treated with 5 μL of a 5 mM SYTOX® Blue solution and incubated for 5 minutes before imaging.

Cell Morphology Changes

HeLa cells at a concentration of 5000-10000 cell/µL were harvested, 75 μL of cells were plated in two 8-well sterile plates, and 125 μL of fresh medium was added to give a total volume of 250 μL. Cells were pre-incubated at 37 °C. After 24 h, cells were washed with sterile PBS and the medium was replaced by 250 μL of L-15 medium containing complex **4** at its LC_{50} concentration. Imaging was performed at different times for a total time of 4 hours.

Results and Discussion

Syntheses and Characterization of the Mono-Substituted Dirhodium Complexes

Compounds **1**, **2**, **4**, **5** and **6** have all been reported previously.[102, 104, 117, 230, 235] The *cis*-[$Rh_2(\mu\text{-}O_2CCH_3)_2(\eta^1\text{-}O_2CCH_3)(dpq)(CH_3OH)](O_2CCH_3)$ (**3**) compound was synthesized in ~ 47% yield by the reaction of $Rh_2(\mu\text{-}O_2C_2H_3)_4(CH_3OH)_2$ with 1 equivalent of the dpq ligand (Figure IV-2). The reaction was performed in two steps. Solvent, temperature and time for the first step are all important factors for the overall yield. The mixture was not heated in order to avoid the formation of the bis-substitued derivative or other undesired by-products. The preparation of mono-substituted compounds using CH_2Cl_2 has also been reported, but, in this case, acetone was the solvent of choice because the reaction is less temperature sensitive with this solvent. The reaction mixture was stirred for 48 h, an optimal reaction time for maximum yield. During the course of the reaction, a green precipitate was obtained, which is the intermediate $Rh_2(\mu\text{-}O_2CCH_3)_2(\eta^2\text{-}O_2CCH_3)(\eta^1\text{-}O_2CCH_3)(dpq)$ in which an acetate ion that occupies an *ax* and an *eq* positions of one rhodium atom. After the intermediate was stirred in methanol for 24 h, the chelating acetate group is displaced by methanol and the diimine ligand rearranges to an *eq*/*eq* binding mode as found in the final product.

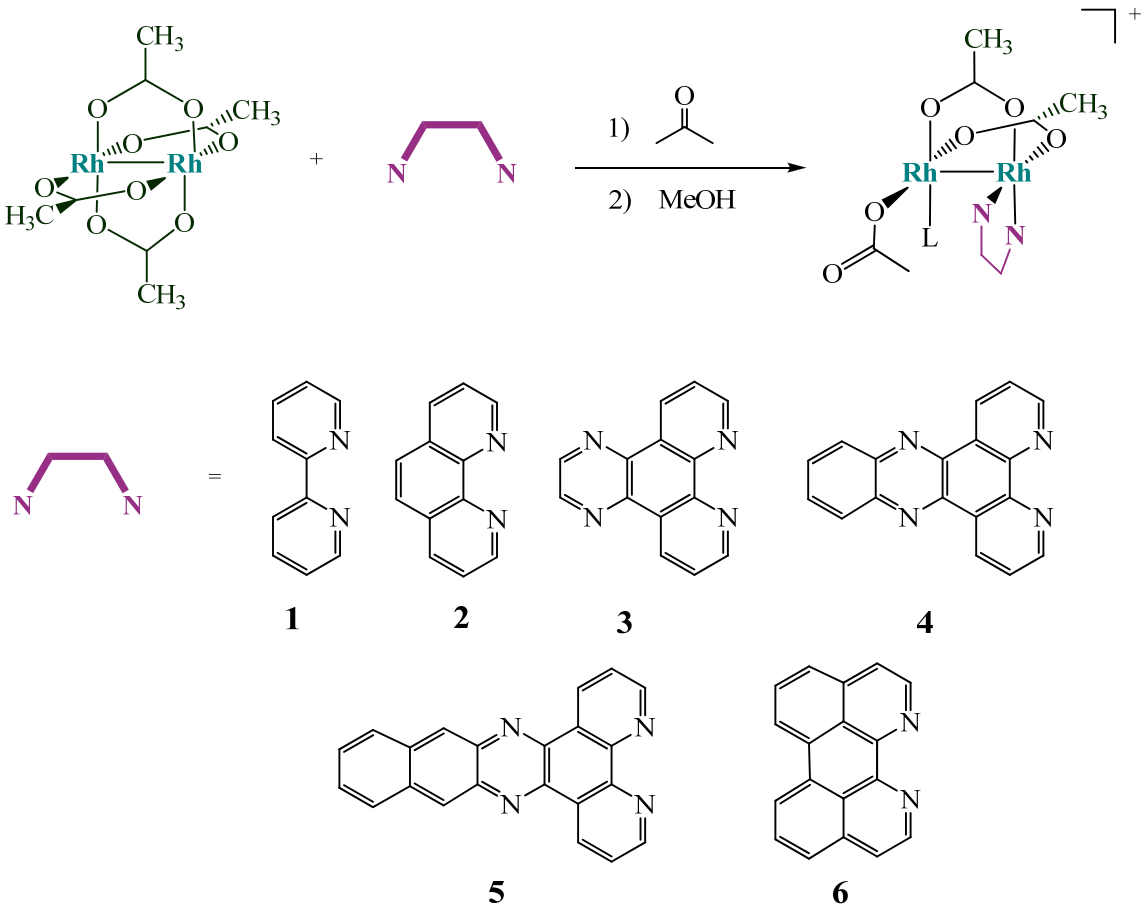

Figure IV-2. Schematic representation of the synthesis of compounds **1**-**6** (L = CH_3OH).

Interactions with DNA in Cell Free Media

The binding constants (K_b) of this family of dirhodium complexes were measured by titrating a fixed concentration of DNA with increasing concentrations of complex. The K_b values (Table IV-1) were determined from fits of the change in the absorption of each complex as a function of the DNA concentration. As expected, compounds **4** and **5**, *viz*., those with the largest intercalating ligands, interact with DNA to the greatest degree with binding constants, K_b, of 4.4×10^5 M^{-1} and 9.7×10^5 M^{-1}, respectively. These values are typical for metal complexes that bind to DNA *via* intercalation. For example, values of $K_b = 1.24 \times 10^5$ M^{-1} and $K_b = 2.0 \times 10^5$ M^{-1} were reported for $[Ru(NH_3)_4(dppz)]^{2+}$,[229] and $[(\eta^6\text{-}C_6Me_6)RuCl(dppz)]^+$,[228] respectively. Similarly, **3** and **6** exhibit binding constants of the same order of magnitude (Table IV-1). The values of K_b for **1** (3.2×10^4 M^{-1}) and **2** (3.2×10^4 M^{-1}) are an order of magnitude lower than the other members of the series. Metal complexes that exhibit binding constants of the same order of magnitude as **1** and **2** have been identified in the literature as intercalating agents,[243] but an inspection of the structure of the two compounds clearly reveals that it would be impossible for these compounds to intercalate without a major change in the ligand binding.

Table IV-1. DNA binding constants and ΔT_m of compounds **1**-**6**

Compound	K_b, M^{-1}	ΔT_m, °C
1	3.2×10^4	2 ± 1
2	3.2×10^4	4 ± 1
3	3.5×10^5	16 ± 1
4	4.4×10^5	18 ± 1
5	9.7×10^5	24 ± 1
6	3.6×10^5	10 ± 1

[a] Binding constants were measured using 1 mM phosphate buffer, 2 mM NaCl, pH 7.2. [b] Melting temperature experiments were performed using 1 mM phosphate buffer, 2 mM NaCl, pH 7.2.

The melting temperature, T_m, of a 16^{mer} DNA sequence (5'-ATCACCTAAAATGGCG-3') in the presence of 20 μM of each complex was measured and compared to that of DNA alone, which is T_m = 53 °C (Figure IV-3). When a compound intercalates into DNA it stabilizes the base stacking which leads to an increase in the DNA melting temperature. The largest difference in melting temperature was recorded for compound **5** (ΔT_m = 24 °C), which has the largest planar surface area in the series. Compounds **1** and **2** with less extended planar ligands show a modest shift, +2 °C and +4 °C, respectively, which is likely due to the ionic character of the compounds. These shifts are comparable to values obtained for species such as $[Ru(tpy)(bpy)OH_2]^{2+}$ (ΔT_m = 2 °C), and $[Ru(tpy)(phen)OH_2]^{2+}$ (ΔT_m = 7.2 °C) that are known to interact with DNA solely through electrostatic interactions.[244] Compounds **3**, **4**, and **6** also exhibit large ΔT_m values (> 10 °C). The values obtained in the present study are in accordance with those observed in the literature for intercalators.[137] For example, the known

metallointercalators $[Rh(phi)_2phen]^{3+}$ and $[Ru(phi)_2phen]^{2+}$, (phi = 9,10-phenanthrenequinone diimine), increase the melting temperature of a 15-mer duplex by 21 °C and 15 °C, respectively.[137] It is important to note that compound **6** has been previously reported to have a change of ΔT_m = -6 °C, but, in this case, compound **6** was first covalently bound to one of the strands of the DNA sequence and then the product was annealed to its complementary strand.[230]

Relative viscosity measurements have proven to be a reliable method for the assignment of the mode of binding of compounds to DNA.[155] Intercalation of molecules between DNA bases causes a change in the relative viscosity of solutions due to the unwinding and elongation of the double helix.[155] For compounds **1** and **2**, no change in the relative viscosity was observed after their addition. This behavior is similar to what one observes with the minor groove binder Hoescht 33258.[245] The addition of compounds **3-4** and **6** increases the relative viscosity of the solution, although to a lesser extent than the changes observed with ethidium bromide.[245] Similar increases in relative viscosity have been documented for other intercalating metal complexes, for example $[(\eta^6\text{-}C_6Me_6)RuCl(dpq)](CF_3SO_3)$ and $[(\eta^6\text{-}C_6Me_6)RuCl(dppz)](CF_3SO_3)$.[228] Finally, compound **5** produces a larger change in the viscosity of DNA as compared to other members of the series with behavior that is similar to the change observed with the intercalator EtBr[153, 154] (Figure IV-4).

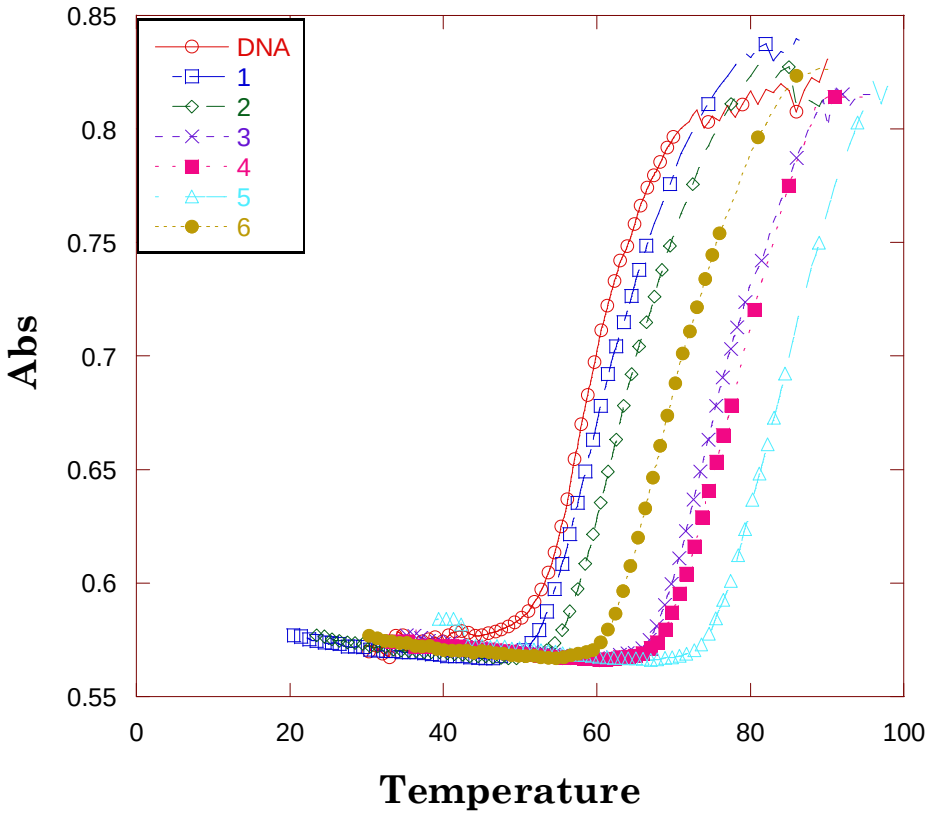

Figure IV-3. Melting profile of compounds **1**-**6**. DNA (○), **1** (□), **2** (◊),**3** (×),**4** (■), **5** (△) and **6** (●).

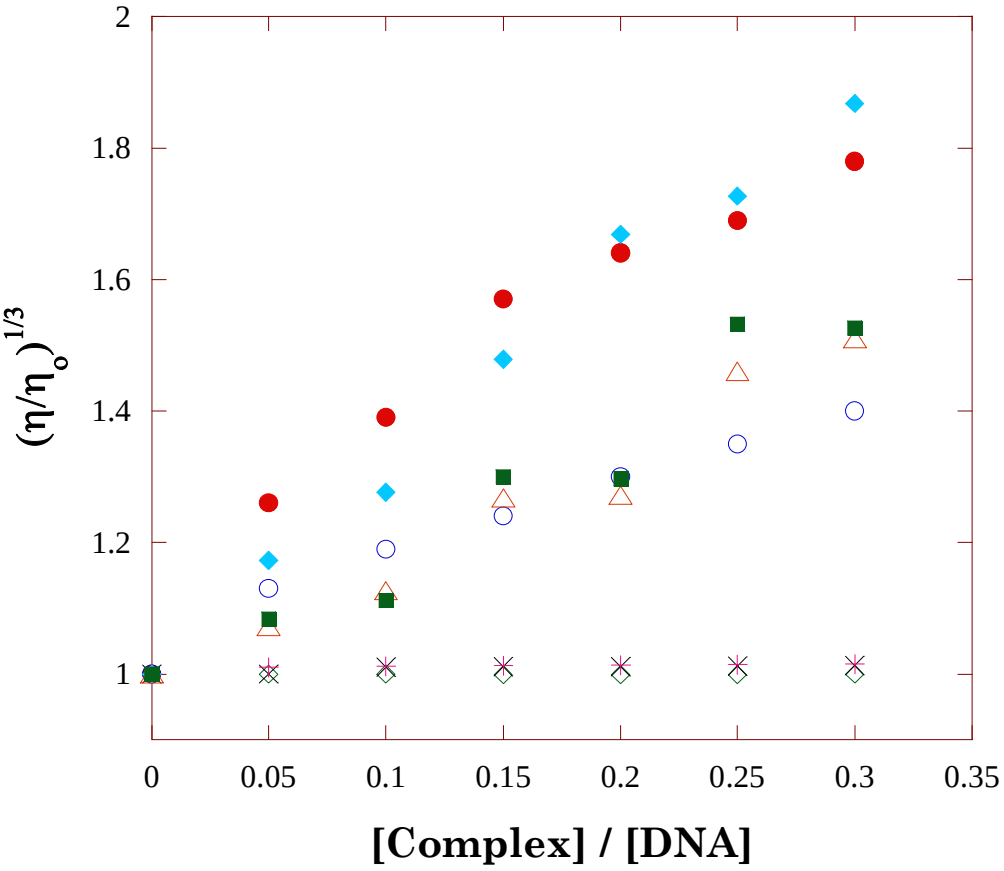

Figure IV-4. Relative viscosity changes of solutions containing 200 μM sonicated herring sperm DNA as the concentration of EtBr (●), **1** (×), **2** (+), **3** (△), **4** (○), **5** (◊), **6** (■) and Hoechst 33258 (◊) is increased.

To further evaluate the formation of adducts with DNA, an electrophoretic mobility shift assay (EMSA) was performed.[236, 237] The binding of molecules such as methylating[246] or intercalating agents[236, 237] to the covalent closed circular (CCC) plasmid DNA generates topoisomers that will migrate at different rates. As the binding increases, the mobility of the CCC topoisomer decreases. In the case of compounds that can potentially both intercalate and bind covalently to DNA, it has been observed that the migration increases as the binding mode progresses from monofunctional (covalent) binding to bifunctional (covalent and intercalating) binding.[238] The incubation was performed in the dark to avoid DNA cleavage by the compounds. This was particularly important for compound **5**, as it is known to be a photocleavage agent.[103] After 24 h of incubation, the solution was loaded into a 1% agarose gel and electrophoresis was carried out for a period of 16 h. The electrophoresis voltage was maintained at a low value (40 V) to ensure a visible shift of the formed adducts. As evidenced by a shift of the DNA on the electrophoresis gel (Figure IV-5 and Figure IV-6), all of the dirhodium complexes in the series were found to form DNA adducts. The most significant shifts were observed with compounds **4** and **5** (Figure IV-5). Compounds **1** and **2** show some degree of interaction although to a lesser extent than the other member of the series (Figure IV-6). Similar shifts have been reported in the literature for the parent compound $Rh_2(\mu\text{-}O_2CCH_3)_4(CH_3OH)_2$.[247]

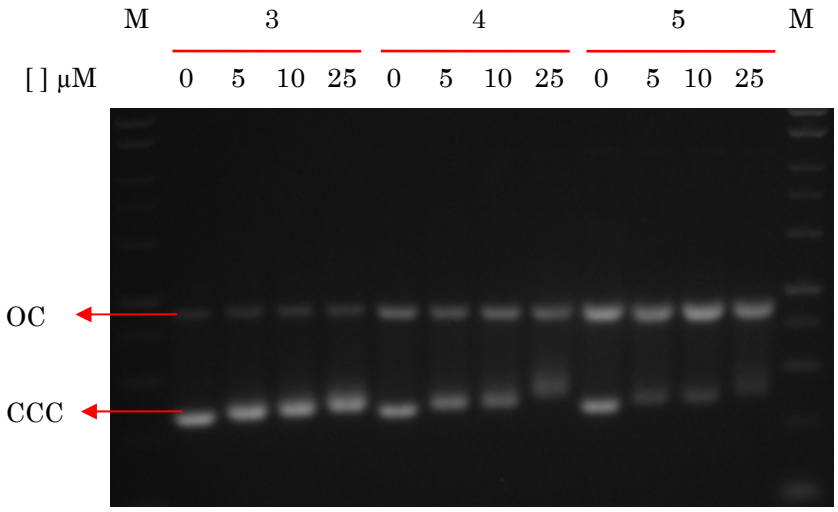

Figure IV-5. Ethidium bromide agarose gel (1%) 100 µM pUC18 incubated with compounds **3-5** at different concentrations. Lane 1, 14: Standard 1 kb leader marker. Lane 2, 6, 10: Native pUC 18, control. Lane 3-5: increasing amounts of compound **3**. Line 7-9: increasing amounts of compound **4**. Line 11-13: increasing amounts of compound **5.**

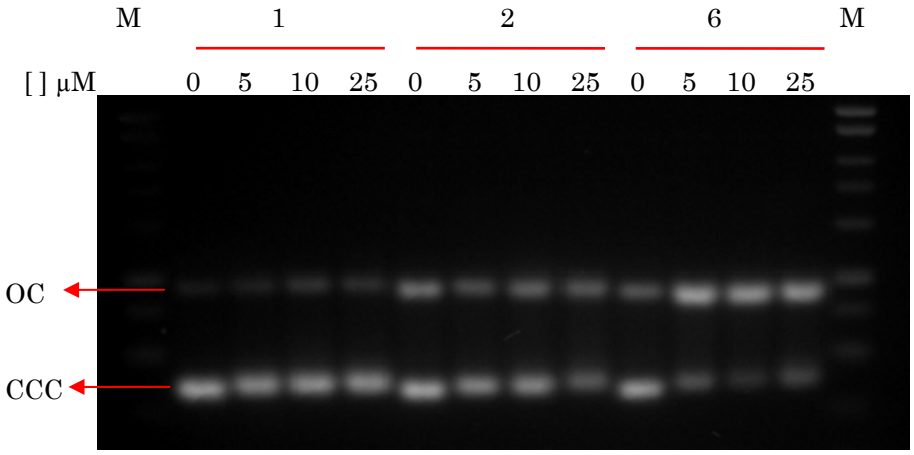

Figure IV-6. Ethidium bromide agarose gel (1%) of 100 μM pUC18 incubated with compounds 1,2 and 6 at different concentrations. Lane 1, 14: Standard 1kb leader marker. Lane 2, 6, 10: Native pUC 18, control. Lane 3-5: increasing amounts of compound 1. Line 7-9: increasing amounts of compound 2. Line 11-13: increasing amounts of compound 6.

The collective aforementioned data support the notion that the progressively increasing ligand size for the series results in a larger affinity for DNA and a change in the binding mode from primarily electrostatic (compounds **1** and **2**) to primarily intercalative (compounds **3-6**) in the initial stages of their interaction. As we have previously observed, mono-substituted diimine complexes of this class are capable of simultaneously intercalating between DNA bases and binding covalently to DNA.[230] Compound **5** exhibits the strongest interactions of the group with the DNA double helix (Table IV-1; Figures IV-3, IV-4 IV-5 and IV-6).

In vitro *Cytotoxicity*

The compounds were tested in a cell proliferation assay on two human cell lines, *viz*., HeLa and COLO-316. The LC_{50} values were calculated after 24 h of incubation with complexes **1**-**6** and are listed in Table IV-2. For this particular dirhodium family, it is obvious that the human ovarian carcinoma cells COLO-316 are more sensitive than HeLa cells. Compound **4** exhibits the highest activity with LC_{50} values of 86 ± 4 μM and 54 ± 1 μM for HeLa and COLO-316 cell lines, respectively. Any further modification of the ligand length or width leads to a decrease in the activity of the dirhodium complex with HeLa cells. When the size of the intercalating moiety was reduced, as in the case of compounds **1** (LC_{50} = 120 ± 4 μM), **2** (LC_{50} = 129 ± 6 μM), and **3** (LC_{50} = 128 ± 5 μM), the cytotoxicity towards HeLa cells was diminished by approximately 1.5 fold. A similar reduction of the activity was observed when the ligand was expanded either in length or width, as in **5** (LC_{50} = 120 ± 7 μM) and **6** (LC_{50} = 130 ± 3 μM), respectively. In the case of COLO-316 cells, a decrease or increase in the length of the aromatic moiety results in lower

activity, approximately 1.3 fold. Compound **6**, however, exhibits activity similar to compound **4** in this cell line.

Partition Coefficient Determination

Compound **5**, which displays the highest affinity towards DNA in cell free media, is not the most cytotoxic of the series in either HeLa or COLO-316 cell lines. It is possible that this dichotomy is due to the difference in the ability of the compounds to cross the cellular plasma membrane. Thus hydrophobic interactions appear to be an important factor for the eventual DNA binding affinity of this family of complexes. Many studies over the years support the conclusion that reactivity and affinity of a compound are not the only important factors in inhibiting a cellular process, but that the availability of the agent to interact with its target also plays an important role.[235] To address this issue, the values of the partition coefficient, log *P*, between *n*-octanol and water of compounds **1**-**6** were measured (Table IV-2). The *P* measurements are based on the difference in solubility that a given compound exhibits in an aqueous medium and in a lipid medium.[240] The correlation of the activity of a compound with its log *P* value depends on the solvent system used as a model for the membrane.[240, 248] The "shake flask" method used during the course of these studies has been shown to work well for molecules with log *P* values that range from -2 (most hydrophilic) to +4 (most hydrophobic).[248-251] The values obtained for the members of this series range from -1.93 to + 0.91 (Table IV-2). By comparing the partition coefficients of these compounds (Table IV-2), it can be seen that the log *P* values become more positive as the π-system of the ligands in the complexes is extended. The difference in the log *P* values of compounds **1** and **2** is small

despite the fact that one more ring is added to the system. Subsequent ring additions to the system increases the log *P* values to a greater extent. Adding the fourth ring, as in the case of compound **3**, increases the log *P* value in 0.55, whereas the fifth and sixth rings in compounds **4** and **5** increase the log *P* value in 1.23 and 1.21, respectively. Extending the width of the system has a more pronounced effect, as can be observed in the log *P* difference (2.16) between compounds **3** and **6**.

Table IV-2. Log *P* and cytotoxicity values of compounds **1**-**6**

Compound	log *P*	LC_{50} ± SD, μM[a]	
		HeLa	COLO-316
1	– 1.90 ± 0.03	129 ± 4	70.8 ± 3
2	– 1.98 ± 0.02	128 ± 6	73.6 ± 4
3	– 1.53 ± 0.03	124 ± 5	71.2 ± 3
4	– 0.30 ± 0.02	86 ± 4	54.0 ± 1
5	0.91 ± 0.01	118 ± 7	71.3 ± 3
6	0.63 ± 0.02	130 ± 3	54.1 ± 3

[a]Determined using the MTT assay. LC_{50} values are concentrations of drug required to kill 50% of the cells. Experiments were performed in triplicate.

As expected, compounds **1** and **2** are the most hydrophilic compounds of the series. The hydrophobicity increases throughout the series as the planar aromatic region is expanded and reaches a maximum at compound **5**. It is a plausible hypothesis that the hydrophobicity of **5** does not permit rapid internalization of the compound which would account for the decreased

cytotoxicity as compared to **4** in HeLa cells or **4** and **6** in COLO-316. Compounds **4** and **6** interact to a lesser degree with DNA but are less hydrophobic and might be able to traverse the cellular membrane more effectively. It must be pointed out that, in a previous study, we did not find any correlation between the partition coefficient and cytotoxicity of the dirhodium complexes studied,[235] but this outcome may be due to the structural differences among the previous compounds which could translate to very different mechanisms of action in live cells. In the present study, however, we have focused on a homologous family of dirhodium complexes that, due to their similarity, would be expected to behave in a comparable manner in the intracellular space. Hence differences in cellular uptake should be reflected in the cytotoxicity of the compounds (Figure IV-7).

Supporting this hypothesis are early data by Bear and coworkers who reported for a the family of dirhodium tetracarboxylate complexes $Rh_2(\mu\text{-}O_2CR)_4$ (R = CH_3, C_2H_5, C_3H_7, and C_4H_9), an increase in cytotoxicity against Ehrlich ascites tumor cell lines in going from the acetate to the butyrate derivative; conversely a decrease in cytotoxicity was observed with a further lengthening of the R group.[72] Similarly, Sheldrick *et al.*, found that the family of compounds $[(\eta^6\text{-}C_6Me_6)RuCl(pp)]^+$ (pp = dpq, dppz, and dppn) exhibited cytotoxicity increases that correlate with the hydrophobicity and the cellular uptake efficiency of the compounds.[228]

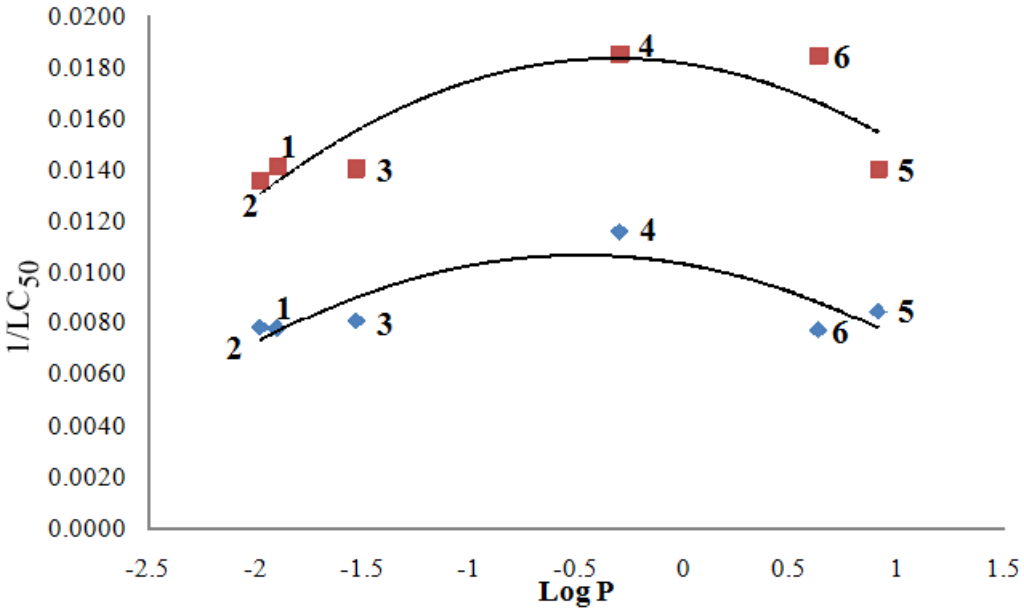

Figure IV-7. Correlation between cytotoxicity and partition coefficient. HeLa (♦) and COLO-316 (■) cells.

Alkaline Comet Assay

An alkaline single cell gel electrophoresis was performed to evaluate the ability of these complexes to form DNA adducts in a cellular environment.[252-255] The Alkaline Comet Assay is a sensitive technique that can be used to detect single-, and double-strand breaks, crosslinks, as well as alkali-labile sites.[252, 253] Assays were performed at a concentration that allows for 75% cell viability using HeLa cells. For each compound, one hundred cells were scored using the CometScore® software.[242] This program allows one to quantify the amount of DNA present in the tail of the comet which is representative of the amount of DNA damage caused by the added agent.[242] As shown in Figure IV-7, all of the compounds produce more damaged DNA (represented as a larger percent of DNA in the tail) than the control.

Compounds **1**, **2**, **3**, and **6** with 48.5 ± 9.6%, 41.7 ± 10.8%, and 39.2 ± 14.7% of the DNA being found in the comet tail, respectively, damage only a small amount of DNA. In fact, these values are quite similar to that observed with $Rh_2(\mu\text{-}O_2CCH_3)_4$ with a percentage of DNA in the tail equal to 37.9 ± 5.8%. On the other hand, compounds **4** and **5** led to the highest DNA damage with 72.4 ± 7.7% and 80.1 ± 7.4% of the DNA being found in the comet tail, respectively. Interestingly, compound **5**, which show to be the most reactive towards DNA in cell free media, shows a better activity than **4** once inside the cell, i.e., this compound causes the greatest amount of DNA damage. The level of damage cause by **5** is similar to that observed with a comparable amount of added cisplatin is added (% DNA in tail = 79.7 ± 8.0) is used. The DNA damage observed in the comet assay could be caused by direct interaction of the compound with DNA, or could be due to the formation of ROS by the metal complex.

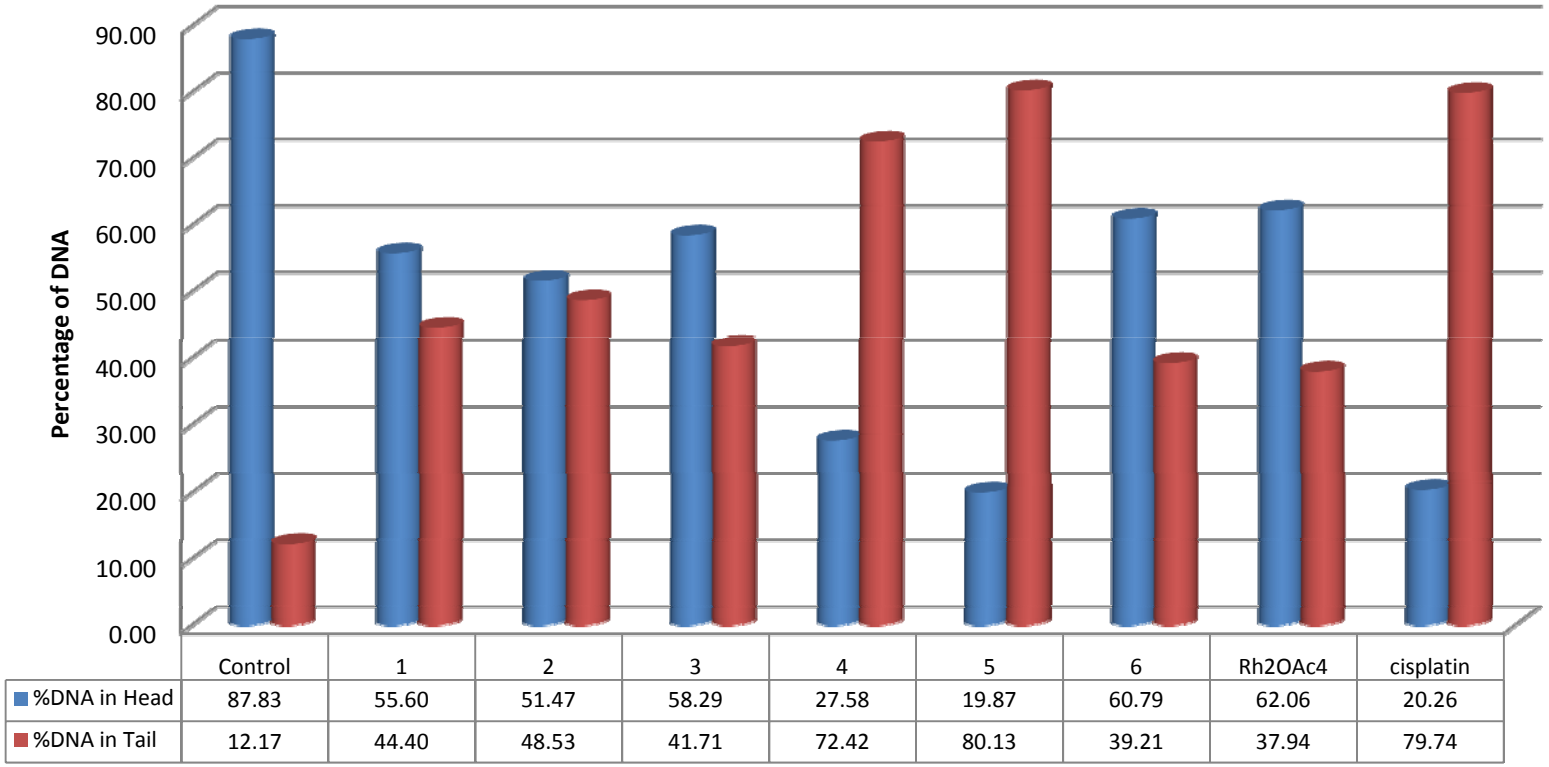

	Control	1	2	3	4	5	6	Rh2OAc4	cisplatin
%DNA in Head	87.83	55.60	51.47	58.29	27.58	19.87	60.79	62.06	20.26
%DNA in Tail	12.17	44.40	48.53	41.71	72.42	80.13	39.21	37.94	79.74

Figure IV-8. Percentage of nuclear DNA damaged after treatment with compounds **1**-**6**, dirhodium tetracetate and cisplatin; represented as percent of DNA in comet tail.

Glutathione Modulation

Glutathione is the most abundant thiol in cells, present at concentrations of 0.5-10 mM depending on the cell type.[256] Some of the functions of glutathione include protection of the cell integrity from reactive oxygen species (ROS) and heavy metal detoxification.[257] It has been observed in some cisplatin resistant cell lines that their glutathione levels are higher than normal.[258] Given this fact, it is of considerable interest to determine the effects of glutathione modulation on the cytotoxicity of this family of dirhodium complexes.

The molecule *N*-acetyl-L-cysteine (NAC) is a compound known to increase levels of glutathione and radical scavengers in cells.[205] The COLO-316 cells were pre-treated with NAC, then incubated with the dirhodium complexes **1**-**6** and the change in the cytotoxicity of these complexes was measured (Figure IV-9). The cells treated with compound **2** showed a slight decrease in activity as observed by the increase in cell viability (+32%), whereas compounds **3** (-2%) and **5** (-8%) showed the greatest activity increase in the series. These variations in activity are considered minimal, and correspond to a small effect of the increase of glutathione and radical scavenger levels on the cytotoxicity of this family of dirhodium complexes.

These results dismiss the hypothesis that the cellular DNA damage is due to the formation of ROS by the metal complex. If the damage caused by the dirhodium complex originated from the presence of ROS, pre-treatment with NAC should increase the cell viability, yet, no market changes in the cytotoxicity of the complexes were observed (Figure IV-9). Therefore, it is

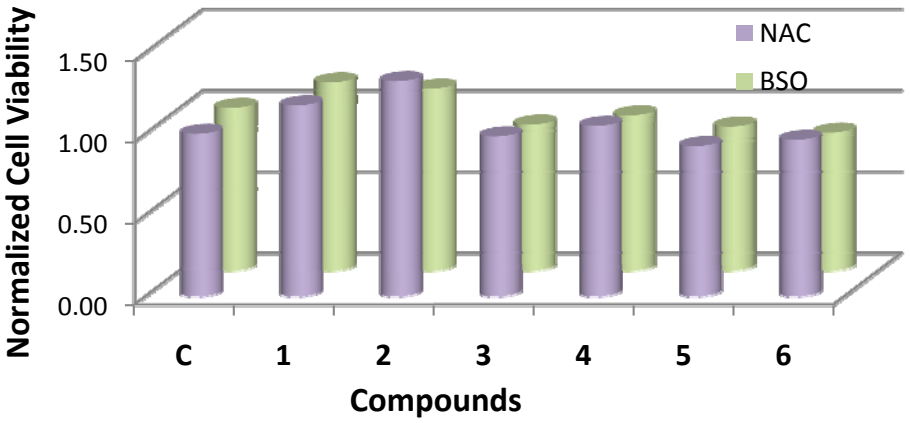

Figure IV-9. Effect of compounds **1**-**6** on COLO-316 cell after glutathione modulation by NAC (increase of cellular glutathione levels) and BSO (decrease of glutathione levels).

reasonable to suggest that direct damage of the nuclear DNA occurs, and that the dirhodium complexes bind to nuclear DNA in living cells.

The levels of glutathione were depleted with BSO, a selective inhibitor of γ-glutamyl cysteine synthase, a key enzyme in the glutathione biosynthetic pathway.[256, 259] Upon exposure to BSO for 20-28 h, levels of glutathione in COLO-316 cells have been shown to decrease to ~13% of its initial value.[260, 261] In COLO-316, depletion of glutathione did not have a major effect on the cytotoxicity of cisplatin,[260] although an increase in cisplatin cytotoxicity has been observed in other cell lines.[262] In the case of the dirhodium complexes used in this study, the depletion of glutathione by BSO did not lead to large variations in their cytotoxicity (Figure IV-9).

Although glutathione, as in the case of cisplatin,[263] is likely to play a role in dirhodium deactivation, it does not seem to be the sole factor involved in this case. The results obtained in the cell viability studies using BSO (Figure IV-9) demonstrate that, despite the decrease in glutathione levels, more dirhodium compound does not reach its cellular target. We note that, in the case of cisplatin, there are other thiols that play a role in its deactivation. For example, the low molecular weight protein metallothionenin contains 20 cysteine residues and is actively involved in the detoxification of heavy metal compounds in cells.[263] It is reasonable to postulate that this protein could also be involved in the detoxification of cells from dirhodium complexes.

Cell Death Mechanism

SYTOX® Blue is a cell impermeable agent that can only enter cells when their membranes have been damaged.[264] Upon entering the cell, SYTOX® Blue binds to nuclear DNA and undergoes a 100-fold increase in fluorescence.[264] After 4 h of incubation of HeLa cells with the dirhodium compound of interest at a concentration equal to their calculated LC_{50} values, ~60 % of the cells contain blue stain in their nuclei. This implies that the cells treated with compounds **1**-**6** have been severely compromised or are no longer viable. From the pictures in Figure IV-10, it is also possible to see that the morphology of the cells differs from that of a viable HeLa cell.

Cells were incubated with compound **4**, the most effective compound of the mono-substituted series, and the changes in cell morphology were monitored. It was observed that compound **4** starts causing cell death after 15 minutes. After 2 h of incubation, almost 90 % of the cells appear to be compromised and the cells change morphology to a globular shape with the appearance of blebs (Figure IV-11). After 4 h incubation, contraction of cell volume and membrane blebbing has been extended to almost all of the cells. These changes, cell shrinkage and membrane blebbing, are hallmarks of apoptosis.[265]

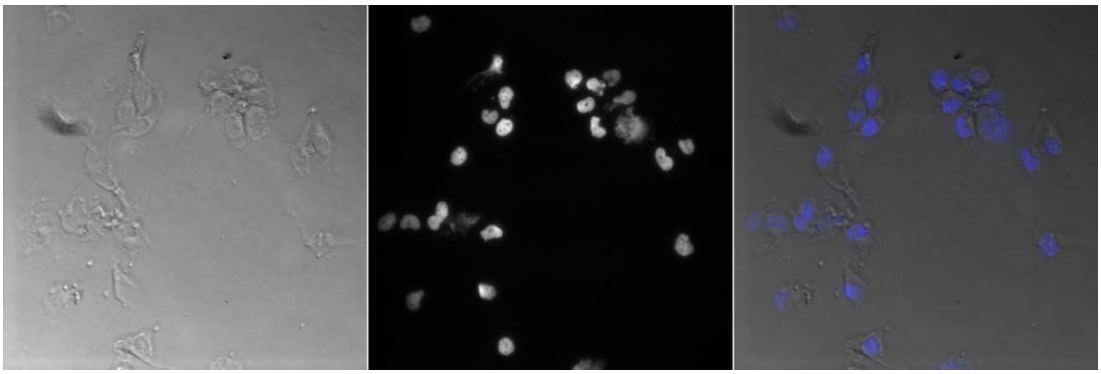

Figure IV-10. Phase contrast and fluorescent image of HeLa cells treated with compound 4. **Left**: Phase contrast. **Center**: SYTOX® Blue fluorescence emission. **Right**: Overlay of the phase contrast and SYTOX® Blue fluorescence emission (pseudo-colored blue) images.

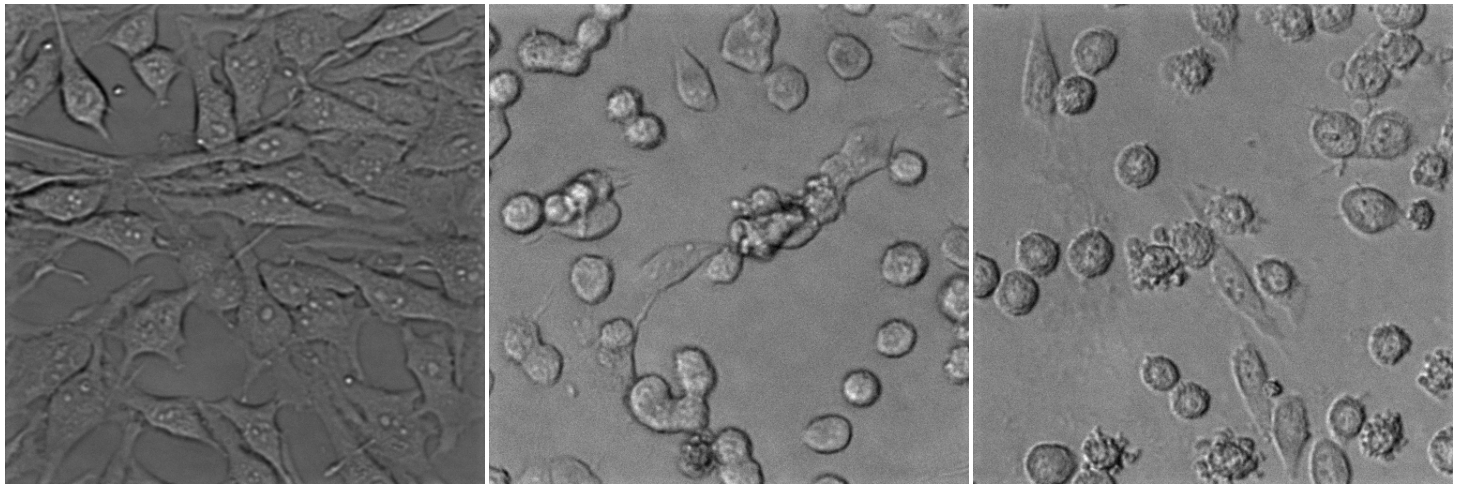

Figure IV-11. Phase contrast images of HeLa cells treated with compound 4. **Left**: Time zero. **Center**: After 2 h incubation. **Right**: After 4 h incubation.

Conclusions

The collective aforementioned data point to the conclusion that this specific family of dirhodium complexes does, in fact, reach nuclear DNA in living cells triggering apoptosis, which is the first time that the longstanding premise of DNA being a target has been verified. The size of the diimine ligands bound to the dirhodium core in compounds **1**-**6** controls the *in-vitro* affinity and interaction with ds-DNA as well as the *in cellulo* reactivity of the complexes. The progressively increasing ligand size for the series results in a larger affinity for DNA and a change in the binding mode from primarily electrostatic (compounds **1** and **2**) to primarily intercalative (compounds **3-6**) in the initial stages of their interaction. As we have previously observed, mono-substituted diimine complexes of this class are capable of simultaneously intercalating between DNA bases and binding covalently to DNA. Thus a clear relationship between the interaction of the compounds with DNA and their cytotoxicity has been established. Moreover, the ability to cross the cellular plasma membrane appears to be another significant factor that affects activity of the compounds *in live cell* assays. Compound **4**, the most effective dirhodium complex of the series, appears to induce apoptosis in HeLa cells. Metal complexes such as **4**-**6** that can potentially intercalate as well as covalently bind to DNA are promising lead compounds certainly deserve further scrutiny.

CHAPTER V

HETEROLEPTIC RHODIUM COMPLEXES AND THEIR INTERACTION WITH CELLULAR DNA*

Introduction

As outlined in the previous chapter, mono-substituted diimine complexes are capable of interacting with DNA both *in-vitro* and *in cellulo*. It was observed that the nature of the diimine ligand bound to the dirhodium core controls the reactivity of the compound, and the progressive increase of the ligand size results in a higher affinity for DNA as well as a change in the binding mode from electrostatic to intercalative in the initial stages of the interaction. Moreover, the studies supported the conclusion that transport through cellular membranes is important and has an effect on the cytotoxicity of the dirhodium complexes.

The membrane permeability can be assessed by measuring the lipophilicity of compounds, with the partition coefficient (P) being the most common parameter used to estimate lipophilicity.[240, 248] The importance of lipophilicity in the observed bioactivity has been previously demonstrated in the class of dirhodium carboxylate paddlewheel compounds of general formula $Rh_2(\mu\text{-}O_2CR)_4$ (R = CH_3, C_2H_5, C_3H_7).[72] In this series, the activity against Ehrlich ascites tumor, Leukemia L1210, and sarcoma 180 cell lines

---

*Reprinted in part from "Anticancer Activity of Heteroleptic Diimine Complexes of Dirhodium: A Study of Intercalating Properties, Hydrophobicity and in cellulo Activity" J. Dafhne Aguirre, Alfredo M. Angeles-Boza, Abdellatif Chouai, Jean-Philippe Pellois, Claudia Turro, and Kim R. Dunbar. *Dalton*. **2009**, . Copyright 2009, with permission from the Royal Society of Chemistry.

increases as the hydrophobicity of the R group increases; further lengthening of the carboxylate group beyond the pentanoate, however, reduces the efficacy.[72]

Another important factor that controls biological activity is the reactivity of the compound.[240] The relative reactivity can be estimated by determining the kinetic parameters of binding to biomolecules.[240] Recent studies of various dirhodium compounds have indicated that there is a correlation between their cytotoxic behavior and the lability of the leaving groups on the dirhodium core.[235] In the series of dirhodium complexes $Rh_2(\mu\text{-}O_2CR)_4$ (R = CH_3; R = CF_3), $[Rh_2(\mu\text{-}O_2CR)_2(phen)_2]^{2+}$ (R = CH_3; R = CF_3) and $[Rh_2(O_2CR)_2(dppz)_2]^{2+}$ (R = CH_3; R = CF_3), the differences in the cytotoxicities are correlated to the higher lability of the trifluoroacetate as compared to the acetate leaving groups.[235] In addition, compounds with one diimine ligand possesing a dangling acetate and a solvent molecule in the equatorial position such as $[Rh_2(\mu\text{-}O_2CCH_3)_2(\eta\text{-}O_2CCH_3)L(MeOH)]^+$ (L = dppz; L = dppn), were shown to be more cytotoxic as compared to the bis-substituted derivatives $[Rh_2(\mu\text{-}O_2CCH_3)_2(bpy)L]^{2+}$ (L = dppz; L = dppn) and $[Rh_2(\mu\text{-}O_2CR)_2L_2]^{2+}$ (L = dppn). This increase in cytotoxicity was correlated to the presence of the labile solvent molecules and the monodentate acetate groups which provide labile sites for substitution chemistry with biomolecules.[235]

The aim of the present chapter is to explore the properties of dirhodium compounds containing two diimine ligands. Specifically the effect of the fused ring size of the second diimine ligand (bpy, phen, dpq, dppz, and dppn) on the biological activity of the compounds and their ability to form adducts with nuclear DNA was investigated for the series of complexes *cis*-$[Rh_2(\mu\text{-}O_2CCH_3)_2(dppn)(L)]^{2+}$, where dppn = benzo[i]dipyrido[3,2-a:2',3'-c] phenazine, and L = bpy (2,2'-bipyridine) (**1**), phen (1,10-phenanthroline) (**2**), dpq (dipyrido[3,2-f:2',3'-h]quinoxaline) (**3**), dppz (dipyrido [3,2-a:2',3'-c] phenazine) (**4**), and dppn (**5**) (Figure V-1). The ability to intercalate DNA due to the presence of the dppn ligand bound to one of the rhodium atoms was systematically reduced by extending the size of the diimine ligand bound to the second rhodium center. The lipophilicity of the compounds was also probed as a function of the increase size of one of the ligands. Finally, the effect of blocking all the "open sites" on the *in cellulo* activity of the complexes was also studied.

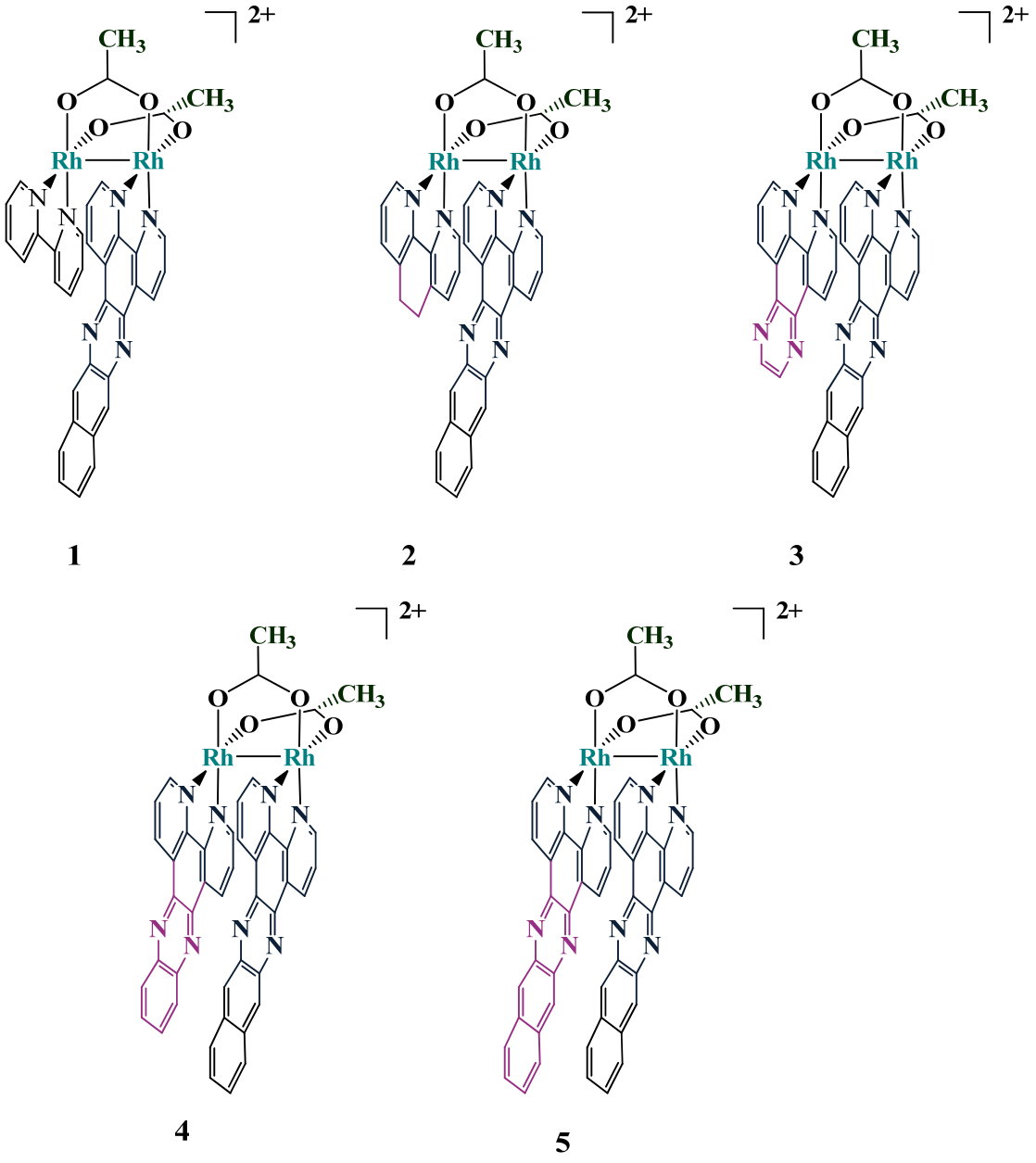

Figure V-1. Schematic representation of compounds **1**-**5** in this study.

Experimental Section

Materials

The reagents 2,2′-bipyridine (bpy), 1,10-phenanthroline (phen), diaminoethylene and 2,3-diaminonaphthalene were purchased from Acros. Calf thymus DNA, ethidium bromide, Hoechst 33258, *n*-octanol and 1,10-phenantroline-5,6-dione were purchased from Sigma-Aldrich and used as received. The HeLa cell line were obtained from the American Type Culture Collection, cell line CCL-2. The COLO-316 cell line was kindly provided by Robert Burghardt (Texas A&M University, Department of Veterinary Anatomy and Public Health).

The starting material $RhCl_3 \bullet H_2O$ was purchased from Pressure Chemicals and used as received. The ligands pyrazino[2,3-f][1,10]phenanthroline (dpq),[231] dipyrido[3,2-*a*:2′,3′-*c*]phenazine (dppz)[232] and benzodipyrido[3,2-*a*:2′,3′-*c*]phenazine (dppn),[233] were synthesized according to reported procedures.[231-233] The dirhodium complexes $Rh_2(\mu\text{-}O_2CCH_3)_4$,[198] *cis*-$[Rh_2(\mu\text{-}O_2CCH_3)_2(\eta^1\text{-}O_2CCH_3)(bpy)(CH_3OH)](O_2CCH_3)$,[117] *cis*-$[Rh_2(\mu\text{-}O_2CCH_3)_2(\eta^1\text{-}O_2CCH_3)(phen)(CH_3OH)]$ (O_2CCH_3),[117] *cis*-$[Rh_2(\mu\text{-}O_2CCH3)_2(\eta^1\text{-}O_2CCH_3)(dpq)(CH_3OH)](O_2CCH_3)$,[266] *cis*-$[Rh_2(\mu\text{-}O_2CCH_3)_2(dppn)(bpy)](O_2CCH_3)_2$ (**1**),[235] and *cis*-$[Rh_2(\mu\text{-}O_2CCH_3)_2(dppn)_2](O_2CCH_3)_2$ (**5**)[235] were synthesized according to published literature procedures.[117, 198, 235, 266]

Synthesis of *cis*-[$Rh_2(\mu\text{-}O_2CCH_3)_2$(dppn)(bpy)]$(O_2CCH_3)_2$ (1)

A suspension of dppn (161 mg, 0.48 mmol) and cis-[$Rh_2(\mu\text{-}O_2CCH_3)_2(\eta^1\text{-}O_2CCH_3)$(bpy)($CH_3OH$)]($O_2CCH_3$) (161 mg, 0.48 mmol) in acetonitrile (13 mL) was refluxed under nitrogen for 24 h. The resulting red precipitate was collected by filtration in air, washed with acetonitrile (3 × 5 mL) and Et_2O, and dried *in vacuo* (280 mg, 63%). ESI-MS: *m*/*z* 405.99 (100%, [$Rh_2(\mu\text{-}O_2CCH_3)_2$(dppn)(bpy)]$^{2+}$). ^{1}H NMR ($CD_3OD/CDCl_3$) δ (ppm): 1.96 (s, 6H), 2.65 (s, 6H), 7.19 (m, 2H), 7.41 (m, 2H), 7.62 (m, 4H), 7.84 (m, 4H), 8.42 (m, 2H), 8.73 (m, 2H), 9.17 (s, 2H), 9.55 (m, 2H). Calcd for $Rh_2C_{40}H_{32}O_8N_6 \cdot 4H_2O$: C, 47.90; H, 4.02; N, 8.38. Found: C, 47.96; H, 3.54; N, 8.69.

Synthesis of *cis*-[$Rh_2(\mu\text{-}O_2CCH_3)_2$(dppn)(phen)]$(O_2CCH_3)_2$ (2)

A suspension of dppn (80 mg, 0.24 mmol) and *cis*-[$Rh_2(\mu\text{-}O_2CCH_3)_2(\eta^1\text{-}O_2CCH_3)$(phen)($CH_3OH$)]($O_2CCH_3$) (150 mg, 0.24 mmol) in acetonitrile (12 mL) was refluxed under nitrogen for 24 h. The red product was collected by filtration, washed with acetonitrile (3 × 5 mL) and Et_2O, and dried *in vacuo* (193 mg, 84%). ESI-MS: *m*/*z* 417.99 (100%, [$Rh_2(\mu\text{-}O_2CCH_3)_2$(dppn)(phen)]$^{2+}$). ^{1}H NMR ($CD_3OD/CDCl_3$) δ (ppm): 1.92 (s, 6H), 2.64 (s, 6H), 7.20 (s, 2H), 7.42 (m, 2H), 7.72 (m, 4H), 8.04 (m, 2H), 8.18 (m, 2H), 8.36 (m, 2H), 8.70 (m, 2H), 9.05 (s, 2H), 9.22 (m, 2H). Calcd for $Rh_2C_{42}H_{32}O_8N_6 \cdot 2H_2O$: C, 50.91; H, 3.66; N, 8.49. Found: C, 50.82; H, 3.62; N, 8.75.

Synthesis of *cis*-[$Rh_2(\mu\text{-}O_2CCH_3)_2$(dppn)(dpq)]$(O_2CCH_3)_2$ (3)

A suspension of dppn (49.3 mg, 0.15 mmol) and *cis*-[$Rh_2(\mu\text{-}O_2CCH_3)_2(\eta^1\text{-}O_2CCH_3)$(dpq)($CH_3OH$)]($O_2CCH_3$) (100 mg, 0.15 mmol) in acetonitrile (10 mL) was refluxed under nitrogen for 24 h. The red precipitate that had formed was collected by filtration, washed with acetonitrile (3 × 5

mL) and Et_2O, and finally dried *in vacuo* (115 mg, 76%). ESI-MS: *m*/*z* 646.9 (100%, $[Rh_2(\mu\text{-}O_2CCH_3)_2(dppn)(phen)](O_2CCH_3)_2$). ^1H NMR (CD_3OD) δ (ppm): 1.90 (s, 6H), 2.66 (s, 6H), 7.52 (m, 2H), 7.68 (m, 2H), 7.80 (s, 2H), 8.10 (m, 2H), 8.30 (s, 2H), 8.39 (m, 2H), 8.63 (m, 2H), 8.71 (m, 2H), 8.99 (m, 2H), 9.08 (m, 2H). Calcd for $Rh_2C_{44}H_{32}O_8N_8 \cdot 3H_2O$: C, 49.81; H, 3.61; N, 10.57. Found: C, 49.64; H, 3.47; N, 10.32.

Instrumentation

The ^1H NMR spectra were recorded on a Varian spectrometer at 300 MHz and referenced to the residual proton impurities in the deuterated solvents. Mass spectra were acquired on a PE SCIEX QSTAR Pulsar electrospray ionization mass spectrometer at Texas A & M University. Elemental analyses were performed by Atlantic Microlab Inc., P.O. Box 2288, Norcross, GA 30091. The UV-visible measurements were performed on a UV-1601PC Shimadzu spectrophotometer. For live-cell imaging, an inverted epifluorescence microscope (Model IX81, Olympus, Center Valley, PA) equipped with a heating stage maintained at 37°C was used. Images were collected using a Rolera-MGI Plus back-illuminated EMCCD camera (Qimaging, Surrey, BC, Canada) mounted on the microscope with UPlanFl 100× / 1.3 NA oil, LCPlan 40× / 0.6 NA, or LCPlan 20× / 0.4 NA objectives.

Methods

Relative Changes in Viscosity Experiment

The relative change in viscosity was measured using an Ubbelohde viscometer maintained at constant temperature (27 °C) in a thermostatic bath. Sonicated herring sperm DNA (200 μM), 5mM Tris/HCl, 20 mM NaCl,

pH 7.5, and increasing concentrations of complexes were used.[134] Data are presented as:

$$(\frac{\eta}{\eta_\circ})^{1/3} \text{ vs } \frac{[M]}{[DNA]}$$

$$\eta = t_1 - t_2$$

$$\eta_0 = t_n - t_0$$

where $\eta = (t_1 - t_2)$ is viscosity of DNA in the presence of the complex, $\eta_0 = (t_n - t_0)$ is viscosity of DNA in the absence of complex.

Partition Coefficient Determination

The lipophilicity of the complexes was determined by the "shake flask" method using a pH 7.4 phosphate buffer (0.129 M NaCl) and *n*-octanol as solvents.[240, 248] Each compound was dissolved in the phase in which it is most soluble, resulting in typical concentrations of 50 to 350 μM. Duplicate determinations using three different solvent ratios were performed for each complex. Following mixing and phase separation according to literature methods,[248] each phase was analyzed for solute content and the concentration was determined using spectrophotometric methods. All the *n*-octanol/water partition coefficients were determined by UV-visible spectroscopy. Octanol and buffer solutions were pre-saturated with each other prior to use. Fifty rotations were performed by hand followed by one hour of settling time. Equilibration and absorption measurements were performed at 20 °C (r. t.).

Cell Culture

All cells lines were cultured in Dulbecco's modified Eagle medium, containing 10% fetal bovine serum (Invitrogen), 50 μg/mL gentamicin, 4.5

mg/mL glucose, and 4 mM L-glutamine (Invitrogen). Cell cultures were incubated in a humidified atmosphere containing 5% CO_2 at 37 °C.

***In Vitro* Cytotoxicity**

The viability of COLO-316 and HeLa cells in the presence of the compounds under investigation was tested using the 3-(4,5-dimethylthiazol-2-yl)-2,5-diphenyltetrazolium bromide (MTT) assay[241] (Invitrogen). Subconfluent (50-80% confluent) monolayers of cells at a concentration of 5000-10000 cell/µl were used. Cells were plated in 96-well sterile plates, at a density of 20-30 cell/µL (volume of 100 µl per well) and were pre-incubated for 48 h. After the cells reached confluence, the medium was replaced by 100 µL of L-15 medium containing different complex concentrations. The plates were incubated for 24 hours. Fresh MTT solution (10 µL) was added, followed by incubation for 4 hours. A 100 µL aliquot of fresh SDS solution in 0.01 M HCl was added and after 16 hours of incubation the absorbance at 570 nm was measured using a Bio-Rad plate reader.

Comet Assay

Single cell gel electrophoresis was performed using a commercially available kit (R&D Systems). HeLa cells were incubated with metal complexes at a concentration that allows for 75% viability. After 4 h, cells were harvested and embedded in 0.75% low-melting point agarose at a volume of 1:10 on microscope slides. Cells were lysed in the dark for a minimum of 1 h at 4 °C. Cells were incubated in an alkaline solution containing NaOH (0.3 M), for a period of 1 h. Electrophoresis was performed for 30 min at 28 V in TBE buffer (pH=13). After electrophoresis, the cells were stained with SYBR® green dye and imaged using an inverted

microscope. A total of 100 cells were scored per sample, using the CometScore® software.[242]

Annexin V

HeLa cells at a concentration of 5000-10000 cell/µL were harvested, 50 µL of cells were plated in an 8-well sterile plate, and 200 µL of fresh medium was added to give a total volume of 250 µL. Cells were pre-incubated at 37 °C and, after 24 h, they were washed with sterile PBS and the medium was replaced by 250 µL of L-15 medium containing the different complexes at their LC_{50} concentration. Plates were incubated for 4 h after which time they were treated with Annexin V-Biotin for 15 minutes at 24 °C in the dark. After washing, the cells were first stained with streptavidin-fluorescein for 15 minutes in the dark and then incubated with PI.

MitoProbe® JC-1 Assay

HeLa cells at a concentration of 5000-10000 cell/µL were harvested, 75 µL of cells were plated in two 8-well sterile plates, and 125 µL of fresh medium was added to give a total volume of 250 µL. Cells were pre-incubated at 37 °C. After 24 h, cells were washed with sterile PBS and the medium was replaced by 250 µL of L-15 medium containing the different complexes at their LC50 concentration. One plate was incubated for 4 h after which time they were treated with 1 µL of a 2 µg/mL JC-1® solution and incubated for 5 minutes before imaging. A 1 µL aliquot of a 2 µg/mL JC-1® solution was added to the second plate and imaging was performed at different time periods for a total time of 4 hours.

Results and Discussion

Synthesis

The new dirhodium complexes reported in this study were synthesized by reacting the monosubstituted complex *cis*-[$Rh_2(\mu\text{-}O_2CCH_3)_2(\eta^1\text{-}O_2CCH_3)$(diimine)($CH_3OH$)]($O_2CCH_3$), (diimine = bpy, phen, dpq) with 1 equivalent of dppn in acetonitrile (Chart 2). The reaction mixture was stirred and heated under nitrogen for 24 h. The green color of the mixture changes to red during the course of the reaction which is a characteristic color for bis-diimine dirhodium complexes with two carboxylate ligands.[103, 235]

Viscosity Measurements

The relative change in viscosity was measured using sonicated herring sperm DNA (200 μM bp) with increasing concentrations of compounds **1** – **5** (Figure V-4). Relative viscosity measurements have proven to be a reliable method for assigning the mode of binding of dirhodium compounds with extended aromatic ligands to DNA.[266] The method is based on the well-known fact that intercalation of molecules between DNA bases causes a change in the relative viscosity of solutions due to the unwinding and elongation of the double helix.[155] For compounds **1** and **2**, a change in the relative viscosity is observed after their addition to the DNA. This behavior is similar to what one observes with the standard intercalator ethidium bromide (EtBr)[245] as well as the complex *cis*-[$Rh_2(\mu\text{-}O_2CCH_3)_2(\eta^1\text{-}O_2CCH_3)$(dppz)($CH_3OH$)]$^+$,[266] which is known to intercalate into DNA. Conversely, the effect of compounds **3 - 5** on the relative viscosity of the solution is more reminiscent of that of the minor groove binder Hoescht 33258[245] as well as *cis*-[$Rh_2(\mu\text{-}O_2CCH_3)_2(dppz)_2$]$^{2+}$ and

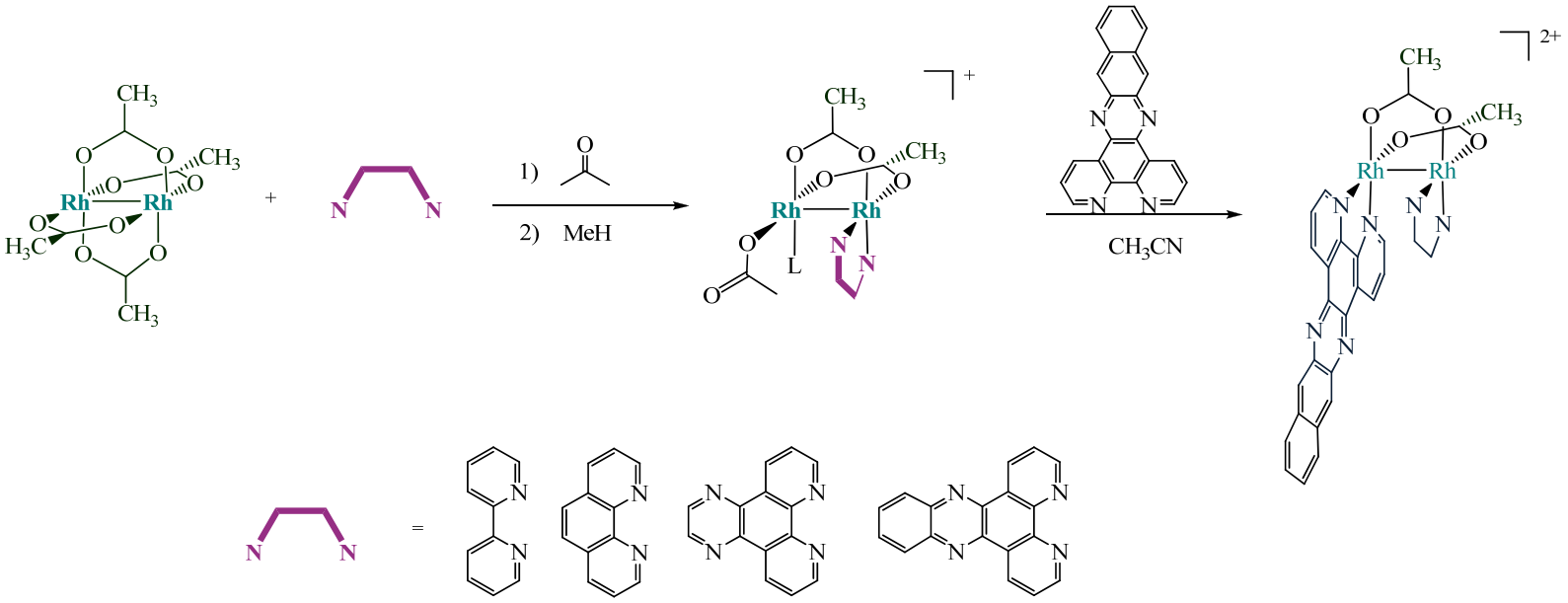

Figure V-2. Schematic representation of the general synthetic procedure to prepare compounds **1**-**4**.

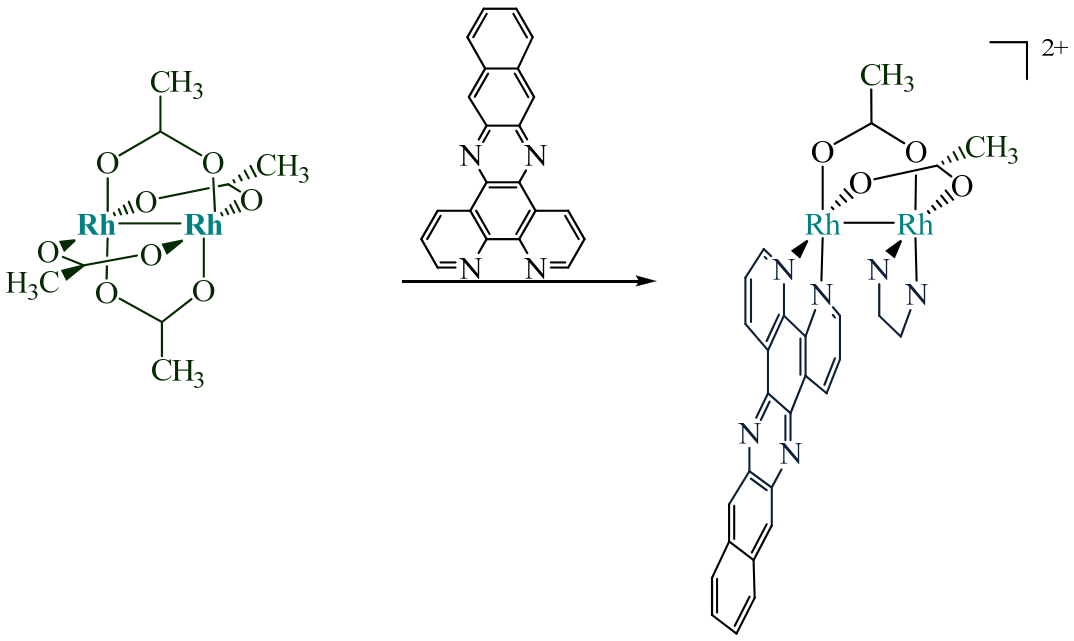

Figure V-3. Schematic representation of the general synthetic procedure to prepare compound **5**.

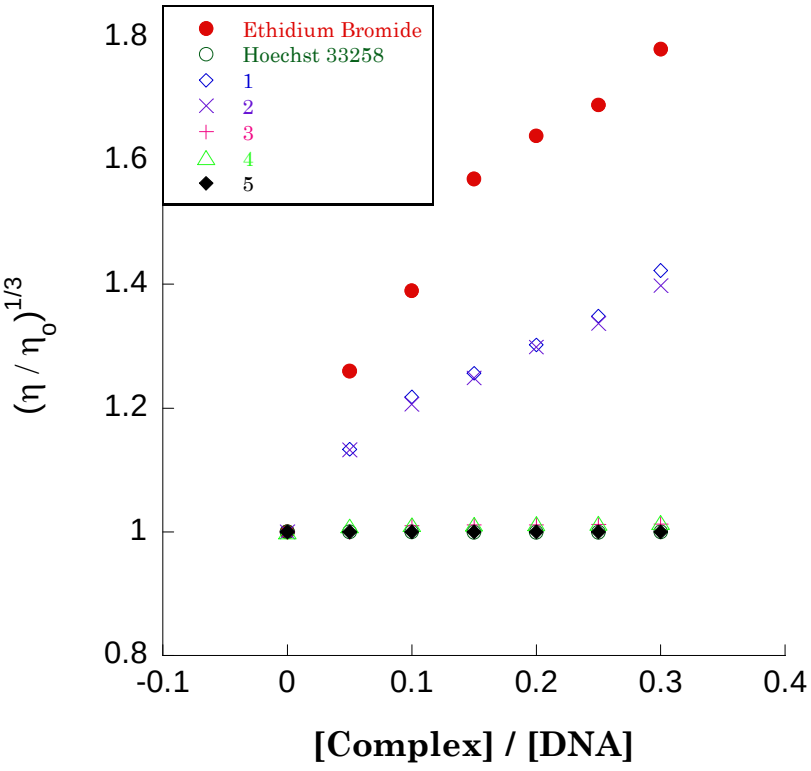

Figure V-4. Relative viscosity changes of solutions containing 200 μM sonicated herring sperm DNA as the concentration of EtBr (●),**1** (◊), **2** (×), **3** (Δ), **4** (Δ), **5** (♦) and Hoechst 33258 (○) is increased.

cis-$[Rh_2(\mu\text{-}O_2CCH_3)_2(dppz)(bpy)]^{2+}$ which had been previously shown to interact with DNA solely by electrostatic interactions.

Partition Coefficient Determination

Partition coefficients, *P*, were measured to help ascertain the ability of these dirhodium compounds to cross lipid bilayers. The *P* measurements are based on the difference in solubility that a given compound exhibits in an aqueous versus a lipid medium.[240] The correlation of the activity of a compound with its log *P* value depends on the solvent system used as a model for the membrane. The log *P* values obtained for compounds **1** - **5** range from 0.32 to 1.02 (Table V-1). The compounds containing the smallest ligands bpy and phen exhibit the lowest values, 0.32 and 0.31, respectively. The hydrophobicity increases as the second diimine ligand increases in length, although it does not do so in a liner progression as expected. The lipophilicity substituent constant of conjugated systems, $\pi_{CH=CHCH=CH}$, is known to be one of the least constitutive, that is to say the effect of adding rings is not greatly influenced by the molecule to which it is attached or to its environment.[267, 268] Giving this situation, one would expect that extending the diimine ligand in compound **3** by one ring will cause a similar increase in the log *P* as would adding an additional ring as in going from compound **4** to compound **5**. As shown in Table V-1, however, the increase in the log *P* for the aforementioned additions of rings is 0.2, and 0.4, respectively. It is possible that the presence of the dppn ligand directly above the second diimine ligand ameliorates the inherent hydrophobicity hence leading to the lack of an additivity effect on the lipophilicity substituent constant for this family of dirhodium complexes.

Table V-1. Log *P* and cytotoxicity values for compounds **1**-**6**.

Compound	**log *P*** [a]	**LC_{50} ± SD, μM**[b]	
		HeLa	**COLO-316**
1	0.32 ± 0.03	138.3 ± 6.7	92.2 ± 5.1
2	0.31 ± 0.03	156.6 ± 10.3	87.0 ± 2.8
3	0.41 ± 0.02	135.3 ± 13.9	92.1 ± 4.1
4	0.63 ± 0.03	81.5 ± 11.1	68.8 ± 1.9
5	1.02 ± 0.03	209.4 ± 11.0	201.3 ± 15.4

[a] Partition coefficient P = Co/Cw (Co and Cw are the complex concentrations in n-octanol and water, respectively). [b] Determined using the MTT assay. LC_{50} values are concentrations of compound required to kill 50% of the cells.

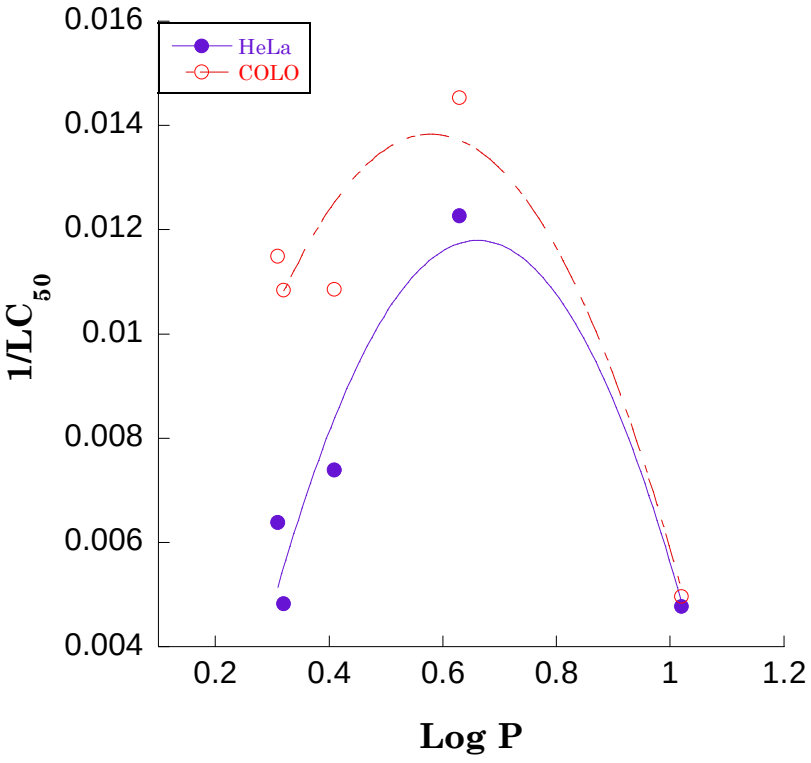

Figure V-5. Correlation between cytotoxicity and partition coefficient: HeLa (○) and COLO-316 (●) cells.

In Vitro *Cytotoxicity*

The cytotoxicity of the compounds was determined by the MTT cell proliferation assay[241] on two human cancer cell lines, *viz*, HeLa and the ovarian carcinoma cells COLO-316. The LC_{50} values were calculated after 24 h of incubation with complexes **1 - 5** and are listed in Table V-1. COLO-316 cells are more sensitive than HeLa cells to this series of dirhodium complexes. A higher sensitivity of COLO-316 cells to dirhodium complexes had been observed previously in our laboratories for a family of mono-substituted dirhodium complexes.[266] Compound **4** exhibits the highest activity with LC_{50} values 81.5 μM and 68.8 μM in HeLa and COLO-316 cell lines. Compounds **1**, **2**, and **3** display very similar cytotoxicity values for the COLO-316 cell line. In the cases of compounds **1** and **2**, these results correlate with their similar log *P* values and DNA binding mode as determined by the change in relative viscosity (Figure V-5, Table V-1). Although compound **3** does not interact with DNA in an analogous fashion as compounds **1** and **2**, it exhibits similar cytotoxic behavior to the aforementioned compounds, which is an indication that specific interactions with DNA are not required in order for cellular death to occur in the presence of this family of complexes. Compound **5** is the least cytotoxic of the family for both cell lines, a fact that is likely related to its hydrophobicity, which is expected to impede its ability to cross the cellular membrane. The relationship between the lipophilicity of the metal complexes and their activity is shown in Figure V-5. A similar decrease in cytotoxicity as the compound becomes more hydrophobic was noted previously for a series of mono-substituted dirhodium complexes, as well as for other families of metal-based compounds.[72, 266, 269] In the case of

the family of mono-substituted dirhodium compounds studied previously, the maximum of the curve occurs at log P ~ - 0.4,[266] whereas in the present case, the maximum is at log P ~ 0.6. This displacement observed in the maximum is suggestion that the two series of compounds likely target different cellular compartments.

Alkaline Comet Assay

The Alkaline Comet Assay, also known as the alkaline single cell gel electrophoresis assay, is a sensitive technique that is used to detect single-, double-strand breaks, crosslinks, and alkali-labile sites.[252, 253] We had used this test in previous studies to evaluate the ability of dirhodium complexes to form DNA adducts in a cellular environment.[266] Assays were performed on HeLa cells at a concentration that allows for 75% cell viability. For each dirhodium complex one hundred cells were scored using the CometScore® software.[242] This program allows one to quantify the amount of intact DNA present in the comet head and that of damaged DNA in the tail of the comet.[242] As shown in Figure V-6, all of the compounds lead to low levels of damaged DNA (represented as a larger percent of DNA in the comet head). These values are in contrast to data observed for $Rh_2(\mu\text{-}O_2CCH_3)_4$, as well as other dirhodium complexes that we have studied, which are known to react with nuclear DNA and produce a lower percentage of DNA in the comet head.[266] The obvious conclusions are either that this family of dirhodium complexes does not reach nuclear DNA or that they produce DNA adducts that are successfully repaired by the cellular machinery. Although nuclear DNA is the target of many transition metal complexes,[6, 42] including some

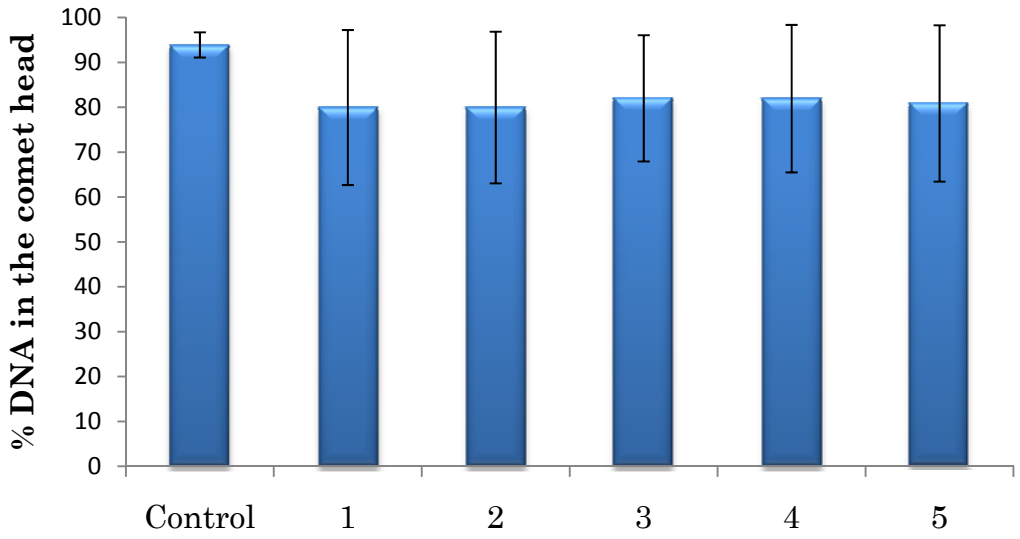

Figure V-6. Comet assay results of compounds **1**-**5** represented as percent of DNA in the comet head.

dirhodium complexes,[266] it is possible that this family of compounds favorably reacts with other biological molecules or reaches other compartments in the cell. For example, lipophilic cations are known to accumulate in the mitochondria due to the negative transmembrane potential leading to cellular toxicity.[270-274] It is also possible that the current dirhodium complexes slow or prohibit important cellular processes from occurring by inhibiting key enzymes involved in the cell cycle.

Annexin V Assay

During apoptosis, which is programmed cell death, several biochemical processes are known to be triggered.[265] One of them leads to the exposure of phosphatidylserine (PS) on the cell surface, the presence of which is commonly used to detect apoptotic events.[275, 276] PS is a phospholipid localized in the cytosolic side on the surface of the cell. When PS flips and gets exposed to the outer leaflet of the cytoplasmic membrane, it can be detected by using Annexin V, a protein that reversibly binds PS.[275, 276]

To obtain insight into the cell death mechanism arising from exposure to the dirhodium compounds in this study, HeLa cells were treated with compounds **1** – **5**, followed by incubation with Annexin V-Biotin for 15 minutes. Next, the cells were stained with streptavidin-fluorescein. Cells treated with compounds **1** – **4** clearly show green fluorescence localized on the outer side of the cellular membrane (Figure V-7a - d). This is indicative of the presence of PS on the outer leaflet of the membrane which means that an apoptotic mechanism of cell death may be occurring. In contrast, cells incubated with compound **5** do not show any degree of staining with the

streptavidin-fluorescein probe, a result that suggests that the cells undergo a necrotic cell death (Figure V-7e).

The cells were also simultaneously stained with propidium iodide (PI), a dye that crosses the cellular membrane of dead cells only and intercalates into DNA (Figure V-7). Because nuclei of normal cells exhibit "structure", slight variations in the hues of the stained nuclei can be observed due to the presence of euchromatin and heterochromatin.[265, 275] In contrast, apoptotic nuclei possess highly condensed chromatin and after staining, they appear as bright spherical beads.[265] As one can see from the data in Figure V-7, several nuclei of the cells treated with compounds **1** - **4**, followed by PI staining appear to contain two or more bright spheres. This is not the case for the more lipophilic dirhodium complex of the group, compound **5**. The PI staining results in combination with the detection of PS flipping by the annexin V assay collectively point towards an apoptotic mechanism of cell death for cells treated with compounds **1** – **4**, and a necrotic pathway for those treated with compound **5**.

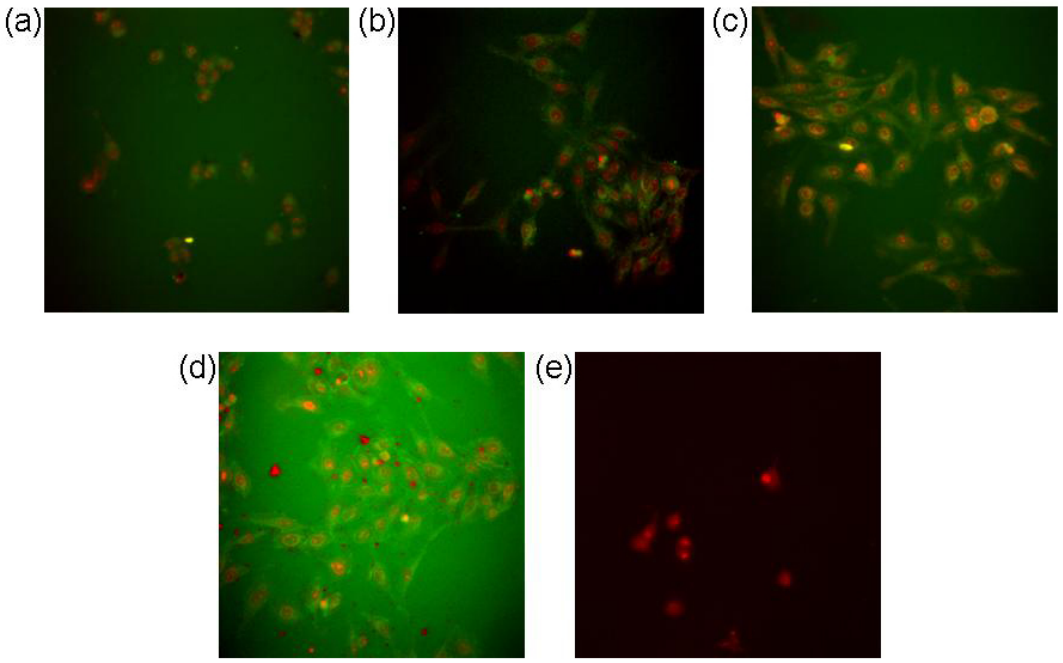

Figure V-7. Confocal microscope images of HeLa cells treated with compounds **1 - 5**, followed by treatment with Annexin V-Biotin, streptavidin-fluorescein, and propidium iodide: (a) **1**, (b) **2**, (c) **3**, (d) **4**, and (e) **5**.

Clues about the Target: Mitochondrial Transmembrane Potential Disruption

It has been recently observed that various hydrophobic compounds with delocalized positive charges accumulate in the inner mitochondrial matrix.[270-272, 274, 277] This behavior has been taken into consideration to develop a new family of drugs that selectively target the mitochondria.[272, 274, 277-279] The compounds described in this chapter possess the two molecular characteristics that cause accumulation in the mitochondria, namely hydrophobicity and positive charge.[270, 271, 277, 280] Therefore, it is possible that the mitochondria are a plausible target of the family of bis-diimine dirhodium complexes.

When compounds accumulate in the mitochondria, they cause disruption of the mitochondrial transmembrane potential ($\Delta\Psi m$).[271] JC-1 (carbony cyanide 3-chlorophenyldydrazone) is a commercially available cationic dye that can selectively enter into mitochondria and change color when $\Delta\Psi m$ is disrupted.[264] In healthy cells, cells with high $\Delta\Psi m$, JC-1 forms complexes (J-aggregates) that posses an intense red fluorescence. In cells whose mitochondria have been compromised and their $\Delta\Psi m$ decreased, JC-1 remains in its monomeric form, which has green fluorescence.

Compound **4** induces changes of the mitochondrial membrane potential as indicated by the changes in color observed in the time-dependent experiment (Figure V-9). Although it is possible that compound **4** is targeting the mitochondria, it is also possible that the decrease of transmembrane potential is due to the apoptosis process triggered by this dirhodium complex as it is known that this is one of the characteristics of programmed cellular death.

In the case of compound **5**, similar changes are observed (Figure V-10). Nevertheless, as described in the previous section, unlike the other members of the series, this compound does not seem to cause apoptosis. Therefore, it can be concluded that this compound causes the disruption of the mitochondrial membrane potential, and most probably targets these organelles.

It is interesting to mention that during the time dependant experiment, it can be observed that both compounds caused different changes in the morphology of the cells (Figure V-8). Whereas compound **4** appears to produce "globular" cells, compound **5** causes the cells to burst out. This is indicative of the two different mechanisms by which they cause cellular death, apoptosis and necrosis for compounds **4** and **5**, respectively.

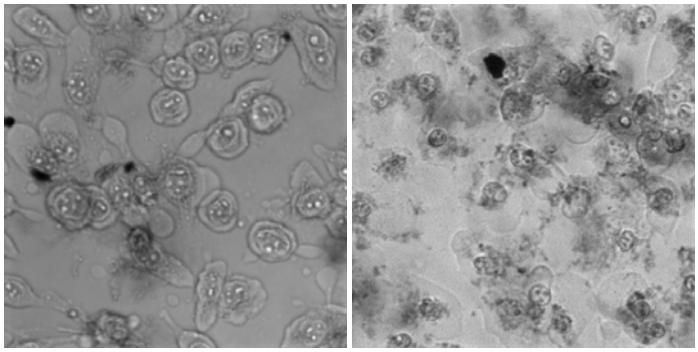

Figure V-8. Phase contrast image of HeLa cells treated with compound **4** and **5**. **Left**: After 4 h incubation with compound **4**. **Right**: After 4 h incubation with compound **5**.

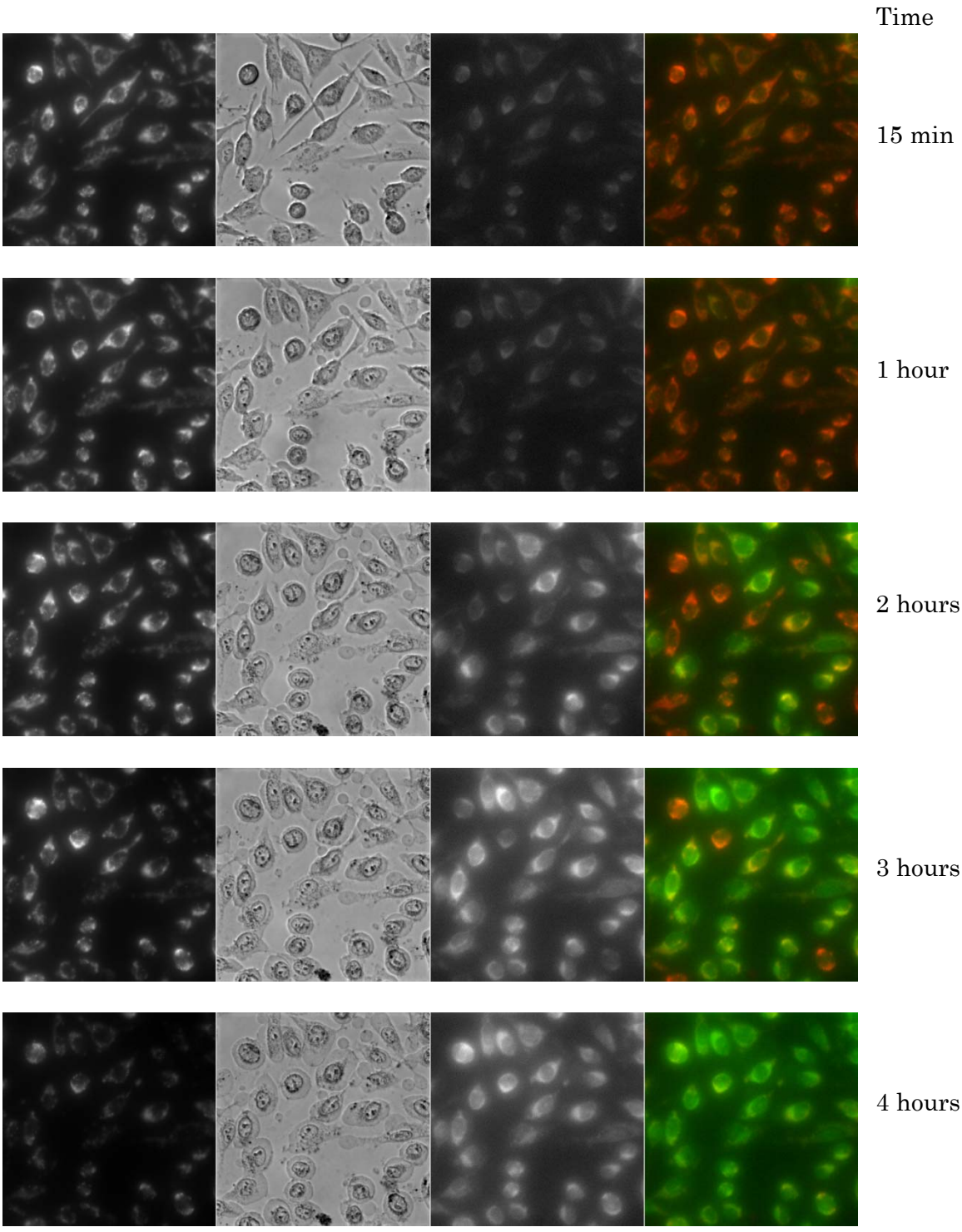

Figure V-9. Phase contrast and fluorescent image of HeLa cells treated with compound **4**, time lapse experiment. **Left**: Red fluorescence emission. **Center**: Phase contrast. **Right**: Green fluorescence emission. **Far Right**: overlay of phase contrast, red and green fluorescence emission (pseudo colored) images.

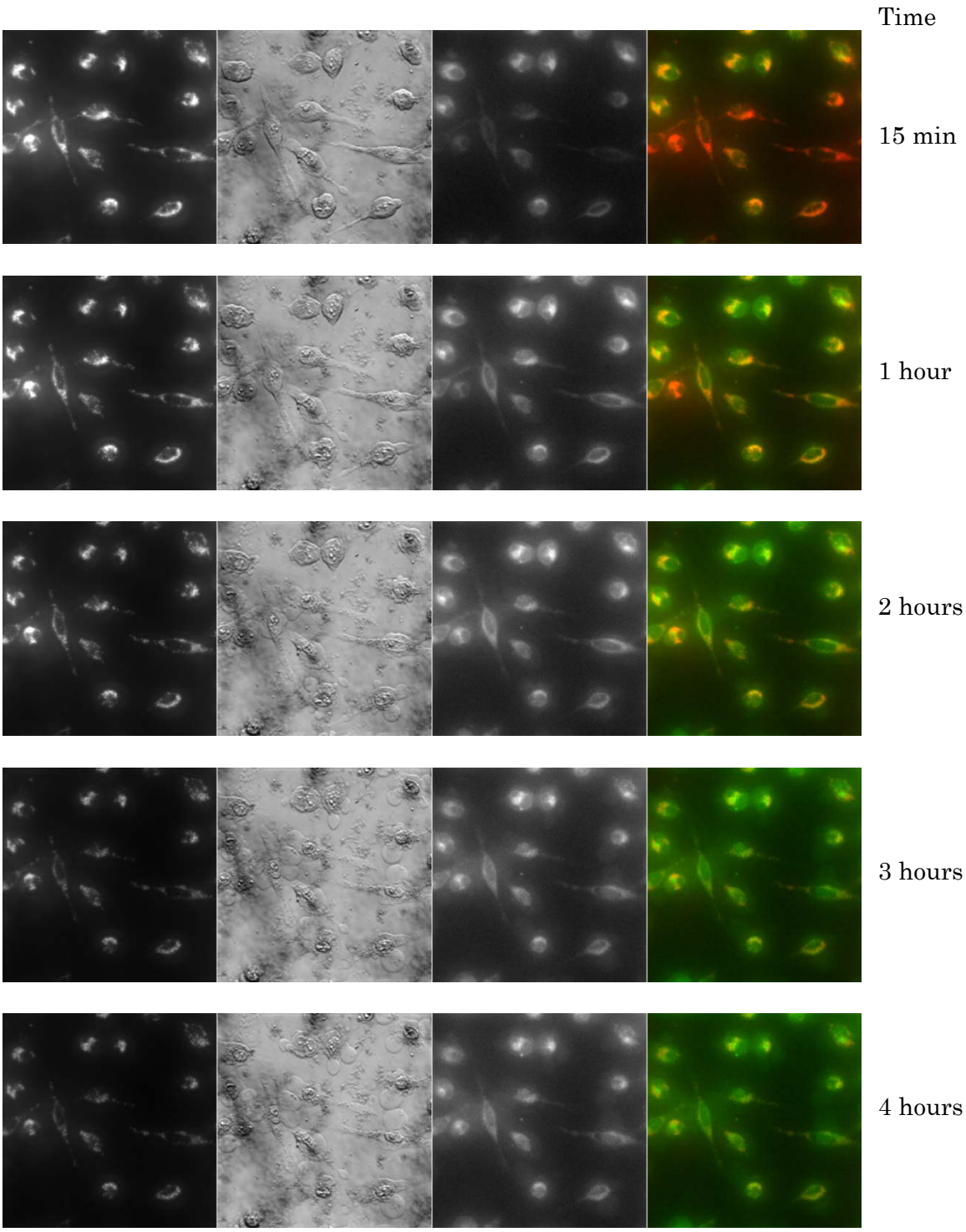

Figure V-10. Phase contrast and fluorescent image of HeLa cells treated with compound **5**, time lapse experiment. **Left**: Red fluorescence emission. **Center**: Phase contrast. **Right**: Green fluorescence emission. **Far Right**: overlay of phase contrast, red and green fluorescence emission (pseudo colored) images.

Conclusions

The present study reveals that the family of dppn-diimine-dirhodium complexes investigated herein exhibits cytotoxicity towards cancer cell lines. Although two of the complexes are capable of intercalating into DNA bases, the ultimate target of these dirhodium compounds does not apper to be nuclear DNA. Clearly the ability to cross the cellular plasma membrane affects the *in cellulo* activity of the compounds with compound **4** being the most effective at inhibiting cell viability of the human cancer cells HeLa and COLO-316. Interestingly, compounds **1** – **4** trigger apoptosis, whereas compound **5** does not. These findings are quite intriguing as they hint at the possibility of being able to exert exquisite control over which process is ultimately responsible for cell death.

CHAPTER VI
FACILITATING CELLULAR TRANSLOCATION USING CELL PENETRATING PEPTIDES

Introduction

In the pharmacological arena, one of the main concerns is the transport of drugs into the cellular media. Solid tumors are resistant to drug penetration through passive diffusion and, in general, drugs have poor transport properties since the plasma membrane of cells is a barrier for molecules that are typically large and hydrophobic.[240, 281, 282] Various delivery methods have been developed to transport molecules across cell membranes and gain access to the cellular interior.[281, 283, 284] For example liposome encapsulation, attachment of polyamines and, more recently, the use of cell penetrating peptides (CPPs) have been shown to have promising applications.[281, 283-286] CPPs, also known as protein transduction domains (PDTs), are short polypeptide sequences with less than 30 amino acids, and with a net positive charge that can facilitate cellular translocation of a variety of molecules, ranging from small molecules, proteins and even large structures with diameters as large as 200 nm.[281, 283-285, 287-289] This class of molecules has been shown to promote translocation of their cargo into cells, both *in vitro* and *in cellulo*.[281-285, 289-291] CPPs include natural occurring sequences derived from toxins or viruses and synthetic analogues (Table VI-1).[281] Among the most extensively investigated CPPs are the HIV TAT sequence GRKKRRQRRRPPQ and its polyarginine derivatives (Table VI-1).[281, 288, 290, 292]

Table VI-1. CPP sequences commonly used.[283, 285, 286, 293]

Name / Sequence	Length	Origin
Penetratin (pAntp) RQIKIWFQNRRMKWKK	16	*D. melanogaster* transcription factor
HIV TAT peptide 48–60 GRKKRRQRRRPPQ	13	Viral transcriptional regulator
Map KLALKLALKALKAALKLA-NH_2	18	Synthetic
Transportan GWTLNSAGYLLGKINLKALAALAKKIL- NH_2	27	Chimeric galanin-mastoparan
Transportan 10 AGYLLGKINLKALAALAKKIL- NH_2	21	Chimeric galanin-mastoparan
R7 peptide RRRRRRR	7	Synthetic
pVEC LLIILRRRIRKQAHAHSK- NH_2	18	Murine sequence of the cell adhesion molecule vascular endothelial cadherin
MPG peptide GALFLGWLGAAGSTMGAPKKKRKV- NH_2	24	Chimeric HIV-1 gp41-SV40 large T antigen
KALA peptide WEAKLAKALAKALAKHLAKALAKALKACEA	30	
YTA2 YTAIAWVKAFIRKLRK- NH_2	16	Synthetic
Buforin 2 TRSSRAGLQFPVGRVHRLLRK	21	Synthetic
Pep-1 KETWWETWWTEWSQPKKKRKV	21	Synthetic
HSV-1 VP22 peptide DAATATRGRSAASRPTERPRAPARSASRPRRVD	33	Viral Capsid protein

From the *in vitro* studies described in the previous two chapters, it is evident that certain dirhodium compounds have a high affinity for DNA, but that they exhibit a low activity according to *in cellulo* studies. Clearly, in order to improve the bio-availability of these dirhodium complexes, their transport into living cells needs to be improved. Cytotoxicity studies of conjugates formed by tethering organic molecules to CPPs have revealed that the cytotoxic activity of the antitumor agent is enhanced as compared to the parent compound.[292, 294, 295] One disadvantage encountered in this approach, however, is the requirement of a chemical bond between the peptide sequence and the cargo molecule, an alteration that can change the properties of the cargo in terms of its toxicity and localization inside the cell.[296] To avoid these issues either a bond that is reversible under biological conditions such as a disulfide bond or an ester bond susceptible to enzymatic hydrolysis has been used with success.

Recently, several groups have reported that co-incubation of a molecule with certain CPP sequences (Table VI-2) is a reliable method to help deliver a cargo when chemical coupling is not possible due to the nature of the cargo or simply to avoid time consuming procedures.[297] The association between the CPP used and the cargo molecule is achieved through non-covalent, electrostatic or hydrophobic interactions. An added advantage of this methodology is that once inside the cell, the cargo is not redirected from its target by the inherent localization of the peptide.[297] Therefore, co-incubation of dirhodium molecules and CPPs seems like a good alternative to avoid purification steps that could modify the coordination sphere of the dirhodium core due to acids used in the purification steps of these systems.

The research presented in this chapter describes the syntheses and characterization of two polyariginine peptide sequences, R_9K and R_7K. The results of the bio-availability changes of five dirhodium compounds as modulated by co-incubation with these two sequences are also reported. The data, although preliminary, shows an improvement of the cytotoxicity after co-incubation as compared to the dirhodium complexes alone. In addition, the synthesis of a diimine ligand functionalized with a CPP and the coupling of this ligand to a ruthenium center is also reported.

Table VI-2. CPP sequences used in co-incubation experiments.[297]

Name	Sequence
YTA2	YTAIAWVKAFIRKLRK- NH_2
pVEC	LLIILRRRIRKQAHAHSK- NH_2
Pep-1	KETWWETWWTEWSQPKKKRKV
Pep-2	KETWFETWFTEWSQPKKKRKV

Experimental Section

Materials

All Fmoc amino acid derivatives and resins were purchased from Novabiochem (San Diego, CA). The HeLa cells were obtained from the American Type Culture Collection, cell line CCL-2. The COLO-316 cell line was kindly provided by Prof. Robert Burghardt (Texas A&M University, Department of Veterinary Anatomy and Public Health).

The starting material $RhCl_3 \cdot H_2O$ was purchased from Pressure Chemicals and used as received. The ligands dipyrido[3,2-*a*:2′,3′-*c*]phenazine (dppz) and benzodipyrido[3,2-*a*:2′,3′-*c*]phenazine (dppn), were synthesized according to reported procedures. The diimine ligand 2-(2-pyridinyl)-4-carboxyquinoline (Yle) was synthesized as described previously.[298] The dirhodium complexes $Rh_2(\mu\text{-}O_2CCH_3)_4$ (**1**),[198] cis-$[Rh_2(\mu\text{-}O_2CCH_3)_2(\eta^1\text{-}O_2CCH_3)(dppz)(CH_3OH)](O_2CCH_3)$ (**2**),[102, 104] cis-$[Rh_2(\mu\text{-}O_2CCH_3)_2(\eta^1\text{-}O_2CCH_3)(dppn)(CH_3OH)](O_2CCH_3)$ (**3**)[235] *cis*-$[Rh_2(\mu\text{-}O_2CCH_3)_2(dppn)(dppz)](O_2CCH_3)_2$ (**4**),[235] and *cis*-$[Rh_2(\mu\text{-}O_2CCH_3)_2(dppn)_2](O_2CCH_3)_2$ (**5**)[235] were synthesized according to published literature procedures.

Synthesis of Peptide Sequences

Cell penetrating peptide sequences R_7K and R_9K were synthesized using the Fmoc synthetic strategy of solid phase peptide synthesis on a rink amide resin using DMF as solvent.[299] For anchoring of the first amino acid to the resin, 740 mg of resin was packed into a SPPS vial and soaked with DMF for 30 minutes. All Fmoc deprotection steps were performed twice by treatment with 20 % piperidine in DMF. Activation of Fmoc protected amino

acids (4 equivalents) was achieved with HBTU (3.9 equivalents) and DIEA (10 equivalents) in minimum amount of DMF. The resulting solution was added directly into the vial with the resin and the coupling reaction was bubbled with a soft nitrogen flow for 4 hours. Completion of each addition was monitored by a ninhydrin test. The coupling cycle was repeated until the required number of amino acids was attached.

After completion of the synthesis, the resin was washed with DCM and dried under vacuum. The peptide was then cleaved from the resin, and the amino acid side chains deprotected by treatment with a mixture of trifluoroacetic acid : water : triisopropyl silane (1 000 μl: 15 μl : 15 μl) for 2 - 3 hours, followed by filtration. Chilled diethylether was added to the filtrate to assist in the precipitation of the crude peptide. After centrifugation the solution was decanted and the crude peptide was dissolved in 0.1 % trifluoroacetic acid in water and dried using a lyophilizer.

Synthesis of $Ru(phen)_2(CH_3CN)_2(PF_6)_2$

The compound *cis*-$[Ru(phen)_2(CH_3CN)_2](PF_6)_2$ was synthesized by mixing *cis*-$Ru(phen)_2Cl_2$ (30 mg, 45 mmol) and an excess of $[NH_4][PF_6]$ in acetonitrile (20 mL) under a nitrogen atmosphere with stirring and refluxing for 12 h. The product was isolated by filtration and used without further purification. Yield: 75%. Found: C, 40.11; H, 2.47; N, 9.86; calculated for $C_{28}H_{16}F_{12}N_6P_2Ru$: C, 40.39; H, 2.31; N, 10.10.

Synthesis of Yle-CPP

The CPP-diimine ligand was synthesized by solid phase peptide synthesis. The Fmoc-R_7K-resin (250 mg) peptide was synthesized as described above. After adding the last aminoacid, Fmoc deprotection was

performed twice by treatment with 20 % piperidine in DMF. Activation of the COOH functional group of 2-(2-pyridinyl)-4-carboxyquinoline was performed by mixing the ligand (55.5 mg, 0.2 mmol) with HBTU (70 μL) and DIEA (96.65 μL) in a minimum volume of DMF. After 10 minutes of activation, the mixture was added to the resin and the coupling reaction proceeded for 48 hours under nitrogen flow. The product was cleavage from the resin and purified using RP-HPLC.

Synthesis of Ru(phen)$_2$(Yle-CPP)

A solution of *cis*-[Ru(phen)$_2$(CH_3CN)$_2$](PF_6)$_2$ (10 mg, mmol) in methanol was treated with Yle-CPP (mg, mmol). The mixture was stirred at 37 °C for 25 hours. An alternative method used was to heat the mixture in a microwave oven (100 power) for 2 minutes.

Instrumentation

Analytical gradient reversed-phase HPLC was performed on a Hewlett-Packard 1200 series instrument and a Vydac C18 column (5 micron, 4 x 150 mm). The flow rate was 1 mL/min and detection was performed at 214, 365, 450 and 525 nm. Preparative HPLC was performed on a Vydac C18 10 × 250 mm column. The flow rate was 4 mL/min and detection was performed at 214, 365, 450 and 525 nm. All runs used linear gradients of 0.1% aqueous TFA (solvent A) and 90% acetonitrile plus 0.1% TFA (solvent B). The identity of the peptides was confirmed by time-of-flight mass spectrometry (MALDI-TOF mass spectrometry) using a Shimadzu/Kratos instrument (AXIMA-CFR, Shimadzu, Kyoto). The UV absorption measurements were performed with a Shimadzu UV 1601PC spectrophotometer.

Methods

Cell Culture

The HeLa and COLO-316 cell lines were cultured in Dulbecco's modified Eagle medium, which contain 10% fetal bovine serum (Invitrogen), 50 μg/mL gentamicin, 4.5 mg/mL glucose, and 4 mM L-glutamine (Invitrogen). Cell cultures were incubated in a humidified atmosphere containing 5% CO_2 at 37 °C.

Co-incubation Experiment

The CPP stock solutions were prepared in dd$H_2$0 and stored at – 20 °C. Peptides were diluted with water prior to co-incubation. CPPs were mixed with each of dirhodium compounds at a concentration that allows for 75% cell viability. Co-incubation was performed at 37° C for 10 minutes after which time the mixture was added to the COLO-316 or HeLa cells and incubated for a period of 3 hours. Cell viability was measured using the MTT assay. Briefly, a 10 μL aliquot of fresh MTT solution was added, followed by incubation for 4 hours. A 100 μL volume of fresh SDS solution in 0.01 M HCl was then added. After 16 hours of incubation the absorbance at 570 nm was measured using a Bio-Rad plate reader.

Results and Discussion

Synthesis and Characterization

The cell penetrating peptide sequences heptaarginine (R_7K) and nonaarginine (R_9K) were synthesized using the Fmoc synthetic strategy of solid phase peptide synthesis on a rink amide resin (Figure VI-1).[299] The peptides were obtained in high yields (~90%) and purified by reverse phase HPLC. Polyarginine peptides were chosen for these studies because of their improved activity as compared to other CPP sequences. Additionally, they were selected because we hypothesized that the guanidine residues of the arginine residues would not bind irreversibly to the dirhodium core under the conditions used for the synthesis and purification of the complex. Interestingly, lack of binding of this residue under similar conditions to those used in this study has recently been reported by Ball *et al.*[300] The ESI-MS spectra of the purified peptides are shown in Figures VI-2 and VI-3. Two peaks are observed in each spectrum, one due to the singly protonated sequence and one at a higher mass due to the presence of the Na^+ peptide adduct.

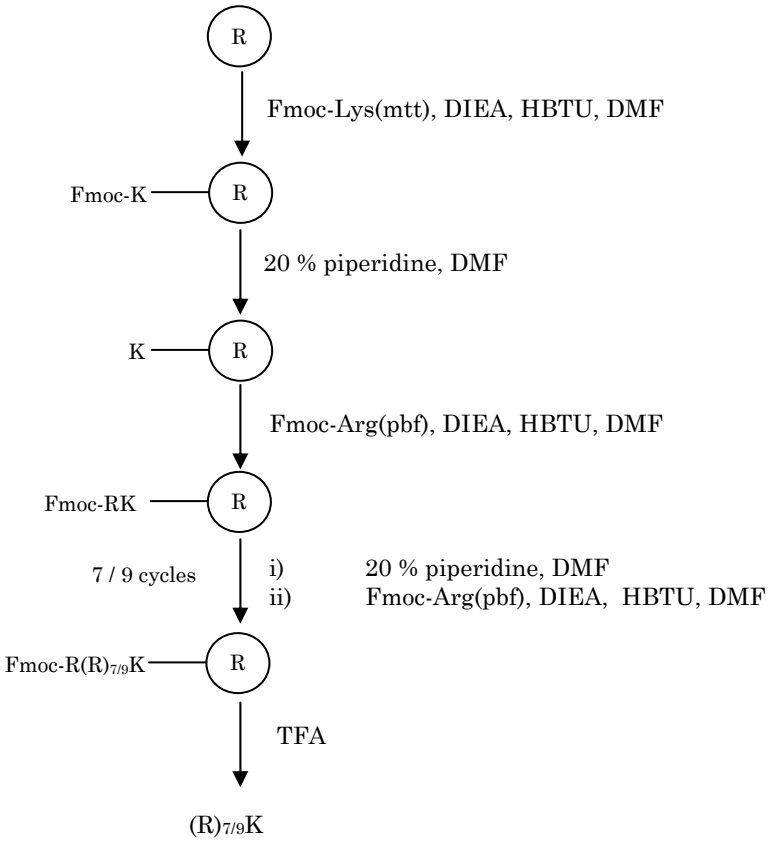

Figure VI-1. Schematic representation of the solid phase synthesis of peptide sequences used in this study.

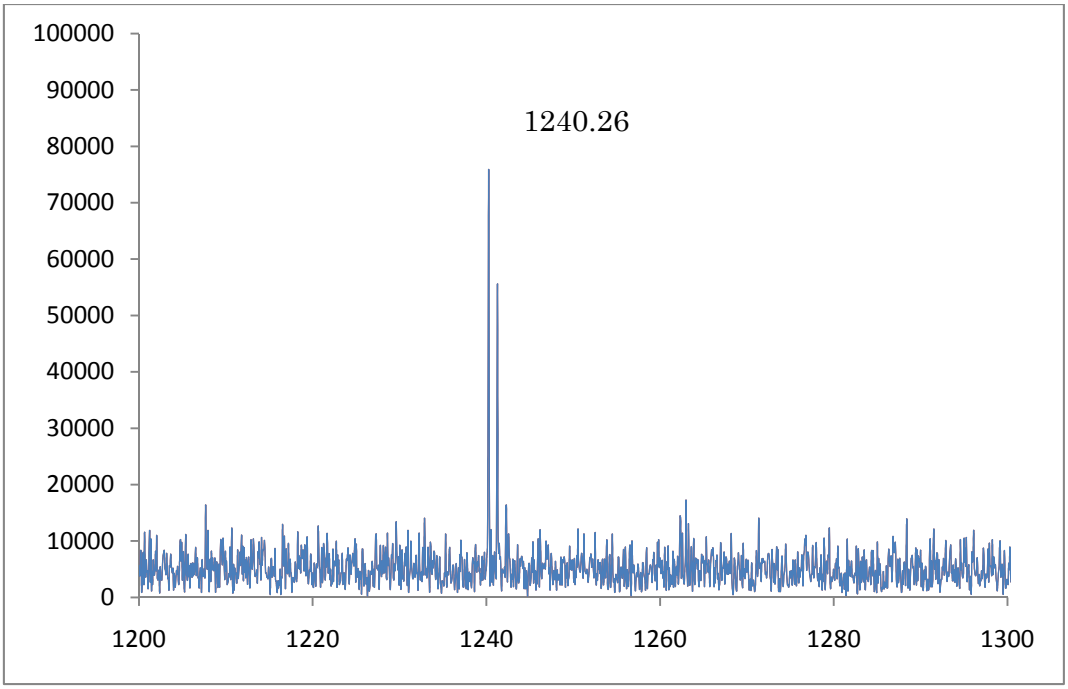

Figure VI-2. ESI-MS spectra of R_7K. Expected mass = 1238.81.

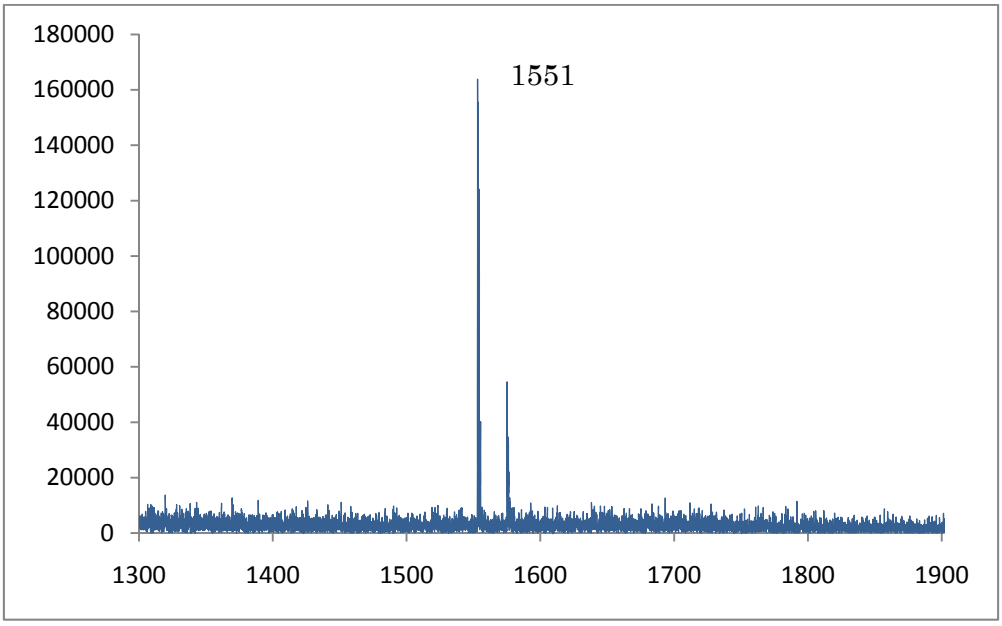

Figure VI-3. ESI-MS spectra of R_9K. Expected mass = 1551.02.

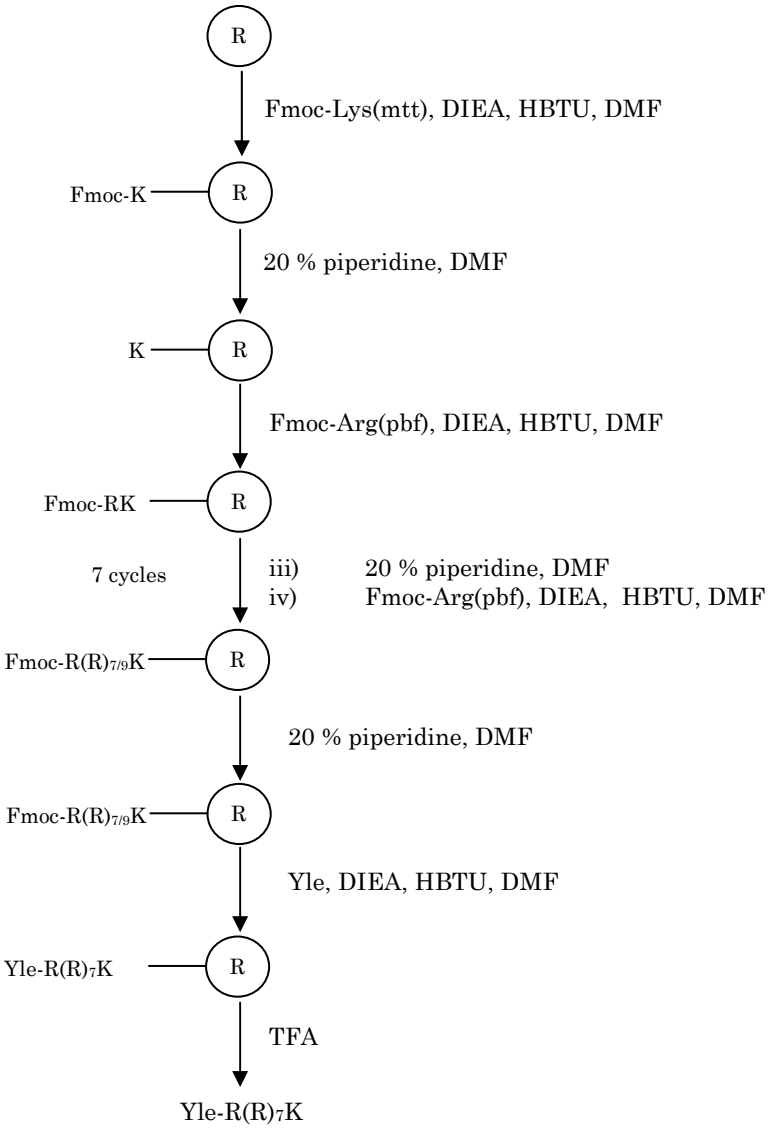

Figure VI-4. Schematic representation of the solid phase synthesis of the diimine-CPP ligand (Yle-CPP).

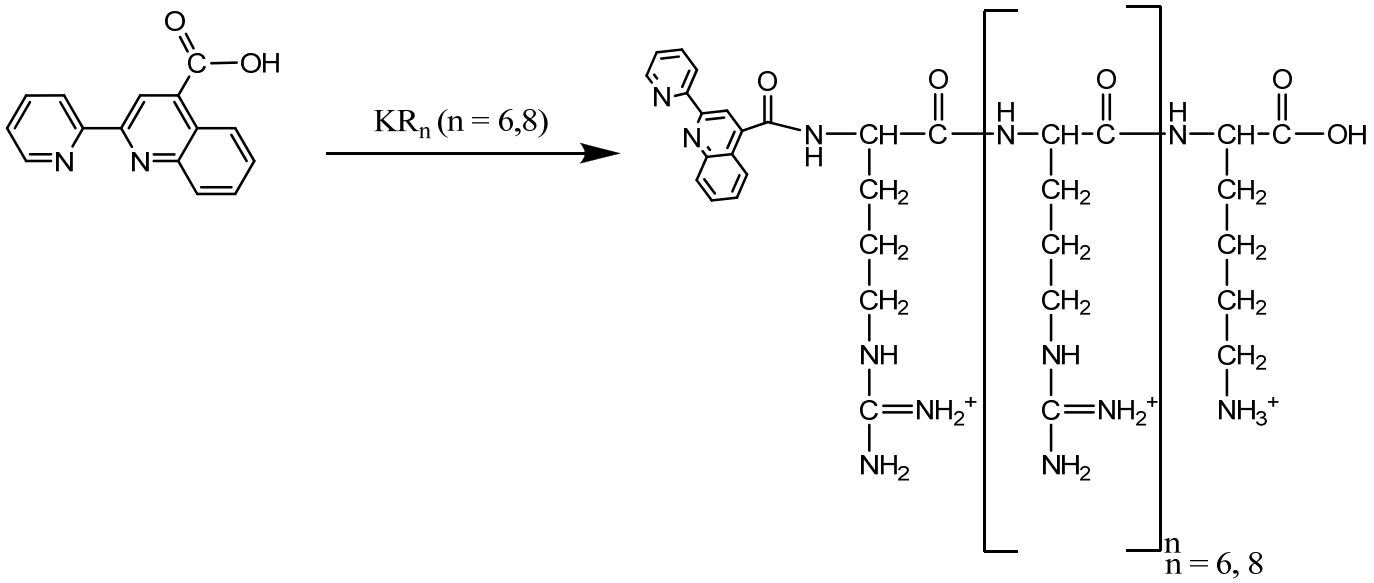

Figure VI-5. Schematic representation of the coupling reaction of Yle with CPP sequences.

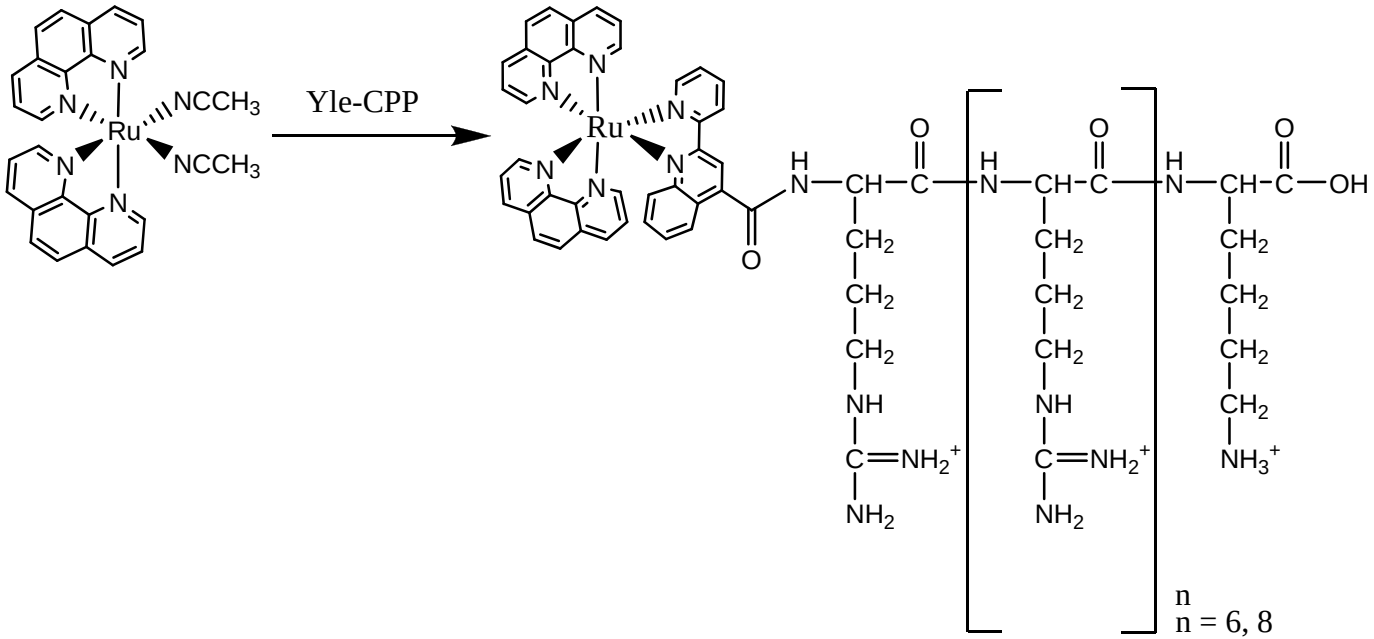

Figure VI-6. Schematic representation of synthesis of the ruthenium-CPP conjugate.

In the case of the diimine-CPP ligand, 2-(2-pyridinyl)-4-carboxyquinoline was chosen due to its ease of synthesis and the presence of a single carboxylic acid group. By taking advance of the -COOH functional group and the solubility of this molecule in DMF, its coupling reaction with the CPP sequence was performed by solid phase peptide synthesis (Figure IV-4 and Figure IV-5). The reaction proceeds in good yields and affords an off-white powder. The final product was purified by reverse phase HPLC using the same conditions used for the purification of the other two peptide sequences described in this chapter.

The reaction between the transporter system (Yle-CPP) and the ruthenium complex $[Ru(phen)_2(CH_3CN)_2](PF_6)_2$ (Figure IV-6) was performed under two different conditions, namely incubation at 37 °C for 25 hours or heating in a commercial microwave oven (100 power) for 2 minutes. As shown in Figure VI-7, the RP-HPLC analysis of the reaction mixture indicates that both methods are equally suitable for the synthesis of the ruthenium complex, both techniques gave similar yields, but the use of microwaves produces faster results. ESI-MS spectrum of the reaction mixture is shown is Figure VI-8.

Reactions between dirhodium carboxylate derivatives were not pursued since preliminary evidence showed that the structural integrity of dirhodium tetraacetate was compromised during the purification by RP-HPLC due to the acidic conditions used.

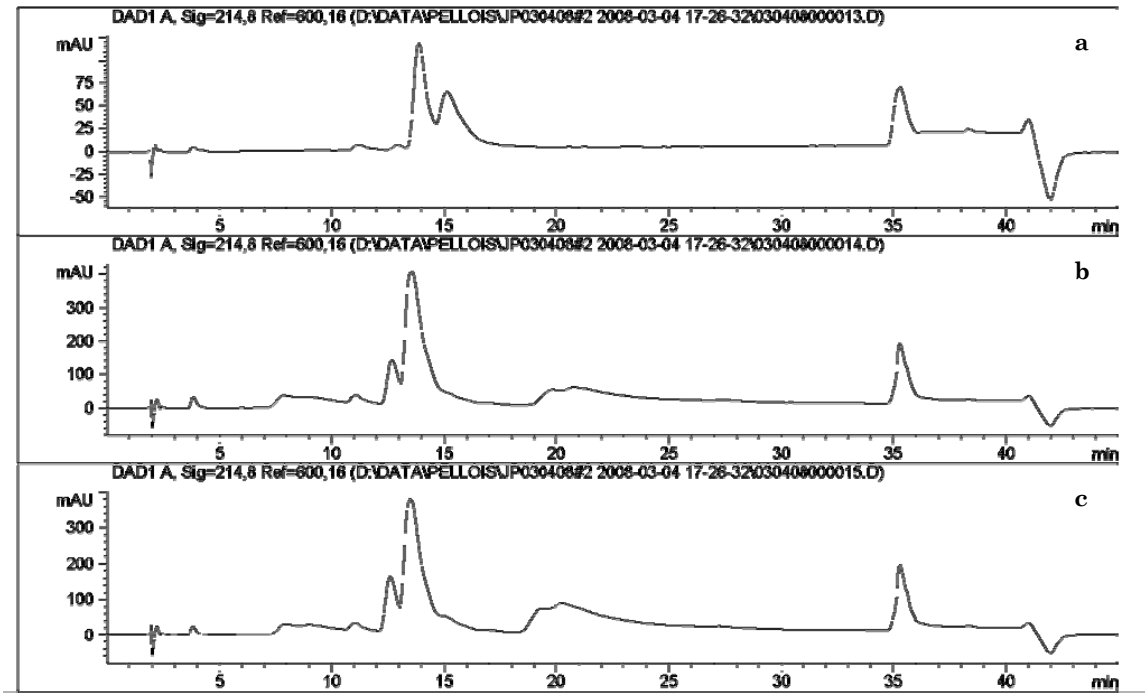

Figure VI-7. RP-HPLC chromatograms a) $[Ru(phen)_2(CH_3CN)_2]^{2+}$ starting material. b) Product of the reaction of $[Ru(phen)_2(CH_3CN)_2]^{2+}$ and Yle-CPP using the microwave. c) Product of the reaction of $[Ru(phen)_2(CH_3CN)_2]^{2+}$ and Yle-CPP after heating and stirring at 37 °C for 25 hours.

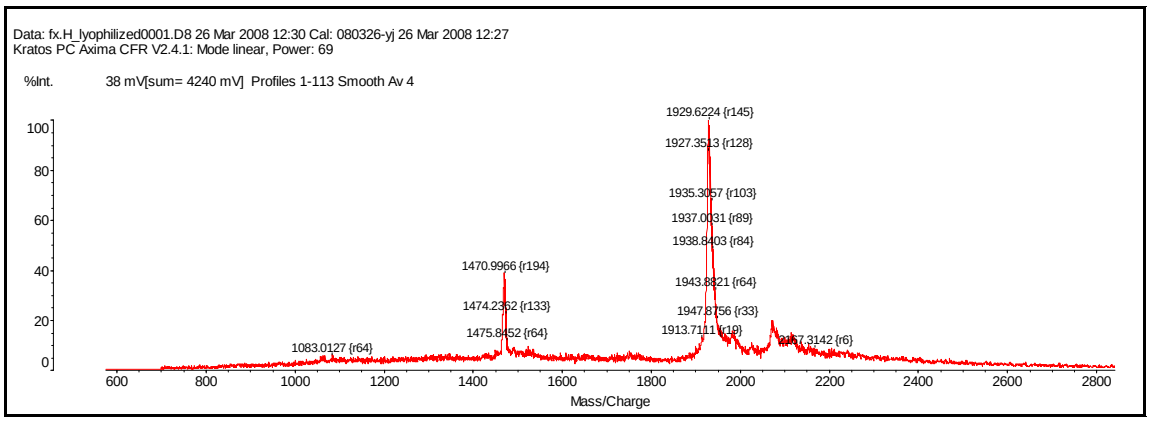

Figure VI-8. ESI-MS spectra of the product of reaction of $[Ru(phen)_2(CH_3CN)_2]^{2+}$ and Yle-CPP.

Co-Incubation Experiments

In order to determine the best concentration of CPP to be used, the cytotoxicities of R_7K and R_9K were studied at different incubation conditions. The MTT assay provided evidence that the CPP sequences at concentrations of 2.5 μM and 5 μM are not toxic when incubation was performed for less than 4 hours.

The dirhodium compounds (Figure VI-9) were mixed with the CPPs for 10 minutes prior to incubation to afford a homogeneous mixture. The dirhodium-CPP mixture was then added to the cells. After 3 hours of incubation the mortality of the cells increases especially at the highest CPP concentration (Table VI-3). As can be seen in Figures VI-10 through VI-13 co-incubation of the dirhodium complexes **1**-**5** with the CPPs R_7K and R_9K results in an enhancement of the cytotoxic properties of the complexes. The increase in cytotoxicity with R_7K is not as prominent as that observed with R_9K, although a significant increase is observed when 5 μM R_7K peptide was used. The delivery using R_9K improves the cytotoxicity of the compounds by 7% to 35% depending on the dirhodium complex when 2.5 μM peptide was used. When 5 μM R_9K was used, the increase in cytotoxicity was greater, reaching as high as 43% as in the case of complex **2**.

As described in chapters IV and V, it was observed that COLO-316 cells are, in general, more sensitive to the dirhodium compounds studied throughout this thesis, but the use of these two CPP sequences, namely R_7K and R_9K, has a greater impact on HeLa cells than on COLO-316. It must be noted that differences in delivery by CPPs on different cell lines have been previously observed, although no globally accepted explanation as to the origin of this effect has been proposed.

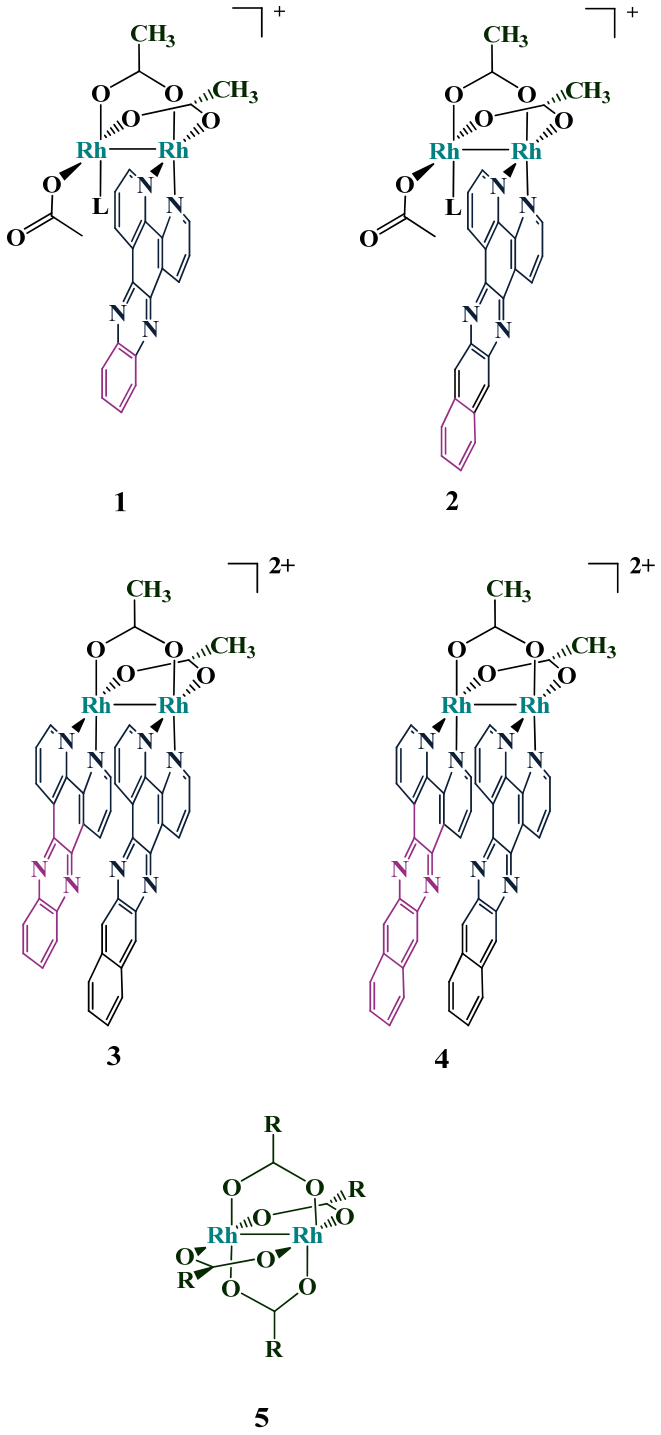

Figure VI-9. Schematic representation of dirhodium compounds used for the co-incubation experiments.

Table VI-3. CPP sequences used in co-incubation experiments.

Compound	CPP Sequence	CPP Concentration μM	% Increase in Cytotoxicity	
			COLO-316	HeLa
1	R_7K	2.5	1.3	13.5
		5	7.9	19.3
	R_9K	2.5	7.9	19.2
		5	19.0	29.0
2	R_7K	2.5	4.8	8.6
		5	57.2	59.0
	R_9K	2.5	68.9	70.1
		5	75.7	76.7
3	R_7K	2.5	2.4	15.8
		5	5.7	18.6
	R_9K	2.5	15.5	27.1
		5	34.4	43.4
4	R_7K	2.5	6.9	10.8
		5	26.0	29.1
	R_9K	2.5	26.7	29.8
		5	41.7	44.1
5	R_7K	2.5	3.5	3.8
		5	10.0	10.0
	R_9K	2.5	3.8	7.4
		5	11.0	11.0

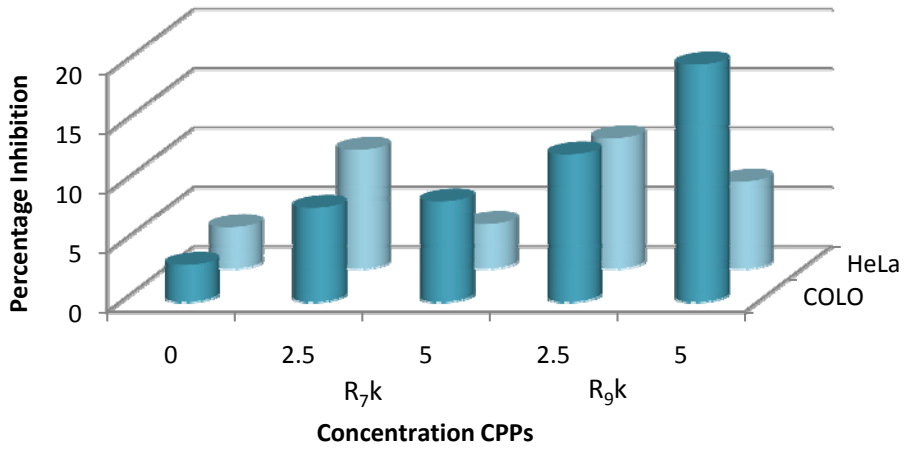

Figure VI-10. Cell mortality increase (%) as a result of co-incubation of compound **1** with the CPPs R_7K and R_9K.

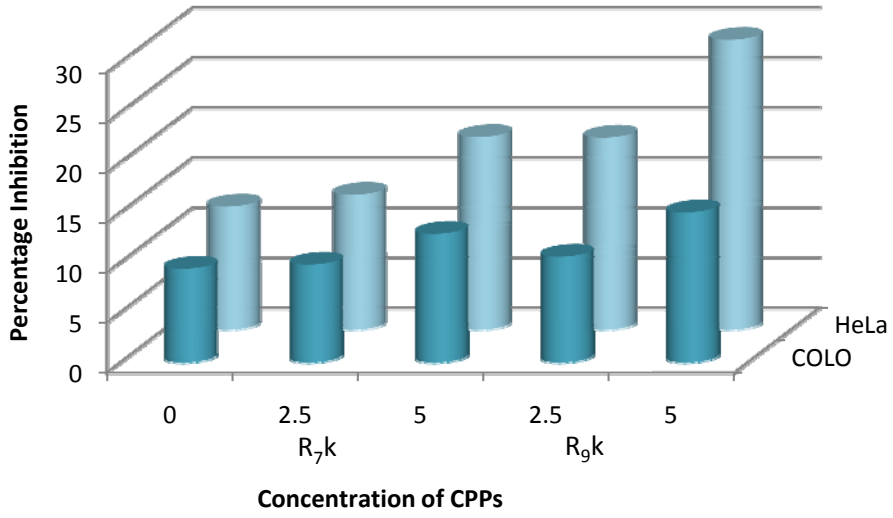

Figure VI-11. Cell mortality increase (%) as a result of co-incubation of compound **2** with the CPPs R_7K and R_9K.

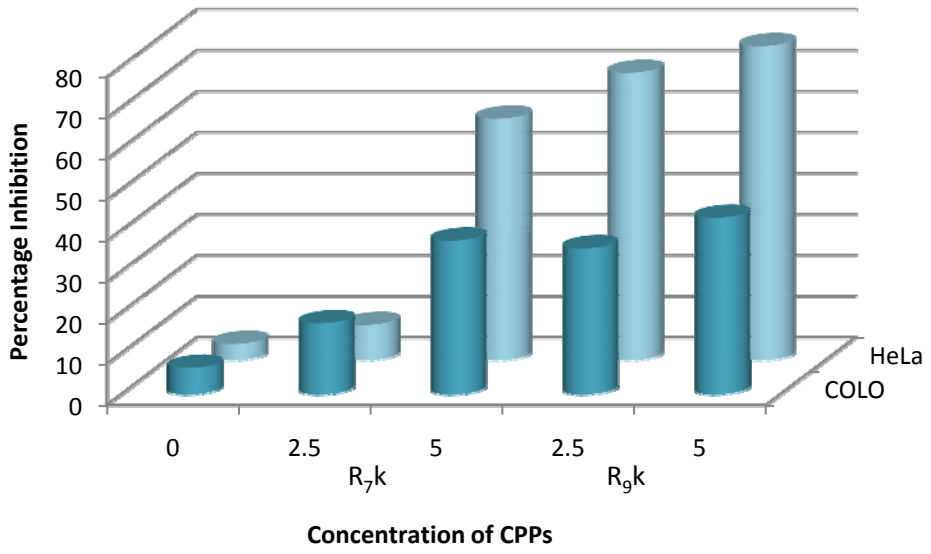

Figure VI-12. Cell mortality increase (%) as a result of co-incubation of compound **3** with the CPPs R_7K and R_9K.

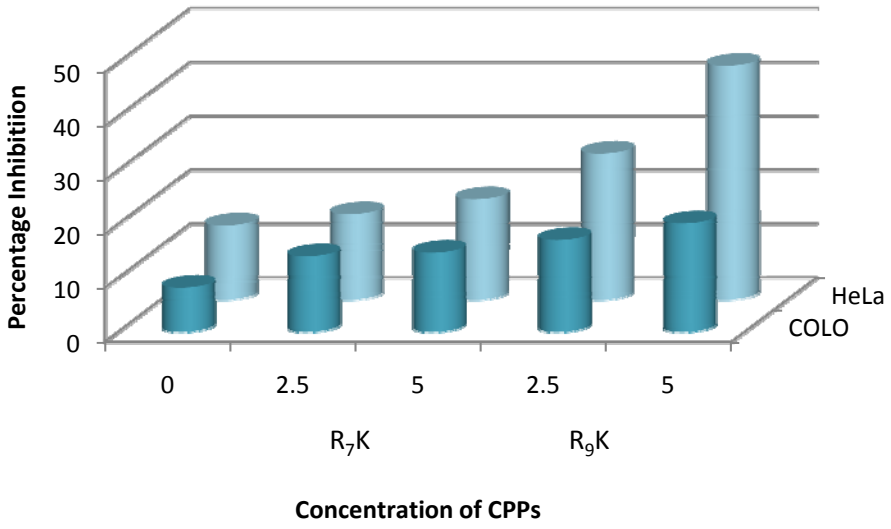

Figure VI-13. Cell mortality increase (%) as a result of co-incubation of compound **4** with the CPPs R_7K and R_9K.

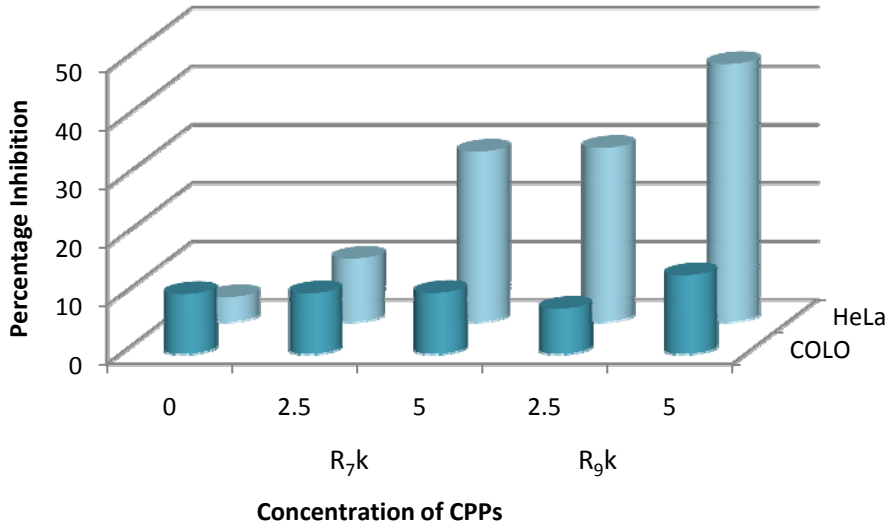

Figure VI-14. Cell mortality increase (%) as a result of co-incubation of compound **5** with the CPPs R_7K and R_9K.

Interactions of Dirhodium Complexes with Polyarginine Peptides

The interactions between compounds **1** – **5** and the CPP sequences used for the co-incubation experiments were followed by UV-Vis spectroscopy. The solutions studied were prepared using the same concentrations used for the co-incubation experiment, for the dirhodium complexes the concentrations that allows for 75% cell viability, while 5 μM for the CPP sequences.

UV-Vis spectroscopy is an excellent tool to follow the axial coordination of ligands of these compounds due to the sensitivity of their electronic spectral properties to the nucleophilic nature of the axial ligand. For example, in $Rh_2(\mu\text{-}O_2CCH_3)_4$, addition of ligands that bind to the axial positions result in a blue-shift of the lowest energy, $Rh_2(\pi^*) \rightarrow Rh_2(\sigma^*)$ metal-centered (MC) transition.[142-145] This shift is due to interaction of the antisymmetric linear combination of the filled orbitals on the axial ligands with the $Rh_2(\sigma^*)$ molecular orbital, which raises the energy of the latter.[130, 140, 146, 147] Addition of coordinative solvents also red-shift the MLCT peaks described as π–π^* transitions centered on the aromatic ligands.

As observed in Figures VI-15 and VI-16 even after 2 hours of incubation of the peptide with the dirhodium complexes no major structural changes are observed. In the case of $Rh_2(\mu\text{-}O_2CCH_3)_4$ the metal-metal bond is still intact since the absorbance at ~ 580 nm decreases in intensity but does not disappear completely. For all the other complexes the $Rh_2(\pi^*) \rightarrow Rh_2(\sigma^*)$ MC transition cannot be observed since the MLCT spreads as far as where this transition appears.[301] The slight blue-shift observed in the MLCT transition, however, hints towards the conclusion that there is an interaction between the peptide and these dirhodium compounds. This interaction does not seem to result in dramatic changes in coordination; therefore, it must probably arise from axial interactions.

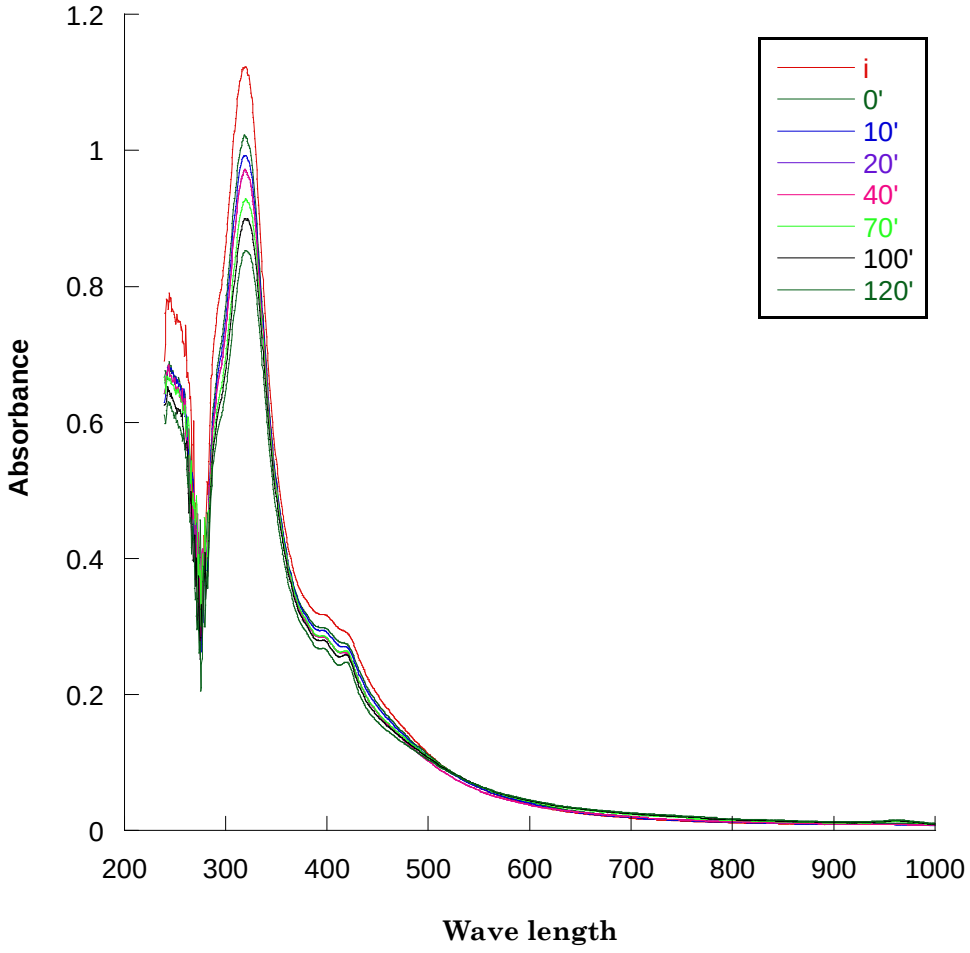

Figure VI-15. Changes over time on the Uv-Vis spectrum of compound **2** when mixed with the CPP R_9K.

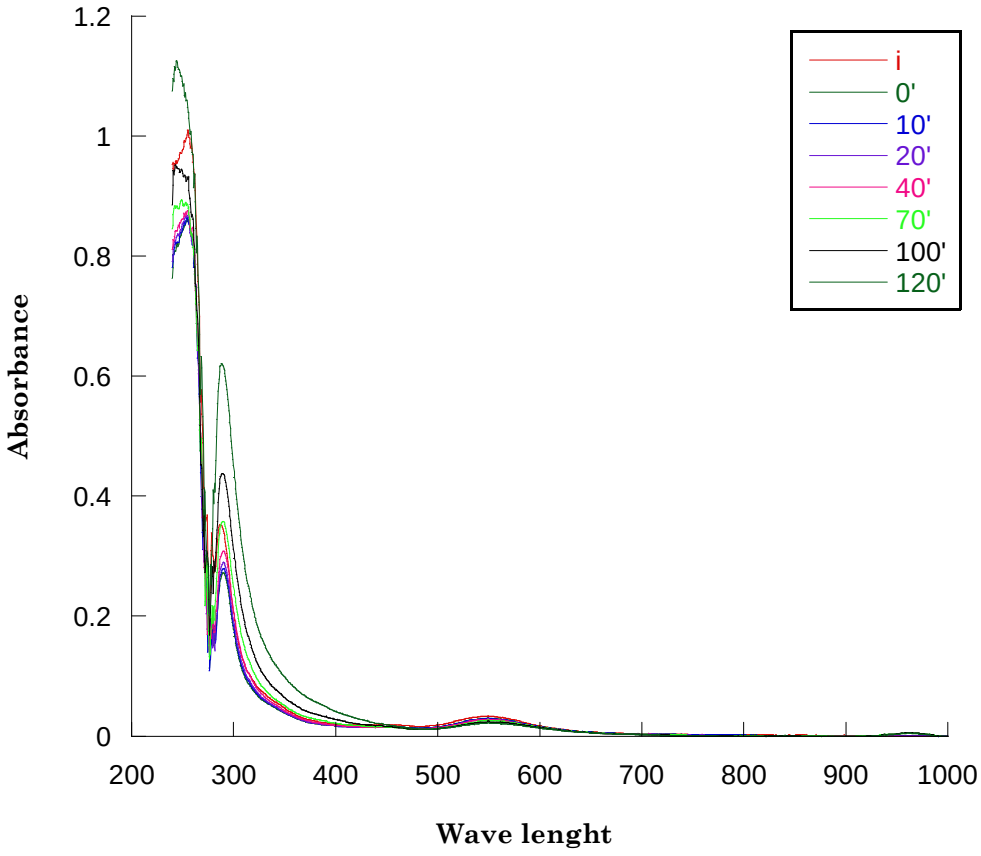

Figure VI-16. Changes over time on the Uv-Vis spectrum of compound **5** when mixed with the CPP R_9K.

Conclusions

Co-incubation of dirhodium complexes with CPP sequences has shown to be a good alternative to increase the effectivity of these compounds. All of the dirhodium complexes studied here become more cytotoxic after co-incubation with the CPPs nonaarginine (R_9K) and heptaarginine (R_7K). Preliminary data indicate that the CPPs bind to the dirhodium complexes through the axial positions. This binding mode is reversible and the dirhodium core can detach from the delivery agent once inside the cell. Overall, R_9K seems to be more effective than R_7K at delivering this type of cargo. In general, co-incubation with these CPP sequences render HeLa cells more sensitive to dirhodium compounds. Surprisingly, this is not the case for $Rh_2(\mu\text{-}O_2CCH_3)_4$ (**1**).

CHAPTER VII
CONCLUDING REMARKS AND FUTURE OUTLOOK

Recent studies of various dirhodium compounds have provided clear evidence that there is a correlation between their molecular characteristics and cytotoxic behavior. These factors include the lability of the groups bound to the dirhodium core, the presence of open coordination sites, the overall charge of the complex, and the hydrophobicity of the ligands bound to the dirhodium core. Tailoring appropriately the groups surrounding the dirhodium core in these complexes may lead to more effective and less toxic drugs.

In chapter II, the interactions with DNA in cell free media and *in cellulo* of dirhodium(II,II) complexes that possess one or two accessible axial coordination sites, *cis*-$[Rh_2(\mu\text{-}O_2CCH_3)_2(np)_2]^{2+}$ and *cis*-$[Rh_2(\mu\text{-}O_2CCH_3)_2(np)(pynp)]^{2+}$, respectively, were compared to a compound in which the axial site positions are blocked, namely *cis*-$[Rh_2(\mu\text{-}O_2CCH_3)_2(pynp)_2]^{2+}$. The results agree with the fact that an accessible axial position is required for the complex to interact with DNA and/or to accomplish biological functions. Whit this knowledge in hand, new compounds can be designed wherein the cytotoxicity may be tuned by controlling the availability of the axial positions. For example, a bifunctional ligand whit binding sites joined together by a flexible linker which forms a strong bond to an equatorial position and a weak bond to an axial may lead to "hemilabile" structures (ON/OFF) whose properties are different from those for which the axial ligand is a permanent leaving group. This design would, in principle, allow

for more exquisite control of the reactivity of the dirhodium complex. Figure VII.1 shows a representation of this approach. In terms of photodynamic therapy, this approach could render compounds with decreased dark toxicity, whereas the photo-cytotoxicity will not be affected since the photochemistry will not be modified.

In chapter III, it has been shown that it is not only possible to modify the reactivity of dirhodium carboxylate and derivatives by changing the axial and/or equatorial ligands directly attached to the dirhodium core but also by adding electron-withdrawing or electron-donating substituents to the dppz ligands. These results underscore the fact that the family of dirhodium complexes of the type *cis*-$[Rh_2(\mu\text{-}O_2CCH_3)_2(R_1R_2dppz)_2]^{2+}$ (R_1R_2dppz = substituted dppz) have a great sensitivity to even subtle changes which makes them promising for tunning the activity by modulating the redox chemistry. It is plausible that dirhodium complexes could be develop as promising candidates for the control of important biochemical processes in which enzymes that use oxidizable residues can be inhibited. Ovbiously, additional studies are required to test the redox activity of this family of compounds *in cellulo*. Assays such as cytotoxicity should be complemented with glutathione modulation experiments to evaluate how the concentration of glutathione affects the properties of the complexes.

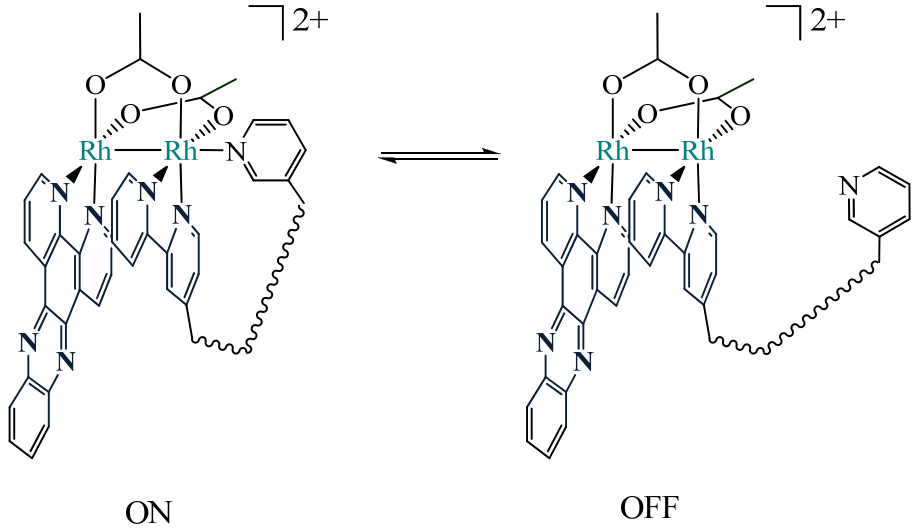

ON OFF

Figure VII-1. Schematic representation of ON and OFF positions of proposed compounds whose biological activity can be modulated through the control of the availability of the axial position.

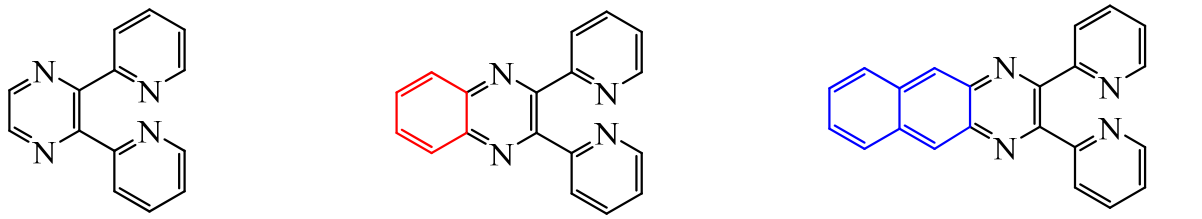

2,3-di(pyridin-2-yl)pyrazine 2,3-di(pyridin-2-yl)quinoxaline 2,3-di(pyridin-2-yl)benzo[*g*]quinoxaline

Figure VII-2. Schematic representation of proposed diimine ligands.

Chapter IV focuses the importance of the structure of the dirhodium carboxylate compounds. Owing to their particular geometry, these compounds are nicely poised for the combination of more than one pharmacological property. In the case of $[Rh_2(\mu\text{-}O_2CCH_3)_2(\eta^1\text{-}O_2CCH_3)(diimine)]^+$, the diimine ligand facilitates the interaction with DNA through intercalation while the dangling acetate allows for covalent bonding of the molecule with DNA. Throughout chapter IV the affinity of the $[Rh_2(\mu\text{-}O_2CCH_3)_2(\eta^1\text{-}O_2CCH_3)(diimine)]^+$ family towards DNA was studied. It was observed that, as the aromatic size of the diimine ligand increases, the higher the affinity for DNA. When the assays were performed *in cellulo*, with the concomitant increase of complexity that exists, other factors such as lipophilicity begin to play a more active role. These compounds are able to damage nuclear DNA as observed from the Comet assay. The hypothesis that DNA damage is caused by ROS and not by direct interaction with the compounds was rejected on the basis of the glutathione modulation experiments. Levels of ROS can be controlled by amounts of glutathione inside the cell, but since there is no effect in the cytotoxicity of the dirhodium complexes studied by changing the levels of glutathione, it can be conclude that the compounds damage DNA directly. Arguably the most important of all the studies presented in chapter IV is the finding that dirhodium complexes are able to reach and react with nuclear DNA. This is the first time that the longstanding premise of DNA being a target of dirhodium complexes in cells has been verified.

Based on the studies presented in chapter IV, a new family of compounds with more flexible diimine ligands ($[Rh_2(\mu\text{-}O_2CCH_3)_2(\eta^1\text{-}$

O_2CCH_3)(flexible-diimine)]$^+$) is proposed that could facilitate the development of a ternary complex between the dirhodium compound, DNA and an enzyme. The idea is that the diimine ligand will still interact with DNA through intercalation but the dirhodium core will have the opportunity to react with an enzyme as well, thereby stalling the function of the latter. This will be possible thanks to the flexibility of the diimine ligand that will facilitate the simultaneous interaction of the dirhodium core with the proteins and DNA.

Chapter V describes the family of compounds of the type [Rh_2(μ-O_2CCH_3)$_2$(*diimine*)(diimine′)]$^{2+}$. These derivatives were used to study the effect of adding a second diimine and gradually increasing its size. Although the cytotoxicity values of this family were similar to those found for the mono-substituted family described in chapter IV ([Rh_2(μ-O_2CCH_3)$_2$(η^1-O_2CCH_3)(diimine)]$^+$) no evidence for nuclear DNA being the possible target was found. Once again, the effect of the lipophilic character of the complexes underscore the point that a delivery system is crucial to aid the most promising complexes to cross the cell membrane where they can interact with their cellular targets.

It is evident from the results reported in chapters IV and V that the reactivity of the dirhodium complexes be tuned by modifying their structure. Dirhodium carboxylate derivatives with one diimine ligand ([Rh_2(μ-O_2CCH_3)$_2$ (η^1-O_2CCH_3)(diimine)]$^+$) are able to reach nuclear DNA, whereas the addition of a second diimine ligand ([Rh_2(μ-O_2CCH_3)$_2$(*diimine*)(diimine′)]$^{2+}$) hinders this ability. Moreover, the size of the second diimine ligand is crucial for determining the mechanism of activity of this family of compounds. When

both diimine ligands are dppn, as in ($[Rh_2(\mu\text{-}O_2CCH_3)_2(dppn)_2]^{2+}$), the mechanism of action is necrosis instead of apoptosis as in the other complexes studied in Chapter V. It is clear that the family of bis-diimine dirhodium complexes deserves more attention with respect to determining the cellular target of these compounds.

Another very important lesson from this work is the usefulness of a delivery agent. As demostrated in Chapter VI, co-incubation of these compounds with two different CPP sequences improves their efficacy, resulting in an increased activity. Although both peptides improved the ability of the dirhodium complexes to decrease the cell viability of HeLa and COLO-316 cell lines, the nonaarginine peptide was the most effective. This peptide was able to increase the cytotoxicity of ($[Rh_2(\mu\text{-}O_2CCH_3)_2(\eta^1\text{-}O_2CCH_3)(dppn)]^+$ in c.a. 75%.

Overall, the collective work described in this thesis has improved our understanding of the molecular properties that affect the activity of dirhodium complexes both *in vitro* and *in cellulo*. This knowledge will help in the future design of molecules based on these systems with improved activity.

REFERENCES

1. Rosenberg, R. B.; Vancamp, L.; Trosko, J. E.; Mansour, V. H., *Nature* **1969,** *222* (5191), 385-387.

2. Orvig, C.; Abrams, M. J., *Chemical Review* **1999,** *99* (9), 2201-2203.

3. Sadler, P. J., *Advanced Inorganic Chemistry* **1991,** *36*, 1-48.

4. Higby, G. J., *Gold Bulletin* **1982,** *15* (4), 130-140.

5. Discher, C. A.; Medwick, T.; Bailey, L. C., *Modern inorganic pharmaceutical chemistry*. 2nd ed.; Waveland Press: Prospect Heights, Ill, 1985.

6. Fricker, S. P., *Dalton Transactions* **2007,** (43), 4903-4917.

7. Bosch, F.; Rosich, L., *Pharmacology* **2008,** *82* (3), 171-179.

8. *Tiekink*, E. R. T., *Critical Reviews in Oncology Hematology* **2002,** *42* (3), 217-224.

9. Manson-Bahr, P. H., *Tropical diseases*. 16th ed.; Tindall & Cassell: London, 1966.

10. Manson, P.; Manson-Bahr, P. H., *Tropical diseases; a manual of the diseases of warm climates*. 14th ed.; Williams & Wilkins: Baltimore, 1954.

11. Rosen, B. P., *Topics in Current Genetics* **2006,** *14*, 485-505.

12. Antman, K. H., *Oncologist* **2001,** *6* (Suppl 2), 1-2.

13. Kinabo, L. D. B., *Acta Tropica* **1993,** *54* (3-4), 169-183.

14. Ravandi, F., *Leukemia* **2004,** *18* (9), 1457-1459.

15. Lloyd Nicholas, C.; Morgan Hugh, W.; Nicholson Brian, K.; Ronimus Ron, S., *Angewandte Chemie International Edition in English* **2005,** *44* (6), 941-944.

16. Merriam-Webster Inc., *The Merriam-Webster dictionary*. Merriam-Webster: Springfield, Mass., 1997.

17. Mertz, W., *Science* **1981,** *213* (4514), 1332-1338.

18. Bertrand, G.; Medigreceanu, F., *Bulletin de la Societe Chimique de France* **1912,** *15*, 37-44.

19. Williams, D. R., *Journal of Inorganic Biochemistry* **2000,** *79* (1-4), 275-283.

20. Desoize, B., *Anticancer Research* **2004,** *24* (3A), 1529-1544.

21. Nguewa, P.; Cepeda, V.; Fuertes, M. A.; Castilla, J.; Alonso, C.; Perez, J. M., *Metal Compounds in Cancer Chemotherapy* **2005**, 1-29.

22. Wolpert, E. A.; Mueller, P., *Archives in General Psychiatry* **1969,** *21* (2), 155-159.

23. Maletzky, B.; Blachly, P. H., *The use of lithium in psychiatry*. CRC Press: Cleveland, 1971.

24. Schrauzer, G. N.; Klippel, K. F., *Lithium in biology and medicine : new applications and developments*. VCH Verlagsgesellschaft; VCH Publishers: Weinheim, Federal Republic of Germany; New York, 1991.

25. Rubin, D. L.; Muller, H. H.; Young, S. W., *Magn. Reson. Med.* **1992,** *23* (1), 154-165.

26. Schibli, R.; Schubiger, P. A., *European Journal of Nuclear Medicine and Molecular Imaging* **2002,** *29* (11), 1529-1542.

27. Bosl, G. J.; Motzer, R., *Journal of Medicine* **1997,** *337*, 242-253.

28. List, A.; Beran, M.; DiPersio, J.; Slack, J.; Vey, N.; Rosenfeld, C. S.; Greenberg, P., *Leukemia* **2003,** *17* (8), 1499-1507.

29. Verstovsek, S.; Estrov, Z., *Leukemia Research* **2004,** *28* (9), 901-903.

30. Rosenberg, R. B.; Vancamp, L.; Krigas, T., *Nature* **1965,** *205* (4972), 698-699.

31. Barabas, K.; Milner, R.; Lurie, D.; Adin, C., *Veterinary and Comparative Oncology* **2008,** *6* (1), 1-18.

32. Barnes, K. R.; Lippard, S. J., *Metal Ions in Biological Systems* **2004,** *42*, 143-177.

33. Jung, Y.; Lippard Stephen, J., *Chemical Reviews* **2007,** *107* (5), 1387-1407.

34. Wong, E.; Giandomenico, C. M., *Chemical Reviews* **1999,** *99* (9), 2451-2466.

35. Graham, M. A.; Lockwood, G. F.; Greenslade, D.; Brienza, S.; Bayssas, M.; Gamelin, E., *Clinical Cancer Research* **2000,** *6* (4), 1205-1218.

36. Misset, J. L.; Bleiberg, H.; Sutherland, W.; Bekradda, M.; Cvitkovic, E., *Critical Reviews in Oncology Hematology* **2000,** *35* (2), 75-93.

37. Itoh, K.; Yamashita, T.; Wakita, H.; Watanabe, Y.; Kodama, K.; Fujii, H.; Minami, H.; Ohtsu, T.; Igarashi, T.; Sasaki, Y. *Successful treatment with nedaplatin in patients with ovarian cancer that recurred after platinum-containing chemotherapy: report of two cases*; Division of Oncology and Hematology, National Cancer Center Hospital East, Chiba, Japan, 1998.

38. Satoh, T.; Tsushima, K.; Saitoh, S.; Hizawa, Y.; Tamura, Y.; Fukuda, S.; Yamada, Y.; Tohno, H.; Takasugi, T.; Sakata, Y.; Munakata, A. *A case of advanced esophageal cancer showing a long-term complete response with chemotherapy with nedaplatin alone*; First Department of Internal Medicine, Hirosaki University School of Medicine, Aomori, Japan, 1999.

39. Uchida, N.; Takeda, Y.; Hojo, K.; Maekawa, R.; Sugita, K.; Yoshioka, T., *European Journal of Cancer* **1998,** *34* (11), 1796-1801.

40. Hannon, M. J., *Pure and Applied Chemistry* **2007,** *79* (12), 2243-2261.

41. Bruijnincx, P. C. A.; Sadler, P. J., *Current Opinion in Chemical Biology* **2008,** *12* (2), 197-206.

42. Jamieson, E. R.; Lippard, S. J., *Chemical Reviews* **1999,** *99* (9), 2467-2498.

43. Foster, B. J.; Clagett-Carr, K.; Hoth, D.; Leyland-Jones, B., *Cancer Treatment Reports* **1986,** *70* (11), 1311-1319.

44. Dreicer, R.; Propert, K. J.; Roth, B. J.; Einhorn, L. H.; Loehrer, P. J., *Cancer* **1997,** *79* (1), 110-114.

45. Dreicer, R.; Lallas, T. A.; Joyce, J. K.; Anderson, B.; Sorosky, J. I.; Buller, R. E., *American Journal of Clinical Oncology* **1998,** *21* (3), 287-290.

46. Kopfmaier, P., *European Journal of Clinical Pharmacology* **1994,** *47* (1), 1-16.

47. Collery, P.; Keppler, B.; Madoulet, C.; Desoize, B., *Critical Reviews in Oncology Hematology* **2002,** *42* (3), 283-296.

48. Vogelzang, N. J.; Gesme, D. H.; Kennedy, B. J., *American Journal of Clinical Oncology* **1985,** *8* (4), 341-344.

49. Crowe, A. J.; Smith, P. J.; Atassi, G., *Chemico-Biological Interactions* **1980,** *32* (1-2), 171-178.

50. Crowe, A. J.; Smith, P. J.; Atassi, G., *Inorganica Chimica Acta* **1984,** *93* (4), 179-184.

51. Chauhan, H. P. S.; Shaik, N. M.; Singh, U. P., *Applied Organometallic Chemistry* **2006,** *20* (2), 142-148.

52. Desoize, B., *Critical Reviews in Oncology Hematology* **2002,** *42* (3), 213-215.

53. Chen, D.; Milacic, V.; Frezza, M.; Dou, Q. P., *Current Pharmaceutical Design* **2009,** *15* (7), 777-791.

54. Wai-Yin Sun, R.; Ma, D.-L.; Wong, E. L.-M.; Che, C.-M., *Dalton Transactions* **2007,** (43), 4884-4892.

55. Guo, M.; Guo, Z.; Sadler, P. J., *Journal of Biological Inorganic Chemistry* **2001,** *6* (7), 698-707.

56. Guo, M. L.; Sun, H. Z.; McArdle, H. J.; Gambling, L.; Sadler, P. J., *Biochemistry* **2000,** *39* (33), 10023-10033.

57. Caruso, F.; Rossi, M., *Metal Ions in Biolgical Systems* **2004,** *42*, 353-384.

58. Kratz, F.; Schutte, M. T., *The Cancer Journal* **1998,** *11* (4), 176-182.

59. Yan, Y. K.; Melchart, M.; Habtemariam, A.; Sadler, P. J., *Chemical Communications* **2005,** (38), 4764-4776.

60. Alessio, E.; Mestroni, G.; Bergamo, A.; Sava, G., *Current Topics in Medicinal Chemistry* **2004,** *4* (15), 1525-1535.

61. Clarke, M. J., *Coordination Chemistry Reviews* **2002,** *232* (1-2), 69-93.

62. Vakifahmetoglu, H.; Olsson, M.; Tamm, C.; Heidari, N.; Orrenius, S.; Zhivotovsky, B., *Cell Death Differ.* **2008,** *15* (3), 555-566.

63. Cepeda, V.; Fuertes, M. A.; Castilla, J.; Alonso, C.; Quevedo, C.; Perez, J. M., *Anti-Cancer Agents in Medicinal Chemistry* **2007,** *7* (1), 3-18.

64. Fuertes, M. A.; Castilla, J.; Alonso, C.; Perez, J. M., *Current Medicinal Chemistry* **2003,** *10* (3), 257-266.

65. Ishida, S.; Lee, J.; Thiele, D. J.; Herskowitz, I., *Proceedings of the National Academy of Sciences of the United States of America* **2002,** *99* (22), 14298-14302.

66. Lin, X.; Okuda, T.; Holzer, A.; Howell, S. B., *Molecular Pharmacology* **2002,** *62* (5), 1154-1159.

67. Cotton, F. A.; Walton, R. A., *Multiple bonds between metal atoms.* 1st ed.; John Wiley & Sons, Inc.: New York, 1982.

68. Chifotides, H. T.; Dunbar, K. R., *Multiple bonds between metal atoms: dirhodium compounds.* 3rd ed.; Springer Science and Business Media, Inc.: New York, 2005.

69. Bear, J. L.; Gray, H. B.; Rainen, L.; Chang, I. M.; Howard, R.; Serio, G.; Kimball, A. P., *Cancer Chemotherapy Reports Part 1* **1975,** *59* (3), 611-620.

70. Bear, J. L.; Howard, R. A.; Dennis, A. M., *Current Chemotherapy, Proc 10th International Congress of Chemotherapy* **1978,** *2*, 1321-1323.

71. Erck, A.; Rainen, L.; Whileyma.J; Chang, I. M.; Kimball, A. P.; Bear, J., *Proceedings of the Society for Experimental Biology and Medicine* **1974,** *145* (4), 1278-1283.

72. Howard, R. A.; Sherwood, E.; Erck, A.; Kimball, A. P.; Bear, J. L., *Journal of Medicinal Chemistry* **1977,** *20* (7), 943-946.

73. Howard, R. A.; Kimball, A. P.; Bear, J. L., *Cancer Research* **1979,** *39* (7, Pt. 1), 2568-2573.

74. Reibscheid, E. M.; Zyngier, S.; Maria, D. A.; Mistrone, R. J.; Sinisterra, R. D.; Couto, L. G.; Najjar, R., *Brazilian Journal of Medical and Biological Research* **1994,** *27* (1), 91-94.

75. Esposito, B. P.; Zyngier, S. B.; de Souza, A. R.; Najjar, R., *Met Based Drugs* **1997,** *4* (6), 333-338.

76. Esposito, B. P.; Zyngier, S. B.; Najjar, R.; Paes, R. P.; Ueda, S. M. Y.; Barros, J. C. A., *Metal-Based Drugs* **1999,** *6* (1), 17-18.

77. Fimiani, V.; Ainis, T.; Cavallaro, A.; Piraino, P., *Journal of Chemotherapy* **1990,** *2* (5), 319-326.

78. Pruchnik, F.; Dus, D., *Journal of Inorganic Biochemistry* **1996,** *61* (1), 55-61.

79. Pruchnik, F. P.; Kluczewska, G.; Wilczok, A.; Mazurek, U.; Wilczok, T., *Journal of Inorganic Biochemistry* **1997,** *65* (1), 25-34.

80. Bien, M.; Pruchnik, F. P.; Seniuk, A.; Lachowicz, T. M.; Jakimowicz, P., *Journal of Inorganic Biochemistry* **1999,** *73* (1-2), 49-55.

81. Rainen, L.; Howard, R. A.; Kimball, A. P.; Bear, J. L., *Inorganic Chemistry* **1975,** *14* (11), 2752-2754.

82. Pneumatikakis, G.; Hadjiliadis, N., *Journal of the Chemical Society, Dalton Transactions* **1979,** (4), 596-599.

83. Rubin, J. R.; Haromy, T. P.; Sundaralingam, M., *Acta Crystallographyca, Sect. C: Crystal Structure Communications* **1991,** *C47* (8), 1712-1714.

84. Farrell, N., *Journal of Inorganic Biochemistry* **1981,** *14* (3), 261-265.

85. Farrell, N., *Journal of the Chemical Society, Chemical Communications* **1980,** (21), 1014-1016.

86. Gil, E. D.; Serrano, S. H. P.; Ferreira, E. I.; Kubota, L. T., *Journal of Pharmaceutical and Biomedical Analysis* **2002,** *29* (4), 579-584.

87. Crawford, C. A.; Day, E. F.; Saharan, V. P.; Folting, K.; Huffman, J. C.; Dunbar, K. R.; Christou, G., *Chemical Communications* **1996,** (10), 1113-1114.

88. Aoki, K.; Salam, M., *Inorganica Chimica Acta* **2002,** *339*, 427-437.

89. Catalan, K. V.; Mindiola, D. J.; Ward, D. L.; Dunbar, K. R., *Inorganic Chemistry* **1997,** *36* (11), 2458-2460.

90. Catalan, K. V.; Hess, J. S.; Maloney, M. M.; Mindiola, D. J.; Ward, D. L.; Dunbar, K. R., *Inorganic Chemistry* **1999,** *38* (17), 3904-3913.

91. Hotze, A. C. G.; Broekhuisen, M. E. T.; Velders, A. H.; Van der Schilden, K.; Haasnoot, J. G.; Reedijk, J., *European Journal of Inorganic Chemistry* **2002,** (2), 369-376.

92. Chifotides, H. T.; Koshlap, K. M.; Perez, L. M.; Dunbar, K. R., *Journal of the American Chemical Society* **2003,** *125* (35), 10703-10713.

93. Chifotides, H. T.; Koshlap, K. M.; Perez, L. M.; Dunbar, K. R., *Journal of the American Chemical Society* **2003,** *125* (35), 10703-10713.

94. Chifotides, H. T.; Dunbar, K. R., *Chemistry-A European Journal* **2006,** *12* (25), 6458-6468.

95. Asara, J. M.; Hess, J. S.; Lozada, E.; Dunbar, K. R.; Allison, J., *Journal of the American Chemical Society* **2000,** *122* (1), 8-13.

96. Chifotides, H. T.; Koomen, J. M.; Kang, M. J.; Tichy, S. E.; Dunbar, K. R.; Russell, D. H., *Inorganic Chemistry* **2004,** *43* (20), 6177-6187.

97. Dunham, S. U.; Chifotides, H. T.; Mikulski, S.; Burr, A. E.; Dunbar, K. R., *Biochemistry* **2005,** *44* (3), 996-1003.

98. Sorasaenee, K.; Fu, P. K. L.; Angeles-Boza, A. M.; Dunbar, K. R.; Turro, C., *Inorganic Chemistry* **2003,** *42* (4), 1267-1271.

99. Chifotides, H. T.; Fu, P. K. L.; Dunbar, K. R.; Turro, C., *Inorganic Chemistry* **2004,** *43* (3), 1175-1183.

100. Bradley, P. M.; Bursten, B. E.; Turro, C., *Inorganic Chemistry* **2001,** *40* (6), 1376-1379.

101. Fu, P. K.; Bradley, P. M.; Turro, C., *Inorganic Chemistry* **2001,** *40* (11), 2476-2477.

102. Bradley, P. M.; Angeles-Boza, A. M.; Dunbar, K. R.; Turro, C., *Inorganic Chemistry* **2004,** *43* (8), 2450-2452.

103. Angeles-Boza, A. M.; Bradley, P. M.; Fu, P. K. L.; Wicke, S. E.; Bacsa, J.; Dunbar, K. R.; Turro, C., *Inorganic Chemistry* **2004,** *43* (26), 8510-8519.

104. Angeles-Boza, A. M.; Bradley, P. M.; Fu, P. K. L.; Shatruk, M.; Hilfiger, M. G.; Dunbar, K. R.; Turro, C., *Inorganic Chemistry* **2005,** *44* (21), 7262-7264.

105. Clarke, M. J.; Zhu, F.; Frasca, D. R., *Chemical Reviews* **1999,** *99* (9), 2511-2533.

106. Chifotides, H. T.; Dunbar, K. R., *Accounts of Chemical Research* **2005,** *38* (2), 146-156.

107. Kitchens, J.; Bear, J. L., *Journal of Inorganic & Nuclear Chemistry* **1969,** *31* (8), 2415-2421.

108. Kitchens, J.; Bear, J. L., *Thermochimica Acta* **1970,** *1* (6), 537-544.

109. Bien, M.; Lachowicz, T. M.; Rybka, A.; Pruchnik, F. P.; Trynda, L., *Metal-based Drugs* **1997,** *4* (2), 81-88.

110. Pruchnik, F. P.; Starosta, R.; Ciunik, Z.; Opolski, A.; Wietrzyk, J.; Wojdat, E.; Dus, D., *Canadian Journal of Chemistry-Revue Canadienne de Chimie* **2001,** *79* (5), 868-877.

111. Hughes, R. G. B., J. L.; Kimball A. P., *Proceedings of the American Association for Cancer Research* **1972,** *13*, 120-123.

112. Lee, S. H.; Chao, D. L.; Bear, J. L.; Kimball, A. P., *Cancer Chemotherapy Reports, Part 1* **1975,** *59* (3), 661-663.

113. Dunbar, K. R.; Matonic, J. H.; Saharan, V. P.; Crawford, C. A.; Christou, G., *Journal of the American Chemical Society* **1994,** *116* (5), 2201-2202.

114. Day, E. F.; Crawford, C. A.; Folting, K.; Dunbar, K. R.; Christou, G., *Journal of the American Chemical Society* **1994,** *116* (20), 9339-9340.

115. Aoki, K.; Salam, M. A., *Inorganica Chimica Acta* **2001,** *316* (1,2), 50-58.

116. Perlepes, S. P.; Huffman, J. C.; Matonic, J. H.; Dunbar, K. R.; Christou, G., *Journal of the American Chemical Society* **1991,** *113* (7), 2770-2771.

117. Crawford, C. A.; Matonic, J. H.; Streib, W. E.; Huffman, J. C.; Dunbar, K. R.; Christou, G., *Inorganic Chemistry* **1993,** *32* (14), 3125-3133.

118. Rotondo, E.; Mann, B. E.; Piraino, P.; Tresoldi, G., *Inorganic Chemistry* **1989,** *28* (15), 3070-3073.

119. Pimblett, G.; Garner, C. D.; Clegg, W., *Dalton Transactions* **1986,** (6), 1257-1263.

120. Campos-Fernandez, C. S.; Thomson, L. M.; Galan-Mascaros, J. R.; Xiang, O.; Dunbar, K. R., *Inorganic Chemistry* **2002,** *41* (6), 1523-1533.

121. SAINT, Version 6.34; Bruker AXS Inc.*:* Madison, WI, 2001.

122. SADABS, Version 2.03; Bruker AXS Inc.*:* Madison, WI, 2002.

123. Sheldrick, G. M. *SHELX, Programs for Solving and Refining Crystal Structures*, University of Gottingen: Germany, 1997.

124. Frisch, M. J. T., G. W.; Schlegel, H. B.; Scuseria, G. E.; Robb, M. A.; Cheeseman, J. R.; Zakrzewski, V. G.; Montgomery, J. A.; Stratmann, R. E.; Burant, J. C.; Dapprich, S.; Millam, J. M.; Daniels, A. D.; Kudin, K. N.; Strain, M. C.; Farkas, O.; Tomasi, J.; Barone, V.; Cossi, M.; Cammi, R.; Mennucci, B.; Pomelli, C.; Adamo, C.; Clifford, S.; Ochterski, J.; Petersson, G. A.; Ayala, P. Y.; Cui, Q.; Morokuma, K.; Malick, D. K.; Rabuck, A. D.; Raghavachari, K.; Foresman, J. B.; Cioslowski, J.; Ortiz, J. V.; Stefanov, B. B.; Liu, G.; Liashenko, A.; Piskorz, P.; Komaromi, I.; Gomperts, R.; Martin, R. L.; Fox, D. J.; Keith, T.; Al-Laham, M. A.; Peng, C. Y.; Nanayakkara, A.; Gonzalez, C.; Challacombe, M.; Gill, P. M. W.; Johnson, B. G.; Chen, W.; Wong, M. W.; Andres, J. L.; Head-Gordon, M.; Replogle, E. S.; Pople J. A. *Gaussian 98, revision A.7;* Gaussian, Inc.: , Pittsburgh, PA, 1998.

125. Becke, A. D., *Physical Review A: General Physics* **1988,** *38* (6), 3098-3100.

126. Becke, A. D., *Journal of Chemical Physics*. **1993,** *98* (7), 5648-5652.

127. Lee, C.; Yang, W.; Parr, R. G., *Physical Review B: Condensed Matter* **1988,** *37* (2), 785-789.

128. Hehre, W. J., *Ab initio molecular orbital theory*. Wiley: New York, 1986.

129. Andrae, D.; Haeussermann, U.; Dolg, M.; Stoll, H.; Preuss, H., *Theor. Chimica Acta* **1990,** *77* (2), 123-141.

130. Bursten, B. E.; Cotton, F. A., *Inorganic Chemistry* **1981,** *20* (9), 3042-3048.

131. Flukiger, P. *Development of molecular graphics package MOLEKEL*. University of Geneva, Switzerland, Geneva, 1992.

132. Gagne, R. R.; Koval, C. A.; Lisensky, G. C., *Inorganic Chemistry* **1980,** *19* (9), 2854-2855.

133. Sawyer, D. T.; Sobkowiak, A.; Roberts, J. L., *Electrochemistry for chemists*. 2nd ed.; Wiley: New York, 1995.

134. Chouai, A.; Wicke, S. E.; Turro, C.; Bacsa, J.; Dunbar, K. R.; Wang, D.; Thummel, R. P., *Inorganic Chemistry* **2005,** *44* (17), 5996-6003.

135. Wozniak, K.; Blasiak, J., *Acta Biochimimica Polonica* **2002,** *49* (3), 583-596.

136. Fu, P. K. L.; Turro, C., *Chemical Communications* **2001,** (3), 279-280.

137. Fu, P. K. L.; Bradley, P. M.; Turro, C., *Inorganic Chemistry* **2003,** *42* (3), 878-884.

138. Campos-Fernandez, C. S.; Xiang, O. Y.; Dunbar, K. R., *Inorganic Chemistry* **2000,** *39* (12), 2432-2433.

139. Pruchnik, F. P.; Jutarska, A.; Ciunik, Z.; Pruchnik, M., *Inorganica Chimica Acta* **2004,** *357* (10), 3019-3026.

140. Sowa, T.; Kawamura, T.; Shida, T.; Yonezawa, T., *Inorganic Chemistry* **1983,** *22* (1), 56-61.

141. Crawford, C. A.; Matonic, J. H.; Huffman, J. C.; Folting, K.; Dunbar, K. R.; Christou, G., *Inorganic Chemistry* **1997,** *36* (11), 2361-2371.

142. Martin, D. S., Jr.; Webb, T. R.; Robbins, G. A.; Fanwick, P. E., *Inorganic Chemistry* **1979,** *18* (2), 475-478.

143. Dubicki, L.; Martin, R. L., *Inorganic Chemistry* **1970,** *9* (3), 673-675.

144. Cotton, F. A.; Felthouse, T. R., *Inorganic Chemistry* **1981,** *20* (2), 584-600.

145. Clark, R. J. H.; Hempleman, A. J., *Inorganic Chemistry* **1989,** *28* (4), 746-752.

146. Norman, J. G., Jr.; Kolari, H. J., *Journal of the American Chemical Society* **1978,** *100* (3), 791-799.

147. Nakatsuji, H.; Ushio, J.; Kanda, K.; Onishi, Y.; Kawamura, T.; Yonezawa, T., *Chemical Physics Letters* **1981,** *79* (2), 299-304.

148. Chavan, M. Y.; Zhu, T. P.; Lin, X. Q.; Ahsan, M. Q.; Bear, J. L.; Kadish, K. M., *Inorganic Chemistry* **1984,** *23* (26), 4538-4545.

149. Boyar, E. B.; Robinson, S. D., *Coordination Chemistry Reviews* **1983,** *50* (1-2), 109-208.

150. Felthouse, T. R., *Progress in Inorganic Chemistry* **1982,** *29*, 73-166.

151. Kalsbeck, W. A.; Thorp, H. H., *Journal of the American Chemical Society* **1993,** *115* (16), 7146-7151.

152. Kalsbeck, W. A.; Thorp, H. H., *Inorganic Chemistry* **1994,** *33* (15), 3427-3429.

153. Tang, T.-C.; Huang, H.-J., *Electroanalysis* **1999,** *11* (16), 1185-1190.

154. Paoletti, C.; LePecq, J. B.; Lehman, I. R., *Journal of Molecular Biology* **1971,** *55* (1), 75-100.

155. Suh, D.; Chaires, J. B., *Bioorganic & Medicinal Chemistry* **1995,** *3* (6), 723-728.

156. Subirana, J. A.; Soler-Lopez, M., *Annual Review of Biophysics and Biomolecular Structure* **2003,** *32*, 27-45.

157. Williams, L. D.; Maher, L. J., III, *Annual Review of Biophysics and Biomolecular Structure* **2000,** *29*, 497-521.

158. Hud, N. V.; Polak, M., *Current Opinion in Structural Biology* **2001,** *11* (3), 293-301.

159. Nakano, S.; Fujimoto, M.; Hara, H.; Sugimoto, N., *Nucleic Acids Research* **1999,** *27* (14), 2957-2965.

160. Duguid, J. G.; Bloomfield, V. A.; Benevides, J. M.; Thomas, G. J., Jr., *Biophysical Journal* **1995,** *69* (6), 2623-2641.

161. Tselepi-Kalouli, E.; Katsaros, N., *Journal of Inorganic Biochemistry* **1989,** *37* (4), 271-282.

162. Karpel, R. L.; Bertelsen, A. H.; Fresco, J. R., *Biochemistry* **1980,** *19* (3), 504-512.

163. Van Garderen, C. J.; Van Houte, L. P. A.; Van den Elst, H.; Van Boom, J. H.; Reedijk, J., *Journal of the American Chemical Society* **1989,** *111* (11), 4123-4125.

164. Brabec, V.; Reedijk, J.; Leng, M., *Biochemistry* **1992,** *31* (49), 12397-12402.

165. Zaludova, R.; Kleinwaechter, V.; Brabec, V., *Biophys.Chem.* **1996,** *60* (3), 135-142.

166. Sorasaenee, K.; Galan-Mascaros, J. R.; Dunbar, K. R., *Inorganic Chemistry* **2003,** *42* (3), 661-663.

167. Imamichi, T.; Murphy, M. A.; Adelsberger, J. W.; Yang, J.; Watkins, C. M.; Berg, S. C.; Baseler, M. W.; Lempicki, R. A.; Guo, J.; Levin, J. G.; Lane, H. C., *Journal of Virology* **2003,** *77* (2), 1011-1020.

168. Chang, T.-C.; Tsai, L.-C.; Hung, M.-W.; Chu, L.-L.; Chu, J.-T.; Chen, Y.-C., *Biochemical Pharmacology* **1997,** *53* (7), 969-977.

169. Blagosklonny, M. V., *Cell Cycle* **2004,** *3* (12), 1537-1542.

170. Phillips, D. R.; Crothers, D. M., *Biochemistry* **1986,** *25* (23), 7355-7362.

171. Mansilla, S.; Rojas, M.; Bataller, M.; Priebe, W.; Portugal, J., *Biochemical Pharmacology* **2007,** *73* (7), 934-942.

172. Bakker, M.; van der Graaf, W. T. A.; Groen, H. J. M.; Smit, E. F.; De Vries, E. G. E., *Current Pharmaceutical Design* **1995,** *1* (1), 133-144.

173. Jiang, X. R.; Macey, M. G.; Kelsey, S. M.; Collins, P. W.; Gutteridge, C. N.; Miki, T.; Adachi, K.; Yamabe, S.; Newland, A. C., *Journal of Chemotherapy* **1993,** *5* (5), 334-343.

174. Antoniou, T.; Tseng, A. L., *Clinical Pharmacokinetics* **2005,** *44* (2), 111-145.

175. Portugal, J.; Martin, B.; Vaquero, A.; Ferrer, N.; Villamarin, S.; Priebe, W., *Current Medicinal Chemistry* **2001,** *8* (1), 1-8.

176. Marin, S.; Mansilla, S.; Garcia-Reyero, N.; Rojas, M.; Portugal, J.; Pina, B., *Biochemical Journal* **2002,** *368* (1), 131-136.

177. O'Dwyer, P. J.; Stevenson, J. P.; Johnson, S. W., *Cisplatin* **1999**, 31-69.

178. Chu, W.; Shinomiya, M.; Kamitori, K. Y.; Kamitori, S.; Carlson, R. G.; Weaver, R. F.; Takusagawa, F., *Journal of the American Chemical Society* **1994,** *116* (18), 7971-7982.

179. Takusagawa, F.; Carlson, R. G.; Weaver, R. F., *Bioorganic & Medicinal Chemistry* **2001,** *9* (3), 719-725.

180. Kester, H. A.; Blanchetot, C.; Den Hertog, J.; Van der Saag, P. T.; Van der Burg, B., *Journal of Biological Chemistry* **1999,** *274* (39), 27439-27447.

181. Taatjes, D. J.; Gaudiano, G.; Resing, K.; Koch, T., *Journal of Medicinal Chemistry* **1997,** *40* (8), 1276-1286.

182. Cullinane, C.; Mazur, S. J.; Essigmann, J. M.; Phillips, D. R.; Bohr, V. A., *Biochemistry* **1999,** *38* (19), 6204-6212.

183. Trimmer, E. E.; Essigmann, J. M., *Essays in Biochemistry* **1999,** *34*, 191-211.

184. Aune, G. J.; Furuta, T.; Pommier, Y., *Anti-Cancer Drugs* **2002,** *13* (6), 545-555.

185. Gojo, I.; Zhang, B.; Fenton, R. G., *Clinical Cancer Research* **2002,** *8* (11), 3527-3538.

186. Gillet, R.; Bobichon, H.; Trentesaux, C., *Biology of the Cell* **2002,** *94* (4-5), 267-273.

187. Jaspers, N. G. J.; Raams, A.; Kelner, M. J.; Ng, J. M. Y.; Yamashita, Y. M.; Takeda, S.; McMorris, T. C.; Hoeijmakers, J. H. J., *DNA Repair* **2002,** *1* (12), 1027-1038.

188. Gajate, C.; An, F.; Mollinedo, F., *Journal of Biological Chemistry* **2002,** *277* (44), 41580-41589.

189. Rokhlin, O. W.; Glover, R. A.; Taghiyev, A. F.; Guseva, N. V.; Seftor, R. E. B.; Shyshynova, I.; Gudkov, A. V.; Cohen, M. B., *Journal of Biological Chemistry* **2002,** *277* (36), 33213-33219.

190. Campbell, E. A.; Korzheva, N.; Mustaev, A.; Murakami, K.; Nair, S.; Goldfarb, A.; Darst, S. A., *Cell* **2001,** *104* (6), 901-912.

191. Luo, G.; Lewis, R. A., *Biochemical Pharmacology* **1992,** *44* (11), 2251-2258.

192. Chao, S.-H.; Price, D. H., *Journal of Biological Chemistry* **2001,** *276* (34), 31793-31799.

193. Bailey, S. A.; Graves, D. E.; Rill, R.; Marsch, G., *Biochemistry* **1993,** *32* (22), 5881-5887.

194. Dickeson, J. E.; Summers, L. A., *Australian Journal of Chemistry* **1970,** *23* (5), 1023-1027.

195. Holmlin, R. E.; Yao, J. A.; Barton, J. K., *Inorganic Chemistry* **1999,** *38* (1), 174-189.

196. Kleineweischede, A.; Mattay, J., *Journal of Organometallic Chemistry* **2006,** *691* (9), 1834-1844.

197. Waterland, M. R.; Gordon, K. C.; McGarvey, J. J.; Jayaweera, P. M., *Journal of the Chemical Society, Dalton Transactions Inorganic Chemistry* **1998,** (4), 609-616.

198. Rempel, G. A.; Legzdins, P.; Smith, H.; Wilkinson, G., *Inorganic Synthesis* **1971,** *13*, 90-91.

199. Cossi, M.; Barone, V.; Cammi, R.; Tomasi, J., *Chemical Physics Letters* **1996,** *255* (4,5,6), 327-335.

200. Miertus, S.; Scrocco, E.; Tomasi, J., *Chemical Physics* **1981,** *55* (1), 117-129.

201. Gill, S. C.; Von Hippel, P. H., *Analytical Biochemistry* **1989,** *182* (2), 319-326.

202. King, G. C.; Martin, C. T.; Thang, T. P.; Coleman, J. E., *Biochemistry* **1986,** *25* (1), 36-40.

203. Waterland, M. R.; Gordon, K. C., *Journal of Raman Spectroscopy* **2000,** *31* (4), 243-253.

204. Lundin, N. J.; Walsh, P. J.; Howell, S. L.; McGarvey, J. J.; Blackman, A. G.; Gordon, K. C., *Inorganic Chemistry* **2005,** *44* (10), 3551-3560.

205. Dougan, S. J.; Habtemariam, A.; McHale, S. E.; Parsons, S.; Sadler, P. J., *Proceedings of the National Academy of Sciences of the United States of America* **2008,** *105* (33), 11628-11633.

206. Fees, J.; Ketterle, M.; Klein, A.; Fiedler, J.; Kaim, W., *Journal of the Chemical Society, Dalton Transactions Inorganic Chemistry* **1999,** (15), 2595-2600.

207. Berger, S.; Fiedler, J.; Reinhardt, R.; Kaim, W., *Inorganic Chemistry* **2004,** *43* (4), 1530-1538.

208. Cheetham, G. M. T.; Steitz, T. A., *Current Opinion in Structural Biology* **2000,** *10* (1), 117-123.

209. McAllister, W. T., *Cellular and Molecular Biology Research* **1993,** *39* (4), 385-391.

210. Sousa, R.; Mukherjee, S., *Progress in Nucleic Acid Research & Molecular Biology* **2003,** *73*, 1-41.

211. Doublie, S.; Tabor, S.; Long, A. M.; Richardson, C. C.; Ellenberger, T., *Nature* **1998,** *391* (6664), 251-258.

212. McAllister, W. T., *Nucleic Acids & Molecular Biology* **1997,** *11*, 15-25.

213. Ujvari, A.; Martin, C. T., *Journal of Molecular Biology* **1997,** *273* (4), 775-781.

214. Nayak, D.; Siller, S.; Guo, Q.; Sousa, R., *Journal of Molecular Biology* **2008,** *376* (2), 541-553.

215. Moffatt, B. A.; Dunn, J. J.; Studier, F. W., *Journal of Molecular Biology* **1984,** *173* (2), 265-269.

216. Mukherjee, S.; Brieba, L. G.; Sousa, R., *Cel* **2002,** *110* (1), 81-91.

217. Oakley, J. L.; Pascale, J. A.; Coleman, J. E., *Biochemistry* **1975,** *14* (21), 4684-4691.

218. Giedroc, D. P.; Keating, K. M.; Martin, C. T.; Williams, K. R.; Coleman, J. E., *Journal of Inorganic Biochemistry* **1986,** *28* (2-3), 155-169.

219. Chamberlin, M.; Ring, J., *Journal of Biological Chemistry* **1973,** *248* (6), 2235-2244.

220. Sanchez, R.; Riddle, M.; Woo, J.; Momand, J., *Protein Science* **2008,** *17* (3), 473-481.

221. Wilcox, D. E.; Schenk, A. D.; Feldman, B. M.; Xu, Y., *Antioxidants & Redox Signaling* **2001,** *3* (4), 549-564.

222. Guo, Q.; Nayak, D.; Brieba, L. G.; Sousa, R., *Journal of Molecular Biology* **2005,** *353* (2), 256-270.

223. Jourd'heuil, D.; Jourd'heuil, F. L.; Feelisch, M., *Journal of Biological Chemistry* **2003,** *278* (18), 15720-15726.

224. Erck, A.; Sherwood, E.; Bear, J. L.; Kimball, A. P., *Cancer Research* **1976,** *36* (7), 2204-2209.

225. Rao, P. N.; Smith, M. L.; Pathak, S.; Howard, R. A.; Bear, J. L., *Journal of the National Cancer Institute* **1980,** *64* (4), 905-912.

226. Howard, R. A.; Spring, T. G.; Bear, J. L., *Cancer Research* **1976,** *36* (12), 4402-4405.

227. Bear, J. L., *Precious Metals* **1986**, 337-344.

228. Schafer, S.; Ott, I.; Gust, R.; Sheldrick, W. S., *European Journal of Inorganic Chemistry* **2007,** (19), 3034-3046.

229. Nair, R. B.; Teng, E. S.; Kirkland, S. L.; Murphy, C. J., *Inorganic Chemistry* **1998,** *37* (1), 139-141.

230. Kang, M.; Chouai, A.; Chifotides, H. T.; Dunbar, K. R., *Angewandte Chemie-International Edition* **2006,** *45* (37), 6148-6151.

231. Delgadillo, A.; Romo, P.; Leiva, A. M.; Loeb, B., *Helvetica Chimica Acta* **2003,** *86* (6), 2110-2120.

232. Lehtonen, K.; Summers, L. A., *Australian Journal of Chemistry* **1970,** *23* (8), 1699-1702.

233. Yam, V. W. W.; Lo, K. K. W.; Cheung, K. K.; Kong, R. Y. C., *Journal of the Chemical Society-Chemical Communications* **1995,** (11), 1191-1193.

234. Schmelz, O.; Mews, A.; Basche, T.; Herrmann, A.; Mullen, K., *Langmuir* **2001,** *17* (9), 2861-2865.

235. Angeles-Boza, A. M.; Chifotides, H. T.; Aguirre, J. D.; Chouai, A.; Fu, P. K. L.; Dunbar, K. R.; Turro, C., *Journal of Medicinal Chemistry* **2006,** *49* (23), 6841-6847.

236. Bauer, W.; Vinograd, J., *Journal of Molecular Biology* **1968,** *33* (1), 141-171.

237. Eriksson, M.; Mehmedovic, M.; Westman, G.; Akerman, B., *Electrophoresis* **2005,** *26* (3), 524-532.

238. Keck, M. V.; Lippard, S. J., *Journal of the American Chemical Society* **1992,** *114* (9), 3386-3390.

239. Rahman, M. M.; Yasuda, H.; Katsura, S.; Mizuno, A., *Archives of Biochemistry and Biophysics* **2007,** *464* (1), 28-35.

240. Graham, L. P., *An introduction to medicinal chemistry*. University Press: Oxford, 1995.

241. Fotakis, G.; Timbrell, J. A., *Toxicol.Lett.* **2006,** *160* (2), 171-177.

242. *CometScore*, 1.5; TriTek Corporation, Sumerduck,VA, 2007.

243. Nagababu, P.; Latha, J. N. L.; Satyanarayana, S., *Chemistry & Biodiversity* **2006,** *3* (11), 1219-1229.

244. Neyhart, G. A.; Grover, N.; Smith, S. R.; Kalsbeck, W. A.; Fairley, T. A.; Cory, M.; Thorp, H. H., *Journal of the American Chemical Society* **1993,** *115* (11), 4423-4428.

245. Comings, D. E., *Chromosoma* **1975,** *52* (3), 229-243.

246. Ushay, H. M.; Tullius, T. D.; Lippard, S. J., *Biochemistry* **1981,** *20* (13), 3744-3748.

247. Rahman, M. M.; Yasuda, H.; Katsura, S.; Mizuno, A., *Journal of Biomolecular Structure & Dynamics* **2007,** *24* (6), 553-560.

248. Sangster, J., *Octanol-water partition coefficients: fundamentals and physical chemistry*. John Wiley: Chichester, England, 1997.

249. Dimitrov, S. D.; Dimitrova, N. C.; Walker, J. D.; Veith, G. D.; Mekenyan, O. G., *Pure and Applied Chemistry* **2002,** *74* (10), 1823-1830.

250. Porcar, I.; Codoner, A.; Gomez, C. M.; Abad, C.; Campos, A., *Journal of Pharmaceutical Sciences* **2003,** *92* (1), 45-57.

251. Avdeef, A., *Current Topics in Medicinal Chemistry* **2001,** *1* (4), 277-351.

252. Olive, P. L.; Banath, J. P., *Nature Protocols* **2006,** *1* (1), 23-29.

253. Tice, R. R.; Agurell, E.; Anderson, D.; Burlinson, B.; Hartmann, A.; Kobayashi, H.; Miyamae, Y.; Rojas, E.; Ryu, J. C.; Sasaki, Y. F., *Environmental and Molecular Mutagenesis* **2000,** *35* (3), 206-221.

254. Heringova, P.; Woods, J.; Mackay, F. S.; Kasparkova, J.; Sadler, P. J.; Brabec, V., *Journal of Medicinal Chemistry* **2006,** *49* (26), 7792-7798.

255. Pang, S. K.; Yu, C. W.; Au-Yeung, S. C. F.; Ho, Y. P., *Biochemical and Biophysical Research Communications* **2007,** *363* (1), 235-240.

256. Meister, A.; Anderson, M. E., *Annu. Rev. Biochem.* **1983,** *52*, 711-760.

257. Balendiran, G. K.; Dabur, R.; Fraser, D., *Cell Biochemistry and Function* **2004,** *22* (6), 343-352.

258. Admiraal, G.; Alink, M.; Altona, C.; Dijt, F. J.; Vangarderen, C. J.; Degraaff, R. A. G.; Reedijk, J., *Journal of the American Chemical Society* **1992,** *114* (3), 930-938.

259. Chen, X.; Carystinos, G. D.; Batist, G., *Chemic.-Biological Interactions* **1998,** *111-112*, 263-275.

260. Andrews, P. A.; Murphy, M. P.; Howell, S. B., *Cancer Research* **1985,** *45* (12, Pt. 1), 6250-6253.

261. Andrews, P. A.; Murphy, M. P.; Howell, S. B., *Molecular Pharmacology* **1986,** *30* (6), 643-650.

262. Hromas, R. A.; Andrews, P. A.; Murphy, M. P.; Burns, C. P., *Cancer Letters* **1987,** *34* (1), 9-13.

263. Reedijk, J., *Chemical Reviews* **1999,** *99* (9), 2499-2510.

264. *Molecular Probes: The Handbook*. Invitrogen: Carlsbad, CA **2007**.

265. Brady, H. J. M.; Editor, *Apoptosis methods and protocols*. CRC, Taylor & Francis: Boca Raton, Fl **2004**.

266. Aguirre, J. D.; Angeles-Boza, A. M.; Chouai, A.; Pellois, J.-P.; Turro, C.; Dunbar, K. R., *Journal of the American Chemical Society* **2009**, *131* (32), 11353-11360.

267. Hansch, C.; Leo, A.; Nikaitani, D., *Journal of Organic Chemistry* **1972,** *37* (20), 3090-3092.

268. Hansch, C.; Leo, A.; Unger, S. H.; Kim, K. H.; Nikaitani, D.; Lien, E. J., *Journal of Medicinal Chemistry* **1973,** *16* (11), 1207-1216.

269. Schaefer, S.; Ott, I.; Gust, R.; Sheldrick, W. S., *European Journal of Inorganic Chemistry* **2007,** (19), 3034-3046.

270. Modica-Napolitano, J. S.; Joyal, J. L.; Ara, G.; Oseroff, A. R.; Aprille, J. R., *Cancer Research* **1990,** *50* (24), 7876-7881.

271. Modica-Napolitano, J. S.; Aprille, J. R., *Advced Drug Delivery Reviews* **2001,** *49* (1-2), 63-70.

272. Modica-Napolitano Josephine, S.; Singh Keshav, K., *Expert Reviews in Molecular Medicine* **2002,** *4* (9), 1-19.

273. Rosania, G. R., *Current Topics in Medicinal Chemistry* **2003,** *3* (6), 659-685.

274. Horobin, R. W.; Trapp, S.; Weissig, V., *Journal of Controlled Release* **2007,** *121* (3), 125-136.

275. Telford, W. G.; Komoriya, A.; Packard, B. Z., *Methods in Molecular Biology* **2004,** *263*, 141-159.

276. Fischer, K.; Voelkl, S.; Berger, J.; Andreesen, R.; Pomorski, T.; Mackensen, A., *Blood* **2006,** *108* (13), 4094-4101.

277. Modica-Napolitano, J. S., *Mitochondrial DNA Mutations in Aging, Disease and Cancer* **1998**, 337-344.

278. Ashley, N.; Poulton, J., *Biochemical & Biophysical Research Communications* **2009,** *378* (3), 450-455.

279. Diaz de la Loza, M. C.; Wellinger, R. E., *Nucleic Acids Research* **2009,** *37* (4), 1- 12.

280. Lansiaux, A.; Dassonneville, L.; Facompre, M.; Kumar, A.; Stephens, C. E.; Bajic, M.; Tanious, F.; Wilson, W. D.; Boykin, D. W.; Bailly, C., *Journal of Medicinal Chemistry* **2002,** *45* (10), 1994-2002.

281. Jarver, P.; Langel, U., *Drug Discovery Today* **2004,** *9* (9), 395-402.

282. Futaki, S., *Advanced Drug Delivery Reviews* **2005,** *57* (4), 547-558.

283. Juliano, R. L.; Alam, R.; Dixit, V.; Kang, H. M., *Wiley Interdisciplinary Reviews: Nanomedicine and Nanobiotechnology* **2009,** *1* (3), 324-335.

284. Heitz, F.; Morris, M. C.; Divita, G., *Br. Journal of Pharmacology* **2009,** *157* (2), 195-206.

285. Langel, U., *Cell-Penetrating Peptides, Mechanisms and Applications.* **2005***, 11(28),* 1-133.

286. Jaerver, P.; Langel, U., *Biochimica & Biophysica Acta, Biomembranes* **2006,** *1758* (3), 260-263.

287. Pujals, S.; Bastus, N. G.; Pereiro, E.; Lopez-Iglesias, C.; Puntes, V. F.; Kogan, M. J.; Giralt, E., *ChemBioChem* **2009,** *10* (6), 1025-1031.

288. El-Sayed, A.; Futaki, S.; Harashima, H., The *Aaps Journal* **2009,** *11* (1), 13-22.

289. Wagstaff, K. M.; Jans, D. A., *Current Medicinal Chemistry* **2006,** *13* (12), 1371-1387.

290. Maitani, Y.; Hattori, Y., *Expert Opinion on Drug Delivery* **2009,** *6* (10), 1065-1077.

291. Graeslund, A.; Eriksson, L. E. G., *Genetic Engineering* **2004,** *26*, 19-31.

292. Tinega, A. N.; Pelle, R.; Kang'a, S.; Gicheru, M. M.; Taracha, E. L. N.; Nene, V.; Graham, S. P., *Veterinary Immunology & Immunopathology* **2009,** *130* (1-2), 107-113.

293. Bertrand, J.-R.; Malvy, C.; Auguste, T.; Toth, G. K.; Kiss-Ivankovits, O.; Illyes, E.; Hollosi, M.; Bottka, S.; Laczko, I., *Bioconjugate Chemistry* **2009,** *20* (7), 1307-1314.

294. Aroui, S.; Brahim, S.; De Waard, M.; Breard, J.; Kenani, A., *Cancer Letters* **2009,** *285* (1), 28-38.

295. Park, K., *Journal of Controlled Release* **2009,** *139* (2), 87.

296. Puckett, C. A.; Barton, J. K., *Journal of the American Chemical Society* **2009,** *131* (25), 8738-8739.

297. Myrberg, H.; Lindgren, M.; Langel, U., *Bioconjugate Chemistry* **2007,** *18* (1), 170-174.

298. Bass, Y.; Morgan, R. J.; Donovan, R. J.; Baker, A. D., *Synthetic Communications* **1997,** *27* (12), 2165-2169.

299. Pellois, J.-P.; Muir, T. W., *Angewandte Chemie International Edition in English* **2005,** *44* (35), 5713-5717.

300. Zaykov, A. N.; MacKenzie, K. R.; Ball, Z. T., *Chemistry A -European Journal* **2009,** *15* (36), 8961-8965.

301. Aguirre, J. D.; Lutterman, D. A.; Angeles, A. M.; Dunbar, K. R.; Turro, C., *Inorganic Chemistry* **2007,** *46* (18), 7494-7502.

VITA

Jessica Dafhne Aguirre Flores received her Bachelor of Science degree in chemistry from the Pontificia Universidad Católica del Perú in 2001. She entered the Ph.D. program at Texas A&M University in 2003, where she joined the group directed by Prof. Dunbar. Her research interests include the history of chemistry, as well as the medicinal properties and toxicology of metal complexes.

Ms. Aguirre Flores may be reached at Elias Aguirre Dpto. 601, Miraflores (Lima18), Lima, Peru. Her e-mail address is jessicadaphne@gmail.com.